THE UNIVERSITY OF CHICAGO

OLEFIN POLYMERIZATION BEHAVIOR AND REACTIVITY OF PALLADIUM(II) ALKYL AND FLUORIDE COMPLEXES BEARING PHOSPHINE-SULFONATE LIGANDS

A DISSERTATION SUBMITTED TO

THE FACULTY OF THE DIVISION OF THE PHYSICAL SCIENCES

IN CANDIDACY FOR THE DEGREE OF

DOCTOR OF PHILOSOPHY

DEPARTMENT OF CHEMISTRY

BY

REBECCA E. BLACK

CHICAGO, ILLINOIS

JUNE 2018

TABLE OF CONTENTS

LIST OF TABLES

CHAPTER FIVE

CHAPTER SIX

LIST OF FIGURES

CHAPTER TWO

LIST OF SCHEMES

CHAPTER ONE

CHAPTER TWO

CHAPTER FOUR

CHAPTER FIVE

CHAPTER SIX

LIST OF CHARTS

LIST OF EQUATIONS

ACKNOWLEDGEMENTS

I must first thank my advisor, Professor Richard Jordan, for his invaluable guidance and constant support throughout my graduate studies. He taught me more about scientific rigor, professionalism, and mentorship than I could have ever imagined. I can only hope to be as good of a mentor to my students in the future. I also thank the other members of my thesis committee, Professors Michael Hopkins and John Anderson, for their mentorship and helpful discussions throughout my graduate studies.

I have been fortunate to work with fantastic chemists in the Jordan group. I am especially grateful to Dr. Ge "David" Feng for his mentorship when I first joined the group, and to Dr. Nathan Contrella, Dr. Frank Olechnowicz, Erik Reinhart, Alison Johnson, Dr. Ka Cheong "Tim" Lau, and Dr. Feng Zhai for their generous help and insightful discussions. I thank the undergraduate students and summer incoming-graduate student who I have worked with over the course of my graduate studies– Kelsey Brown, Eleanor Mayes, Hannah Yi, and Jennifer Zhang– for being excellent mentees. I also thank other past and current group members who have provided insightful discussions and a great work environment, including Dr. Qian Liu, Dr. Jia Wei, Dr. Ryan Zarkesh, and undergraduates Tabatha Bohoc, Naomi Clayman, Joseph Solomon, James Earl, Amanda Waterbury, Max Weinberg, and Isabel Jensen.

I am grateful to my undergraduate research advisor at Augustana College, Professor Gregory Domski, for his support and helpful discussions both during college and graduate school. He fostered my interests in teaching and catalysis that I now take with me into my independent career.

The research described in this thesis relied heavily on departmental facilities, and I thank Dr. Antoni Jurkiewicz for his assistance with NMR Spectroscopy, Dr. Chang-Jin Qin for his assistance

with mass spectrometry, and Dr. Alexander Filatov and Dr. Ian Steele for their assistance with X-ray crystallography. I also thank Melinda Moore, Vera Dragisich, and Laura Baker for their various responsibilities outside of research.

Having the support of friends both inside and outside of the department has been a vital component of graduate school. From exploring Chicago's food to cat sitting to board game binges and to everything in between, I thank Joseph Mastron, Michael Lueckheide, Polina Navotnaya, Airi Kawamura, Andrew McNeece, the rest of the Anderson lab clan, Joel and Jess Dodge, Dan Micheroni, Dr. Preston Scrape, Dr. Judith Kamm, Hunter Vibbert, Dr. Wayne Lau, the Rosenberger/Anderson family, Sarah and JR Lehuta, and my RB folks.

I thank my family and especially my parents, Judy and Jim Black, for a lifetime of unconditional support and encouragement. Finally, I thank my partner, Austin, for his love and support, and for standing by my side through the ups and downs of graduate school. Now, on to the next adventure!

ABSTRACT

The unique ability for (PO)PdR(L) complexes that contain phosphine-arenesulfonate ligands to copolymerize ethylene (E) with a wide range of polar vinyl monomers motivates the objectives of this thesis: to identify new ways of modifying the (PO)Pd scaffold (i.e. incorporating a cyclopentane linker), to elucidate the effects of these modifications on polymerization performance, and to study the olefin polymerization and insertion behavior by new (PO)Pd alkyl and fluoride complexes.

This thesis describes new Pd-based catalysts for E homopolymerization and ethylene/vinyl-fluoride (VF) and ethylene/methyl-acrylate (MA) copolymerization. These catalysts feature chelating ligands that contain a strong phosphine donor and a weak sulfonate donor group, which are bridged by a cyclopentane ring. This thesis also describes the synthesis and olefin insertion behavior of a new (PO)Pd fluoride complex. Finally, the solution and solid-state structures of a high performing (PO)PdRL polymerization catalyst were investigated by NMR spectroscopy and X-ray crystallography.

Chapter One introduces palladium(II) alkyl complexes that contain ancillary phosphine-arenesulfonate ligands. This class of catalysts is one of the few that catalyze the copolymerization of E and polar vinyl monomers to afford copolymers with the polar functionalities incorporated into a highly linear polyethylene (PE) backbone. The electronic asymmetry of the phosphine-arenesulfonate ligand is believed to be important for the unique reactivity of these (PO)Pd alkyl complexes by suppressing β-eliminations that deactivate the catalyst or lead to non-linear polymers. Importantly, the catalyst activity and the molecular weight (MW) of the PEs and

copolymers produced by (PO)Pd alkyl catalysts can be significantly modified by changing the substituents on the phosphine.

Chapter Two describes the synthesis and characterization of Pd(II) alkyl complexes that contain PPh_2-cyclopentanesulfonate ([PO-C5-Ph]$^-$) and P(2-OMe-Ph)$_2$-cyclopentanesulfonate ([PO-C5-OMe]$^-$) ligands. A sulfonate-bridged, base-free dimer species of type {(PO-C5-OMe)PdMe}$_2$ was synthesized by abstraction of pyridine from the analogous (PO)PdMe(py) complex using $B(C_6F_5)_3$. Borane-coordinated base-free dimer [{(PO-C5-OMe)•$B(C_6F_5)_3$}PdMe]$_2$, in which $B(C_6F_5)_3$ binds to a sulfonate oxygen, was prepared by addition of one equiv of $B(C_6F_5)_3$ per Pd to {(PO-C5-OMe)PdMe}$_2$ base-free dimer or addition of two equiv of $B(C_6F_5)_3$ to (PO-C5-OMe)PdMe(py). The solution behavior and solid-state structures of these complexes are described.

Chapter Three describes the olefin polymerization performance of the complexes prepared in Chapter Two. (PO-C5-OMe)PdMe(py), {(PO-C5-OMe)PdMe}$_2$, and [{(PO-C5-OMe)•$B(C_6F_5)_3$}PdMe]$_2$ polymerize E with low activity (up to 210 kg mol^{-1} h^{-1} at 250 psi and 80 °C) to linear polyethylene (M_n = 1950 – 5250 Da) with predominantly internal olefin placements. (PO-C5-OMe)PdMe(py) and {(PO-C5-OMe)PdMe}$_2$ copolymerize E with MA to linear copolymers that contain up to 11.7 mol % MA, which is incorporated as –$CH_2CH(CO_2Me)CH_2$– (80%) in-chain units and –$CH_2CH(CO_2Me)Me$ (8%) and –CH_2CH=$CH(CO_2Me)$ (12%) chain-end units. (PO-C5-OMe)PdMe(py) and {(PO-C5-OMe)PdMe}$_2$ also copolymerize E with VF to linear copolymers that contain up to 0.41 mol % VF, which is incorporated as –CH_2CHFCH_2– (~80%) in-chain units and –CH_2CF_2H (7%), –CH_2CHFCH_3 (5%) and –CH_2CH_2F (8%) chain-end units. The cyclopentane linker in the phosphine-sulfonate ligand strongly affects the activity of the catalysts and the PE MW. (PO-C5-OMe)PdMe(py) and {(PO-C5-OMe)PdMe}$_2$ are much more stable and active in E polymerization than analogous (PAr_2-*CH_2CH_2*SO_3)PdR catalysts, and are

less active but less inhibited by polar vinyl monomers than analogous (PAr_2-*arene*sulfonate)PdR catalysts.

Chapter Four describes experimental and computational investigations of the ethylene polymerization mechanism for complexes prepared in Chapter Two. Low-temperature NMR studies show that {(PO-C5-OMe)PdMe}$_2$ reacts with ethylene below –10 °C to form ethylene-adduct *cis-P,R*-(PO-C5-OMe)PdMe(ethylene), which undergoes insertion at 5 °C. DFT calculations for a model (PMe_2-*cyclopentane*sulfonate)Pd(Pr)(ethylene) species show that E insertion proceeds by *cis-P,R*/*trans-P,R* isomerization followed by migratory insertion, and that the lower activity of (PO-C5-OMe)PdMe(py) and {(PO-C5-OMe)PdMe}$_2$ vis-à-vis analogous (PAr_2-*arene*sulfonate)PdR catalysts results from a higher barrier for migratory insertion of the *trans-P,R* isomer.

Chapter Five describes the synthesis and characterization of new (PO-OMe)PdX(lut) complexes (X= Br, F, FHF) bearing a P(2-OMe-Ph)$_2$-*p*-Me-benzenesulfonate ligand. (PO-OMe)PdF(lut) exists as a mixture of *cis-/trans-P,F* isomers that interconvert both in CD_2Cl_2 and in the solid-state. Rather than the formation of a {(PO-OMe)PdF}$_2$ species by abstraction of lutidine, the addition of $B(C_6F_5)_3$ to *cis/trans-P,F*-(PO-OMe)PdF(lut) results in F/C_6F_5 exchange to yield (PO-OMe)Pd$(C_6F_5)_3$, which is likely generated through an ion-paired $[(PO)Pd(II)(lut)]^+[FB(C_6F_5)_3]^-$ intermediate followed by aryl elimination. *Cis*/*trans-P,F*-(PO-OMe)PdF(lut) reacts cleanly with VF, vinyl bromide (VBr), vinyl acetate (VOAc), and 1,5-hexadiene to give net insertion products. For example, (PO-OMe)PdCH_2CHF_2(lut) is generated from net VF insertion into *cis-P,F*-(PO-OMe)PdF(lut) and *trans-P,F*-(PO-OMe)PdF(lut). Notably, at room temperature, *cis-P,F*-(PO-OMe)PdF(lut) reacts with VF eight times faster than does *trans-P,F*-(PO-OMe)PdF(lut). Another net insertion product, (PO-OMe)Pd(CH_2CHF(OAc))(lut), was

observed from net VOAc insertion into *cis/trans-P,F*-(PO-OMe)PdF(lut) at 50 °C. However, (PO-OMe)Pd($CH_2CHF(OAc)$)(lut) reacts further at 50 °C to give an unusual Pd-enolate complex (PO-OMe)Pd{$CH_2C(=O)H$}(lut). VBr insertion into the Pd–F bond is followed by rapid *β*-Br elimination to yield (PO-OMe)PdBr(lut). *Cis/trans-P,F*-(PO-OMe)PdF(lut) reacts with 1,5-hexadiene by insertion and cyclization to give a Pd-fluoro-cyclopentylmethyl compound. Reaction with *trans,trans*-1,6-dideuterium-1,5-hexadiene may provide a means of determining whether fluoropalladation occurs via *cis*- or *trans*-addition.

Chapter Six describes the synthesis and structures of the 2-{PH(2-{2,6-$(OMe)_2$-Ph}-Ph)(2-OMe-Ph))}-4-Me-benzenesulfonate (H[PO-Bp/Ph^{OMe}]) proligand and the corresponding (PO-Bp/Ph^{OMe})PdMeL catalysts (L = py, lut). ^1H-^1H NOESY NMR experiments establish that the solution-state structure of (PO-Bp/Ph^{OMe})PdMe(lut) is similar to the solid-state structure and contains a π-stacking interaction between the Ar^2Bp and Ar^{SO3} rings of the PO^- ligand. (PO-Bp/Ph^{OMe})PdMe(py) exists as a mixture of two isomers in solution. The solid-state of one of these isomers was determined by X-ray crystallography. Interestingly, rather than participating in a π-stacking interaction, the Ar^2Bp ring in this structure is positioned over an axial site of the Pd square plane. Therefore, it is most likely that the two (PO-Bp/Ph^{OMe})PdMe(py) species seen in solution at low temperature differ in the rotational conformation of the Bp unit.

PREFACE

Each chapter has an independent numbering system for compounds. A given compound may have a different number in different chapters. For each chapter, the relevant experimental information, references and notes are provided at the end of the chapter.

Chapter One

(Phosphine-Arenesulfonate)Palladium-Alkyl Olefin Polymerization Catalysts

1.1 Introduction

(PO)PdRL complexes bearing *ortho*-phosphino-arenesulfonate ligands (PO^-) have been widely studied because of their ability to polymerize ethylene (E) to highly-linear polyethylene (PE) and to copolymerize E with a variety of "polar" CH_2=CHX vinyl monomers. In 2002, Pugh and Drent first reported that a Pd catalyst generated *in situ* from $Pd(OAc)_2$ or $Pd(dba)_2$ (dba = dibenzylideneacetone) and the phosphonium sulfonate zwitterion 1-PH^+(2-OMe-Ph)$_2$-2-SO_3^--Ph (H[PO-OMe]) copolymerizes E and alkyl acrylates to linear copolymers with the acrylate monomer incorporated into the polymer backbone (Scheme 1.1).[1] It was proposed that polymerization proceeds by insertion of monomers into active (PO)PdR complexes.

Scheme 1.1. First copolymerization of ethylene and acrylates by (PO)PdR catalysts

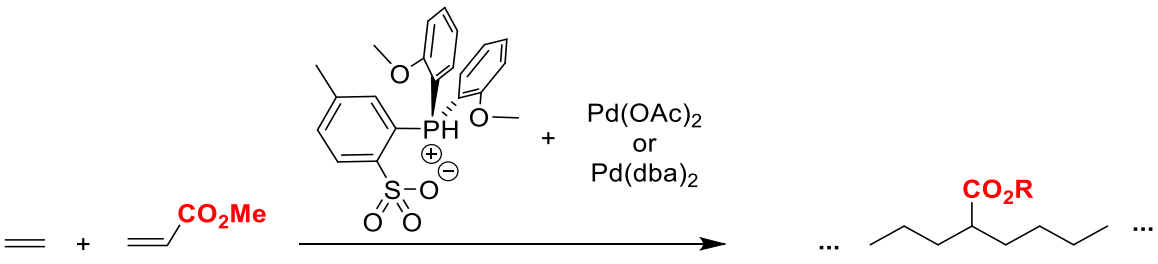

Due to the unique reactivity of this system, following Pugh and Drent's seminal report, several industrial and academic groups–Claverie,[2–13] Jordan,[14–25] Mecking,[26–51] Nozaki,[52–67] Rieger,[68–72] Sen,[73–76] Chen,[77–84] and others[85–91]–have studied the E polymerization and E/CH_2=CHX copolymerization behavior of discrete (PO)PdMe(L) complexes (L = pyridine or other labile ligands, Scheme 1.2, **A**).[92–94]

Some of these studies have focused on the comonomer scope of these catalysts (Scheme 1.2).[95] (PO)PdR-type complexes are now known to copolymerize E with vinyl ethers,[14] vinyl fluoride,[16,17,25] vinyl chloride (terminal incorporation only),[38] acrylonitrile,[53,59] vinyl acetate,[57] acrylates,[1,3,5,9,10,27,30,32,96,97] acrylic acid,[6,8,31] vinyl ketone,[75] styrene,[75] acrylamides,[4,34] N-vinyl-2-pyrrolidinone,[4] vinyl sulfone,[29] vinyl phosphonic acid and vinyl phosphonate,[98] norbornene,[2,74,88] 3,3,3-trifluoropropene,[72] allyl monomers,[48,60] diallyl ether,[44] and norbornene anhydride.[51] (PO)PdR-type complexes can also catalyze the non-alternating copolymerization of ethylene and CO,[69,73,76,86,87,99,100] and the alternating copolymerization of CO with vinyl acetate or methyl acrylate.[54,55,61,65]

Scheme 1.2. Copolymerization of ethylene and polar vinyl monomers by (PO)PdRL catalysts

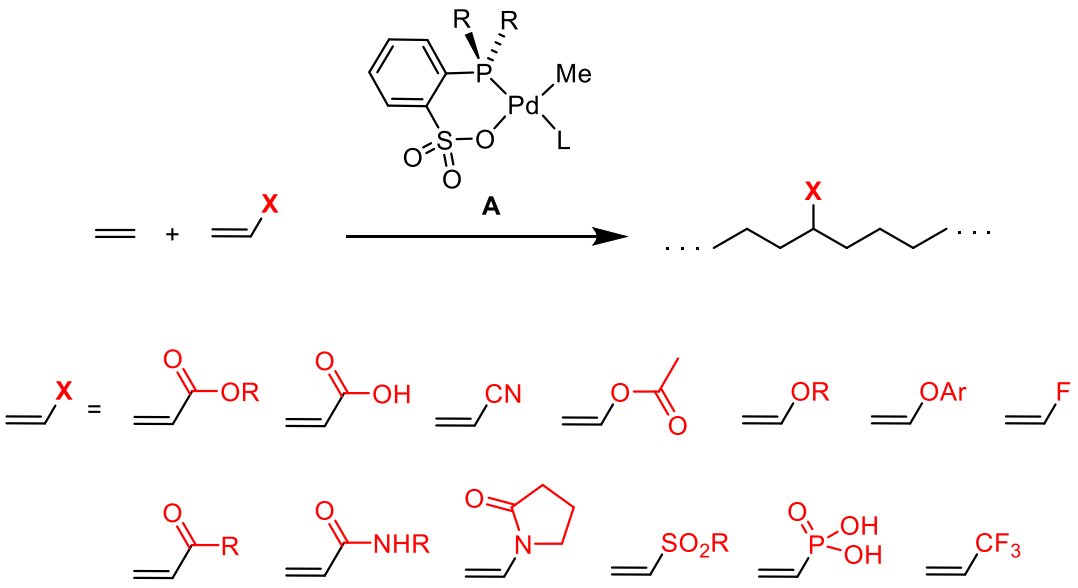

A general scheme for olefin polymerization by (PO)PdRL complexes is shown in Scheme 1.3. First, replacement of labile ligand L by E takes place by an associative mechanism to form *cis-P,C*-(PO)PdR(ethylene).[56] This species then isomerizes to a less stable, more reactive *trans-P,C*-(PO)PdR(ethylene) isomer. The isomerization likely involves coordination of a second oxygen atom of the sulfonate group with the PO^- ligand binding to the Pd center in a κ^3-*P,O,O* fashion, to afford a five-coordinate species, followed by decoordination of the second sulfonate oxygen (Berry's pseudorotation pattern).[19,56,92,93,101] The *trans-P,C* isomer can then undergo 1,2-migratory insertion to give a *β*-agostic *cis-P,C*-alkyl species, followed by ethylene trapping to regenerate the *cis-P,R* complex with an extended polymeryl chain. The *β*-agostic *cis*-alkyl species can also undergo *β*-H elimination, isomerization via a five-coordinate species to a *cis-P,H* species, and olefin displacement. The latter process typically occurs by associative substitution in these systems,

i.e. axial coordination of ethylene, Berry pseudorotation, and dissociation of the vinyl-capped polymer from the opposite axial site.[19,85,92,93,101] Catalyst activity is influenced by the off-cycle (PO)PdR(L) and (PO)PdR(ethylene) ligand exchange, and the PE molecular weight is controlled by the relative rates of chain growth and chain transfer, $M_n = (\frac{R_{growth}}{R_{transfer}})$(monomer MW).

Scheme 1.3. General scheme for olefin polymerization by (PO)PdR catalysts. R = growing chain or hydride, ancillary ligands are not shown.

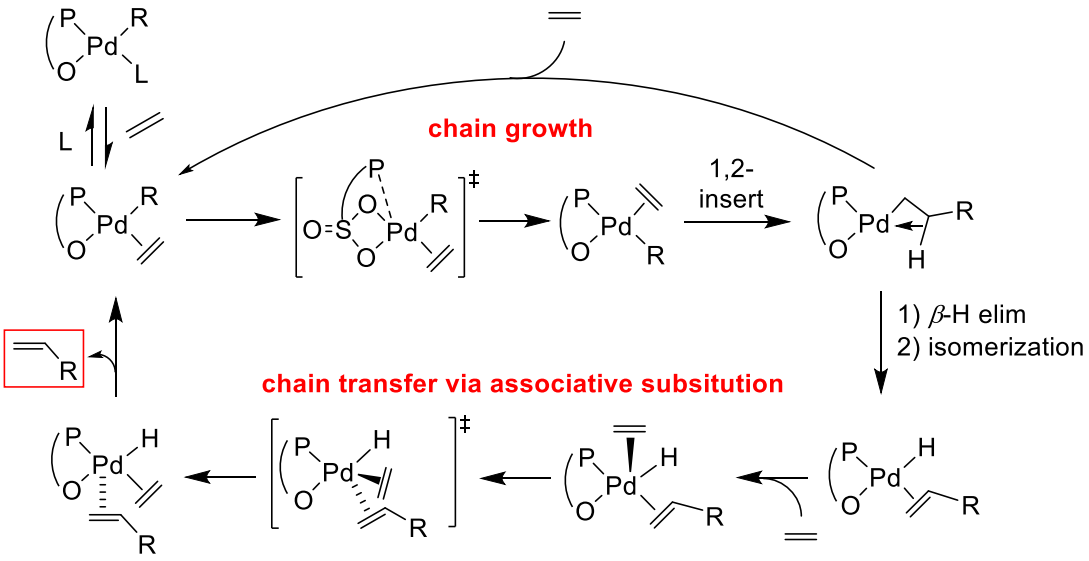

The production of linear polymers by (PO)PdRL catalysts is atypical of Pd(II) catalysts, which usually undergo rapid chain walking to form highly-branched polymers.[102] It is also remarkable that (PO)PdRL complexes incorporate monomers such as vinyl fluoride, vinyl ethers, and vinyl acetate, since these olefins typically insert into Pd–R bonds to give $PdCH_2CRX$ species that undergo rapid β-X elimination to form in active (PO)PdX species. The production of linear PEs and incorporation of polar monomers by (PO)PdRL catalysts is believed to arise from the

"electronic asymmetry" of the bidentate phosphine-sulfonate ligand,[85] which arises from the different *trans* influences of the strong phosphine donor and the exceedingly weak sulfonate donor.

In ethylene homopolymerization (Scheme 1.4, right-hand side), *β*-H elimination is disfavored because it would result in the generation of a species with a strong phosphine ligand and a strong hydride ligand in a mutually *trans* arrangement. Binding ethylene, on the other hand, generates a more stable species that has two favorable *trans* arrangements: (i) the sulfonate (very weak) *trans* to the alkyl (very strong) group and (ii) the phosphine (very strong) *trans* to the olefin (medium, weaker than hydride). Subsequent ethylene coordination and chain growth is favored over *β*-H elimination, which would result in chain transfer or branching via chain walking. Similarly, in the copolymerization of ethylene and polar monomers (Scheme 1.4, left-hand side), ethylene coordination is favored over *β*-X elimination because the ethylene-coordinated species maintains a favorable *trans* arrangement of the sulfonate (very weak) and alkyl (very strong) ligands. The *trans* arrangement of the phosphine and dative X ligand is also likely preferred over a *trans* phosphine/X^- arrangement. Therefore, chain growth by subsequent ethylene coordination and insertion is favored over catalyst deactivation by *β*-X elimination. These kinds of *trans* influence effects are more pronounced for "soft" Pd(II) metal centers where metal-ligand bonds are more covalent compared to "hard" metal centers.

Scheme 1.4. Electronic asymmetry of (PO)PdR olefin polymerization catalysts

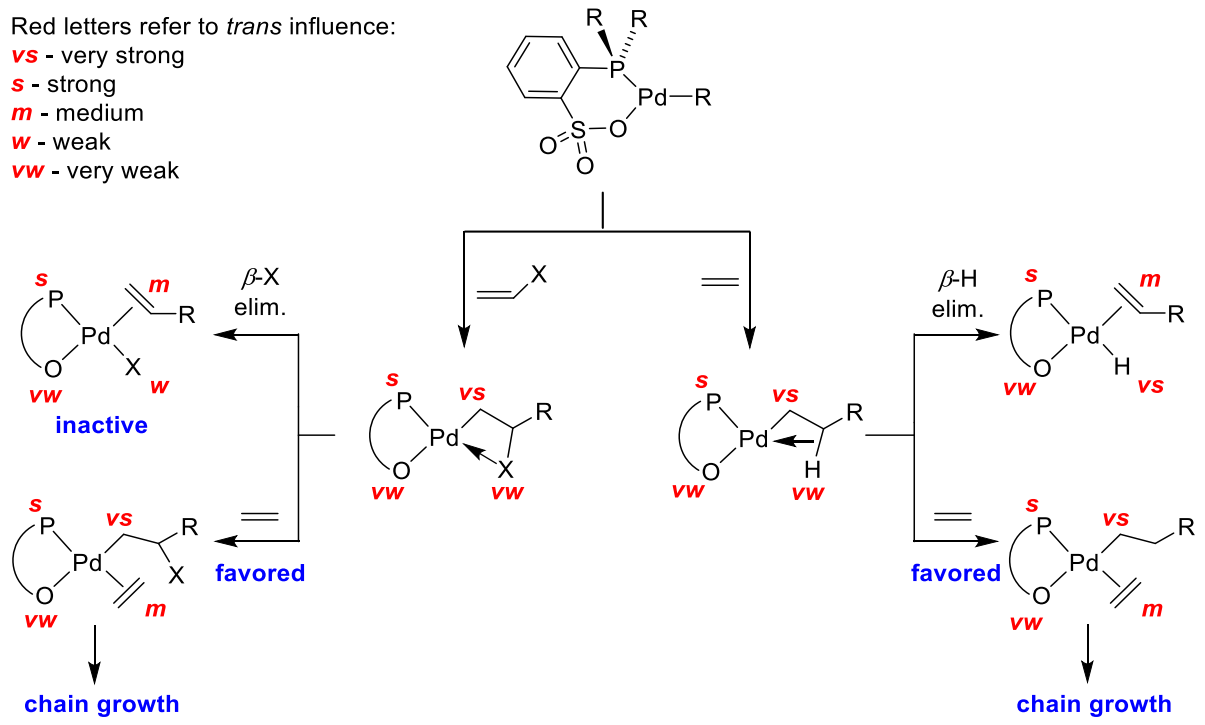

Other catalyst features that strongly influence polymerization reactivity include: (i) steric crowding of the Pd axial coordination sites by the (PO) ligand to inhibit chain transfer by blocking associative exchange of the alpha olefin with ethylene,[66] (ii) limited backbonding ability of Pd(II) ensures that the coordinated olefin is electron deficient and activated for nucleophilic attack by the alkyl group, and (iii) a neutral Pd(II) center favors binding polar vinyl monomers to form π-complexes rather than X-bound σ-complexes, which promotes incorporation of polar vinyl monomers.

1.2 Modifications to (Phosphine-Arenesulfonate)PdRL Catalysts

While the ability to incorporate diverse comonomers is an advantage of the (PO)PdR system, the original (PO-OMe)PdMeL catalysts (**1,** Chart 1.1) generate PE with relatively low molecular weight and activity compared to what is observed for other single-site catalysts.[103,104] Furthermore, the addition of polar monomers invariably reduces activities and MWs further. Therefore, many new structures have been designed in efforts to produce better performing catalysts.

Chart 1.1. Structures of new (PO)Pd -type complexes, L = labile ligand.

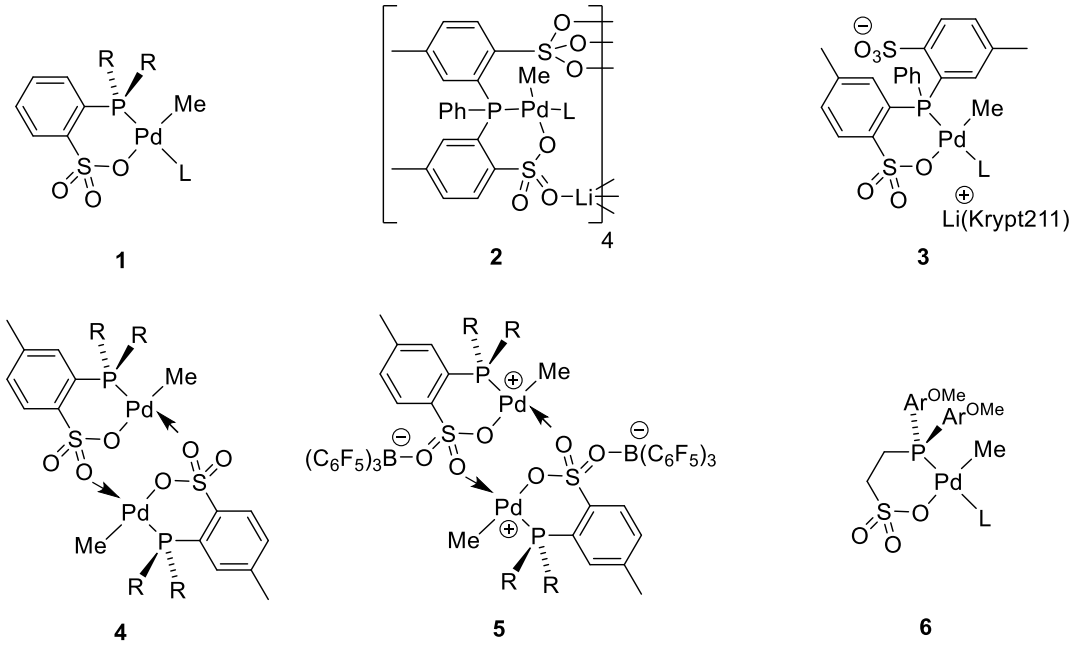

One approach to improve polymerization performance of **1**-type complexes has been to modify the PR_2 group to change the electronic and steric properties of the phosphine.[7,37,40,66] Generally, more electron-donating $–PR_2$ units increase the catalyst activity and more sterically-

crowded $–PR_2$ units increase the polymer molecular weight. For example, Claverie and co-workers[10] compared the ethylene polymerization performance of type-**1** complexes with a range of $–PAr_2$, $–P(alkyl)_2$ and –PAr(alkyl) units and found a strong positive correlation between the phosphine donor ability, as assessed by the BE(B) descriptor within the ligand knowledge base for monodentate P donors (LKB-P),[105] and catalyst activity. In another example, phenyl-substituted (κ^2-1-*PPh_2*-2-SO_3-Ph)PdMe(py) catalyst generates PE with a number-average molecular weight (M_n) of 9.3 kDa, while dimethyoxy-biphenyl-substituted catalyst (κ^2-1-*$P(2\text{-}(2,6\text{-}OMe_2\text{-}Ph)\text{-}Ph)_2$*-2-$SO_3$-Ph)PdMe(py) generates PE with M_n = 227 kDa, under the same conditions (toluene, 290 psi E, 85 °C).[10] The higher MW arises from the steric size of the ($PO^–$) ligand, which blocks the axial sites of Pd and suppresses associative chain transfer.

A second approach to improving catalyst performance is to incorporate the (PO)PdRL unit into multinuclear structures (**2** and **3**, Chart 1.1). Complex **2** adopts a tetrameric cage structure that produces ultra-high MW (M_w up to 10^6 Da) PE and incorporates a higher level of vinyl fluoride in copolymerizations (2.4 mol%) compared to mononuclear analogous **1** catalysts (0.6 mol%) under identical conditions (120 psi VF/130 psi E).[17,18] **2** is converted to mononuclear species **3** by abstraction of Li^+ with a cryptand. **3** shows similar activity to **2**, but only produces low MW oligomers (C_4-C_{18}) rather than ultra-high MW PE.[17] The free, pendant sulfonate moiety in **2** may be able to displace α-olefins formed by *β*-H elimination, thereby increasing chain transfer.[106]

The polymerization activity of (PO)PdRL catalysts depends on the steric profile and electron-donation of the $-PR_2$ unit, as well as the lability of the L ligand.[35] Under the same ethylene

polymerization conditions (toluene, 73 psi E, 80 °C), (PO-OMe)PdMeL has an activity of 170 kg mol^{-1} h^{-1} bar^{-1} when L = pyridine and 560 kg mol^{-1} h^{-1} bar^{-1} when L = DMSO.[35] Since the L ligand competes with ethylene during polymerization and DMSO is a weaker base than pyridine (i.e. more labile), the equilibrium between Pd-L and Pd-(ethylene) lies more toward Pd-(ethylene) during polymerization, resulting in higher activity. Complete abstraction of L by a borane, such as $B(C_6F_5)_3$, to yield $\{(PO)PdMe\}_2$ base-free dimers (**4**) also increases polymerization activity.[20] For example, {(PO-Et)PdMe(py) based on the o-$\{(2\text{-Et-Ph})_2P\}$-*p*-toluenesulfonate ligand produces linear PE (M_n = 21,800) with an activity of 1,470 kg mol^{-1} h^{-1},[15] and base-free $\{(PO\text{-Et})PdMe\}_2$ gives PE (M_n = 29,300) with an activity of 1,570 kg mol^{-1} h^{-1}.[20]

The coordination of $B(C_6F_5)_3$ to the sulfonate oxygen of the $\{(PO)PdMe\}_2$ dimer **4** to afford **5** has a dramatic effect on catalyst performance (Chart 1.1). For example, $\{(PO\text{-Et})PdMe\}_2$ is 4-times more active (3,870 kg mol^{-1} h^{-1}) than (PO-Et)PdMe(py) (i.e. 4-fold increase in R_{growth}), but there is a ca. 10-fold reduction in polymer M_n (19,600) due to an 40-fold increase in $R_{transfer}$.[20] Similarly, when R = 3,5-^{t}Bu$_2$-Ph, coordination of borane increases activity three-fold (**4**: activity = 110 kg mol^{-1} h^{-1}; **5**: activity = 360 kg mol^{-1} h^{-1}) but decreases the M_n of the PE significantly due to an 80-fold increase in chain transfer (**4**: M_n = 3000 Da; **5**: M_n = 170 Da).[20]

While many type-**1** complexes containing benzene or toluene backbones have been prepared and tested in polymerization, complex **6** is the only (PO)PdMeL complex with a different linker to be tested in polymerization.[100,107] Complex **6** is discussed in more detail in Chapter 2.

1.3 Thesis Objectives

Despite the many variations made to (PO)PdR(L) catalysts, these complexes typically exhibit low to moderate E polymerization activities, relative to other olefin polymerization catalysts.[103,104] The promising ability for (PO)Pdr(L) catalysts to copolymerize E with a wide range of polar vinyl monomers and these limitations have motivated the objectives of this thesis: to identify new ways of modifying the (PO)Pd scaffold (i.e. incorporating a cyclopentane linker), to elucidate the effects of these modifications on polymerization performance, and to study the olefin polymerization and insertion behavior by new (PO)Pd alkyl and fluoride complexes.

Chapter Two describes the synthesis and characterization of Pd(II) alkyl complexes that contain PPh_2-cyclopentanesulfonate ($[PO\text{-}C5\text{-}Ph]^-$) or P(2-OMe-Ph)$_2$-cyclopentanesulfonate ($[PO\text{-}C5\text{-}OMe]^-$) ligands. A sulfonate-bridged, base-free dimer species of type {(PO-C5-OMe)PdMe}$_2$ and a borane-coordinated base-free dimer species of type [{(PO-C5-OMe)•$B(C_6F_5)_3$}PdMe]$_2$ were prepared by addition of one equiv or two equiv of $B(C_6F_5)_3$ per Pd, respectively, to (PO-C5-OMe)PdMe(py). The solution behavior and solid-state structures of these complexes are described.

Chapter Three describes the olefin polymerization performance of complexes prepared in Chapter Two. (PO-C5-OMe)PdMe(py), {(PO-C5-OMe)PdMe}$_2$, and [{(PO-C5-OMe)•$B(C_6F_5)_3$}PdMe]$_2$ are active in E polymerization and copolymerization with methyl acrylate and vinyl fluoride (VF) to form linear PEs and copolymers. The cyclopentane linker in the phosphine-sulfonate ligand strongly affects the activity of the catalysts and the PE MW. (PO-C5-

OMe)PdMe(py) and {(PO-C5-OMe)PdMe}$_2$ are much more stable and active in E polymerization than analogous (PAr$_2$-*CH$_2$CH$_2$*SO$_3$)PdR catalysts, and are less active but less inhibited by polar vinyl monomers than analogous (PAr$_2$-*arene*sulfonate)PdR catalysts.

Chapter Four describes experimental and computational investigations of the polymerization mechanism for complexes prepared in Chapter Two. Low temperature NMR studies show that {(PO-C5-OMe)PdMe}$_2$ reacts with E below –10 °C to form the ethylene adduct *cis-P,R*-(PO-C5-OMe)PdMe(ethylene), which undergoes insertion at 5 °C. DFT calculations for a model (PMe$_2$-*cyclopentane*sulfonate)Pd(Pr)(ethylene) species show that E insertion proceeds by *cis-P,R*/*trans-P,R* isomerization followed by migratory insertion, and that the lower activity of (PO-C5-OMe)PdMe(py) and {(PO-C5-OMe)PdMe}$_2$ vis-à-vis analogous (PAr$_2$-*arene*sulfonate)PdR catalysts results from a higher barrier for migratory insertion of the *trans-P,R* isomer.

Chapter Five describes the synthesis and characterization of new (PO-OMe)PdX(lut) complexes (X= Br, F, FHF) bearing a P(2-OMe-Ph)$_2$-*p*-Me-benzenesulfonate ligand. (PO-OMe)PdF(lut) exists as a mixture of *cis/trans-P,F* isomers that interconvert both in CD_2Cl_2 and in the solid-state. The olefin insertion behavior of *cis*/*trans*-P,F-(PO-OMe)PdF(lut) with VF, vinyl bromide, vinyl acetate, vinyl benzoate, and 1,4-hexadiene is described. (PO-OMe)Pd(enolate)(lut) and (PO-OMe)Pd(C_6F_5)(lut) products were isolated and characterized by X-ray crystallography from reaction of (PO-OMe)PdF(lut) with vinyl-acetate/vinyl-benzoate and B(C_6F_5)$_3$, respectively.

Chapter Six describes the synthesis of the 2-{PH(2-{2,6-(OMe)$_2$-Ph}-Ph)(2-OMe-Ph))}-

4-Me-benzenesulfonate (H[PO-Bp/Ph^{OMe}]) proligand and the corresponding (PO-Bp/Ph^{OMe})PdMeL catalysts (L = py, lut). The systematic process by which the NMR spectra for H[PO-Bp/Ph^{OMe}]) and (PO-Bp/Ph^{OMe})PdMe(lut) were assigned and how these assignments were exploited in NOESY studies to probe the solution structures are described. (PO-Bp/Ph^{OMe})PdMe(py) exists as a mixture of two isomers in solution. The solid-state of one of these isomers was determined by X-ray crystallography. The solution-behavior of (PO-Bp/Ph^{OMe})PdMe(py) is re-analyzed based on these structural studies.

1.4 References and Notes

(1) Drent, E.; van Dijk, R.; van Ginkel, R.; van Oort, B.; Pugh, R. I. *Chem. Commun.* **2002**, 744.

(2) Skupov, K. M.; Marella, P. R.; Hobbs, J. L.; McIntosh, L. H.; Goodall, B. L.; Claverie, J. P. *Macromolecules* **2006**, *39*, 4279.

(3) Skupov, K. M.; Marella, P. R.; Simard, M.; Yap, G. P. A.; Allen, N.; Conner, D.; Goodall, B. L.; Claverie, J. P. *Macromol. Rapid Commun.* **2007**, *28*, 2033.

(4) Skupov, K. M.; Piche, L.; Claverie, J. P. *Macromolecules* **2008**, *41*, 2309.

(5) Skupov, K. M.; Hobbs, J.; Marella, P.; Conner, D.; Golisz, S.; Goodall, B. L.; Claverie, J. P. *Macromolecules* **2009**, *42*, 6953.

(6) Kryuchkov, V. A.; Daigle, J.-C.; Skupov, K. M.; Claverie, J. P.; Winnik, F. M. *J. Am. Chem. Soc.* **2010**, *132*, 15573.

(7) Piche, L.; Daigle, J.-C.; Poli, R.; Claverie, J. P. *Eur. J. Inorg. Chem.* **2010**, *2010*, 4595.

(8) Daigle, J.-C.; Piche, L.; Claverie, J. P. *Macromolecules* **2011**, *44*, 1760.

(9) Daigle, J.-C.; Piche, L.; Arnold, A.; Claverie, J. P. *ACS Macro Lett.* **2012**, *1*, 343.

(10) Piche, L.; Daigle, J. C.; Rehse, G.; Claverie, J. P. *Chem. Eur. J.* **2012**, *18*, 3277.

(11) Daigle, J.-C.; Arnold, A. A.; Piche, L.; Claverie, J. P. *Polym. Chem.* **2013**, *4*, 449.

(12) Piche, L.; Daigle, J.-C.; Claverie, J. P. *Chem. Commun.* **2011**, *47*, 7836.

(13) Bashir, O.; Piche, L.; Claverie, J. P. *Organometallics* **2014**, *33*, 3695.

(14) Luo, S.; Vela, J.; Lief, G. R.; Jordan, R. F. *J. Am. Chem. Soc.* **2007**, *129*, 8946.

(15) Vela, J.; Lief, G. R.; Shen, Z.; Jordan, R. F. *Organometallics* **2007**, *26*, 6624.

(16) Weng, W.; Shen, Z.; Jordan, R. F. *J. Am. Chem. Soc.* **2007**, *129*, 15450.

(17) Shen, Z.; Jordan, R. F. *J. Am. Chem. Soc.* **2010**, *132*, 52.

(18) Shen, Z.; Jordan, R. F. *Macromolecules* **2010**, *43*, 8706.

(19) Conley, M. P.; Jordan, R. F. *Angew. Chem. Int. Ed. Engl.* **2011**, *50*, 3744.

(20) Cai, Z.; Shen, Z.; Zhou, X.; Jordan, R. F. *ACS Catal.* **2012**, *2*, 1187.

(21) Feng, G.; Conley, M. P.; Jordan, R. F. *Organometallics* **2014**, *33*, 4486.

(22) Zhou, X.; Lau, K.-C.; Petro, B. J.; Jordan, R. F. *Organometallics* **2014**, *33*, 7209.

(23) Zhou, X.; Bontemps, S.; Jordan, R. F. *Organometallics* **2008**, *27*, 4821.

(24) Lau, K.-C.; Petro, B. J.; Bontemps, S.; Jordan, R. F. *Organometallics* **2013**, *32*, 6895.

(25) Wada, S.; Jordan, R. F. *Angew. Chem. Int. Ed.* **2017**, *56*, 1820.

(26) Guironnet, D.; Rünzi, T.; Göttker-Schnetmann, I.; Mecking, S. *Chem. Commun.* **2008**, 4965.

(27) Guironnet, D.; Roesle, P.; Rünzi, T.; Göttker-Schnetmann, I.; Mecking, S. *J. Am. Chem. Soc.* **2009**, *131*, 422.

(28) Zhang, D.; Guironnet, D.; Göttker-Schnetmann, I.; Mecking, S. *Organometallics* **2009**, *28*, 4072.

(29) Bouilhac, C.; Rünzi, T.; Mecking, S. *Macromolecules* **2010**, *43*, 3589.

(30) Guironnet, D.; Caporaso, L.; Neuwald, B.; Göttker-Schnetmann, I.; Cavallo, L.; Mecking, S. *J. Am. Chem. Soc.* **2010**, *132*, 4418.

(31) Rünzi, T.; Fröhlich, D.; Mecking, S. *J. Am. Chem. Soc.* **2010**, *132*, 17690.

(32) Rünzi, T.; Guironnet, D.; Göttker-Schnetmann, I.; Mecking, S. *J. Am. Chem. Soc.* **2010**, *132*, 16623.

(33) Wucher, P.; Caporaso, L.; Roesle, P.; Ragone, F.; Cavallo, L.; Mecking, S.; Göttker-Schnetmann, I. *Proc. Natl. Acad. Sci. USA* **2011**, *108*, 8955.

(34) Friedberger, T.; Wucher, P.; Mecking, S. *J. Am. Chem. Soc.* **2012**, *134*, 1010.

(35) Neuwald, B.; Ölscher, F.; Göttker-Schnetmann, I.; Mecking, S. *Organometallics* **2012**, *31*, 3128.

(36) Rünzi, T.; Tritschler, U.; Roesle, P.; Göttker-Schnetmann, I.; Möller, H. M.; Caporaso, L.; Poater, A.; Cavallo, L.; Mecking, S. *Organometallics* **2012**, *31*, 8388.

(37) Wucher, P.; Goldbach, V.; Mecking, S. *Organometallics* **2013**, *32*, 4516.

(38) Leicht, H.; Göttker-Schnetmann, I.; Mecking, S. *Angew. Chem. Int. Ed.* **2013**, *52*, 3963.

(39) Neuwald, B.; Caporaso, L.; Cavallo, L.; Mecking, S. *J. Am. Chem. Soc.* **2013**, *135*, 1026.

(40) Neuwald, B.; Falivene, L.; Caporaso, L.; Cavallo, L.; Mecking, S. *Chem. Eur. J.* **2013**, *19*, 17773.

(41) Wucher, P.; Schwaderer, J. B.; Mecking, S. *ACS Catal.* **2014**, *4*, 2672.

(42) Jian, Z.; Wucher, P.; Mecking, S. *Organometallics* **2014**, *33*, 2879.

(43) Jian, Z.; Mecking, S. *Angew. Chem. Int. Ed. Engl.* **2015**, *54*, 15845.

(44) Jian, Z.; Mecking, S. *Angew. Chem. Int. Ed. Engl.* **2015**, *127*, 16071.

(45) Jian, Z.; Baier, M. C.; Mecking, S. *J. Am. Chem. Soc.* **2015**, *137*, 2836.

(46) Leicht, H.; Göttker-Schnetmann, I.; Mecking, S. *J. Am. Chem. Soc.* **2017**, *139*, 6823.

(47) Schuster, N.; Rünzi, T.; Mecking, S. *Macromolecules* **2016**, *49*, 1172.

(48) Jian, Z.; Leicht, H.; Mecking, S. *Macromol. Rapid Commun.* **2016**, *37*, 934.

(49) Jian, Z.; Mecking, S. *Macromolecules* **2016**, *49*, 4057.

(50) Jian, Z.; Mecking, S. *Macromolecules* **2016**, *49*, 4395.

(51) Schuster, N.; Krumova, M.; Richter, F.; Schneller, A.; Mecking, S. *Macromol. Mater. Eng.*

2018, *303*, 1700276.

(52) Kochi, T.; Yoshimura, K.; Nozaki, K. *Dalton Trans.* **2006**, 25.

(53) Kochi, T.; Noda, S.; Yoshimura, K.; Nozaki, K. *J. Am. Chem. Soc.* **2007**, *129*, 8948.

(54) Kochi, T.; Nakamura, A.; Ida, H.; Nozaki, K. *J. Am. Chem. Soc.* **2007**, *129*, 7770.

(55) Nakamura, A.; Munakata, K.; Kochi, T.; Nozaki, K. *J. Am. Chem. Soc.* **2008**, *130*, 8128.

(56) Noda, S.; Nakamura, A.; Kochi, T.; Chung, L. W.; Morokuma, K.; Nozaki, K. *J. Am. Chem. Soc.* **2009**, *131*, 14088.

(57) Ito, S.; Munakata, K.; Nakamura, A.; Nozaki, K. *J. Am. Chem. Soc.* **2009**, *131*, 14606.

(58) Noda, S.; Kochi, T.; Nozaki, K. *Organometallics* **2009**, *28*, 656.

(59) Nozaki, K.; Kusumoto, S.; Noda, S.; Kochi, T.; Chung, L. W.; Morokuma, K. *J. Am. Chem. Soc.* **2010**, *132*, 16030.

(60) Ito, S.; Kanazawa, M.; Munakata, K.; Kuroda, J.; Okumura, Y.; Nozaki, K. *J. Am. Chem. Soc.* **2011**, *133*, 1232.

(61) Nakamura, A.; Munakata, K.; Ito, S.; Kochi, T.; Chung, L. W.; Morokuma, K.; Nozaki, K. *J. Am. Chem. Soc.* **2011**, *133*, 6761.

(62) Kageyama, T.; Ito, S.; Nozaki, K. *Chem. Asian. J.* **2011**, *6*, 690.

(63) Kanazawa, M.; Ito, S.; Nozaki, K. *Organometallics* **2011**, *30*, 6049.

(64) Ito, S.; Ota, Y.; Nozaki, K. *Dalton Trans.* **2012**, *41*, 13807.

(65) Nakamura, A.; Kageyama, T.; Goto, H.; Carrow, B. P.; Ito, S.; Nozaki, K. *J. Am. Chem. Soc.* **2012**, *134*, 12366.

(66) Ota, Y.; Ito, S.; Kuroda, J.; Okumura, Y.; Nozaki, K. *J. Am. Chem. Soc.* **2014**, *136*, 11898.

(67) Ota, Y.; Ito, S.; Kobayashi, M.; Kitade, S.; Sakata, K.; Tayano, T.; Nozaki, K. *Angew. Chem. Int. Ed. Engl.* **2016**, *55*, 7505.

(68) Nowack, R. J.; Hearley, A. K.; Rieger, B. *Z. anorg. allg. Chem.* **2005**, *631*, 2775.

(69) Hearley, A. K.; Nowack, R. J.; Rieger, B. *Organometallics* **2005**, *24*, 2755.

(70) Anselment, T. M. J.; Wichmann, C.; Anderson, C. E.; Herdtweck, E.; Rieger, B. *Organometallics* **2011**, *30*, 6602.

(71) Anselment, T. M. J.; Anderson, C. E.; Rieger, B.; Boeddinghaus, M. B.; Fässler, T. F. *Dalton Trans.* **2011**, *40*, 8304.

(72) Lanzinger, D.; Giuman, M. M.; Anselment, T. M. J.; Rieger, B. *ACS Macro Lett.* **2014**, *3*, 931.

(73) Newsham, D. K.; Borkar, S.; Sen, A.; Conner, D. M.; Goodall, B. L. *Organometallics* **2007**, *26*, 3636.

(74) Liu, S.; Borkar, S.; Newsham, D.; Yennawar, H.; Sen, A. *Organometallics* **2007**, *26*, 210.

(75) Borkar, S.; Newsham, D. K.; Sen, A. *Organometallics* **2008**, *27*, 3331.

(76) Luo, R.; Newsham, D. K.; Sen, A. *Organometallics* **2009**, *28*, 6994.

(77) Chen, M.; Yang, B.; Chen, C. *Angew. Chem. Int. Ed.* **2015**, *54*, 15520.

(78) Wu, Z.; Chen, M.; Chen, C. *Organometallics* **2016**, *35*, 1472.

(79) Chen, M.; Yang, B.; Chen, C. *Synlett* **2016**, *27*, 1297.

(80) Chen, M.; Chen, C. *ACS Catal.* **2017**, *7*, 1308.

(81) Song, G.; Pang, W.; Li, W.; Chen, M.; Chen, C. *Polym. Chem.* **2017**, *8*, 7400.

(82) Liang, T.; Chen, C. *Organometallics* **2017**, *36*, 2338.

(83) Wu, Z.; Hong, C.; Hongxu Du; Pang, W.; Chen, C. *Polymers* **2017**, *9*, 168.

(84) Yang, B.; Xiong, S.; Chen, C. *Polym. Chem.* **2017**, *8*, 6272.

(85) Haras, A.; Anderson, G. D. W.; Michalak, A.; Rieger, B.; Ziegler, T. *Organometallics* **2006**, *25*, 4491.

(86) Haras, A.; Michalak, A.; Rieger, B.; Ziegler, T. *Organometallics* **2006**, *25*, 946.

(87) Chen, C.; Anselment, T. M. J.; Fröhlich, R.; Rieger, B.; Kehr, G.; Erker, G. *Organometallics* **2011**, *30*, 5248.

(88) Ravasio, A.; Boggioni, L.; Tritto, I. *Macromolecules* **2011**, *44*, 4180.

(89) Perrotin, P.; McCahill, J. S. J.; Wu, G.; Scott, S. L. *Chem. Commun.* **2011**, *47*, 6948.

(90) Friedberger, T.; Ziller, J. W.; Guan, Z. *Organometallics* **2014**, *33*, 1913.

(91) Rezabal, E.; Ugalde, J. M.; Frenking, G. *J. Phys. Chem. A* **2017**, *121*, 7709.

(92) Nakamura, A.; Ito, S.; Nozaki, K. *Chem. Rev.* **2009**, *109*, 5215.

(93) Nakamura, A.; Anselment, T. M. J.; Claverie, J.; Goodall, B.; Jordan, R. F.; Mecking, S.; Rieger, B.; Sen, A.; van Leeuwen, P. W. N. M.; Nozaki, K. *Acc. Chem. Res.* **2013**, *46*, 1438.

(94) Ito, S.; Nozaki, K. *Chem. Rec.* **2010**, *10*, 315.

(95) Berkefeld, A.; Mecking, S. *Angew. Chem. Int. Ed. Engl.* **2008**, *47*, 2538.

(96) Yasuda, H.; Nakano, R.; Ito, S.; Nozaki, K. *J. Am. Chem. Soc.* **2018**, *140*, 1876.

(97) Mitsushige, Y.; Yasuda, H.; Carrow, B. P.; Ito, S.; Kobayashi, M.; Tayano, T.; Watanabe, Y.; Okuno, Y.; Hayashi, S.; Kuroda, J.; Okumura, Y.; Nozaki, K. *ACS Macro Lett.* **2018**, *7*, 305.

(98) Rünzi, T.; Baier, M. C.; Negele, C.; Krumova, M.; Mecking, S. *Macromol. Rapid Commun.* **2015**, *36*, 165.

(99) Drent, E.; van Dijk, R.; van Ginkel, R.; van Oort, B.; Pugh, R. I. Ch*em. Commun.* ***2*****002,** 964.

(100) Bettucci, L.; Bianchini, C.; Claver, C.; Suarez, E. J. G.; Ruiz, A.; Meli, A.; Oberhauser, W.

Dalton Trans. **2007**, 5590.

(101) Zhou, X.; Jordan, R. F. *Organometallics* **2011**, *30*, 4632.

(102) Ittel, S. D.; Johnson, L. K.; Brookhart, M. *Chem. Rev.* **2000**, *100*, 1169.

(103) Britovsek, George J. P.; Gibson, V. C.; Wass, D. F. *Angew. Chem. Int. Ed.* **1999**, 428.

(104) Gibson, V. C.; Spitzmesser, S. K. *Chem. Rev.* **2003**, *103*, 283.

(105) Jover, J.; Fey, N.; Harvey, J. N.; Lloyd-Jones, G. C.; Orpen, A. G.; Owen-Smith, G. J. J.; Murray, P.; Hose, D. R. J.; Osborne, R.; Purdie, M. *Organometallics* **2010**, *29*, 6245.

(106) Stephenson, C. J.; McInnis, J. P.; Chen, C.; Weberski, M. P.; Motta, A.; Delferro, M.; Marks, T. J. *ACS Catal.* **2014**, *4*, 999.

(107) García Suárez, E. J.; Ruiz, A.; Castillón, S.; Oberhauser, W.; Bianchini, C.; Claver, C. *Dalton Trans.* **2007**, 2859.

(108) Defoe, J., J. Doctoral dissertation, The University of Chicago, **2011**.

Chapter Two

Synthesis and Characterization of Palladium(II) Alkyl Complexes that Contain Phosphine-cyclopentanesulfonate Ligands

2.1 Introduction

As described in Chapter One, Pd(II) alkyl complexes that contain *ortho*-phosphine-arenesulfonate (PO^-) ligands (**A**, Chart 1) polymerize ethylene to linear polyethylene (PE) and copolymerize ethylene with a wide variety of polar vinyl monomers to functionalized linear PEs.[1–19] While the ability to incorporate diverse comonomers is an advantage of the (PO)PdR system, ethylene polymerization activities and PE molecular weights (MWs) are generally low for these catalysts compared to what is observed for other single-site catalysts,[20,21] and the polar monomers further reduce activities and MWs.

Many electronic and steric modifications of the $–PR_2$ unit of (PO)PdRL catalysts **A** have been explored in efforts to improve the performance of these catalysts.[14,17,22–24] Mecking and co-workers investigated the ethylene polymerization properties of diarylphosphine-benzenesulfonate catalysts (**B**, L = dmso, Chart 2.1), in which the *para*-R substituent was varied to probe electronic effects.[24] Catalysts with electron-donating substituents produced PE with higher MW but exhibited somewhat lower activity (R = OMe: M_n = 17000, Activity = 2128 kg mol^{-1} h^{-1}) compared to catalysts with electron-withdrawing substituents (R = CF_3: M_n = 8000, Activity = 2632 kg mol^{-1} h^{-1}). Nozaki and co-workers examined the polymerization behavior of type-**A** catalysts that

incorporate –P(alkyl)$_2$ units of varying size to probe steric effects.[14] Catalysts with more sterically-demanding –PR$_2$ units produced PE with higher MW than those with smaller phosphines, likely due to steric blockage of the axial positions of the square-planar metal center (R = ^{i}Pr: M_n = 6700; R = menthyl: M_n = 169000). Catalyst activity generally increased with increasing steric bulk of the –PR$_2$ unit (R = ^{t}Bu: 1860 kg mol^{-1} h^{-1}), but decreased when the phosphine substituents became too bulky (R = menthyl: 205 kg mol^{-1} h^{-1}). Claverie and co-workers compared the ethylene polymerization performance of type-**A** complexes with a range of –PAr$_2$, –P(alkyl)$_2$ and –PAr(alkyl) units (L = pyridine or lutidine, Chart 2.1).[22] While no clear relationship between the size of the –PR$_2$ unit and the MW of the PE emerged, a strong positive correlation between the phosphine donor ability, as assessed by the BE(B) descriptor within the ligand knowledge base for monodentate P donors (LKB-P),[25] and catalyst activity was observed.

Chart 2.1. (PO)PdR complexes

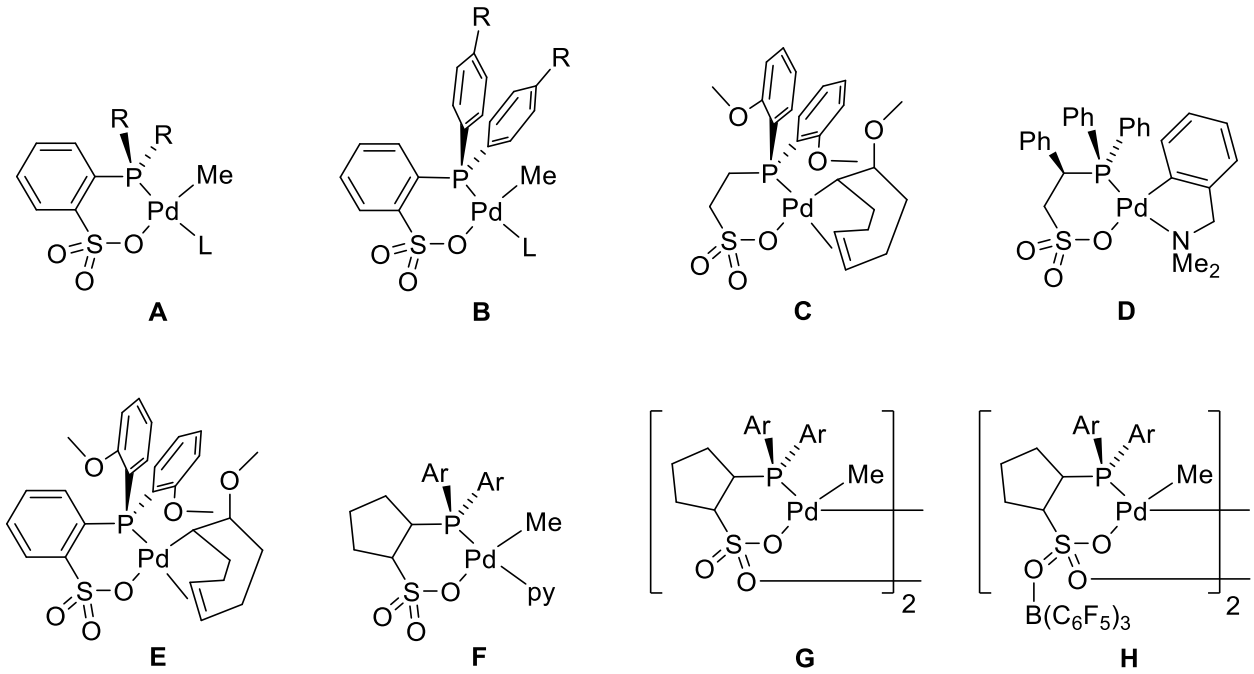

Mecking and co-workers analyzed the performance of type-**A** complexes with a range of –PAr_2 units in ethylene/methyl acrylate (MA) copolymerization.[17] Catalysts with more strongly electron-donating phosphines were less active but did not deactivate as quickly as catalysts with less electron-donating phosphines, and sterically-crowded catalysts produced copolymers with higher MW than sterically-open catalysts. Claverie and coworkers noted that while type-**A** catalysts with $–PR_2$ = – $P(^tBu)_2$ or –PPh^tBu are both very active for ethylene homopolymerization, the latter incorporates MA much more effectively than the former.[22] This difference was ascribed to steric effects.

The marked dependence of the behavior of (PR_2- arenesulfonate)PdR catalysts on the structure of the PR_2 unit suggests that replacement of the arene linker in type-**A** catalysts with an

alkane linker may also strongly influence catalyst performance.[26] However, to date, only a few phosphine-*alkane*sulfonate ligands[27,28] and Pd^{II} alkyl complexes thereof (**C**[29] and **D**[30], Chart 2.1) have been reported. The (PAr_2-$CH_2CH_2SO_3$)PdR complex **C** oligomerizes ethylene to butenes and hexenes, but rapidly degrades to catalytically inactive species.[31] Compound **C** also catalyzes the non-alternating copolymerization of ethylene and CO, but is less active and produces polyketones with lower MW and fewer non-alternating ethylene units compared to the benzene-linked analogue **E**.[29,31] The reactivity of **D** has not been reported.[30]

The low stability of the presumed active {P(2-OMe-Ph)$_2$CH$_2$CH$_2$SO$_3$}PdR species derived from **C** is likely due to the high skeletal flexibility that results from facile rotation around the PC–CS bond. As shown in Scheme 2.1, dissociation of the sulfonate ligand and rotation around the PC–CS bond would generate κ^1-PO species **I**, which is expected to decompose to Pd^0. In contrast, if sulfonate decoordination occurs in the arene-linker case, recoordination is favored because rotation around the PC–CS bond is not possible. Rotation around the C(Ar^{SO3})–P bond could lead to κ^1-species **J**, but is likely to have a barrier of 10–15 kcal/mol,[18,32] so sulfonate recoordination is favored.[33,34] To date, de-coordination of the sulfonate oxygen in a (diarylphosphine-arenesulfonate)Pd species has only been observed in the presence of an excess of strong Lewis base. For example, the reaction of [{2-P(2-OMe-Ph)$_2$-benzenesulfonate}Pd(py)$_2$][SbF_6] and pyridine generates [{κ^1-*P*-2-P(2-OMe-Ph)$_2$-benzenesulfonate}Pd(py)$_3$][SbF_6], but this reaction is reversible.[35] Even coordination of the strong Lewis acid B(C_6F_5)$_3$ to the sulfonate group does not cleave the Pd–sulfonate bond.[36]

Scheme 2.1. Proposed decomposition pathways

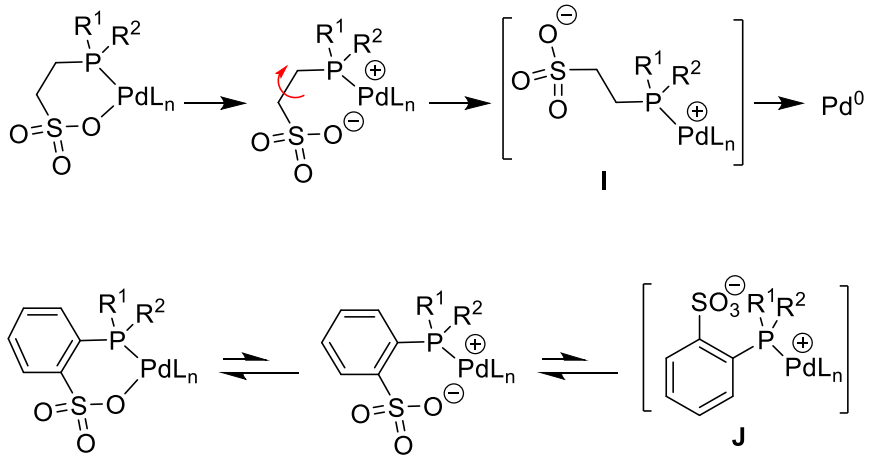

One potential strategy for stabilizing (diarylphosphine-*alkane*sulfonate)PdRL compounds is to incorporate a cyclic alkane linker to preclude PC–CS bond rotation. Here, we report the synthesis of two 2-diarylphosphine-*cyclopentane*sulfonate ligands (C5-PO$^-$), and the corresponding Pd(II) complexes (C5-PO)PdMe(py) (**F**), {(C5-PO)PdMe}$_2$ (**G**) and {(C5-PO•B(C_6F_5)$_3$)PdMe}$_2$ (**H**, Chart 2.1). We also describe the behavior of these complexes in ethylene polymerization and ethylene copolymerization with methyl acrylate (MA) and vinyl fluoride (VF).

2.2 Results and Discussion

Diarylphosphine-cyclopentanesulfonate Ligands (C5-PO$^-$). Salts of 2-diarylphosphine-cyclopentanesulfonate ligands that contain –PPh_2 (Li/K[**2a**]) or –P(2-OMe-Ph)$_2$ (Li/K[**2b**]) units were synthesized according to Scheme 2.2. K[*trans*-2-Br- cylopentanesulfonate] **(**K[**1**]) was prepared by nucleophilic opening of cyclopentane-β-sultone[37] by [NBu_4]Br followed by aqueous salt exchange with K[PF_6]. The *trans* orientation of K[**1**] was established by quantitative ^{1}H–^{1}H NOESY experiments and an X-ray diffraction analysis of [K(18-crown-6)][**1**] (Figure 2.1). The reaction of K[**1**] with the appropriate lithium phosphide[38–41] gave *trans*-Li/K[**2a**] and *trans*-Li/K[**2b**]. The amount of Li^+ and K^+ in Li/K[**2a**] was quantified by ICP-MS.

Scheme 2.2. PAr_2-cyclopentanesulfonate ligand synthesis

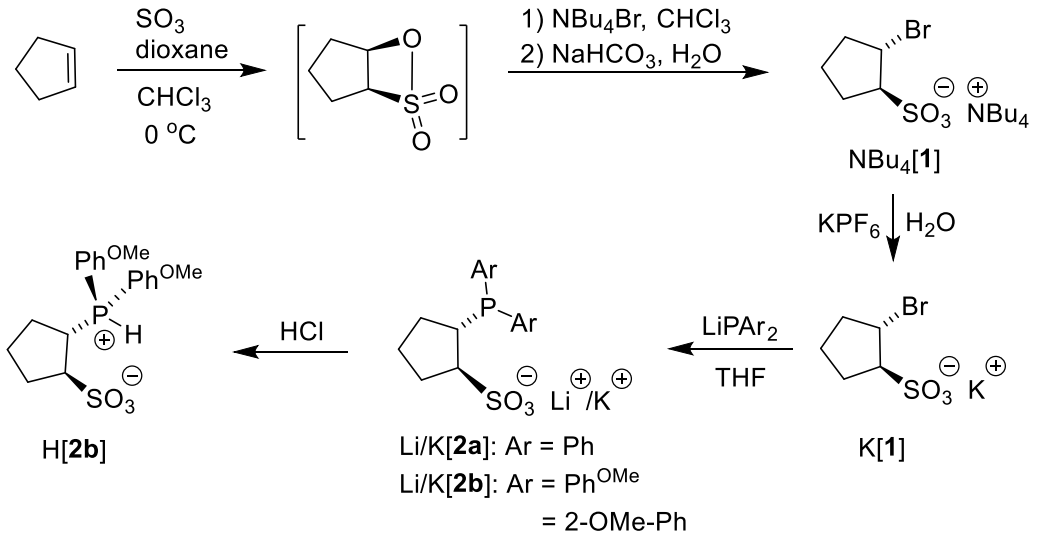

Figure 2.1. Molecular structure of [K(18-crown-6)][**1**]. The H atoms on the 18-crown-6 unit are omitted. Selected bond lengths (Å): Br1–C1 1.972(4), S1–C5 1.820(4), S1–O1 1.444(3), S1–O2 1.446(3), S1–O3 1.447(3), K1–O2 2.782(3), K1–O3 2.902(3).

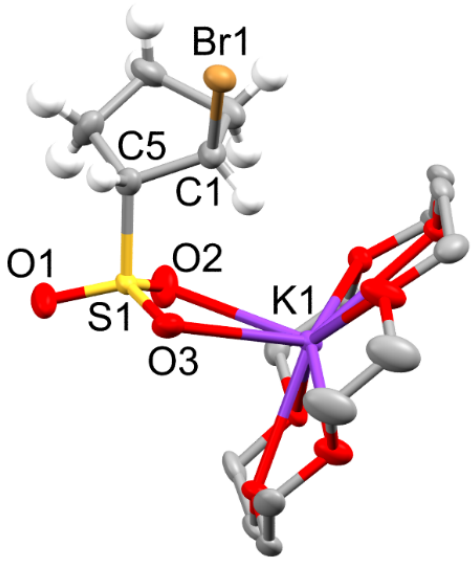

The retention of stereochemistry in these substitution reactions likely results from anchimeric assistance by the neighboring sulfonate group.[42] Li/K[**2b**] was converted to the phosphonium sulfonate zwitterion H[**2b**] by reaction with excess HCl. The ^{31}P NMR spectrum of H[**2b**] comprises a doublet at δ 9.9 with a large $^{1}J_{PH}$ value (446 Hz), which confirms that H[**2b**] exists as a zwitterion.

In order to develop more PR_2-cyclopentanesulfonate ligands that are more electron-rich than H[**2b**], similar routes for the synthesis of ligands bearing –P^{i}Pr$_2$ (Scheme 2.3), –P(menthyl)$_2$ (Scheme 2.4), and –P(2',6'-dimethoxybiphenyl)$_2$ (Scheme 2.5) units were explored. As shown in Scheme 2.3, the reaction of K[**1**] with LiP^{i}Pr$_2$ in hexane/THF solution gave *trans*-Li/K[P^{i}Pr$_2$-cyclopentanesulfonate], which was identified by ESI-MS and 2D-NMR. However, attempts to

purify this salt and convert it to the corresponding H[PO] zwitterion, (phosphine oxide)-sulfonate, and (phosphine borane)-sulfonate derivatives were unsuccessful. Attempts to metalate impure samples Li/K[P^{i}Pr$_2$-cyclopentanesulfonate] and H[P^{i}Pr$_2$-cyclopentanesulfonate] did not yield isolable metal complexes. Similarly, attempts to prepare dimenthylphoshine, the precursor to Li[P(Men)$_2$], were unsuccessful. As shown in Scheme 2.4, the attempted reduction of dimenthyl phosphine oxide yielded tetramenthyldiphosphine as the major product rather than dimenthylphoshine. Finally, di(biphenyl)phosphine was successfully prepared as shown in Scheme 2.5, by reduction of HP(=O)Bp$_2$ (solid-state structure shown in Figure 2.2). HPBp$_2$ was cleanly deprotonated by ^{n}BuLi in hexanes but LiPBp$_2$ did not react with Li/K[**1**] in this solvent. LiPBp$_2$ was also generated in THF, ether, and dioxane, but decomposes to the Bp$_2$PPBp$_2$ diphosphine as the major product in these solvents.

Scheme 2.3. Synthetic route to P^{i}Pr$_2$-cyclopentanesulfonate

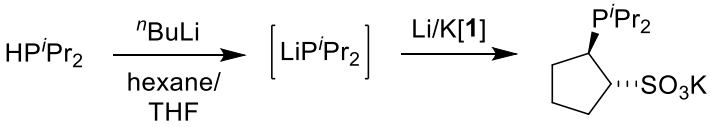

Scheme 2.4. Synthetic route toward dimenthylphosphine

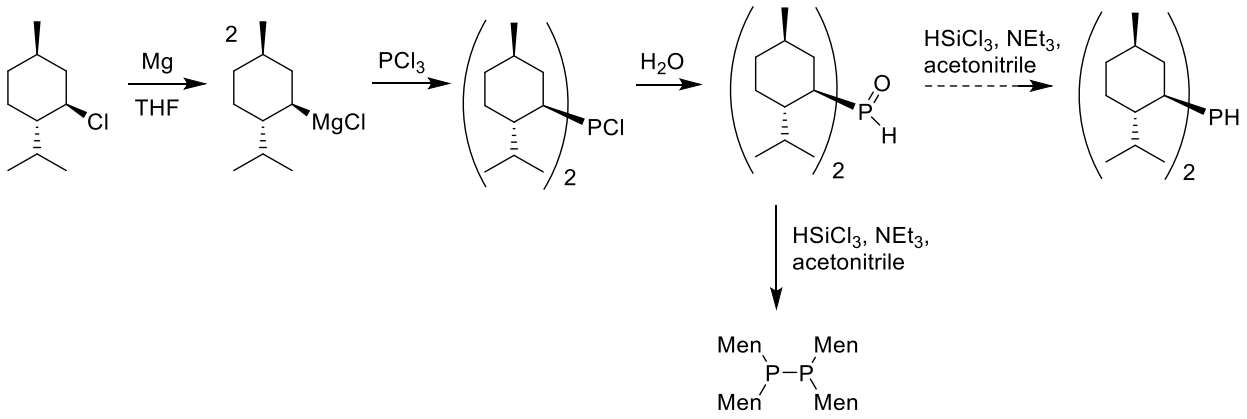

Scheme 2.5. Synthetic route toward di(biphenyl)phosphine

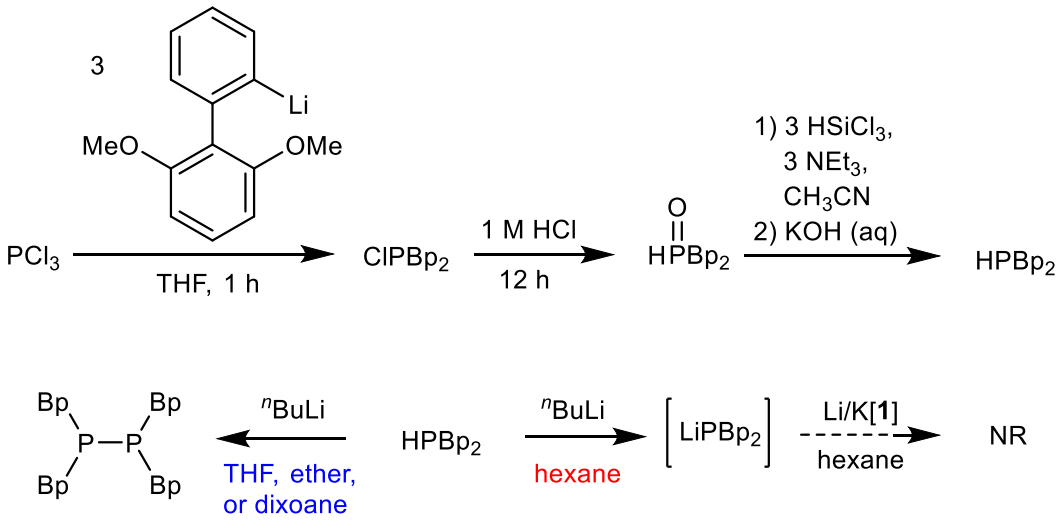

Figure 2.2. Molecular structure of HP(=O)Bp_2. The hydrogen atoms are omitted, except for the P–H hydrogen atom.

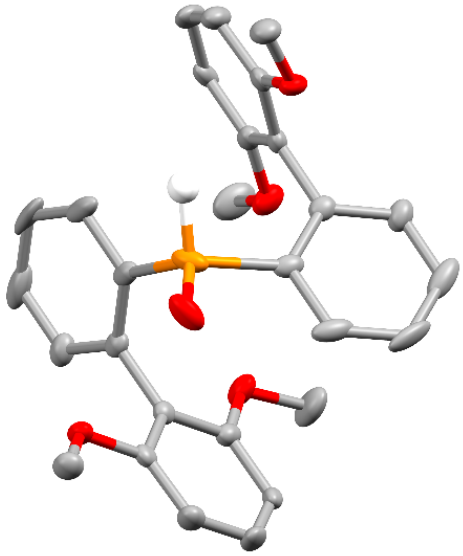

(C5-PO)PdMe(py) Complexes. The reaction of Li/K[**2a**] with (COD)PdMeCl, followed by addition of pyridine affords (**2a**)PdMe(py) (**3a**) in 85% yield (Eq. 2.1). The analogous reaction with Li/K[**2b**] gave a mixture of products, from which {[Li(THF)][(**2b**)PdMeCl]}$_2$ was isolated in low yield (Eq. 2.2). The reaction of H[**2b**] with (TMEDA)$PdMe_2$ followed by addition of pyridine affords (**2b**)PdMe(py) (**3b**) in 91% yield (Eq. 2.3).

Eq. 2.1

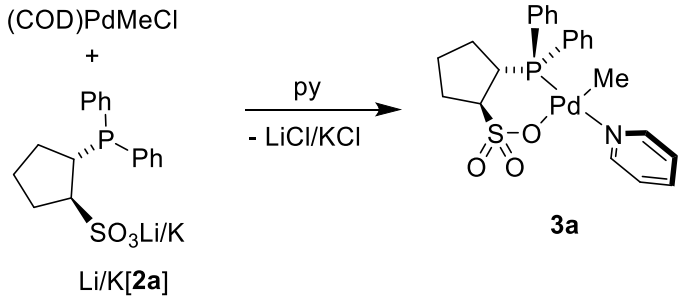

Eq. 2.2

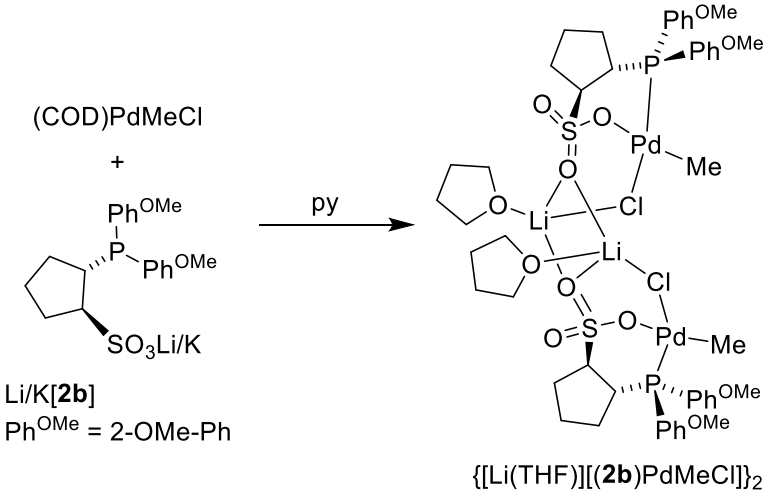

Eq. 2.3

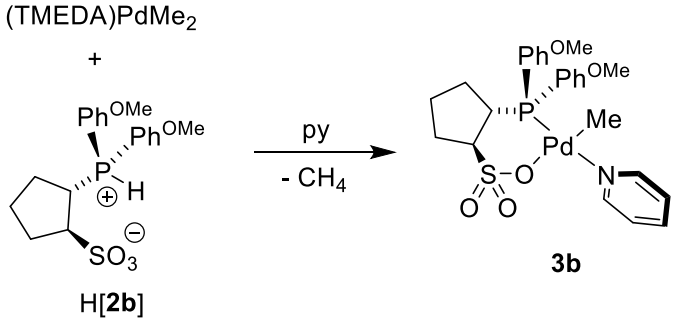

Compound **3a** decomposes thermally within 1 h at 40 °C in chlorobenzene-d_5 to Pd^0 and unidentified ligand-derived species. In contrast, **3b** is thermally stable in chlorobenzene-d_5 and toluene-d_8 at 80 °C for at least 20 h.

Solid-state Structures of 3a and 3b. The solid-state structures of **3a** and **3b** are shown in Figure 2.3 and Figure 2.4 and are very similar to those of the analogous *benzo*-linked complexes (2-PPh_2-benzenesulfonate)PdMe(py) (**3c**)[23] and (2-P(2-OMe-Ph)$_2$-benzenesulfonate)PdMe(py)

(**3d**)[43] (Chart 2.2). Each complex features square-planar geometry at Pd, a six-membered phosphine-sulfonate)Pd chelate ring and a *cis* arrangement of the phosphine and methyl ligands. The Pd–ligand bond distances and the O–Pd–P angles of **3a** and **3b** are nearly identical to those in **3c** and **3d**, respectively (Table 2.1).[44] The conformations of the *o*-anisolyl rings in **3b** and **3d** are also similar. In each structure, the –OMe substituent of one *o*-anisolyl ring is directed toward Pd (*exo*) and the –OMe substituent of the other *o*-anisolyl ring is directed away from Pd (*endo*).[18,32,45,46] The *ortho*-H on the *endo* ring (H13 in Figure 2.4) and the methoxy group on the *exo* ring (O4 in Figure 2.4) of **3b** are directed toward Pd, but the Pd···H13 (2.799 Å) and Pd···O4 (3.438 Å) distances are close to or greater than the sums of the relevant van der Waals radii (Pd, H: 2.83 Å; Pd, O: 3.18 Å).

Figure 2.3. Molecular structure of **3a**. Hydrogen atoms are omitted. Bond lengths (Å) and angles (deg): Pd1–C1 2.020(3), Pd1–N1 2.122(2), Pd1–O1 2.1816(18), Pd1–P1 2.2308(7), C1–Pd1–N1 88.65(10), N1–Pd1–O1 88.64(8), C1–Pd1–P1 89.82(9), O1–Pd1–P1 93.04(5).

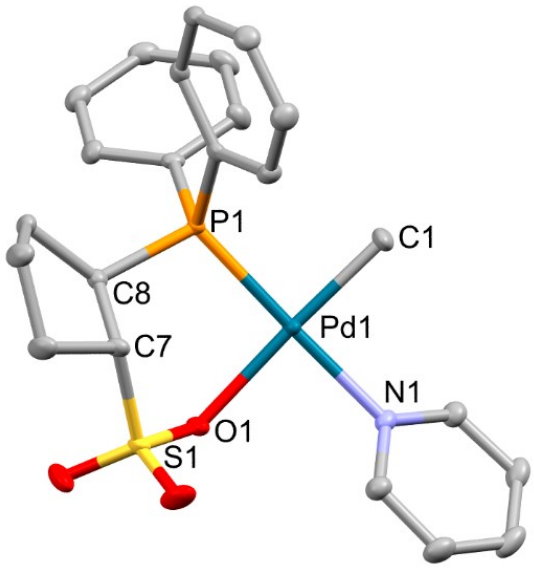

Figure 2.4. Molecular structure of **3b**•CH_2Cl_2. Hydrogen atoms except H13 and a CH_2Cl_2 solvent molecule are omitted. Bond lengths (Å) and angles (deg): Pd1–C1 2.019(3), Pd1–N1 2.106(2), Pd1–O1 2.195(2), Pd1–P1 2.2324(7), C1–Pd1–N1 91.04(11), N1–Pd1–O1 88.91(8), C1–Pd1–P1 89.96(9), O1–Pd1–P1 90.25(6).

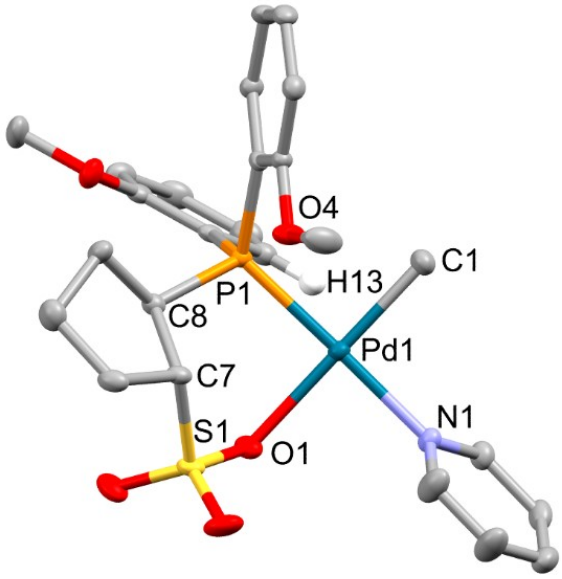

Chart 2.2. (PAr$_2$-arenesulfonate)PdRL complexes

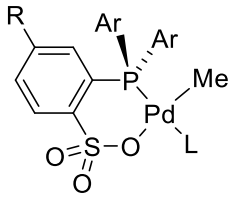

3c, R = H, Ar = Ph, L = py
3d, R = H, Ar = Ph^{OMe}, L = py
3e, R = Me, Ar = Ph^{OMe}, L = py
3f, R = Me, Ar = Ph^{OMe}, L = dmso
3g, R = Me, Ar =3,5-$^{t}Bu_2$-Ph, L = py

Table 2.1. Comparison of bond lengths (Å) and angles (degrees) in **3a-d**

Parameter	**3a**	**3c**	**3b**	**3d**
Pd1– P1	2.2307(8)	2.224(3)	2.2324(7)	2.232(1)
Pd1– O1	2.182(2)	2.151(7)	2.195(2)	2.165(3)
Pd1– N1	2.123(2)	2.114(9)	2.106(2)	2.108(4)
Pd1– C1	2.020(3)	2.03(1)	2.019(3)	2.028(5)
P1– Pd1– C1	89.80(9)	89.8(3)	89.96(9)	90.0(1)
C1–Pd1–N1	88.7(1)	89.2(4)	91.04(11)	90.8(2)
N1– Pd1– O1	88.64(8)	86.4(3)	88.91(8)	84.9(1)
O1– Pd1– P1	93.04(6)	94.8(2)	90.25(6)	94.63(9)
Angle between py plane and Pd square plane	44.40	76.89	70.20	67.37
Angle between O–S–C–C and O–Pd–P planes	63.45	30.91	68.78	27.16

The major difference between **3a**,**b** and their *arene*sulfonate analogues **3c**,**d** is that the (PO)Pd chelate rings in **3a**,**b** are more strongly puckered than those in **3c**,**d**, as illustrated in Figure 2.5. One measure of chelate ring puckering is the angle between the O–S–C–C and O–Pd–P planes, which is much larger in **3a** and **3b** (63°, 69°) than in **3c** and **3d** (31°, 27°), as illustrated in Figure 2.6.[47]

Figure 2.5. Views of **3a** (top left), **3c** (top right), **3b** (bottom left), and **3d**[43] (bottom right) highlighting the puckering of the (PO)Pd chelate rings.

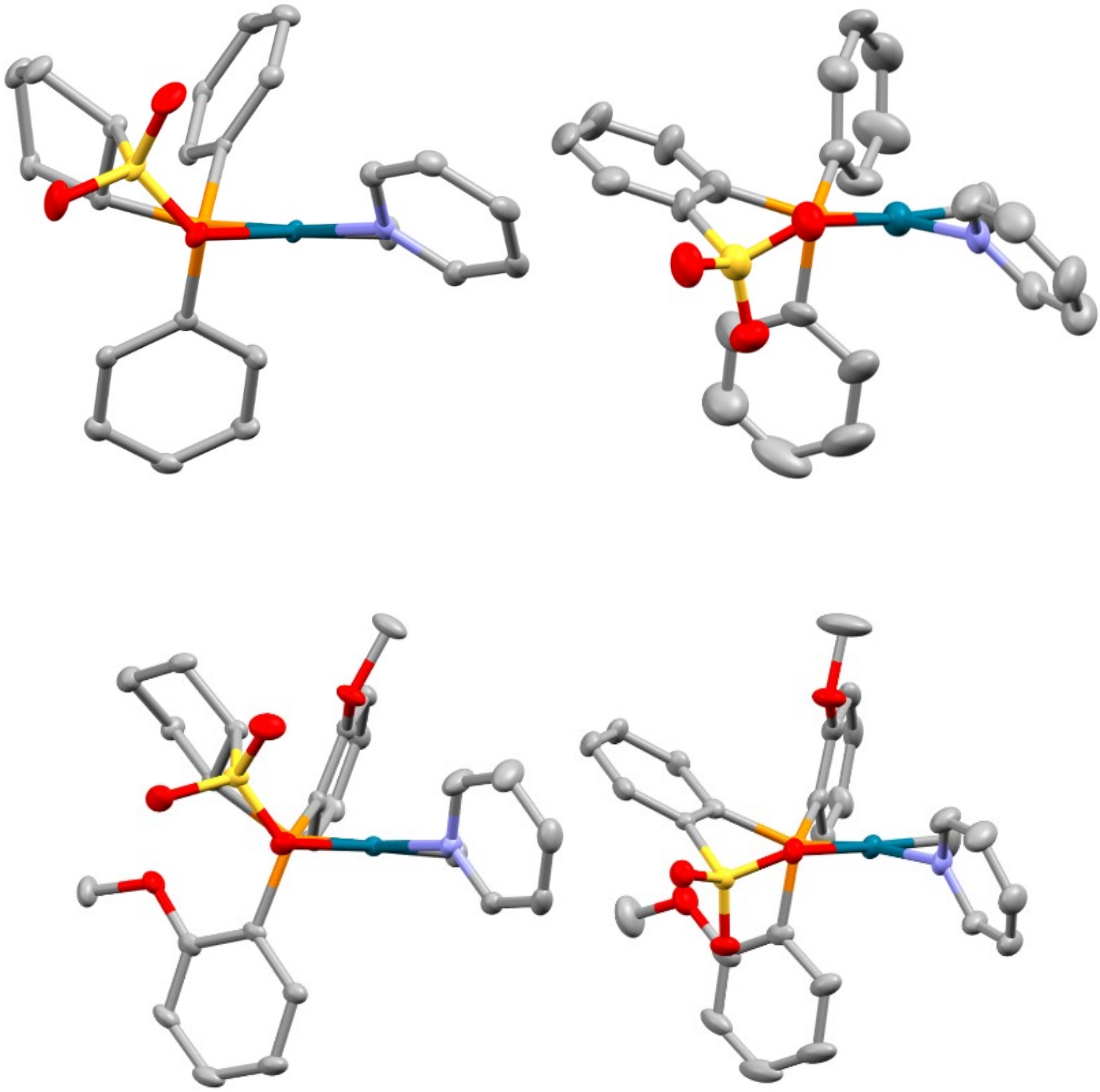

Figure 2.6. Visualization of the O-S-C-C plane (blue) and Pd square-plane (red) in **3a** (top left), **3c**[23] (top right), **3b** (bottom left), and **3d**[43] (bottom right).

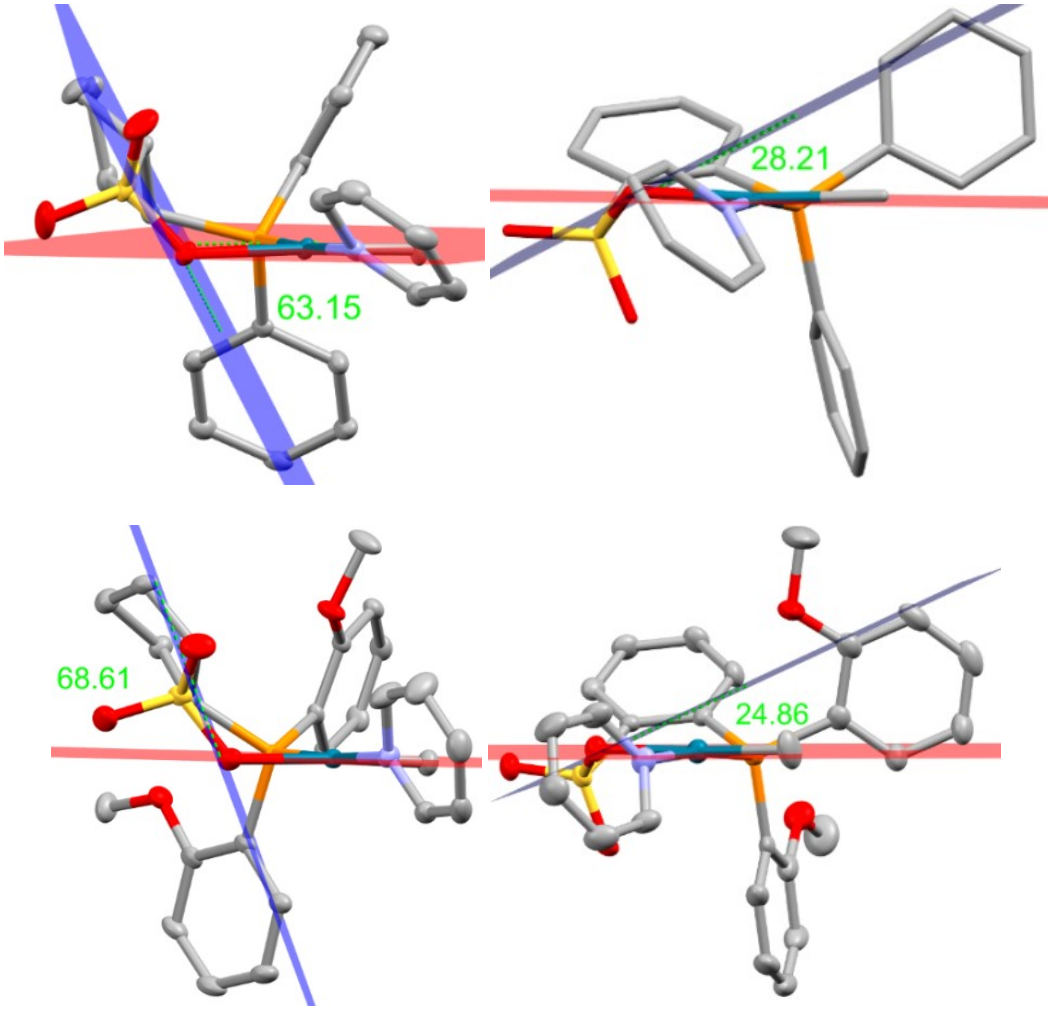

Solution Structure of 3b. Room temperature NMR data show that the solution structure of **3b** contains one *exo* and one *endo o*-anisolyl ring as observed in the solid-state. The ^{1}H NMR spectrum of **3b** contains a low-field resonance (δ 8.5) that integrates to 1H, which is characteristic of an *ortho* hydrogen of a P-*aryl* ring that is positioned in the axial, deshielding region of the Pd square plane.[32,48–53] This resonance is assigned to H13 in reference to the numbering scheme in Figure 3. The ^{1}H–^{1}H NOESY spectrum contains correlations between H13 and the *ortho* hydrogens of the pyridine ligand and the Pd-C*H*$_3$ hydrogens, confirming that H13 is directed toward Pd. The *ortho* hydrogen resonance of the other *o*-anisolyl ring appears in the normal range (δ 7.2) and does not have NOESY correlations to the Pd–C*H*$_3$ or pyridine resonances, indicating that it is directed away from Pd.

Structure of {[Li(THF)][(2b)PdMeCl]}$_2$. In the solid-state, {[Li(THF)][(**2b**)PdMeCl]}$_2$ adopts a C_2-symmetric structure in which two (**2b**)PdMeCl$^-$ anions are linked by two Li(THF)$^+$ cations (Figure 2.7). Each Li(THF)$^+$ cation binds one S=*O* atom of each [(**2b**)PdMeCl]$^-$ unit and one Pd-*Cl* atom to form a 4-membered Li_2O_2 ring and two 6-membered Li-Cl-Pd-O-S-O rings. Several other solvated Li^+/Na^+-linked dinuclear (PO)Pd(II) complexes are known, and their structures vary depending on the PO$^-$ ligand, alkali metal cation, solvent, and crystallization conditions.[15,24,54–57]

Figure 2.7. Molecular structure of {[Li(THF)][(**2b**)PdMeCl]}$_2$. Hydrogen atoms are omitted. Selected bond lengths (Å) and angles (deg): Pd1–C1 2.012(2), Pd1–Cl1 2.3898(8), Pd1–O1 2.246(2), Pd1–P1 2.2238(8), Cl1–Li1 2.334(3), O2–Li1 2.094(4), O2–Li1* 1.927(3), C1–Pd1–Cl1 93.09(7), Cl1–Pd1–O1 89.78(5), C1–Pd1–P1 89.17(7), O1–Pd1–P1 88.01(5).

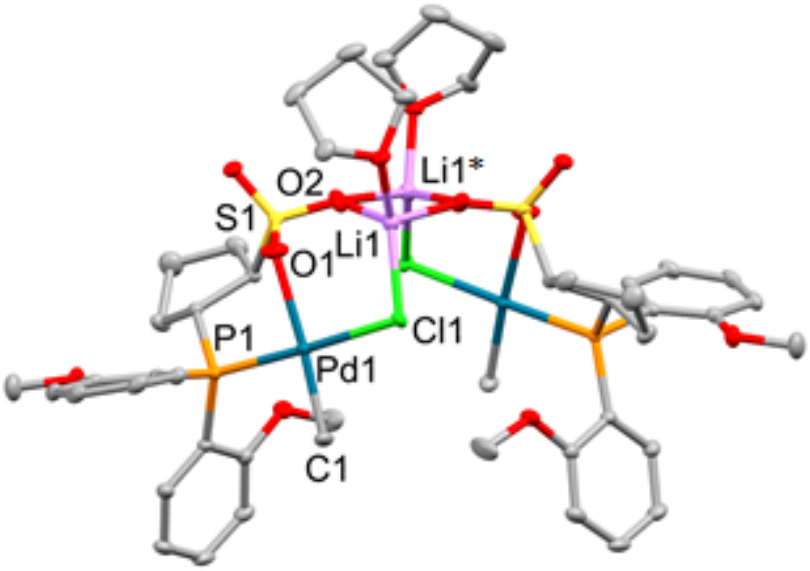

Abstraction of Pyridine from 3b by B(C$_6$F$_5$)$_3$ to Generate {(2b)PdMe}$_2$ (4b). The reaction of **3b** with 1 equiv of B(C$_6$F$_5$)$_3$ in CH$_2$Cl$_2$ produces soluble B(C$_6$F$_5$)$_3$(py) and the base-free dimer **4b**, which precipitates as a white powder (Scheme 2.6). Addition of 1 equiv of pyridine or dissolution in a coordinating solvent (Et$_2$O, THF-d_8, dmso-d_6) converts **4b** to the corresponding (**2b**)PdMe(L) complex. **4b** is insoluble in CH$_2$Cl$_2$, C$_6$H$_5$Cl, toluene, and benzene, but dissolves in 1,1,2,2-tetrachloroethane-d_2.

Scheme 2.6. Synthesis of **4b** and **5b**

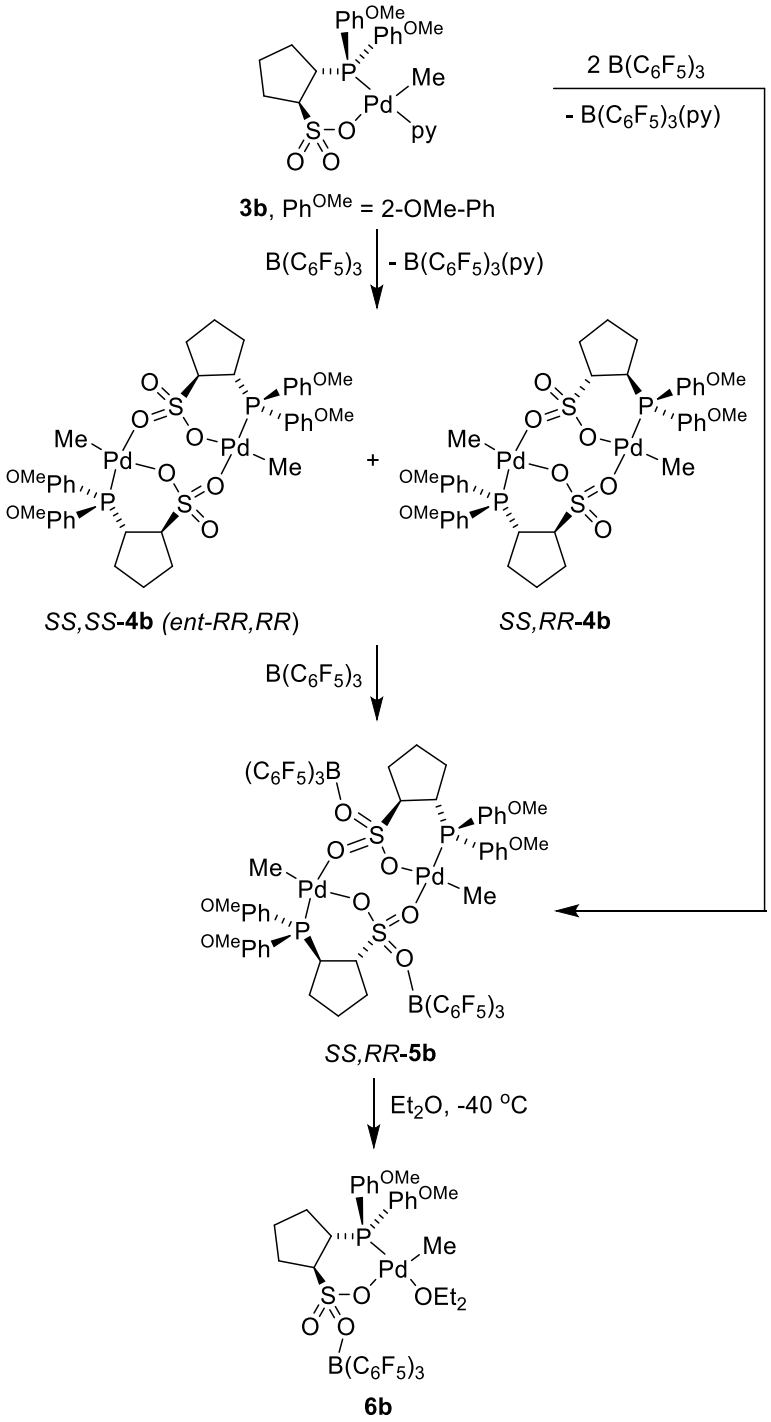

Crystals of **4b**•4($CHCl_2CHCl_2$) were grown from a concentrated $CHCl_2CHCl_2$ solution and characterized by X-ray crystallography (Figure 2.8). Compound **4b** adopts an approximately C_2-symmetric dinuclear structure comprising two *S,S*-(**2b**)PdMe units or two *R,R*-(**2b**)PdMe units that are linked through two sulfonate bridges. The *S,S* and *R,R* stereochemical descriptors denote the configurations of C^1 and C^2 in the cyclopentane ring. The central eight-membered $(PdSO_2)_2$ ring of **4b** adopts a boat–boat conformation,[58,59] in which Pd1 and Pd2 lie on the same side of the plane formed by O1, S2, O3, O6, S1, and O4 (Figure 2.9). The unit cell contains one *SS*,*SS*-**4b** molecule and one *RR*,*RR*-**4b** molecule. Interestingly, there are hydrogen bonds between three of the $CHCl_2CHCl_2$ molecules and the sulfonate oxygens in **4b**•4($CHCl_2CHCl_2$) (Figure 2.10). The CH···O distances range from 2.3–2.7 Å and are shorter than the sum of the H and O van der Waals radii (2.72 Å). These hydrogen bonding interactions provide an explanation for why **4b** is soluble in $CHCl_2CHCl_2$ but not CH_2Cl_2. CH_2Cl_2 is ca. 2 pK_a units less acidic and is a poorer hydrogen bond donor compared to $CHCl_2CHCl_2$.[60,61]

Figure 2.8. Molecular structure of **4b**•4($CHCl_2CHCl_2$). The *SS,SS*-stereoisomer is shown. Hydrogen atoms and the $CHCl_2CHCl_2$ solvent molecules are omitted. Selected bond lengths (Å) and angles (deg): Pd1–P2 2.208(2), Pd1–O1 2.152(5), Pd1–O4 2.172(5), Pd1–C1 2.060(7), Pd2–P1 2.202(2), Pd2–O3 2.176(5), Pd2–O6 2.152(5), Pd2–C2 2.049(7), O1–Pd1–O4 87.55(19), O4–Pd1–P2 91.98(15), C1–Pd1–P2 89.7(2), C1–Pd1–O1 90.3(3), O3–Pd2–P1 92.51(14), O6–Pd2–O3 87.26(19), C2–Pd2–P1 88.2(2), C2–Pd2–O6 91.8(2).

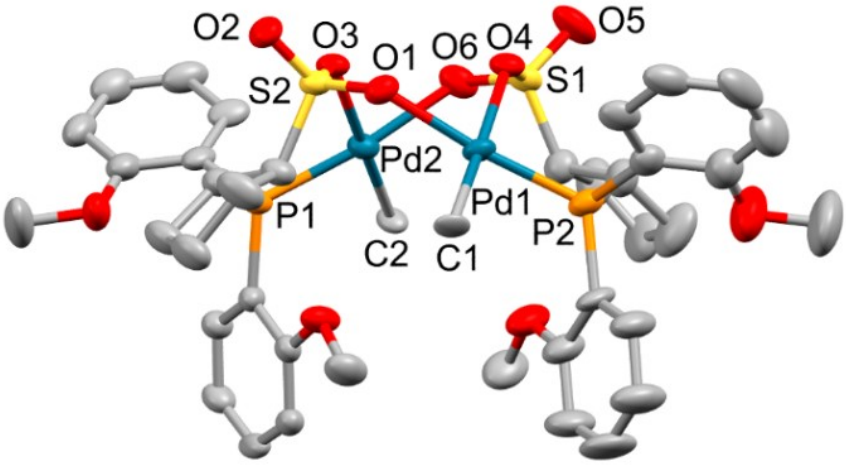

Figure 2.9. View of ***SS,SS*-4b•4(CDCl₂CDCl₂)** showing the boat conformation of the eight-membered $[PdSO_2]_2$ ring. The hydrogen atoms, full anisole rings, and $CDCl_2CDCl_2$ molecules are not shown.

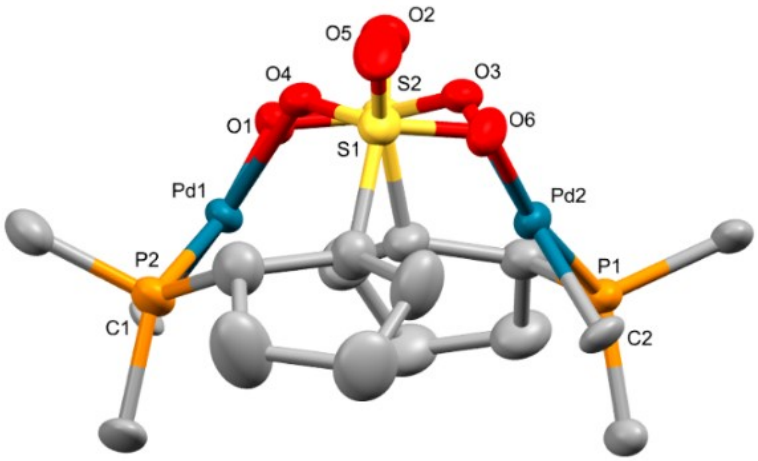

Figure 2.10. Molecular structure of **4b**•4($CHCl_2CHCl_2$) highlighting the hydrogen bonding interactions involving the $CHCl_2CHCl_2$ solvent molecules and the sulfonate groups of **4b**. The *SS,SS* stereoisomer is shown. The hydrogen atoms of **4b** and the $CHCl_2CHCl_2$ molecule that is not involved in hydrogen bonding are omitted. The disorder in two solvent molecules and the cyclopentane rings is not shown.

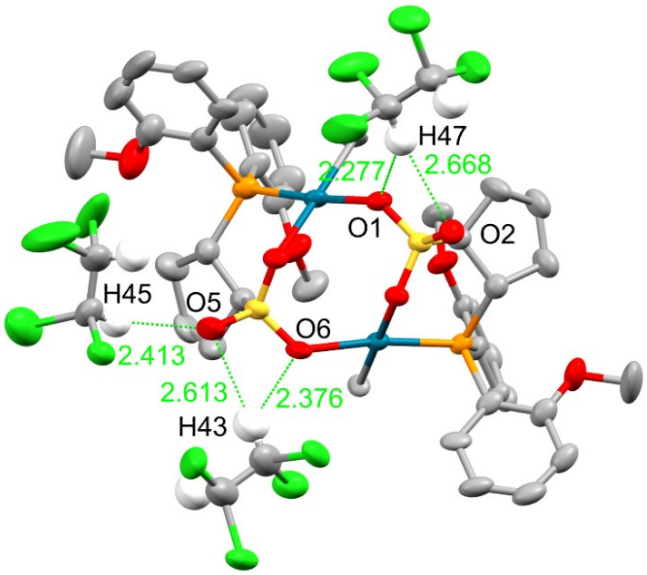

The structure of **4b** is similar to those of {(*o*-{(2-Et-Ph)$_2$P}-*p*-toluenesulfonate)PdMe}$_2$,[36] and {(*o*-{(2-OMe-Ph)$_2$P}-*p*-toluenesulfonate)Pd(CH_2SiMe_3)}$_2$.[62] The main difference is that the central $(PdSO_2)_2$ ring in **4b** adopts a boat–boat conformation, while those in the latter compounds adopt chair–chair conformations.[36,62] {(*o*-{(3,5-^{t}Bu$_2$-Ph)$_2$P}-*p*-toluenesulfonate)PdMe}$_2$ is also known but differs from **4b** in that the (PO-3,5-^{t}Bu$_2$)PdMe units are linked through a four-membered Pd_2O_2 ring.[36]

The ^{1}H NMR spectrum of **4b** in $CDCl_2CDCl_2$ solution contains two Pd–Me resonances in a 3/1 intensity ratio, and the ^{31}P spectrum contains one broad resonance, which is most likely a result of two overlapping signals. The NMR spectra of **4b** are concentration-independent, which

implies that **4b** is not in equilibrium with a monomeric (**2b**)PdMe($CDCl_2CDCl_2$) species, since the fraction of the latter species is expected to increase as $[Pd]_{total}$ is decreased, likely resulting in changes to the spectra. Therefore, the two species are assigned as the *SS*,*SS*-**4b** (*ent*- *RR*,*RR*) and *SS,RR*-**4b** diastereomers, which differ in relative configurations of the cyclopentane units in the two halves of the dimer.[63]

Borane-coordinated Base-free Dimer 5b. The reaction of **3b** with 2 equiv of $B(C_6F_5)_3$ in CH_2Cl_2 at room temperature yields $B(C_6F_5)_3$(py) and the soluble borane adduct {(**2b**•$B(C_6F_5)_3$)PdMe}$_2$ (**5b**, Scheme 2.6). **5b** is also formed by the reaction of **4b** with 2 equiv of $B(C_6F_5)_3$ (i.e. one equiv per Pd). Crystallization of **5b** from $CHCl_2CHCl_2$/hexanes in the presence of excess $B(C_6F_5)_3$ affords *SS,RR*-**5b** as colorless crystals. In the solid-state, *SS,RR*-**5b** adopts an S_2-symmetric dinuclear structure consisting of two (**2b**•$B(C_6F_5)_3$)PdMe units linked by two sulfonate bridges (Figure 2.11). The central eight-membered ring adopts a chair–chair conformation, and the two $B(C_6F_5)_3$ units are located on opposite sides of the central ring.

Figure 2.11. Molecular structure of **5b•**($CHCl_2CHCl_2$). Hydrogen atoms and the $CHCl_2CHCl_2$ solvent molecule are omitted. Selected bond lengths (Å) and angles (deg): Pd1–P1 2.208(2), Pd1–O1 2.2101(19), Pd1–O2 2.204(2), Pd1–C1 2.024(3), S1–O1 1.450(2), O2–S1 1.450(2), S1–O3 1.507(2), O3–B1 1.584(5), O1–Pd1–O2 86.67(7), O2–Pd1–P1 93.56(5), C1–Pd1–P1 88.91(10), C1–Pd1–O1 91.17(11).

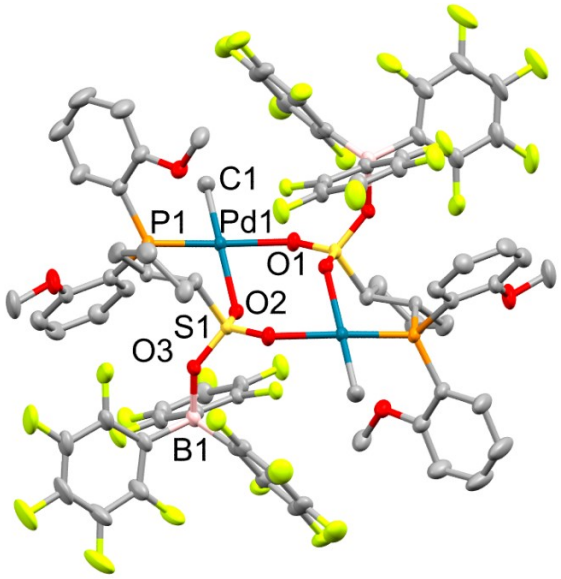

The ^{1}H NMR spectrum of **5b** contains several Pd–Me resonances, indicating the presence of several species, which may include stereoisomers and complexes that contain either one or two $B(C_6F_5)_3$ molecules. However, dissolution of **5b** in Et_2O cleanly generates {**2b•**$B(C_6F_5)_3$}$PdMe(Et_2O)$ (**6b**), which crystallizes at –40 °C as the **6b•**Et_2O solvate (Scheme 2.6). The ^{1}H NMR spectrum of **6b•**Et_2O at –60 °C in CD_2Cl_2 solution contains separate resonances for free and bound Et_2O (1:1 integral ratio), indicating that only 1 equiv of Et_2O is coordinated. However, exchange of free and **6b**-coordinated Et_2O is fast on the NMR time scale at room temperature, and under these conditions, one set of exchange-averaged Et_2O resonances is observed. Attempts to remove the excess Et_2O from **6b•**Et_2O led to decomposition of the complex.

2.3 Conclusions

A new class of phosphine-sulfonate ligands bearing a cyclopentane linker, which is more electron-donating relative to the traditional benzene linker, was designed and several pro-ligands were synthesized, characterized, and used in the synthesis of Pd(II) alkyl complexes. Synthetic routes toward (cation)[PR_2-cyclopentanesulfonate] ligands are discussed, where R = Ph (**2a**), 2-OMe-Ph (**2b**), iPr, menthyl (Men), and 2',6'-dimethoxy-biphenyl (Bp). The solid-state structures and solution behavior of Pd(II) alkyl complexes are reported and discussed in detail, including {PPh_2-cyclopentanesulfonate}PdMe(pyridine) (**3a**), {$P(2\text{-OMe-Ph})_2$-cyclopentanesulfonate}PdMe(pyridine) (**3b**), base-free dimer [{$P(2\text{-OMe-Ph})_2$-cyclopentanesulfonate}PdMe]$_2$ (**4b**), borane-coordinated base-free dimer [{$P(2\text{-OMe-Ph})_2$-cyclopentanesulfonate}PdMe]$_2$ (**5b**), a LiCl-(PO)PdMe dimer, and a (BAr_3^F•PO)PdMe(Et_2O) complex.

2.4 Experimental Section

General Procedures. All experiments were performed using drybox or Schlenk techniques under a nitrogen atmosphere unless noted otherwise. Nitrogen was purified by passage through Q-5 oxygen scavenger and activated molecular sieves. CH_2Cl_2, Et_2O, and THF were dried by passage through activated alumina. Pentane, hexanes, and toluene were purified by passage through BASF R3-11 oxygen scavenger and activated alumina. CD_2Cl_2 was distilled from and stored over P_2O_5. Toluene-d_8 and THF-d_8 were distilled from Na/benzophenone. DMSO-d_6, cyclopentene, sulfur trioxide (stored in a 35 °C oil bath to prevent formation of fibrous β-SO_3[64]),

$CHCl_3$ (50 ppm hexanes as preservative), dioxane (anhydrous), NBu_4Br, KPF_6, $HPPh_2$, ^nBuLi solution (1.6 M or 2.5 M in hexanes), 2-bromoanisole, diethylphosphite, $HSiCl_3$, NEt_3 (99.5%), ethanol (anhydrous), acetonitrile (anhydrous, 99.8%), $NaHCO_3$, KOH, HCl solution (2.0 M in Et_2O), pyridine (Fisher), 2,6-lutidine (99+%), and 3-phenylpyridine were purchased from Sigma Aldrich and used without further purification. $B(C_6F_5)_3$ was donated by Boulder Scientific. Ethylene (polymer grade) and vinyl fluoride (VF) were purchased from Matheson. 1-lithio-2-methoxybenzene,[65] 2-lithio-2',6'-dimethoxy-biphenyl, $LiP(2\text{-}OMe\text{-}Ph)_2$,[38–41] (COD)PdMeCl (COD = cyclooctadiene),[66] and (TMEDA)$PdMe_2$ (TMEDA = tetramethylenediamine)[67,68] were prepared according to the literature.

NMR spectra were recorded on Bruker DMX-500 or DRX-400 spectrometers at ambient temperature unless otherwise indicated. ^1H and ^{13}C chemical shifts are reported relative to $SiMe_4$ and internally referenced to residual ^1H and ^{13}C solvent resonances. ^{31}P chemical shifts are externally referenced to 85% H_3PO_4 (δ 0.0). ^{11}B and ^{19}F chemical shifts are externally referenced to $BF_3(OEt_2)$ (δ 0.0 for ^{11}B and δ –153 for ^{19}F).

Electrospray mass spectra (ESI-MS) and atmospheric pressure chemical ionization mass spectra (APCI-MS) were recorded using Agilent 6224 TOF–MS (high resolution) or 6130 LCMS (low resolution) instruments. The observed isotope patterns closely matched calculated isotope patterns. The listed *m/z* value corresponds to the most intense peak in the isotope pattern.

Tetrabutylammonium 2-bromocyclopentanesulfonate, NBu_4[1]. Cyclopentane-β-sultone was generated according to the literature.[37,69] A solution of dioxane (28.2 mL, 0.331 mol)

and chloroform (80 mL) was cooled in an ice bath for 20 min and stirred. The septum of the flask was removed while the flask was flushed with N_2 and SO_3 (6.9 mL, 0.17 mmol) was added in one portion via a graduated pipet (CAUTION: SO_3 reacts rapidly and exothermically with water and generates white sulfuric acid fumes when the bottle is opened. Work in a well-ventilated fume hood and avoid inhalation). A white, sticky precipitate (SO_3-dioxane adduct)[70] formed as the SO_3 was added and dissolved over a period of 10 min. Cyclopentene (13.3 mL, 0.145 mol) was added dropwise to the solution via syringe over 10 min. A yellow, sticky solid formed and gradually dissolved to give a pale-yellow solution. The solution was stirred at 0 °C for 1.5 h. The septum was briefly removed while the flask was flushed with N_2 and NBu_4Br (48.3 g, 0.150 mol) was added in one portion. The mixture was stirred until the NBu_4Br dissolved. The cold bath was removed and the solution was allowed to warm to room temperature over 30 min. The mixture was transferred to a separatory funnel and washed with 40 mL water, and then saturated $NaHCO_3$ solution (3 x 20 mL) until the *p*H of the wash was 6. The organic layer was dried with $MgSO_4$, filtered, and concentrated on a rotary evaporator. Most of the remaining dioxane was removed on a vacuum line to afford NBu_4[**1**] as a gummy brown solid. The crude product contained ca. 0.2 excess equiv of NBu_4Br, which was removed by the salt exchange procedure discussed below. The numbering scheme for NBu_4[**1**] is shown in Figure 2.12. All ^1H and ^{13}C signals on the ring were identified in the next step of the reaction. ^1H NMR ($CDCl_3$), Figure 2.13: δ 4.92 (m, 1H, H^2), 3.67 (m, 1H, H^1), 3.3 (m, 9H (excess from 8), H^a), 2.41–2.50 (m, 1H), 2.14–2.29 (m, 2H), 1.99–2.06 (m, 1H), 1.86–1.99 (m, 2H), 1.66 (m, 9H (excess from 8), H^b), 1.46 (sex, $^3J_{HH}$ = 7.5 Hz, 9H (excess

from 8), H^c), 1.02 (t, $^3J_{HH}$ = 7.5 Hz, 13.5H (excess from 12), H^d).

Figure 2.12. Numbering scheme for NBu_4[**1**].

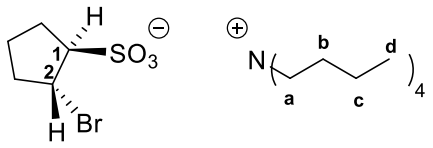

Figure 2.13. ^{1}H NMR spectrum of tetrabutylammonium (2-bromo)cyclopentylsulfonate (NBu_4[**1**]) ($CDCl_3$, 500 MHz).

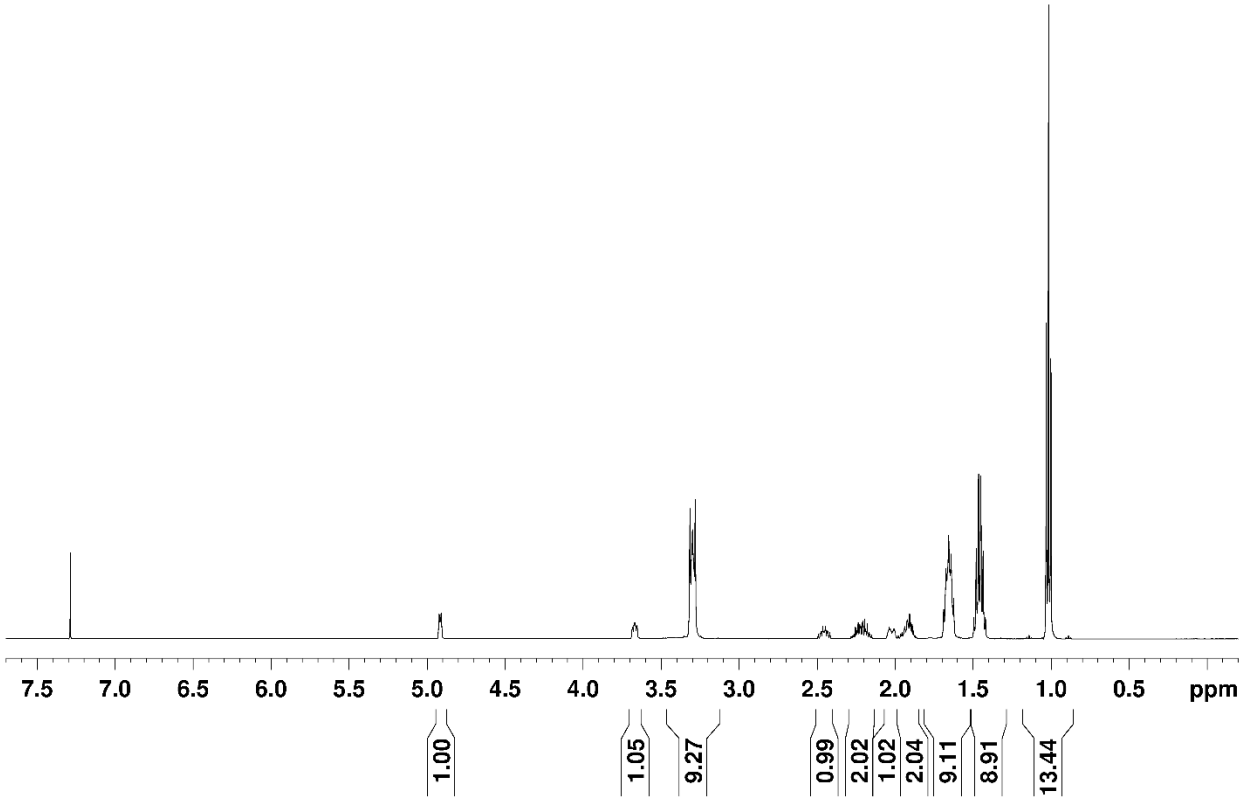

Potassium 2-bromocyclopentanesulfonate, K[1]. The crude NBu_4[**1**] prepared above, which contained ca. 0.2 equiv of NBu_4Br, was dissolved in water (150 mL). A solution of KPF_6 (27.7 g, 0.150 mol) in water (150 mL) was added dropwise while the mixture was stirred. White NBu_4PF_6 precipitated. The thick slurry was stirred overnight, and the precipitate was removed by filtration. The filtrate was taken to dryness on a vacuum line to afford crude a yellow solid that contained K[**1**] and a small amount of KPF_6 (by ^{31}P NMR). This material was suspended in acetone (50 mL) and stirred vigorously for 15 min to dissolve the KPF_6. The white solid was collected by filtration, washed 3 times with acetone, and dried under vacuum to afford K[**1**] as a white powder (26.843 g, 67% from cyclopentene). X-ray quality crystals of [K(18-crown-6)][**1**] were grown from a CH_2Cl_2 (0.5 mL) and ether (1 mL) solution of K[**1**] (50 mg) and 18-crown-6 (50 mg) stored at 0 °C for 2 days. X-ray crystallographic data for [K(18-crown-6)][**1**] are shown in Table 2.2. The numbering scheme for K[**1**] is shown in Figure 2.14. ^1H NMR (D_2O), Figure 2.15(a): δ 4.43–4.51 (m, 1H, H^2), 3.58–3.68 (m, 1H, H^1), 2.10–2.26 (dt, ^3J = 6 Hz, 4.5 Hz, 2H, H^{3a}, H^{5b}), 1.94–2.04 (m, 1H, H^{3b}), 1.76–1.89 (m, 2H, H^{4b}, H^{5a}), 1.65–1.76 (m, 1H, H^{4a}). ^{13}C NMR (D_2O), Figure 2.15 (b): δ 69.2 (C^1), 50.1 (C^2), 38.1 (C^3), 27.6 (C^5), 23.8 (C^4). The *trans* configuration of the Br and SO_3K groups was also established by quantitative ^1H–^1H NOESY NMR, Figure 2.15 (c). ES–HRMS (*m/z*): Calcd for $[C_5H_8BrO_3S - H]^-$: 228.9362, Found: 228.9364.

Figure 2.14. Numbering scheme for K[**1**].

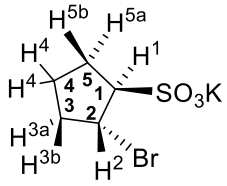

Figure 2.15. NMR spectra of K[**1**].

(a) ^{1}H NMR (D_2O, 500 MHz)

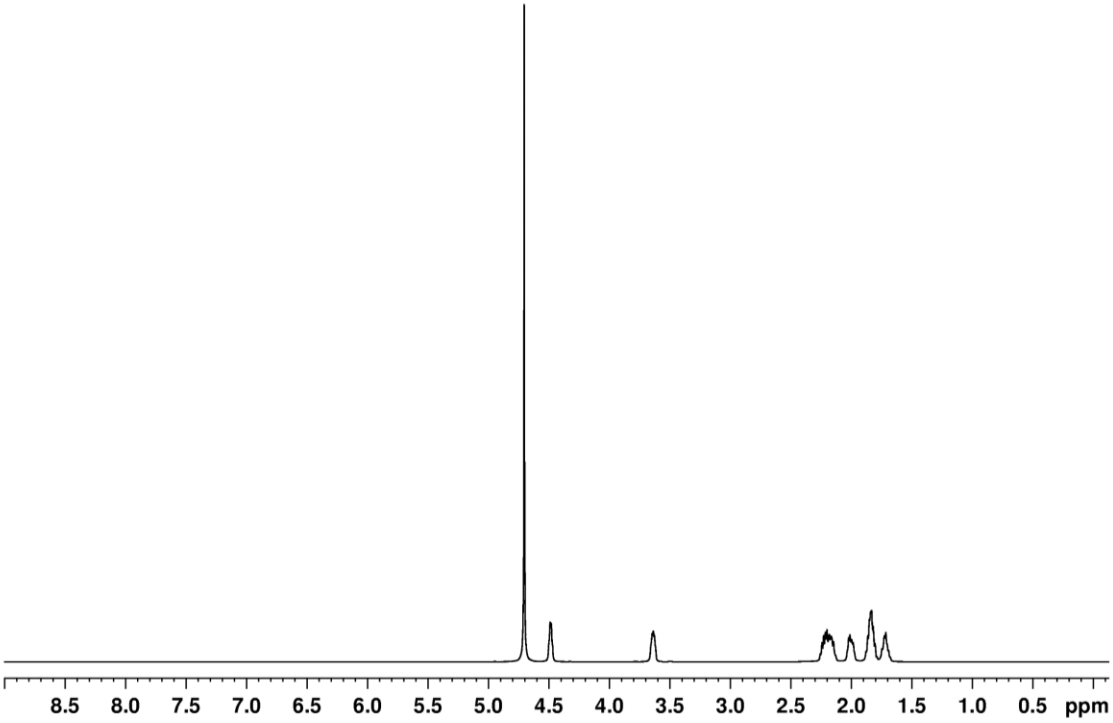

Figure 2.15, continued.

(b) ^{13}C NMR (D_2O, 125 MHz)

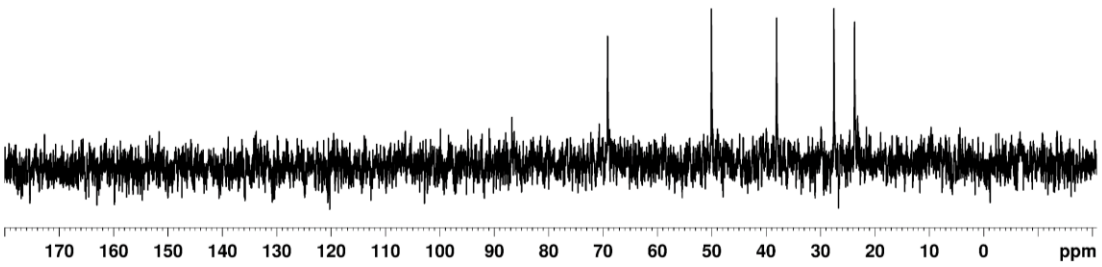

(c) ^{1}H–^{1}H NOESY (D_2O, 500 MHz)

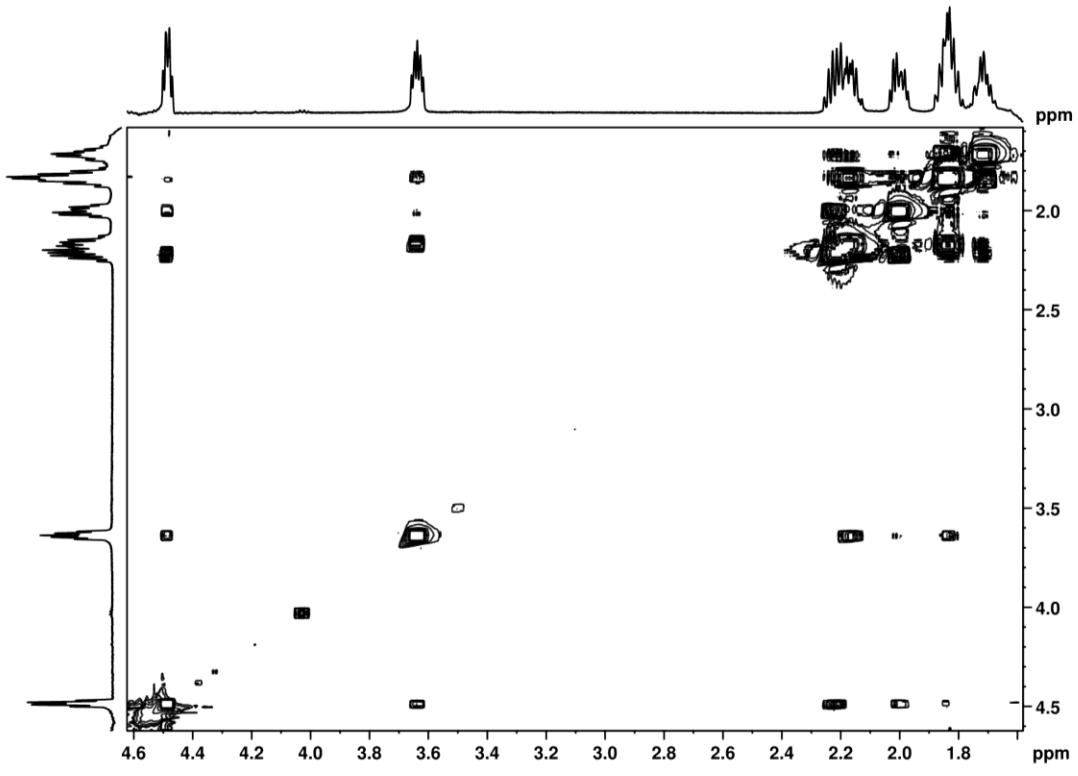

Generation of lithium diphenylphosphide, $LiPPh_2$. A solution of diphenylphosphine (2.14 mL, 11.5 mmol) in THF (25 mL) was cooled in a dry ice/acetone bath for 20 min. ^{n}BuLi solution (2.5 M in ether, 5.0 mL, 13 mmol) was added dropwise over 15 min via syringe to yield a red-orange solution. The solution was stirred for 30 min at –78 °C. The cold bath was removed. The solution was stirred at room temperature for 1.5 h and then used for the synthesis of Li/K[**2a**] as described below. $^{31}P\{^1H\}$ NMR (THF): δ –22.4.

Li/K[PPh2(2-SO3-cyclopentyl)], Li/K[2a]. A solution of K[**1**] (3.04 g, 11.8 mmol) in THF (20 mL) was stirred at room temperature and a solution of $LiPPh_2$ (11.5 mmol) in THF (25 mL) was added dropwise over 10 min. The solution became orange. The solution was stirred at room temperature overnight. The solvent was removed under vacuum and the remaining yellow solid was dissolved in degassed water (25 mL). The pale-green aqueous solution was washed with dichloromethane (3 x 15 mL), and the water was removed under vacuum in a 40 °C bath to afford a white solid. The solid was dissolved in dichloromethane and filtered to remove LiBr. The volatiles from the filtrate were removed under vacuum to yield a white powder (2.97 g, 15% Li[**2a**] and 85.3% K[**2a**], Li vs. K content determined by ICP-MS, 70% yield). ^1H NMR (CD_3OD): δ 7.67 (2H, H^4), 7.52 (2H, H^2), 7.35 (6H, $4H^3$, $2H^2$), 3.40 (m, 1H, H^6), 3.20 (m, 1H, H^5), 2.25 (m, 2H, H^7, H^9), 2.05 (m, 1H, H^9), 1.95 (m, 1H, H^8), 1.70 (m, 1H, H^8), 1.55 (m, 1H, H^7). ^{13}C NMR (CD_3OD): δ 134.8 (s, 2C, C^4), 134.8 (d, $^2J_{PC}$ = 40.5 Hz, 2C, C^2), 131.5 (d, $^1J_{PC}$ = 158 Hz, 2C, C^1), 129.8 (d, $^2J_{PC}$ = 40.5 Hz, 2C, C^2), 129.3 (4C, C^3), 67.7 (d, $^1J_{PC}$ = 18 Hz, C^5), 39.7 (d, $^2J_{PC}$ = 13 Hz, C^6), 30.1 (d, $^3J_{PC}$ = 13 Hz, C^7), 29.4 (C^9), 25.6 (C^8). ^{31}P NMR (CD_3OD): δ –2.6. ES/CI–HRMS (*m/z*): Calcd

for $[C_{17}H_{18}KO_3PS - H]^-$, ($[M - H]^-$) : 372.0351, Found: 372.0350.

Figure 2.16. Numbering scheme for Li/K[**2a**].

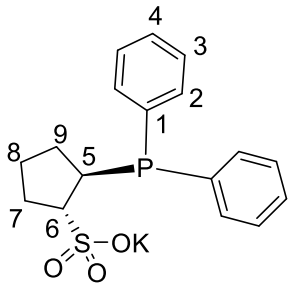

Figure 2.17. NMR spectra of Li/K[**2a**].

(a) ^{1}H NMR (MeOD, 500 MHz) (*CH_2Cl_2)

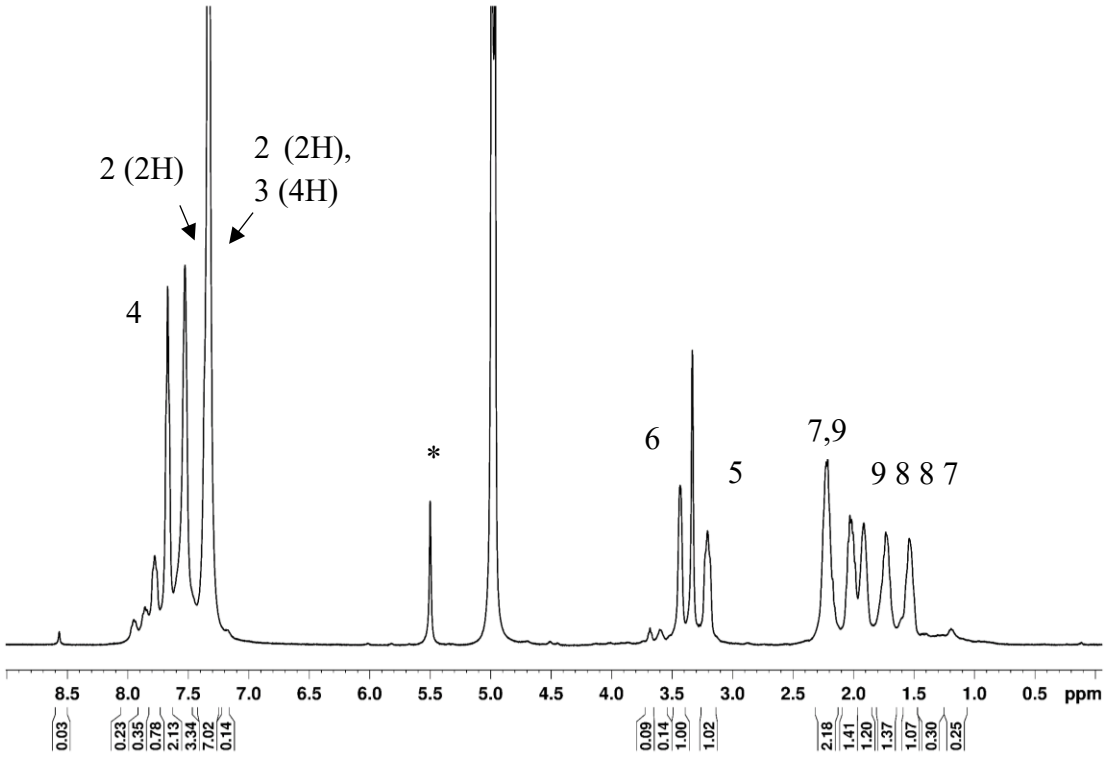

Figure 2.17, continued.

(b)$^{31}P\{^{1}H\}$ NMR spectrum (MeOD, 202 MHz)

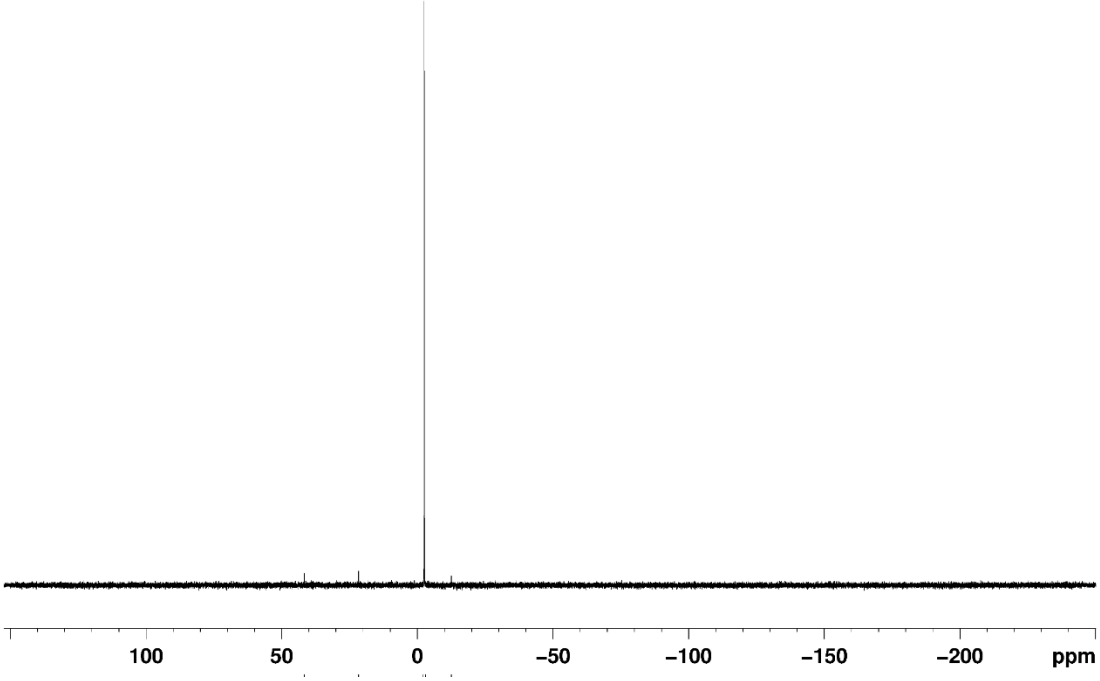

(c) $^{13}C\{^{1}H\}$ NMR spectrum (MeOD, 125 MHz)

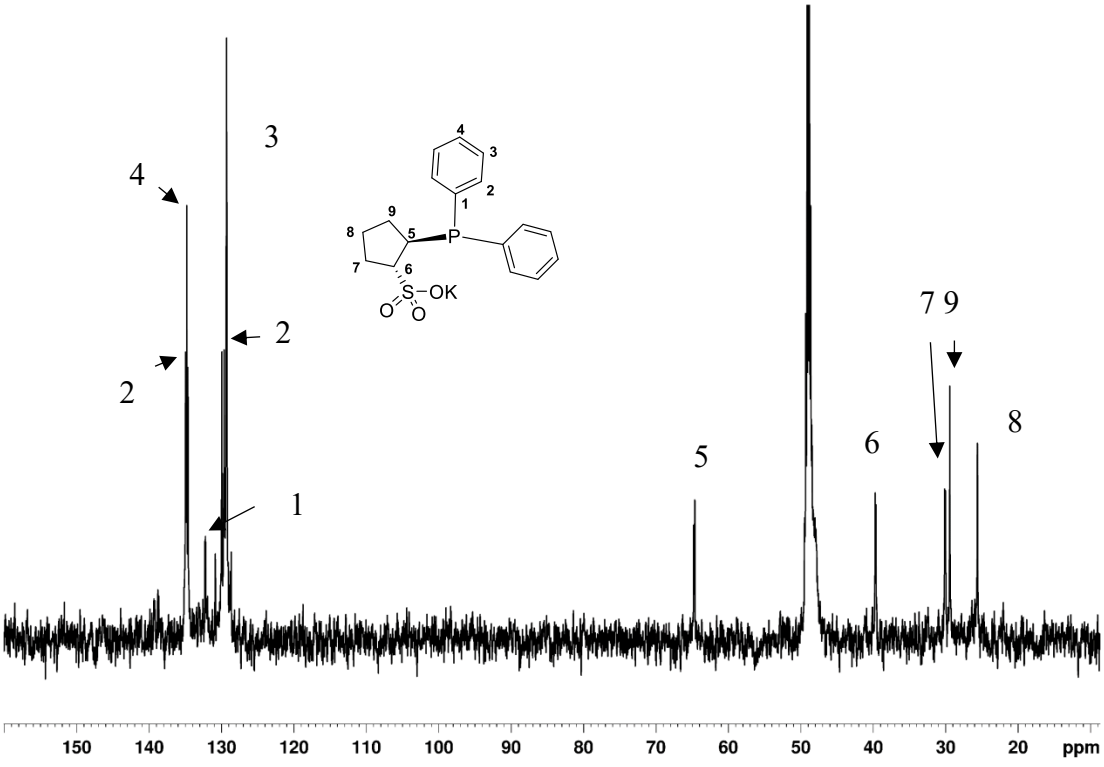

Lithium o-anisole, Li[2-OMe-Ph]. Adapted from the literature.[38] A solution of 2-bromoanisole (23.5 mL, 0.189 mmol) in pentane (50 mL) was cooled to 0 °C and stirred, and ^{n}BuLi solution (2.5 M in hex, 75.0 mL, 0.188 mmol) was added dropwise over 10 min. A copious amount of a white solid precipitated. The mixture was allowed to warm to room temperature and was stirred overnight. The solvent was removed under vacuum and the resulting off-white solid was washed with pentane (100 mL) and dried under vacuum to yield a white powder (22.0 g, 100%). ^{1}H NMR (THF-d_8), Figure 2.18: δ 7.73 (d, $^{3}J_{HH}$ = 6 Hz, 1H, H^{1}), 6.98 (t, $^{3}J_{HH}$ = 7 Hz, 1H, H^{2}), 6.74 (t, $^{3}J_{HH}$ = 6.5 Hz, 1H, H^{3}), 6.64 (d, $^{3}J_{HH}$ = 8 Hz, 1H, H^{4}), 3.73 (s, 3H, –OCH_3).

Figure 2.18. Numbering scheme for Li-anisole.

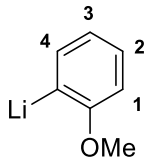

Di(o-anisolyl)phosphine oxide, PH(=O)(2-OMe-Ph)$_2$. Adapted from the literature.[38,40] A solution of o-lithium anisole (13.7 g, 0.120 mol) in Et_2O (80 mL) was stirred and cooled in a 1,2-dichlorobenzene/N_2(l) slush bath (–25 °C) for 10 min. Diethylphosphite (5.4 mL, 0.042 mol) was added dropwise over 15 min. The mixture was stirred for 10 min and then allowed to warm to room temperature over 30 min. The mixture was refluxed for 2 h and cooled to room temperature. A degassed, aqueous solution of HCl (0.1 M, 100 mL) was added dropwise. Under air, the water layer was extracted with dichloromethane (3 x 25 mL). The combined organic layers were dried

over $MgSO_4$, filtered, and dried on a rotary evaporator at 70 °C. The elevated temperature was used to remove the excess anisole. The crude yellow-white powder was washed with ether (100 mL) to afford a white powder (8.682 g, 79%). The NMR numbering scheme for PH(=O)(2-OMe-Ph)$_2$ is shown in Figure 2.19. ^{1}H NMR ($CDCl_3$), Figure 2.20(a): δ 8.27 (d, $^1J_{PH}$ = 516 Hz, 1H, P*H*), 7.69 (dd, $^2J_{PH}$ = 15 Hz, $^3J_{HH}$ = 7 Hz, 2H, H^4), 7.52 (t, $^3J_{PH}$ = 7.5 Hz, 2H, H$^{2 \text{ or } 3}$), 7.07 (t, $^3J_{PH}$ = 7.5 Hz, 2H, H$^{2 \text{ or } 3}$), 6.91 (dd, $^3J_{PH}$ = 8 Hz, $^3J_{HH}$ = 6 Hz, 2H, H^1), 3.77 (s, 6H, –OC*H*$_3$). ^{31}P{^{1}H} NMR ($CDCl_3$), Figure 2.20(b): δ 9.3 (s). X-ray quality crystals were obtained from a concentrated ether solution at 0 °C. X-ray crystallographic data for PH(=O)(2-OMe-Ph)$_2$ are shown in Table 2.2.

Figure 2.19. Numbering scheme for PH(=O)(2-OMe-Ph)$_2$.

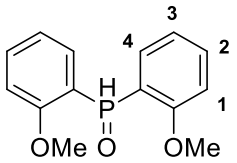

Figure 2.20. NMR spectra of (O=)PH(2-MeO-Ph)$_2$

(a)^{1}H NMR spectrum ($CDCl_3$, 500 MHz)

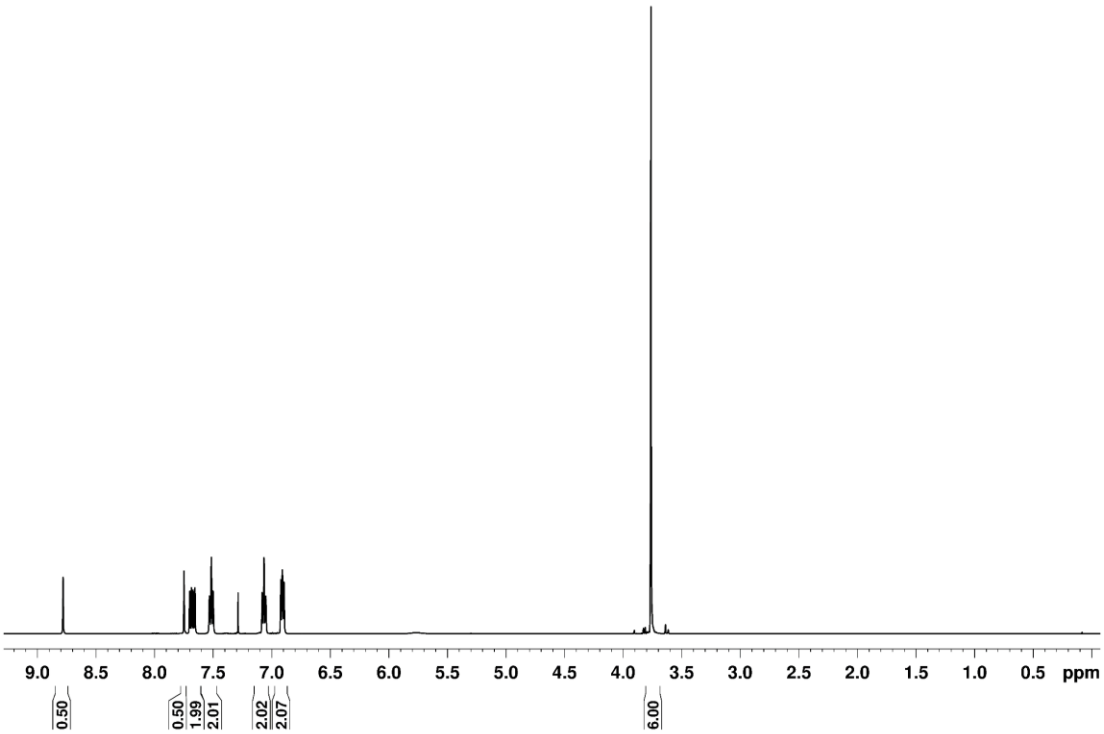

(b)^{31}P NMR spectrum ($CDCl_3$, 202 MHz)

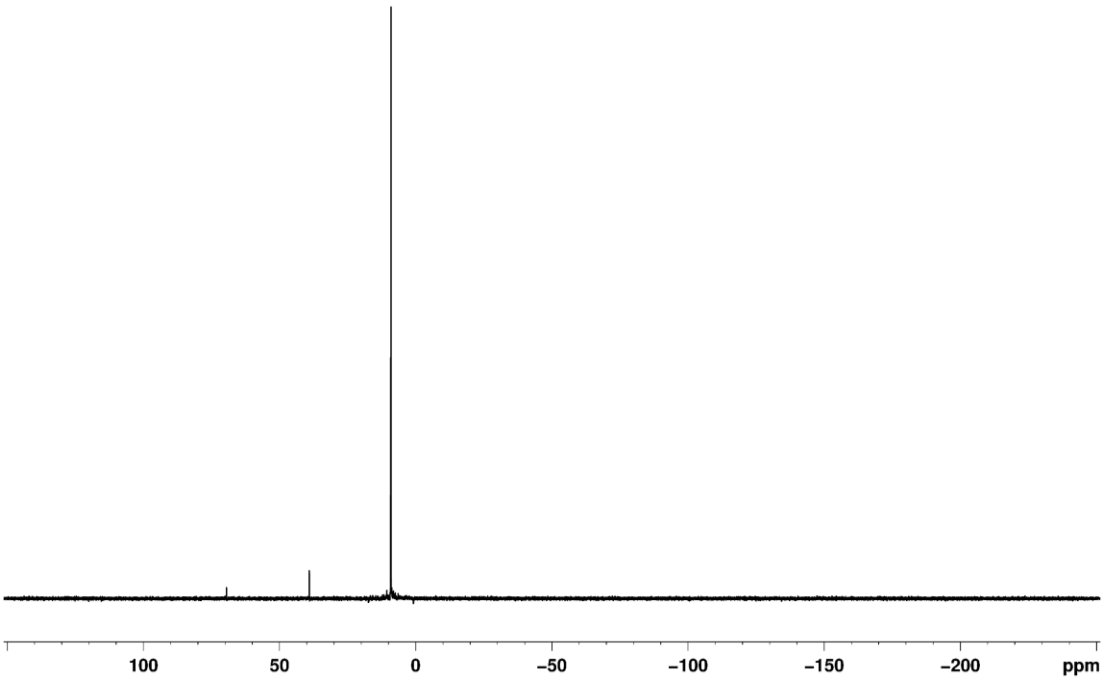

Di(o-anisolyl)phosphine, PH(2-OMe-Ph)$_2$. Adapted from the literature.[39–41] A solution of triethylamine (2.2 mL, 15 mmol) in anhydrous acetonitrile (30 mL) was degassed by bubbling N_2 through the solution for 20 min. This solution was stirred and $HSiCl_3$ (1.6 mL, 16 mmol) was added dropwise at room temperature. The mixture was refluxed for 6 h. The yellow solution was allowed to cool to room temperature and then was cooled in an ice bath. White solid precipitated. A degassed solution of KOH (5.3 g, 94 mmol) in water (20 mL) was added dropwise while the mixture was stirred. The top, yellow acetonitrile layer was separated and the aqueous layer was extracted with acetonitrile (3 x 10 mL). The acetonitrile fractions were combined and dried under vacuum to afford a pale-pink solid. This material was suspended in minimal anhydrous degassed EtOH (10 mL), collected by filtration, and dried under vacuum to give a white solid (1.393 g, 50% yield). ^{1}H NMR (CD_2Cl_2): δ 7.38 (t, $^3J_{HH}$ = 7.5 Hz, 2H), 7.27 (t, $^3J_{HH}$ = 7 Hz, 2H), 6.98–6.91 (m, 4H), 5.24 (d, $^1J_{PH}$ = 228 Hz, 1H, P*H*), 3.88 (s, 6H, –OC*H*$_3$). ^{31}P{^{1}H} NMR (CD_2Cl_2): δ –72.3 (s).

Lithium di(o-anisolyl)phosphide, LiP(2-OMe-Ph)$_2$. *In-situ generation:* A solution of di(o-anisolyl)phosphine (0.32 g, 1.3 mmol) in THF (25 mL) was cooled in an ice bath and stirred for 10 min. A solution of ^{n}BuLi (2.5 M in hexanes, 0.55 mL, 1.3 mmol) was added dropwise. A small amount of bright yellow solid precipitated from the bright yellow solution. The cold bath was removed and the mixture was allowed to warm to room temperature over 30 min. This mixture was used for the synthesis of **Li/K[2b]** as described below. *Isolation:* A solution of ^{n}BuLi (2.5 M in hexanes, 3.0 mL, 7.5 mmol) was added dropwise to a solution of di(o-anisolyl)phosphine (1.54 g, 6.26 mmol) in hexane (40 mL) over 1 min while the mixture was stirred at room temperature.

The solution became neon yellow and a bright yellow precipitate formed. The slurry was stirred for 1 h at room temperature. The bright yellow solid was collected by filtration and dried under vacuum (1.5 g, 95%). ^{1}H NMR (THF-d_8): δ 7.67 (br, 2H), 6.69 (br, 2H), 6.64 (br, 2H), 6.58 (br, 2H), 3.76 (s, 6H, –OCH_3). ^{31}P{^{1}H} NMR (THF-d_8): δ –73.5.

Li/K[P(2-OMe-Ph)2(2-SO3-cyclopentyl)], **Li/K[2b]**. A colorless slurry of K[**1**] (1.08 g, 4.06 mmol) in THF (25 mL) was cooled in an ice bath and stirred for 10 min. A bright orange slurry of LiP(2-OMe-Ph)$_2$ (1.0 g, 4.06 mmol) in THF (60 mL) was added dropwise over 10 min. The cold bath was removed and the slurry was allowed to warm to room temperature and stirred for 5 h. The volatiles were removed under vacuum and the resulting yellow solid was dissolved in degassed water (30 mL). The aqueous layer was washed with CH_2Cl_2 (5 x 10 mL) and then the water was removed under vacuum using a warm water bath. The resulting white powder was dissolved in dichloromethane (25 mL) and dried over $MgSO_4$. The mixture was filtered and the volatiles of the filtrate were removed to afford Li/K[**2b**] as a white powder (0.580 g, 31%). The product contained minor impurities (likely alkanesulfonates formed via elimination) that were difficult to remove because of their similar solubility to Li/K[**2b**]. The numbering scheme for Li/K[2b] is shown in Figure 2.21. ^{1}H NMR (MeOD), Figure 2.22 (a): δ 7.7–7.66 (m, 1H, H^4), 7.34–7.28 (m, 2H, H^6, H^{12}), 7.22–7.17 (t, 1H, H^{10}), 7.0–6.86 (m, 4H, H^3, H^5, H^9, H^{11}), 3.76 (s, 3H, –OCH_3), 3.68 (s, 3H, –OCH_3), 3.51–3.44 (m, 1H, H^{13}), 3.42–3.38 (m, 1H, H^{14}), 2.26–2.13 (m, 2H, H^{15}, H^{17}), 2.13–2.02 (m, 1H, H^{17}), 1.92–1.81 (m, 1H, H^{16}), 1.7–1.6 (m, 1H, H^{16}), 1.55–1.46 (m, 1H, H^{15}). ^{31}P{^{1}H} NMR (MeOD, Figure 2.22(b): δ -25.2 (s). ESI-MS (*m/z*): 393

(negative scan, $[C_{23}H_{26}NO_3PPdS]^-$) and 395 (positive scan, $[C_{23}H_{26}NO_3PPdS + 2H]^+$).

Figure 2.21. Numbering scheme for Li/K[**2b**].

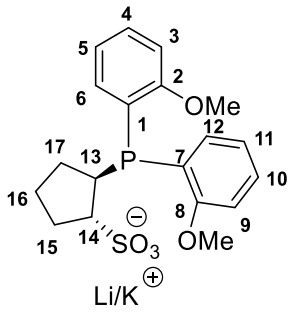

Figure 2.22. NMR spectra of Li/K[**2b**].

(a) ^{1}H NMR spectrum (MeOD, 500 MHz)

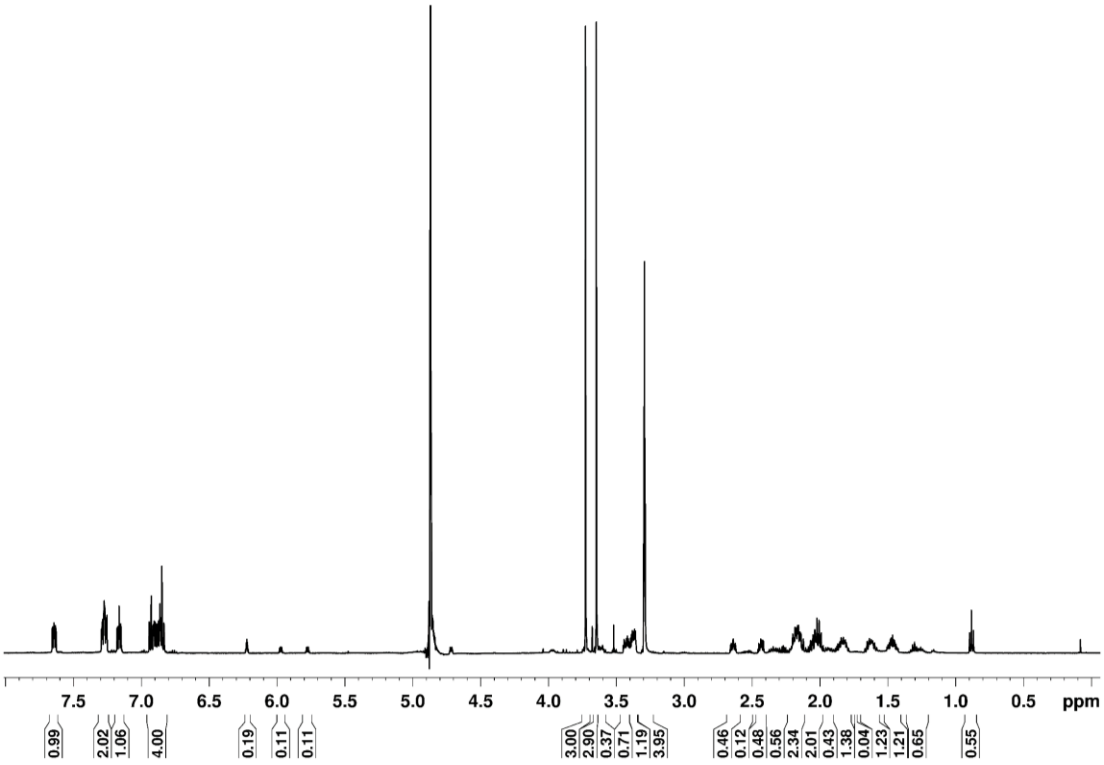

Figure 2.22, continued.

(b)^{31}P NMR spectrum (MeOD, 202 MHz)

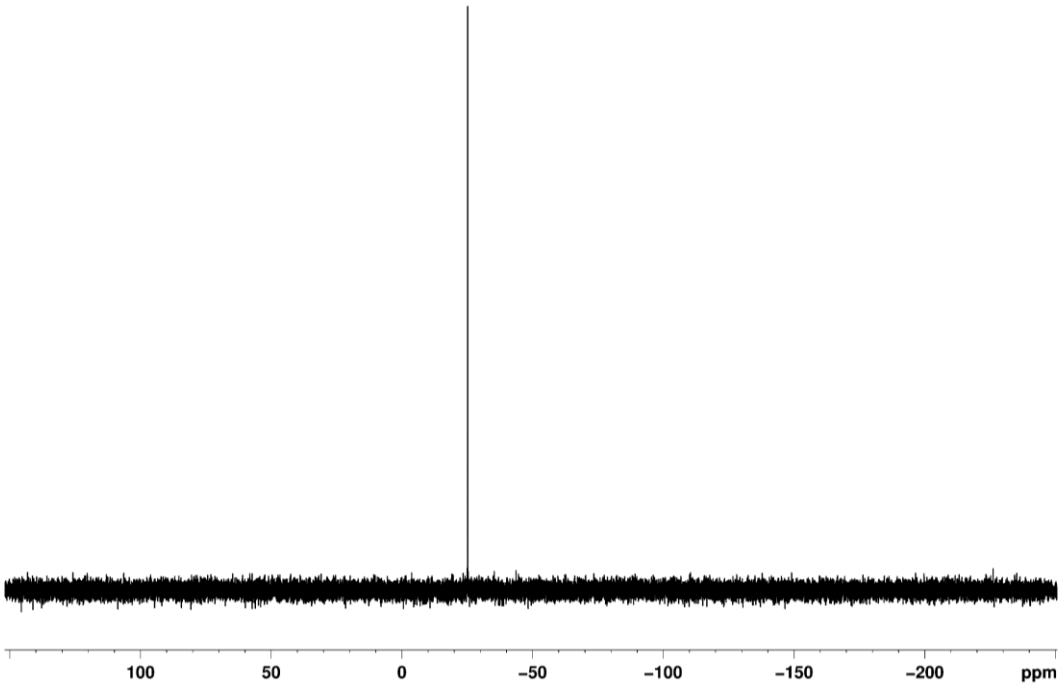

H[P(2-OMe-Ph)2(2-SO3-cyclopentyl)], **H[2b]**. A slurry of K[**1**] (1.67 g, 6.26 mmol) in THF (25 mL) was cooled in an ice bath and stirred for 10 min. A bright orange slurry of LiP(2-OMe-Ph)$_2$ (1.54 g, 6.26 mmol) in THF (60 mL) was added *dropwise over 50 min* to maintain a dark orange slurry color. The cold bath was removed and the reaction was stirred at room temperature for 18 h. The volatiles were removed under vacuum to give a yellow solid, which was dissolved in degassed water (30 mL). The aqueous layer was washed with CH_2Cl_2 (5 x 10 mL) and then acidified to a *p*H of 1 by addition of conc. HCl (0.3 mL). A yellow solid precipitated from the yellow solution. Under air, the aqueous layer was extracted with CH_2Cl_2 (5 x 10 mL). The combined CH_2Cl_2 fractions were dried over $MgSO_4$, filtered, and the volatiles of the filtrate were

removed under vacuum to afford H[**2b**] as a crystalline white powder (1.40 g, 57% yield from $HP(2\text{-}OMe\text{-}Ph)_2$). The numbering scheme for H[**2b**] is shown in Figure 2.23. ^1H NMR ($CDCl_3$), Figure 2.24(a): δ 7.77–7.69 (m, 2H, H^4), 7.57–7.50 (m, 2H, H^6), 7.20–7.10 (m, 4H, H^5, H^3), 3.96 (s, 3H, –OC*H*$_3$), 3.94 (s, 3H, –OC*H*$_3$), 3.81–3.72 (m, 1H, H^7), 3.60–3.49 (m, 1H, H^8), 2.35–2.25 (m, 1H, H^9), 2.23–2.10 (m, 2H, H^9, H^{11}), 2.03–1.94 (m, 1H, H^{10}), 1.77–1.66 (m, 2H, H^{10}, H^{11}). $^{13}C\{^1H\}$ NMR ($CDCl_3$), Figure 2.24(c): δ 161.3 (d, $^2J_{PC}$ = 6.9 Hz, 2C, C^2), 137.3 (d, J_{PC} = 13 Hz, 2C, C^4), 136.0 (d, $^2J_{PC}$ = 7.6 Hz, C^6), 135.0 (d, $^2J_{PC}$ = 7.5 Hz, C^6), 122.7 (d, $^3J_{PC}$ = 12.9 Hz, C^5), 122.4 (d, $^3J_{PC}$ = 12.9 Hz, C^5), 111.7 (s, 2C, C^3), 104.7 (d, $^1J_{PC}$ = 88.6 Hz, C^1), 103.5 (d, $^1J_{PC}$ = 88.6 Hz, C^1), 62.3 (s, C^8), 56.6 (s, –O*C*H$_3$), 56.4 (s, –O*C*H$_3$), 34.6 (d, $^1J_{PC}$ = 54 Hz, C^7), 29.4 (d, $^3J_{PC}$ = 8.2 Hz, C^9), 28.8 (s, C^{11}), 25.8 (d, $^3J_{PC}$ = 11.4 Hz, C^{10}). $^{31}P\{^1H\}$ NMR ($CDCl_3$), Figure 2.24(b): δ 9.7 (s). ES/CI–HRMS (*m/z*): Calcd for $[C_{19}H_{23}O_5PS+H^+]^+$: 395.1077, Found: 395.1085.

Figure 2.23. Numbering scheme for H[**2b**].

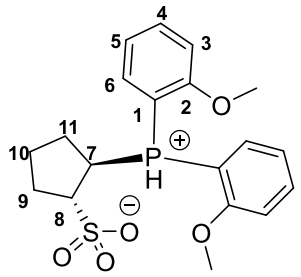

Figure 2.24. NMR spectra of H[**2b**].

(a)^{1}H NMR spectrum of H[**2b**] (CD_2Cl_2, 500 MHz):

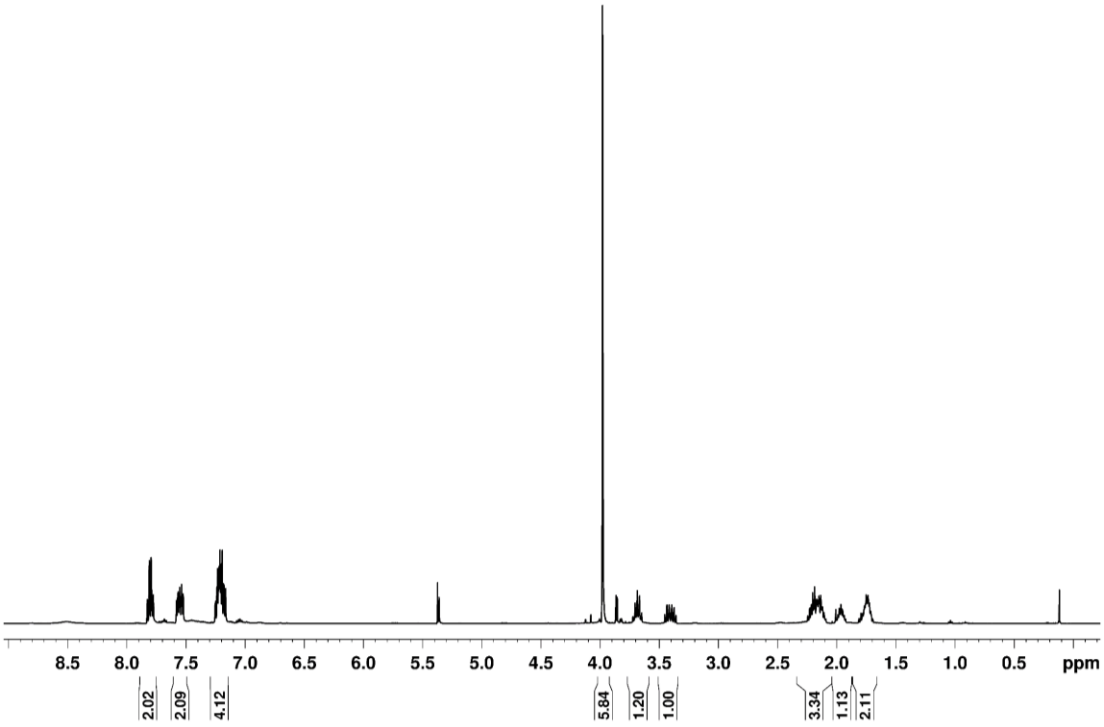

(b)^{31}P NMR spectrum (CD2Cl2, 202 MHz)

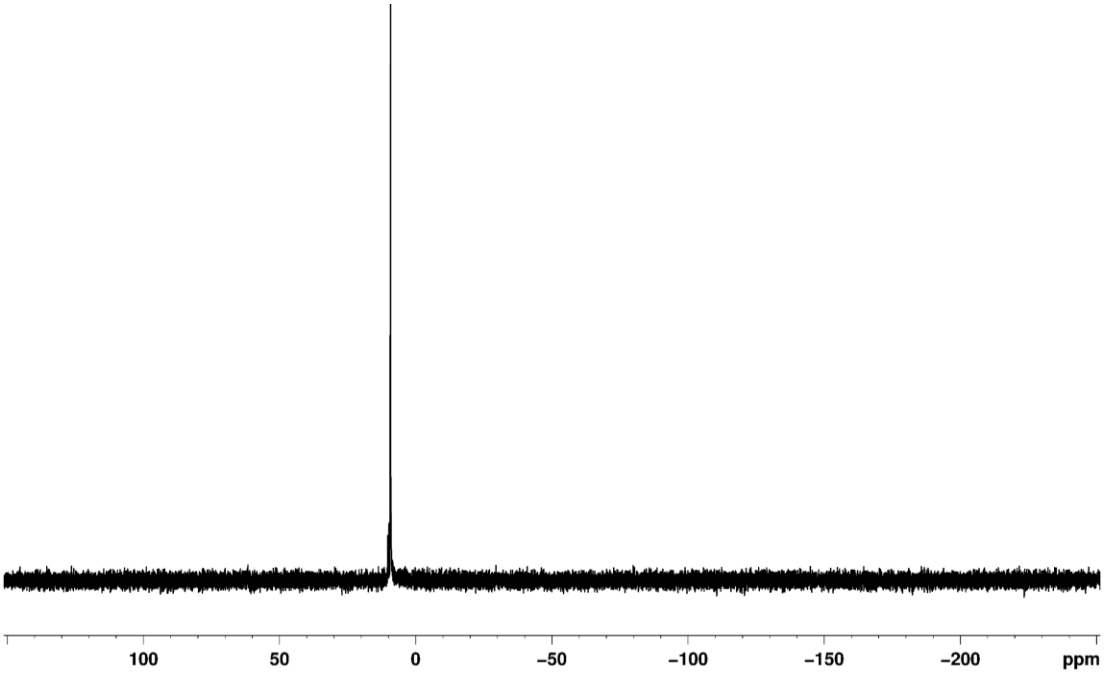

Figure 2.24, continued.

(c) $^{13}C\{^{1}H\}$ NMR spectrum with expansions (CD_2Cl_2, 125 MHz)

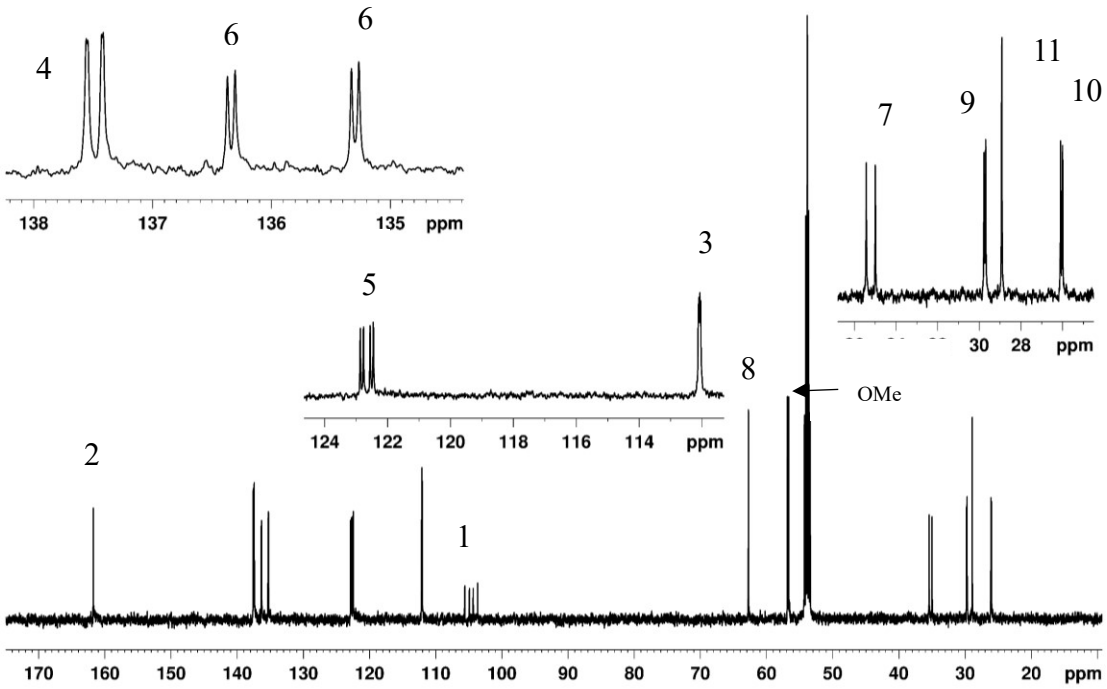

(2a)PdMe(py) (3a). Li/K[**2a**] (0.1925 g, 0.5170 mmol) and (COD)PdMeCl (0.140 g, 0.509 mmol) were dissolved in CH_2Cl_2 (20 mL) and the mixture was stirred at room temperature for 1.5 h. Pyridine (41 μL, 0.51 mmol) was added and the mixture was stirred at room temperature for 30 min. The mixture was filtered through a fine porosity frit and concentrated under vacuum to 4 mL. Pentane (40 mL) was added to precipitate the product as a white solid. The product was collected by filtration and dried under vacuum (0.22 g, 85%). The numbering scheme for **3a** is shown in Figure 2.25. ^{1}H NMR (CD_3OD), Figure 2.26(a):δ 8.76 (d, $^{3}J_{HH}$ = 3.5 Hz, 2H, H^{10}), 8.10 (t, $^{3}J_{HH}$ = 9 Hz, 2H, H^{4}), 8.02 (t, $^{3}J_{HH}$ = 7.5 Hz, 1H, H^{12}), 7.72 (t, $^{3}J_{HH}$ = 8.5 Hz, 2H, H^{2}), 7.65 (t,

$^3J_{HH}$ = 6.5 Hz, 2H, H^{11}), 7.59 (br m, 6H, 4-H^3, 2-H^2), 3.50–3.60 (m, 1H, H^6), 3.20–3.30 (m, 1H, H^5), 2.00–2.15 (m, 2H, H^7, H^9), 1.82–1.93 (m, 1H, H^9), 1.69–1.80 (m, 1H, H^8), 1.54–1.66 (m, 1H, H^7), 1.30–1.40 (m, 1H, H^8), 0.46 (s, 3H, PdCH_3). ^{13}C NMR (CD_3OD), Figure 2.26(b): δ 151.6 (2-C^{10}), 137.5 (C^4), 133.4 (C^2), 132.0 (C^{12}), 130.1 (br, 3C, C^3, 2-C^{11}), 126.6 (C^2), 62.7 (C^5), 41.1 (d, $^2J_{PC}$ = 24 Hz, C^6), 30.3 (C^7), 29.9 (C^9), 26.6 (C^8), 0.3 (PdCH$_3$). ^{31}P{^{1}H} NMR (CD_3OD), Figure 2.26(c): δ 39.9. ES-HRMS (*m/z*): Calcd. for $[C_{23}H_{26}NO_3PPdS - py + H]^+$ 455.0063, Found: 455.0063. X-ray quality crystals of **3a** were obtained by crystallization from a solution of **3a** (20 mg) in CD_3OD (0.5 mL) at room temperature. The crystallographic parameters for **3a** are shown in Table 2.2.

Figure 2.25. Numbering scheme for **3a**.

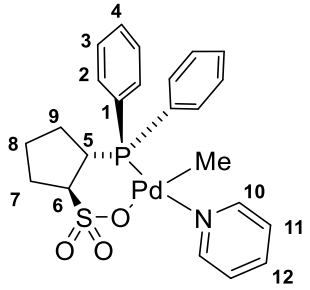

Figure 2.26. NMR spectra for **3a**.

(a)^{1}H NMR spectrum (MeOD, 500 MHz):

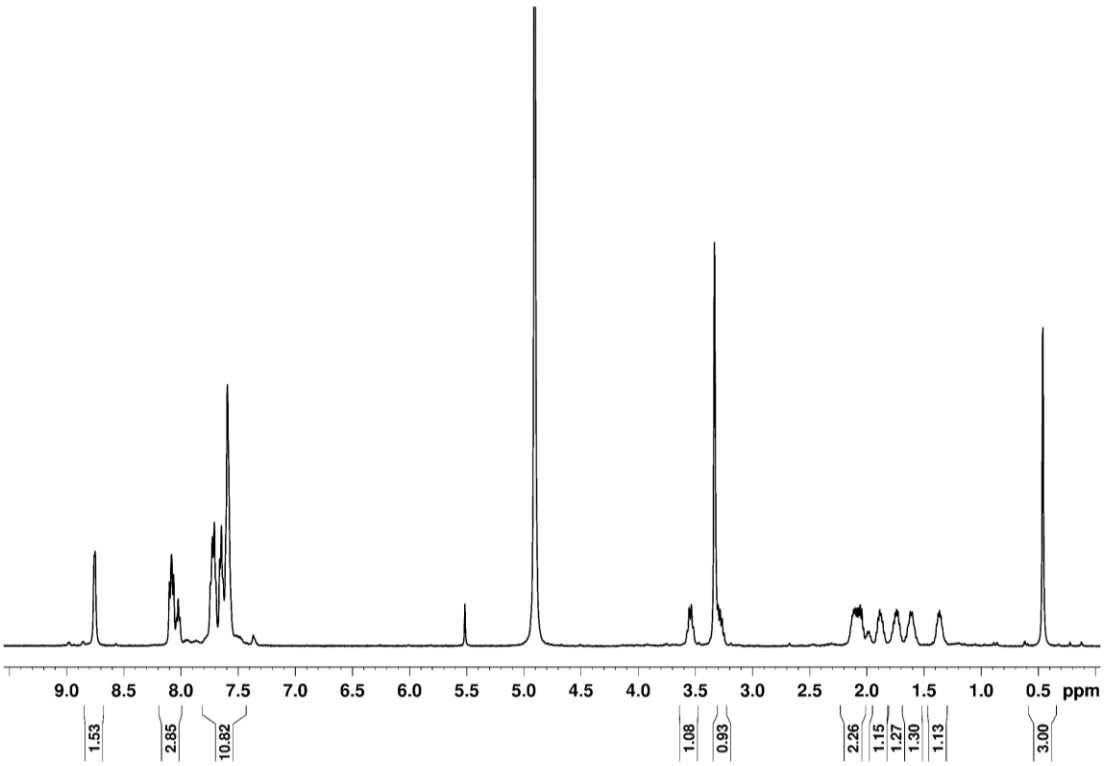

(b) ^{13}C{^{1}H} NMR spectrum (MeOD, 125 MHz)

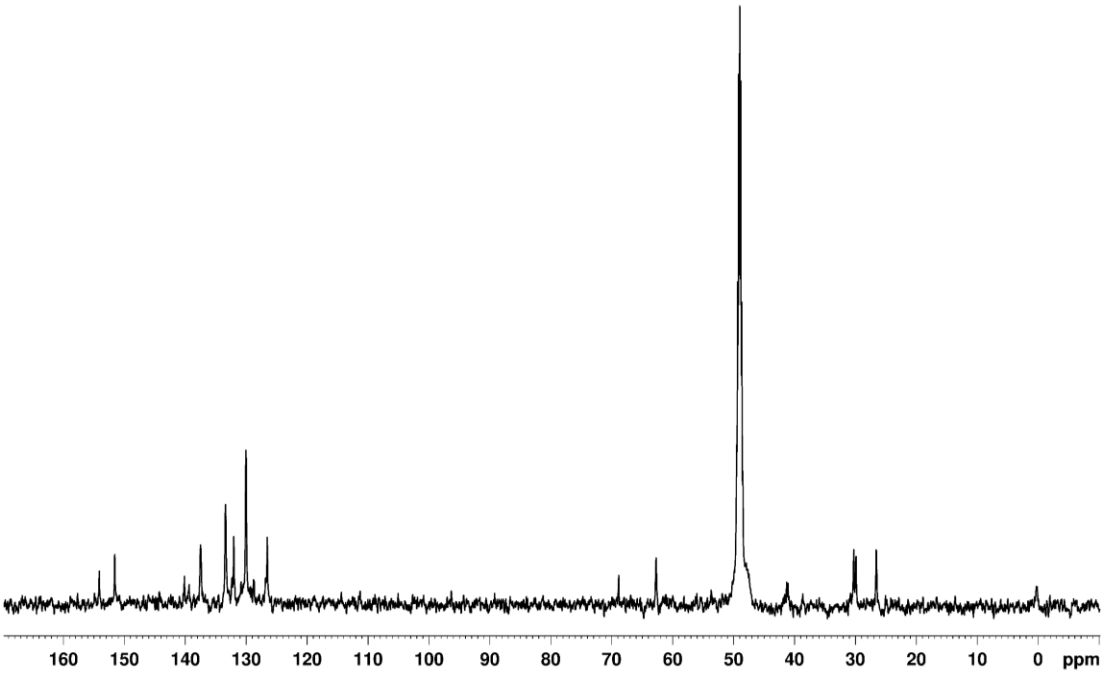

Figure 2.26, continued.

(c) $^{31}P\{^{1}H\}$ NMR spectrum (MeOD, 202 MHz)

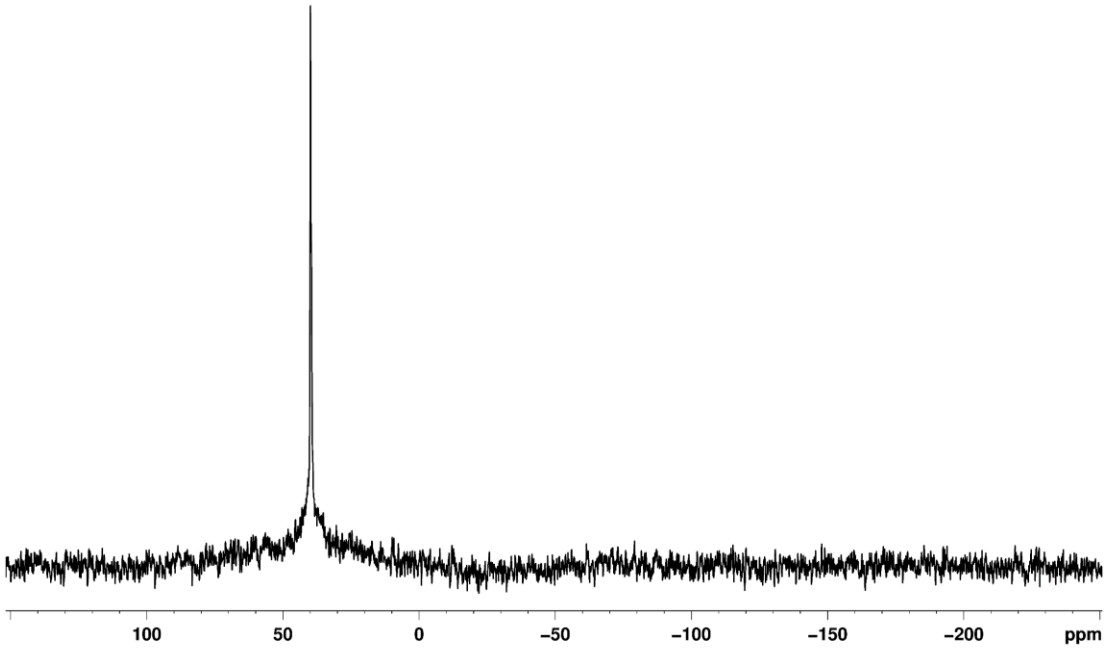

(2b)PdMe(py) (3b). H[**2b**] (0.3005 g, 0.7610 mmol) and (TMEDA)$PdMe_2$ (0.1925 g, 0.7610 mmol) were dissolved in CH_2Cl_2 (16 mL) and the mixture was stirred at room temperature for 1 h. Pyridine (92 μL, 1.2 mmol) was added and the mixture was stirred at room temperature for 30 min. The mixture was filtered through a fine porosity frit and the volatiles were removed under vacuum overnight to yield **3b** as a white solid (0.3297 g, 73%). The numbering scheme for **3b** is shown in Figure 2.27. ^{1}H NMR (CD_2Cl_2), Figure 2.28(a): δ 8.85 (d, $^{3}J_{HH}$ = 5 Hz, 2H, H^{20}), 8.50 (br s, 1H, H^{6}), 7.92 (t, $^{3}J_{HH}$ = 7.5 Hz, 1H, H^{22}), 7.64 (t, $^{3}J_{HH}$ = 8 Hz, 1H, H^{4}), 7.52 (m, $^{2}J_{HH}$ = 7.5 Hz, 3H, H^{10}, H^{21}), 7.17 (br s, H^{12}), 7.16 (t, $^{3}J_{HH}$ = 7 Hz, 1H, H^{5}), 7.06 (m, 2H, H^{9}, H^{3}), 6.98 (t, $^{3}J_{HH}$ = 7.5 Hz, 1H, H^{9}, H^{11}), 4.08 (br m, 1H, H^{14}), 3.99 (s, 3H, H^{18}), 3.82 (s, 3H, H^{19}), 3.23 (br m,

1H, H^{13}), 2.17–2.26 (m, 1H, H^{15}), 2.08–2.17 (m, 1H, H^{17}), 2.01–2.08 (m, 1H, H^{15}), 1.77–1.86 (m, 1H, H^{16}), 1.62–1.77 (m, 2H, H^{17}, H^{16}), 0.17 (d, 3H, $^{3}J_{PH}$ = 2.5 Hz, PdC*H*$_3$). $^{13}C\{^{1}H\}$ NMR (CD_2Cl_2), Figure 2.28(b): δ 160.5 (C^2), 160.0 (C^8), 150.6 (C^{20}), 139.9 (br s, C^6), 138.3 (C^{22}), 135.5 (br s, C^{12}), 133.8 (C^4), 132.7 (C^{10}), 125.0 (C^{21}), 120.8 (d, J_{PC} = 14 Hz, C^{11}), 120.7 (d, $^{3}J_{PC}$ = 10 Hz, C^5), 117.5 (d, $^{1}J_{PC}$ = 50 Hz, C^1), 115.2 (d, $^{1}J_{PC}$ = 50 Hz, C^7), 110.9 (d, $^{3}J_{PC}$ = 4 Hz, C^3), 110.5 (d, $^{3}J_{PC}$ = 5 Hz, C^9), 65.7 (d, $^{2}J_{PC}$ = 9 Hz, C^{14}), 55.3 (C^{18}), 55.1 (C^{19}), 40.9 (d, $^{1}J_{PC}$ = 32 Hz, C^{13}), 30.8 (d, $^{2}J_{PC}$ = 6 Hz, C^{17}), 29.7 (d, $^{3}J_{PC}$ = 11 Hz, C^{15}), 26.0 (d, $^{3}J_{PC}$ = 7 Hz, C^{16}), –1.0 (d, $^{2}J_{PC}$ = 4 Hz, Pd*C*H$_3$). $^{31}P\{^{1}H\}$ NMR (CD_2Cl_2), Figure 2.28(c): δ 46.3 (s). ES-HRMS (*m/z*): Calcd for $[C_{25}H_{30}NO_5PPdS - py + H]^+$ 515.027, Found: 515.026. Crystalline **3b** was obtained by slow diffusion of ether (10 mL) into a solution of **3b** (77 mg) in CH_2Cl_2 (2 mL) at –40 °C. X-ray quality crystals of **4b** were obtained by a second slow diffusion crystallization of this material at –40 °C. The crystallographic parameters for **3b** are shown in Table 2.2.

Figure 2.27. Numbering scheme for **3b**.

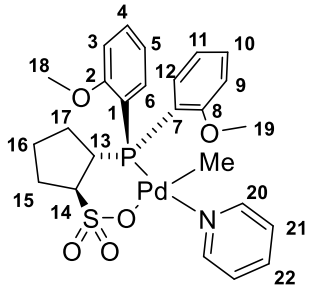

Figure 2.28. NMR spectra of **3b**.

(a)^{1}H NMR spectrum (CD_2Cl_2, 500 MHz)

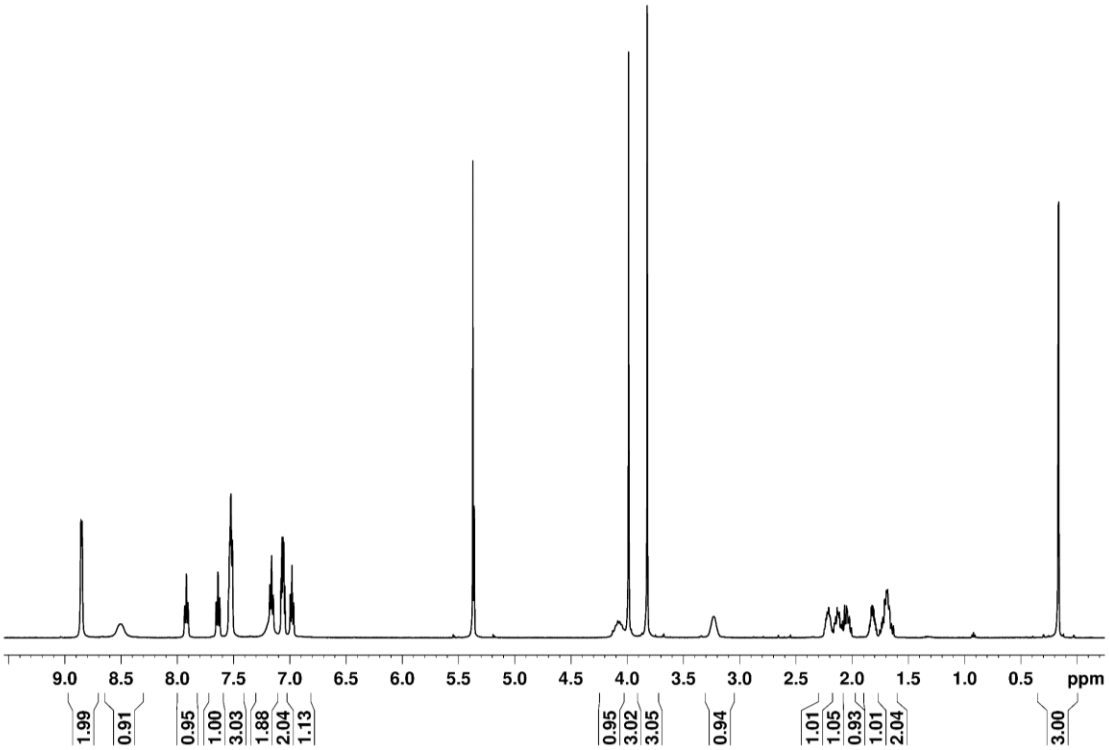

(b)^{13}C{^{1}H} NMR spectrum of **3b** (CD_2Cl_2, 125 MHz)

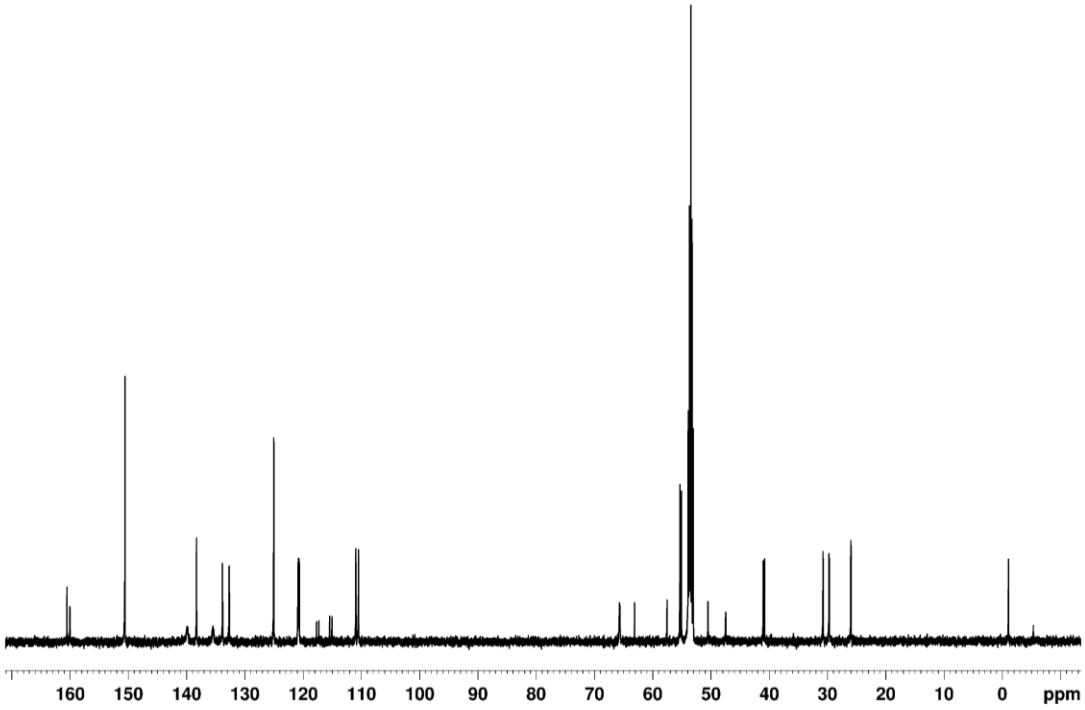

Figure 2.28, continued.

(c) ^{31}P NMR spectrum (CD_2Cl_2, 202 MHz)

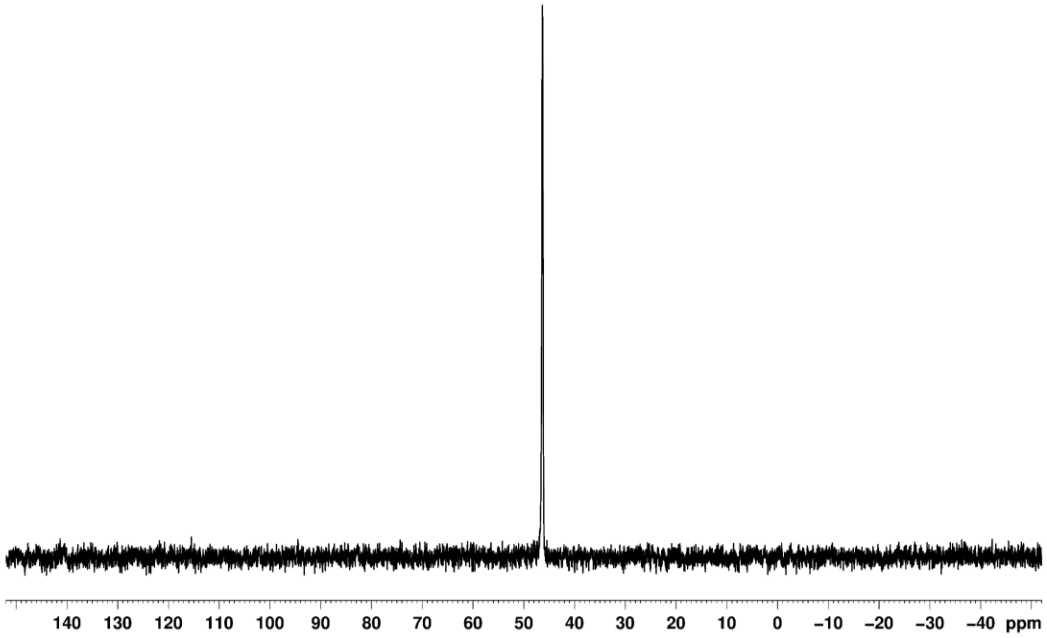

{(2b)PdMeCl(Li-THF)}$_2$. Li/K[**2b**] (0.100 g, 0.230 mmol) and (COD)PdMeCl (0.051 g, 0.19 mmol) were dissolved in CH_2Cl_2 (20 mL) and the mixture was stirred at room temperature for 1 h. Pyridine (16 μL, 0.19 mmol) was added and the mixture was stirred at room temperature for 30 min. The mixture was filtered through a fine porosity frit and concentrated under vacuum to 3 mL. Ether (40 mL) was added to precipitate the product as a yellow solid. The crude was collected by filtration and dried under vacuum to afford a mixture of Pd–Me containing compounds (by ^{1}H and ^{31}P NMR) as a yellow powder. A small amount of x-ray quality crystals of {(**2b**)PdMeCl(Li-THF)}$_2$ was obtained from a THF-d_8 (0.5 mL) solution containing this yellow powder (20 mg) that was stored at –20 °C. X-ray crystallographic data for {(**2b**)PdMeCl(Li-

THF)}$_2$ is shown in Table 2.3.

{(2b)PdMe}$_2$ (4b). **3b** (0.250 g, 0.420 mmol) and B(C_6F_5)$_3$ (0.215 g, 0.420 mmol) were dissolved in CH_2Cl_2 (12 mL) and the mixture was stirred in an aluminum foil-coated vial at room temperature for 30 min. The mixture was left to stand overnight resulting in the precipitation of a white solid. The precipitate was collected by filtration, washed with CH_2Cl_2, and dried under vacuum to yield **4b** as a white powder (0.135 g, 62%). NMR studies show that **4b** exists as a 3/1 mixture of two Pd-Me species in $CDCl_2CDCl_2$ solution. ^{1}H NMR ($CDCl_2CDCl_2$): 8.52 (Ar*H*), 7.61 (Ar*H*), 7.45 (Ar*H*), 7.20 (Ar*H*), 7.00 (Ar*H*), 6.85 (Ar*H*), 6.65 (Ar*H*), 4.49 (C5-ring C*H*), 3.98 (9.3H, –OC*H*$_3$), 3.89 (4.1H, –OC*H*$_3$), 3.72 (13.2H, –OC*H*$_3$), 3.04 (C5-ring C*H*), 2.28 (C5-ring C*H*$_2$), 2.09 (C5-ring C*H*$_2$), 1.74 (C5-ring C*H*$_2$), 1.64 (C5-ring C*H*$_2$), 0.39 (s, 3H, Pd–Me), 0.27 (s, 9.8H, PdC*H*$_3$). ^{31}P NMR ($CDCl_2CDCl_2$): δ 50.8 (br). CI/ESI-HRMS (*m/z*): Calcd. for $[C_{40}H_{50}O_{10}P_2Pd_2S_2 + H]^+$: 1029.0463, Found: 1029.0471. X-ray quality crystals of **4b**•4($C_2H_2Cl_4$) were obtained from a concentrated solution of **4b** in $CHCl_2CHCl_2$ in a sealed tube at room temperature. X-ray crystallographic parameters for **4b**•4($C_2H_2Cl_4$) are shown in Table 2.3.

Interconversion of 3b and 4b. CD_2Cl_2 (ca. 0.5 mL) was vacuum transferred into a J-Young tube containing **3b** (6.5 mg, 0.011 mmol) and the ^{1}H NMR spectrum was collected. Tris(pentafluorophenyl)borane (5.6 mg, 0.011 mmol) was added to the solution and the tube was inverted for 2 h. A white solid precipitated upon inverting the tube. The ^{1}H, ^{19}F, and ^{31}P NMR spectra were collected. Pyridine (0.8 μL, 0.011 mmol) was added and the tube was inverted several times. The white precipitate dissolved. The ^{1}H and ^{31}P NMR spectra were collected and were

identical to the spectra for isolated **3b**.

Thermal stability of 3a, 3b, and 3e in chlorobenzene. ^{1}H NMR spectra of **3a**, and **3b**, and **3e** (10 mg each) in chlorobenzene-d_5 (0.5 mL) were collected at room temperature. The J-Young sample tubes were heated at 80 °C for 1 h, cooled to room temperature, and assayed by ^{1}H NMR. The ^{1}H NMR spectra and color of the solutions containing **3b** and **3e** did not change upon heating. The solution containing **3a** became much darker yellow and Pd black precipitated. The ^{1}H NMR of **3a** also became very broad.

Thermal stability of 3b and 3e in toluene. ^{1}H NMR spectra of **3b** (10 mg) and **3e** (12 mg) in toluene-*d*$_8$ (0.5 mL) were collected at room temperature. Neither compound dissolved completely in toluene at room temperature. The samples were heated at 40 °C for 1 h, cooled to room temperature, and then the ^{1}H NMR spectra were collected. This process was repeated at 60 °C for 1 h and then an 80 °C for 1 h. The spectra were unchanged upon heating.

{(2b•B(C$_6$F$_5$)$_3$)PdMe}$_2$ (5b). *From 3b:* **3b** (0.20 g, 0.34 mmol) and B(C_6F_5)$_3$ (0.35 g, 0.67 mmol) were dissolved in CH_2Cl_2 (12 mL) and the mixture was stirred at room temperature for 2 h. The mixture was concentrated to 4 mL under vacuum, filtered through a syringe filter, and layered with hexanes (12 mL). After 7 d at room temperature, pale yellow crystals formed. The crystalline solid was collected by filtration, washed with hexanes, and dried under vacuum overnight to remove all methylene chloride (220 mg, 32%). X-ray quality crystals of **5b**•$C_2H_2Cl_4$ were obtained from a solution of this crystalline material and excess B(C_6F_5)$_3$ (ca. 2 equiv) in $CHCl_2CHCl_2$ (3 mL) that was layered with hexanes (15 mL) and stored at room temperature. X-

ray crystallographic parameters for **5b**•$C_2H_2Cl_4$ can be found in Table 2.3. ^{1}H NMR ($CDCl_2CDCl_2$): 8.21 (Ar*H*), 7.64 (Ar*H*), 7.46 (Ar*H*), 7.05 (Ar*H*), 6.88 (Ar*H*), 6.84 (Ar*H*), 6.37 (Ar*H*), 4.49 (C5-ring C*H*), 4.00 (–OC*H*$_3$), 3.75 (–OC*H*$_3$), 3.48 (C5-ring C*H*), 2.55–1.55 (C5-ring 3C*H*$_2$), 0.31 (s, 1.1H, PdC*H*$_3$), 0.11 (s, 6.2H, PdC*H*$_3$), –0.32 (s, 2H, PdC*H*$_3$). ^{31}P NMR (CD_2Cl_2): δ 51.1. CI/ESI-HRMS (*m/z*): Calcd. for $[C_{76}H_{50}B_2F_{30}O_{10}P_2Pd_2S_2 + Li]^+$: 2059.0252, Found: 2059.0730. *From **4b**:* The reaction of **4b** (0.010 g, 9.7 μmol) and $B(C_6F_5)_3$ (0.100 g, 19.4 μmol) in CD_2Cl_2 afforded **5b** quantitatively by NMR.

{(2b-B(C$_6$F$_5$)$_3$)PdMe(Et$_2$O)•Et$_2$O (6b•Et$_2$O). Crystals of **6b**•Et_2O were obtained from a concentrated Et_2O solution of **5b** at –40 °C. Drying **6b**•Et_2O under vacuum for 48 h, sublimation from a frozen benzene solution, and freeze/thaw/pumping the crystals to remove the equiv of free Et_2O resulted in significant decomposition. ^{1}H NMR (CD_2Cl_2): 7.61 (m, 2H, Ar*H*), 7.12 (m, 4H, Ar*H*), 7.06 (m, 2H, Ar*H*), 4.03 (–OC*H*$_3$), 3.33 (–OC*H*$_3$), 3.52 (free Et_2O and Pd–OEt_2), 2.15 (C5-ring 3C*H*$_2$), 1.83 (C5-ring 3C*H*$_2$), 1.65 (C5-ring 3C*H*$_2$), 1.29 (free Et_2O and Pd–OEt_2), 0.23 (s, PdC*H*$_3$). ^{31}P NMR (CD_2Cl_2): δ 49.9. ESI-HRMS (*m/z*): Calcd. for $[C_{24}H_{35}O_6PPdS + H]^+$: 1101.0854, Found: 1101.0663.

Li/K[C5-PO-^{i}Pr]. ^{n}BuLi (2.5 M in hexanes, 3.7 mL, 9.3 mmol) was added dropwise to a solution of HP^{i}Pr$_2$ (1.0 g/5 mL hexane, 8.5 mmol) in THF (15 mL) at -78 °C while the contents were stirred. The cold bath was removed and the slurry was allowed to warm to room temperature over 30 min. The yellow mixture was cooled to -20 °C (1,2-dichlorobenzene/dry ice) and added dropwise to a slurry of K[**1**] (2.28 g, 8.50 mmol) in THF (40 mL) over 10 min. The mixture was

allowed to warm to room temperature and was stirred overnight. The volatiles were removed under vacuum and the resulting yellow powder was rinsed with hexanes to remove any remaining HP^iPr_2. The resulting solid contained white powder and an orange-brown brittle solid. The white powder was not soluble in CH_2Cl_2 and was removed by filtration. The volatiles of the filtrate were taken to dryness to give an orange-brown brittle solid (0.686 g, 28% yield), which contained one major species by ^{31}P NMR (Li/K[**2c**]) but contained alkane/alkanesulfonate impurities by ^1H NMR. In the ^1H NMR (THF-d_8), overlapping signals in the aliphatic region from 3.2–1.5 correspond to the cyclopentane ring and *ipso*-Hs on the two ^{i}Pr groups. The ^{i}Pr methyl groups make up a broad multiplet centered at δ 1.1. $^{31}P\{^1H\}$ NMR (THF-d_8): δ 18.8 (s). ESI-MS (*m/z*): Calcd for $[C_{11}H_{22}PSO_3]^-$, $[M]^-$: 265, Found: 273 ($[M + Li + H]^+$). Attempts to metallate Li/K[**2c**] with (COD)PdMeCl and ligands (L = py, lut, PhPy, DMSO) led to inseparable mixtures of products.

Dimenthylphosphine oxide, (O=)HP(Men)$_2$. MenMgCl was generated by a procedure adapted from Krause, et al.[4] Dry THF (30 mL) was added to magnesium turnings (3.47 g, 0.140 mol), dibromoethane was added in one portion, and the solution was refluxed with rapid stirring. Upon heating to reflux, bubbles evolved from the mixture and the magnesium turnings lost their luster. Menthylchloride (5.4 mL, 0.029 mol) was added dropwise to the mixture and refluxed for 1 h. The mixture became gray-black. The Grignard solution was titrated with iodine (recorded amount of Grignard solution needed to quench color of 0.1 g I_2 in 1 mL THF). Three duplicate titrations were performed. The Grignard mixture (0.460 M, 30.0 mL, 0.0137 mol) was cooled to room temperature and then cooled in an ice/salt bath. Another flask containing PCl_3 (0.54 mL, 62

mmol) in hexane (40 mL) was cooled in an ice/salt bath and the Grignard mixture was added dropwise over 15 min. The mixture was stirred for 30 min and then the cold bath was removed and the mixture was allowed to come to room temperature. The mixture was assayed by ^{31}P NMR and no PCl_3 remained (^{31}P (hex/THF): δ121.7, Men_2PCl). The reaction mixture was vacuum filtered over a course frit under air to remove the MgX_2 salts. Water (15 mL) was added to the filtrate to convert Men_2PCl to $Men_2P(=O)H$. The water layer was separated from the hexanes/THF organic fraction and then extracted with CH_2Cl_2 (3 x 20 mL). The combined hexanes/THF/CH_2Cl_2 organic layers were washed with brine (15 mL), dried over MgSO4, and filtered. The solvents were removed by rotary evaporation to give an impure yellow liquid (4.55 g). $Men_2P(=O)H$ oxide was isolated as a light yellow oil by column chromatography (4:6 EA:hex as eluent, Yield: 0.866 g, 45% yield from PCl_3). Crystals grew from the neat oil upon standing for 2 d. The numbering scheme for dimenthylphosphine oxide is shown in Figure 2.29. ^{1}H NMR ($CDCl_3$): δ 6.80 ($^1J_{PH}$ = 435 Hz, $^3J_{HH}$ = 5.5 Hz, P–H), 2.69–2.59 (m, 1H, H^1), 2.25–2.18 (m, 1H, H^1), 2.00–1.90 (m, 1H), 1.81–1.72 (m, 6H), 1.72–1.59 (m, 2H), 1.57–1.48 (m, 1H), 1.45–1.33 (m, 3H), 1.15–1.02 (m, 2H), 1.00–0.90 (4 doublets, each d: $^3J_{HH}$ = 6 Hz, 12H, 2 ^{i}Pr-C*H*$_3$'s, 2 Me's), 0.90–0.86 (m, 2H), 0.86–0.81 (d, $^3J_{HH}$ = 6 Hz, 3H, 1 ^{i}Pr-C*H*$_3$), 0.81–0.78 (d, 3H, $^3J_{HH}$ = 6 Hz, ^{i}Pr-C*H*$_3$). ^{13}C{^{1}H} NMR ($CDCl_3$): δ 44.6 (d, $^2J_{PC}$ = 3 Hz, C^2), 41.4 (d, $^2J_{PC}$ = 3 Hz, C^2), 37.0 (d, $^1J_{PC}$ = 63 Hz, C^1), 36.5 (d, $^1J_{PC}$ = 63 Hz, C^1), 34.4 (s, 2 C^4), 34.3 (d, $^2J_{PC}$ = 6 Hz, C^6), 32.7 (d, $^3J_{PC}$ = 3.5 Hz, C^5), 32.6 (d, $^3J_{PC}$ = 3 Hz, C^5), 32.3 (d, $^2J_{PC}$ = 4 Hz, C^6), 28.3 (d, $^3J_{PC}$ = 2 Hz, C^7), 27.4 (d, $^3J_{PC}$ = 5 Hz, C^7), 24.6 (d, $^3J_{PC}$ = 12 Hz, C^3), 24.2 (d, $^3J_{PC}$ = 11 Hz, C^3), 22.6 (s, -*C*H$_3$), 22.5 (s, -*C*H$_3$), 21.6 (s, -*C*H$_3$), 21.4 (s, -*C*H$_3$), 15.7 (s, -

CH_3), 15.5 (s, -CH_3). $^{31}P\{^1H\}$ NMR (THF-d_8): δ 42.3 (s).

Figure 2.29. Numbering scheme for dimenthylphosphine oxide.

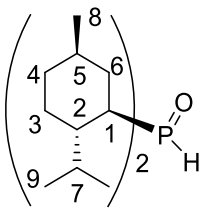

$Men_2P–PMen_2$. Attempted reduction of $H(O)PMen_2$ to $HPMen_2$ gave diphosphine $Men_2P–PMen_2$ as the major product. A solution of NEt_3 (1.0 mL, 7.4 mmol) and $H(O)PMen_2$ (0.801 g, 2.45 mmol) in anhydrous acetonitrile (50 mL) was degassed by bubbling N_2 through the solution for 20 min. $HSiCl_3$ (0.74 mL, 7.4 mmol) was added dropwise at room temperature. White precipitate formed. The mixture was stirred and refluxed for 4 h. A ^{31}P NMR assay of the reaction mixture (NEt_3/ acetonitrile) showed a single species (δ –44). The solution was allowed to come to room temperature and then cooled in an ice bath. White solid precipitated from the yellow solution. A solution of KOH (5.0 g) in water (20 mL) was degassed by N_2 bubbling and added dropwise while the mixture was stirred. The top, yellow acetonitrile layer was transferred to another Schlenk flask and the aqueous layer was extracted with acetonitrile (3 x 15 mL). The combined acetonitrile layers were dried under vacuum to afford a pale-pink solid. This material was suspended in anhydrous and degassed EtOH (10 mL total), collected by filtration, and dried under vacuum to give a white solid (0.053 g, 3% yield, used for characterization). The EtOH was evaporated to give

more of the product that was clean by ^{31}P NMR, but which contained many impurities by ^{1}H NMR. No further purification was performed. ^{1}H NMR (CD_2Cl_2): δ 2.99–2.89 (m, 2H), 2.81–2.71 (m, 2H), 2.4–2.28 (m, 4H), 1.8–1.68 (m, 8H), 1.68–1.56 (m, 2H), 1.56–1.42 (m, 4H), 1.42–1.31 (m, 2H), 1.3–1.18 (m, 4H), 1.18–1.0 (m, 12H), 0.97–0.85 (4 doublets, each d: $^{3}J_{HH}$ = 6.5 Hz, 24H), 0.75–0.69 (2 d, $^{3}J_{HH}$ = 6.5 Hz, 12H). ^{31}P{^{1}H} NMR (CD_2Cl_2): δ –42.1 (s). ESI–MS (*m/z*): Calcd for $C_{40}H_{76}P_2$, M: 618, Found: 619 (positive scan, $[M + H]^+$).

PH(=O)(2,6-dimethoxybiphenyl)$_2$, H(O)PBp$_2$. 2'-bromo-2,6-dimethoxybiphenyl (4.50 g, 15.0 mmol) was dissolved in ether (60 mL). ^{n}BuLi solution (2.5 M in hexanes, 6.8 mL, 17 mmol) was added dropwise at room temperature and the mixture was stirred for 1 h. White solid precipitated from the solution. The white precipitate (LiBp) was collected by filtration, washed with ether, and dried. LiBp (15 mmol) was partially dissolved in 60 mL THF and added dropwise over 30 min to a solution of PCl_3 (0.5 mL, 6 mmol) in THF (20 mL) at room temperature. The LiBp completely dissolved upon addition to the PCl_3 solution and the homogenous solution transitioned from light yellow to dark yellow during the addition. The reaction mixture was assayed after 1 h (^{31}P NMR (ether/THF): one signal at δ 81.5, $ClPBp_2$). HCl (1M, 20 mL) was degassed by N_2 bubbling and added dropwise to the solution of $ClPBp_2$. The mixture was stirred overnight. Under air, CH_2Cl_2 (30 mL) was added. The organic fraction was separated and washed twice with water (2 x 10 mL). The organic layer was dried over $MgSO_3$, filtered, and dried on a rotary evaporator. The crude solid was suspended in 100 mL ether to dissolve 2,6-dimethoxybiphenyl and the product was collected by filtration (Yield: 2.656 g, 97% yield from

PCl_3). X-ray quality crystals were grown by layering ether on a concentrated CH_2Cl_2 solution of this solid. The crystallographic data and structure refinement parameters are shown in Table 2.3. The numbering scheme for H(O)PBp$_2$ is shown in Figure 2.30. ^{1}H NMR ($CDCl_3$): δ 7.37 ($^1J_{PH}$ = 497 Hz, P*H*), 7.52–7.42 (t, $^3J_{HH}$ = 7 Hz, 2H^4), 7.38–7.3 (t, $^3J_{HH}$ = 8 Hz, 2H^{10}), 7.26–7.18 (t, $^3J_{HH}$ = 7.5 Hz, 2H^5), 7.15–7.08 (m, 2H^3), 7.08–7.0 (dd, $^3J_{HH}$ = 7.5 Hz, 2H^6), 6.58–6.45 (t, $^3J_{HH}$ = 8 Hz, 2H^9, 2H^{11}), 3.42 (3H, –OC*H*$_3$), 3.38 (3H, –OC*H*$_3$). ^{13}C{^{1}H} NMR (CDC_3): δ 158.5 (s, C$^{8/12}$), 157.4 (s, C$^{8/12}$), 138.5 (d, $^1J_{PC}$ = 10 Hz, C^1), 132.4 (d, J_{PC} = 12 Hz, C^6), 131.4 (s, 3C, C$^{2,\ 3,\ \text{and}\ 4}$), 129.7 (s, C^{10}), 126.4 (d, $^3J_{PC}$ = 13 Hz, C^5), 116.2 (s, C^7), 104.0 (s, C$^{9/11}$), 103.2 (s, C$^{9/11}$), 55.3 (s, –O*C*H$_3$), 55.2 (s, –O*C*H$_3$). ^{31}P{^{1}H} NMR (CD_2Cl_2): δ 42.3 (s). ^{31}P–^{1}H NMR (CD_2Cl_2): δ 42.3 (d, $^1J_{PH}$ = 495 Hz).

Figure 2.30. Numbering scheme for PH(=O)(2,6-dimethoxybiphenyl)$_2$.

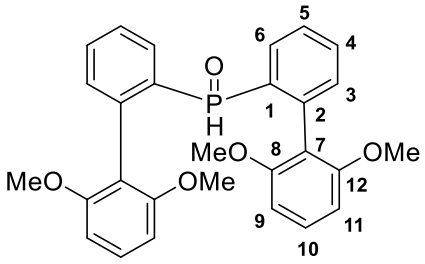

PH(2,6-dimethoxybiphenyl)$_2$, HPBp$_2$. A solution of NEt_3 (1.76 mL, 17.4 mmol) and H(O)PBp$_2$ (2.66 g, 5.60 mmol) in anhydrous acetonitrile (120 mL) was degassed by bubbling N_2 through the solution for 20 min. $HSiCl_3$ (0.74 mL, 7.4 mmol) was added dropwise at room temperature. White precipitate formed. The mixture was stirred and refluxed overnight. The bright

orange-yellow mixture was assayed by ^{31}P NMR (60% δ -40.8 $NEt_3H[PBp_2]$, 40% δ -57 target). The solution was allowed to cool to room temperature and then cooled in an ice bath. White solid precipitated. A solution of KOH (20 g) in water (20 mL) was degassed by N_2 bubbling and *added dropwise* while the mixture was stirred (Caution: this process is very exothermic and generated many bubbles). The mixture became light yellow upon adding the first drop of KOH water. The yellow acetonitrile layer was transferred to another Schlenk flask and the volatiles were removed (Yield 0.38 g white solid that was 2/3 $HPBp_2$ and 1/3 $H(O)PBp_2$). The aqueous layer was extracted with CH_2Cl_2 (3 x 15 mL) and the CH_2Cl_2 was removed under vacuum to afford a pale yellow solid. This material was suspended in degassed anhydrous EtOH (3 x 5 mL), collected by filtration, and dried under vacuum to give a white solid (1.34 g, 52% yield). ^{1}H NMR (CD_2Cl_2): δ 7.33 (br s), 7.28 (br s), 7.23 (br s), 7.14 (br s), 6.64 (br s), 4.6 ($^1J_{PH}$ = 600 Hz, P*H*), 3.67 (3H, –OC*H*$_3$), 3.62 (3H, –OC*H*$_3$). ^{31}P{^{1}H} NMR (CD_2Cl_2): δ –58.5 (s).

(2-{2,6-dimethoxybiphenyl})$_2$P–P(2-{2,6-dimethoxybiphenyl})$_2$, Bp$_2$P–PBp$_2$. Attempted lithiation of $HPBp_2$ gave diphosphine $Bp_2P–PBp_2$ as the major product. There is precedent in the literature of the reduction of sterically crowded dialkylphosphorous halides to radical species that dimerize to diphosphines.[5] ^{n}BuLi solution (2.2 mL, 0.88 mmol) was added dropwise to a hexane (40 mL) solution of $HPBp_2$ (0.33 g, 0.72 mmol). The bright yellow mixture was stirred for 1 h at room temperature (^{31}P NMR assay: single species, δ –43.3 $LiPBp_2$). This solution was added *dropwise over 1 h* to a slurry of Li/K[**1**] (0.19 g, 0.72 mmol) in THF (20 mL). The mixture was orange-brown after addition and became dark red upon 1 h of stirring. The

volatiles were removed under vacuum, and the resulting red solid was brought into the glovebox, dissolved in CH_2Cl_2 (20 mL), and filtered to remove the LiBr and KBr salts. The volatiles were removed from the filtrate to yield a yellow powder (0.42 g), which contained K[**1**] and the title compound. $Bp_2P–PBp_2$ was isolated by dissolution in THF and filtering off Li/[**1**]. The volatiles of the filtrate were removed to afford $Bp_2P–PBp_2$ as a white powder (0.32 g, 48% from $LiPBp_2$). ^1H NMR (THF-d_8): δ 8.44 (d, $^3J_{HH}$ = 8 Hz, 1H), 7.38 (t, 1H), 7.25 (m, 1H), 7.12 (q, 2H), 7.02 (m, 3H), 6.93 (d, $^3J_{HH}$ = 12 Hz, 2H), 6.88 (br d, 1H), 6.79 (t, $^3J_{HH}$ = 7 Hz, 1H), 6.69 (d, $^3J_{HH}$ = 10 Hz, 2H), 6.43 (m, 1H), 3.95 (s, 3H, –OC*H*$_3$), 3.79 (s, 3H, –OC*H*$_3$), 3.78 (s, 3H, –OC*H*$_3$), 3.59 (s, 3H, –OC*H*$_3$). $^{31}P\{^1H\}$ NMR (CD_2Cl_2): δ –58.5 (s).

X-ray Crystallography. Data were measured on a Bruker D8 VENTURE diffractometer using a PHOTON 100 CMOS detector system equipped with a Mo-target micro-focus X-ray tube and Kα radiation (0.71073 Å). Direct methods were used to locate many atoms from the E-map. Repeated difference Fourier maps enabled location of all expected non-hydrogen atoms. Following anisotropic refinement of all non-H atoms, ideal H atom positions were calculated. Final refinement was anisotropic for all non-H atoms and isotropic-riding for H atoms. ORTEP diagrams are drawn with 50 % probability ellipsoids.

Table 2.2. Crystal data and structure refinement for [K(18-crown-6)][**1**], P(=O)H(2-OMe-Ph)$_2$, **3a**, and **3b**•CH_2Cl_2.

	[K(18-crown-6)][**1**]	P(=O)H(2-OMe-Ph)$_2$	(**2a**)PdMe(py), **3a**	(**2b**)PdMe(py)•CH_2Cl_2 (**3b**•CH_2Cl_2)
Identification code	0089_black_a	tw4ful_a	0080_bl	0130_black
CCDC deposition Nº	1557505	1557503	1557504	1557502
Empirical formula	$C_{17}H_{32}BrKO_9S$	$C_{14}H_{15}O_3P$	$C_{23}H_{26}NO_3PPdS$	$C_{26}H_{32}Cl_2NO_5PPdS$
Formula weight	531.49	262.23	533.88	678.85
Temperature (K)	100(2)	100(2)	100(2)	100(2)
Crystal system	Triclinic	monoclinic	triclinic	monoclinic
Space group	P-1	$P2_1/c$	P-1	$P2_1/c$
a (Å)	8.6727(7)	8.0582(5)	10.6642(14)	9.2922(5)
b (Å)	8.9433(8)	20.4060(12)	10.9186(14)	25.9157(12)
c (Å)	14.8064(13)	8.4524(5)	11.1022(14)	12.2400(6)
α (°)	85.750(2)	90	72.600(3)	90
β (°)	87.106(2)	116.482(2)	63.320(3)	104.850(2)
γ (°)	80.364(2)	90	84.527(3)	90
Volume (Å^3)	1128.26(17)	1244.04(13)	1101.1(2)	2849.1(2)
Z	2	4	2	4
Density (calculated, Mg/m3)	1.564	1.4	1.61	1.583
Absorption coefficient (mm^{-1})	2.143	0.218	1.035	1.005
F(000)	552	552	544	1384
Crystal size (mm^3)	0.140x0.100x0.040	0.32×0.24x0.16	0.14×0.06×0.04	0.16×0.1x0.06
Radiation	MoKα (λ = 0.71073)	MoKα	MoKα	MoKα
Theta range for collection (°)	2.315 to 26.150°	5.648 to 54.21	4.522 to 55.164	4.534 to 57.526
Index ranges	-10 ≤ h ≤ 10, -11 ≤ k ≤ 11, -18 ≤ l ≤ 18	-10 ≤ h ≤ 8, 0 ≤ k ≤ 26, 0 ≤ l ≤ 10	-12 ≤ h ≤ 13, -13 ≤ k ≤ 14, 0 ≤ l ≤ 14	-12 ≤ h ≤ 12, -34 ≤ k ≤ 35, -15 ≤ l ≤ 16

Table 2.2, continued.

Reflections collected	18500	2555	5028	48314
Independent reflections	4495 [R(int) = 0.0433]	2555 [R_{int} = 0.0351, R_{sigma} = 0.0342]	5028 [R_{int} = 0.0431, R_{sigma} = 0.0310]	7205 [R_{int} = 0.0607, R_{sigma} = 0.0578]
Data / restraints / parameters	4495 / 0 / 262	2555/0/169	5028/0/273	7205/0/337
Goodness-of-fit on F^2	1.042	1.08	1.066	1.017
Final R indices [I>2sigma(I)]	R1 = 0.0476, wR2 = 0.1095	R_1 = 0.0403, wR_2 = 0.0812	R_1 = 0.0268, wR_2 = 0.0554	R_1 = 0.0394, wR_2 = 0.0770
R indices (all data)	R1 = 0.0665, wR2 = 0.1176	R_1 = 0.0548, wR_2 = 0.0866	R_1 = 0.0325, wR_2 = 0.0576	R_1 = 0.0753, wR_2 = 0.0875
Largest diff. peak and hole ($e.Å^{-3}$)	1.595 and -0.474	0.30/-0.38	0.55/-0.44	0.79/-0.82

Table 2.3. Crystal data and structure refinement for {[Li(THF)][(**2b**)PdMeCl]}$_2$, **4b**•4($C_2H_2Cl_4$), **5b**•$C_2H_2Cl_4$, and PH(=O)Bp_2.

	{[Li(THF)][(**2b**)PdMeCl]}$_2$	{(**2b**)PdMe}$_2$•4($C_2H_2Cl_4$), **4b**•4($C_2H_2Cl_4$)	{(**2b**•B(C_6F_5)$_3$)PdMe}$_2$• $C_2H_2Cl_4$, **5b**•$C_2H_2Cl_4$	PH(=O)(2,6-dimethoxybiphenyl)$_2$
Identification code	0105_black	0370_black	aps_br1	0313_black
CCDC deposition Nº	1557509	1557506	1557507	
Empirical formula	$C_{48}H_{66}Cl_2Li_2O_{12}P_2Pd_2S_2$	$C_{48}H_{58}Cl_{16}O_{10}P_2Pd_2S_2$	$C_{78}H_{52}B_2Cl_4F_{30}O_{10}P_2Pd_2S_2$	$C_{28}H_{27}O_5P$
Formula weight	1258.64	1701	2221.47	474.46
Temperature (K)	100(2)	100(2)	195	100(2)
Crystal system	monoclinic	triclinic	triclinic	tetragonal
Space group	C2/c	P-1	P-1	$I4_1/a$
a (Å)	29.5251(17)	9.5265(8)	10.0959(12)	14.3826(12)
b (Å)	11.9106(7)	14.0160(12)	13.6561(14)	14.3826(12)

Table 2.3, continued.

c (Å)	15.4762(9)	25.532(2)	16.6519(15)	22.764(2)
α (°)	90	84.037(2)	69.505(7)	90
β (°)	104.5375(14)	89.631(2)	88.116(5)	90
γ (°)	90	74.743(2)	80.207(4)	90
Volume ($Å^3$)	5268.1(5)	3270.4(5)	2118.3(4)	4709.0(9)
Z	4	2	1	8
Density (calculated, Mg/m3)	1.587	1.727	1.741	1.338
Absorption coefficient (mm^{-1})	0.983	1.368	0.669	0.155
F(000)	2576	1704	1102	2000.0
Crystal size (mm^3)	0.32 × 0.22 × 0.14	0.21 × 0.15 × 0.12	0.02 × 0.015 × 0.015	0.32 × 0.16 × 0.14
Radiation	MoKα (λ = 0.71073)	MoKα (λ = 0.71073)	synchrotron (λ = 0.41328)	MoKα (λ = 0.71073)
Theta range for data collection (°)	4.378 to 59.21	4.172 to 50.182	3.038 to 31	5.372 to 52.828
Index ranges	-40 ≤ h ≤ 40, -16 ≤ k ≤ 16, -20 ≤ l ≤ 21	-11 ≤ h ≤ 11, -16 ≤ k ≤ 16, -30 ≤ l ≤ 29	-13 ≤ h ≤ 13, -17 ≤ k ≤ 13, -21 ≤ l ≤ 19	-17 ≤ h ≤ 16, -17 ≤ k ≤ 15, -28 ≤ l ≤ 28
Reflections collected	91456	47518	47490	21579
Independent reflections	6926 [R_{int} = 0.0314, R_{sigma} = 0.0191]	11616 [R_{int} = 0.0660, R_{sigma} = 0.0659]	8592 [R_{int} = 0.0673, R_{sigma} = 0.0544]	2413 [R_{int} = 0.0568, R_{sigma} = 0.0362] –
Data / restraints / parameters	6926/0/319	11616/387/833	8592/3/609	2413/2/164
Goodness-of-fit on F^2	1.024	1.037	1.027	1.096
Final R indices [I>2sigma(I)]	R_1 = 0.0288, wR_2 = 0.0673	R_1 = 0.0671, wR_2 = 0.1521	R_1 = 0.0385, wR_2 = 0.0926	R_1 = 0.0880, wR_2 = 0.1848
R indices (all data)	R_1 = 0.0376, wR_2 = 0.0712	R_1 = 0.1082, wR_2 = 0.1721	R_1 = 0.0540, wR_2 = 0.0990	R_1 = 0.1017, wR_2 = 0.1907
Largest diff. peak/hole ($e.Å^{-3}$)	1.70/-0.53	2.02/-1.47	0.60/-0.81	0.26/-0.29

2.5 References and Notes

(1) Nakamura, A.; Ito, S.; Nozaki, K. *Chem. Rev.* **2009**, *109*, 5215.

(2) Ito, S.; Nozaki, K. *Chem. Rec.* **2010**, *10*, 315.

(3) Nakamura, A.; Anselment, T. M. J.; Claverie, J.; Goodall, B.; Jordan, R. F.; Mecking, S.; Rieger, B.; Sen, A.; van Leeuwen, P. W. N. M.; Nozaki, K. *Acc. Chem. Res.* **2013**, *46*, 1438.

(4) Franssen, N. M. G.; Reek, J. N. H.; de Bruin, B. *Chem. Soc. Rev.* **2013**, *42*, 5809.

(5) Drent, E.; van Dijk, R.; van Ginkel, R.; van Oort, B.; Pugh, R. I. *Chem. Commun.* **2002**, 744.

(6) Guironnet, D.; Roesle, P.; Rünzi, T.; Göttker-Schnetmann, I.; Mecking, S. *J. Am. Chem. Soc.* **2009**, *131*, 422.

(7) Kochi, T.; Nakamura, A.; Ida, H.; Nozaki, K. *J. Am. Chem. Soc.* **2007**, *129*, 7770.

(8) Luo, S.; Vela, J.; Lief, G. R.; Jordan, R. F. *J. Am. Chem. Soc.* **2007**, *129*, 8946.

(9) Ito, S.; Munakata, K.; Nakamura, A.; Nozaki, K. *J. Am. Chem. Soc.* **2009**, *131*, 14606.

(10) Weng, W.; Shen, Z.; Jordan, R. F. *J. Am. Chem. Soc.* **2007**, *129*, 15450.

(11) Leicht, H.; Göttker-Schnetmann, I.; Mecking, S. *Angew. Chem. Int. Ed.* **2013**, *52*, 3963.

(12) Borkar, S.; Newsham, D. K.; Sen, A. *Organometallics* **2008**, *27*, 3331.

(13) Skupov, K. M.; Piche, L.; Claverie, J. P. *Macromolecules* **2008**, *41*, 2309.

(14) Ota, Y.; Ito, S.; Kuroda, J.; Okumura, Y.; Nozaki, K. *J. Am. Chem. Soc.* **2014**, *136*, 11898.

(15) Jian, Z.; Wucher, P.; Mecking, S. *Organometallics* **2014**, *33*, 2879.

(16) Contrella, N. D.; Sampson, J. R.; Jordan, R. F. *Organometallics* **2014**, *33*, 3546.

(17) Neuwald, B.; Falivene, L.; Caporaso, L.; Cavallo, L.; Mecking, S. *Chem. Eur. J.* **2013**, *19*, 17773.

(18) Neuwald, B.; Caporaso, L.; Cavallo, L.; Mecking, S. *J. Am. Chem. Soc.* **2013**, *135*, 1026.

(19) Wada, S.; Jordan, R. F. *Angew. Chem. Int. Ed.* **2017**, *56*, 1820.

(20) Britovsek, George J. P.; Gibson, V. C.; Wass, D. F. *Angew. Chem. Int. Ed.* **1999**, 428.

(21) Gibson, V. C.; Spitzmesser, S. K. *Chem. Rev.* **2003**, *103*, 283.

(22) Piche, L.; Daigle, J. C.; Rehse, G.; Claverie, J. P. *Chem. Eur. J.* **2012**, *18*, 3277.

(23) Piche, L.; Daigle, J.-C.; Poli, R.; Claverie, J. P. *Eur J Inorg Chem* **2010**, *2010*, 4595.

(24) Wucher, P.; Goldbach, V.; Mecking, S. *Organometallics* **2013**, *32*, 4516.

(25) Jover, J.; Fey, N.; Harvey, J. N.; Lloyd-Jones, G. C.; Orpen, A. G.; Owen-Smith, G. J. J.; Murray, P.; Hose, D. R. J.; Osborne, R.; Purdie, M. *Organometallics* **2010**, *29*, 6245.

(26) Replacement of the arene linker with an alkane linker will enhance the donor ability of the phosphine and sulfonate group. The Tolman electronic parameter for P(2-OMe-Ph)$_2$(*m*-tolyl) (2061.6 cm^{-1}) is larger than that for P(2-OMe-Ph)$_2$Cy (2058 cm^{-1}). Alkanesulfonates are 1 to 2 pK_a units more basic than aryl sulfonates (e.g. pK_a: PhSO$_3$H –2.8, EtSO$_3$H –1.8). A small alkane linker should not exert significant steric effects, while a bulky alkane linker may influence the conformation of the –PR$_2$ units.

(27) Paetzold, E.; Kinting, A.; Oehme, G. *J. Prakt. Chem.* **1987**, *329*, 725.

(28) Ganguly, S.; Mague, J. T.; Roundhill, D. M. *Inorg. Chem.* **1992**, *31*, 3500.

(29) García Suárez, E. J.; Ruiz, A.; Castillón, S.; Oberhauser, W.; Bianchini, C.; Claver, C. *Dalton Trans.* **2007**, 2859.

(30) Lu, J.; Ye, J.; Duan, W.-L. *Org. Lett.* **2013**, *15*, 5016.

(31) Bettucci, L.; Bianchini, C.; Claver, C.; Suarez, E. J. G.; Ruiz, A.; Meli, A.; Oberhauser, W. *Dalton Trans.* **2007**, 5590.

(32) Feng, G.; Conley, M. P.; Jordan, R. F. *Organometallics* **2014**, *33*, 4486.

(33) Rotation around the C–S bond before recoordination will permute the Pd-coordinated and

terminal oxygens.

(34) Noda, S.; Nakamura, A.; Kochi, T.; Chung, L. W.; Morokuma, K.; Nozaki, K. *J. Am. Chem. Soc.* **2009**, *131*, 14088.

(35) Conley, M. P.; Jordan, R. F. *Angew. Chem. Int. Ed.* **2011**, *50*, 3744.

(36) Cai, Z.; Shen, Z.; Zhou, X.; Jordan, R. F. *ACS Catal.* **2012**, *2*, 1187.

(37) Bakker, B.; Cerfontain, H.; Tomassen, H. *J. Org. Chem.* **1989**, *54*, 1680.

(38) Wife, R. L.; Van Oort, A. B.; Van Doorn, J. A.; Van Leeuwen, P. W. N. M. *Synthesis* **1983**, *1983*, 71.

(39) Aspinall, H. C.; Moore, S. R.; Smith, A. K. *J. Chem. Soc., Dalton Trans.* **1993**, 993.

(40) Bianchini, C.; Lenoble, G.; Oberhauser, W.; Parisel, S.; Zanobini, F. *Eur. J. Inorg. Chem.* **2005**, *2005*, 4794.

(41) Aspinall, H. C.; Tillotson, M. R. *Inorg. Chem.* **1996**, *35*, 5.

(42) Miljkovic, M. In *Carbohydrates: Synthesis, Mechanisms, and Stereoelectronic Effects*; Springer: New York, 2009; pp. 169–190.

(43) Newsham, D. K.; Borkar, S.; Sen, A.; Conner, D. M.; Goodall, B. L. *Organometallics* **2007**, *26*, 3636.

(44) The N–Pd–O angles in **3a,b** are 2–4° larger and the O–Pd–P angles are 2–4° smaller than in **3c,d**.

(45) Howell, J. A. S.; Palin, M. G.; Yates, P. C.; McArdle, P.; Cunningham, D.; Goldschmidt, Z.; Gottlieb, H. E.; Hezroni-Langerman, D. *J. Chem. Soc., Perkin Trans. 2* **1992**, 1769.

(46) Howell, J. A. S.; Fey, N.; Lovatt, J. D.; Yates, P. C.; McArdle, P.; Cunningham, D.; Sadeh, E.; Gottlieb, H. E.; Goldschmidt, Z.; Hursthouse, M. B.; Light, M. E. *J. Chem. Soc., Dalton Trans.* **1999**, 3015.

(47) Another metric that can be used to compare the puckering in **3a** and **3d** is the distance between the O–Pd–P plane and the S atom and two C atoms within the chelate ring. These

distances are as follows: **3a**: 1.030, 1.661, and 0.507 Å; **3c**: 0.565, –0.477, and –0.656 Å; **3b**: 1.099, 1.964, and 1.032 Å; **3d**: 0.485, –0.518, and –0.654 Å. These data confirm that the chelate rings of **3a,b** are more puckered than those in **3c,d**.

(48) Sundquist, W. I.; Bancroft, D. P.; Lippard, S. J. *J. Am. Chem. Soc.* **1990**, *112*, 1590.

(49) Mukhopadhyay, A.; Pal, S. *Eur. J. Inorg. Chem.* **2006**, *2006*, 4879.

(50) Buckingham, A. D.; Stephens, P. J. *J. Chem. Soc.* **1964**, 4583.

(51) Miller, R. G.; Stauffer, R. D.; Fahey, D. R.; Parnell, D. R. *J. Am. Chem. Soc.* **1970**, *92*, 1511.

(52) Brookhart, M.; Green, M. L. H.; Parkin, G. *Proc. Natl. Acad. Sci. USA* **2007**, *104*, 6908.

(53) Zhang, Y.; Lewis, J. C.; Bergman, R. G.; Ellman, J. A.; Oldfield, E. *Organometallics* **2006**, *25*, 3515.

(54) Lau, K.-C.; Petro, B. J.; Bontemps, S.; Jordan, R. F. *Organometallics* **2013**, *32*, 6895.

(55) Wucher, P.; Roesle, P.; Falivene, L.; Cavallo, L.; Caporaso, L.; Göttker-Schnetmann, I.; Mecking, S. *Organometallics* **2012**, *31*, 8505.

(56) Wucher, P.; Caporaso, L.; Roesle, P.; Ragone, F.; Cavallo, L.; Mecking, S.; Göttker-Schnetmann, I. *Proc. Natl. Acad. Sci. USA* **2011**, *108*, 8955.

(57) Rünzi, T.; Guironnet, D.; Göttker-Schnetmann, I.; Mecking, S. *J. Am. Chem. Soc.* **2010**, *132*, 16623.

(58) Still, W. C.; Galynker, I. *Tetrahedron* **1981**, *37*, 3981.

(59) Anet, F. A. L. In *Dynamic Chemistry*; Springer Berlin Heidelberg: Berlin, Heidelberg, 1974; pp. 169–220.

(60) Replacing an H atom in CH_2Cl_2 with a -$CHCl_2$ unit is expected to decrease pK_a by ca. 2 units based on pK_a trends for the analogous carboxylic acids. For example, the pK_a of CCl_2HCO_2H (1.35) is 2.42 units lower than that of HCO_2H (3.77).

(61) The isodesmic reaction $CHCl_2CHCl_2 + CHCl_2^- = CH_2Cl_2 + CHCl_2CCl_2^-$ were calculated by DFT (B3LYP/6-311+G**) to be exergonic by –52.5 kcal/mol.

(62) Vela, J.; Lief, G. R.; Shen, Z.; Jordan, R. F. *Organometallics* **2007**, *26*, 6624.

(63) Stereoisomers that differ in configurations at the S atoms are also possible for **4b**. If the two S atoms have opposite configurations the central ring adopts a chair–chair conformation, as seen for formulas from p 13, whereas if they have the same configuration, the central ring adopts a boat–boat conformation, which is the case for *SS,SS*-**4b**. However, the isolation of *SS,RR*-**5b** from the reaction of **4b** with $B(C_6F_5)_3$ suggests that the two isomers of **4b** differ in the relative configurations of the cyclopentane rings.

(64) Cotton, A. F.; Wilkinson, G.; Murillo, C. A.; Bochmann, M. In *Advanced Inorganic Chemistry* ; Wiley-Interscience: New York, 1999; pp. 521–522.

(65) Harder, S.; Boersma, J.; Brandsma, L.; van Mier, G. P. M.; Kanters, J. A. *J Organomet Chem* **1989**, *364*, 1.

(66) Rulke, R. E.; Ernsting, J. M.; Spek, A. L.; Elsevier, C. J.; van Leeuwen, P. W. N. M.; Vrieze, K. *Inorg. Chem.* **1993**, *32*, 5769.

(67) Biscoe, M. R.; Fors, B. P.; Buchwald, S. L. *J. Am. Chem. Soc.* **2008**, *130*, 6686.

(68) De Graaf, W.; Boersma, J.; Smeets, W. J. J.; Spek, A. L.; Van Koten, G. *Organometallics* **1989**, *8*, 2907.

(69) Bakker, B. H.; Cerfontain, H. *Euro. J. Org. Chem.***1998**, *1999*, 91.

(70) Suter, C. M.; Evans, P. B.; Kiefer, J. M. *J. Am. Chem. Soc.* **1938**, *60*, 538.

Chapter Three

Ethylene Polymerization and Copolymerizations with Methyl Acrylate and Vinyl Fluoride by Palladium(II) Alkyl Complexes that Contain Phosphine-cyclopentanesulfonate Ligands

3.1 Introduction

As described in Chapters One and Two, the marked dependence of the behavior of (PR_2-arenesulfonate)PdR catalysts on the structure of the PR_2 unit suggests that replacement of the arene linker in type-**A** catalysts with an alkane linker may also strongly influence catalyst performance. However, only one (phosphine-alkanesulfonate)PdR complex that contains an alkane linker, specifically a *–CH_2CH_2–* linker, has been tested for olefin polymerization. This (PO)PdRL complex, (P(2-OMe-Ph)$_2$-ethanesulfonate)Pd(η^1,η^2-2-methoxycyclooct-5-enyl), oligomerizes ethylene to butenes and hexenes but rapidly degrades to catalytically inactive species, [1] most likely because the –CH_2CH_2– linker is highly flexible. One potential strategy for stabilizing (diarylphosphine-alkanesulfonate)PdRL compounds is to incorporate a cyclic alkane linker to preclude PC–CS bond rotation. In this chapter, the behavior of (C5-PO)PdMe(py) (**3b**), {(C5-PO)PdMe}$_2$ (**4b**) and {(C5-PO•B(C_6F_5)$_3$)PdMe}$_2$ (**5b**) in ethylene polymerization and ethylene copolymerization with methyl acrylate (MA) and vinyl fluoride (VF) is described (Chart 3.1). The synthesis and characterization of **3, 4,** and **5b** were described in Chapter Two.

Chart 3.1. New (Phosphine-cyclopentanesulfonate)PdR complexes

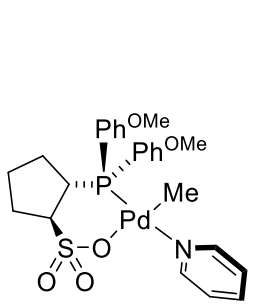

3b

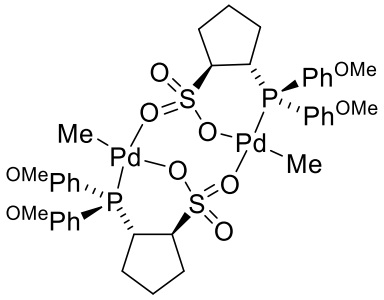

SS,SS-**4b** (*ent-RR,RR*)

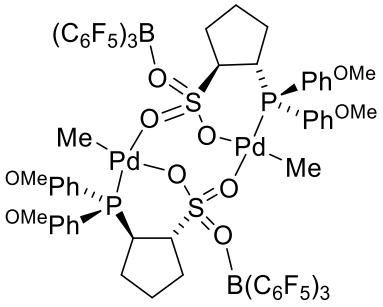

SS,RR-**5b**

3.2 Results and Discussion

Ethylene Polymerization Studies. Ethylene polymerization results are summarized in Table 3.1.[2] Compound **3b** produces PE with a M_n of ca. 4000 Da with an activity of 100 kg mol^{-1} h^{-1} at 250 psi ethylene and 80 ºC in toluene (entry 1). Base-free dimer **4b** is ca. twice as active as **3b** and produces PE with similar MW as **3b**, consistent with both complexes forming the same active (**2b**)PdMe(ethylene) species (entry 2). The two-fold increase in activity is a result of removing the off-cycle equilibrium between active (**2b**)PdR(ethylene) and inactive (**2b**)PdR(py) species (R = growing chain).[3–6] {(PO)PdR}$_2$ catalysts that contain phosphine-arenesulfonate ligands show similar enhancements in activity compared to the corresponding (PO)PdR(py)complexes.[3,4,7,8] The observed activity of **4b** is very similar for 1 h and 2 h polymerization reactions, indicating that the catalyst is quite stable under these conditions (entries 2 and 4). Increasing the ethylene pressure to 800 psi has little effect on the catalyst activity or the MW of the resulting PE, suggesting that the rate-determining step is insertion of the (PO)PdR(ethylene) catalyst resting state (entries 2 and 5) and that chain transfer occurs by an

associative mechanism.[9] The borane adduct **5b** is less active and produces PE with a 2-fold lower MW compared to **3b** and **4b** (entries 6, 7). In contrast, binding of $B(C_6F_5)_3$ to (PAr_2-arenesulfonate)PdR catalysts increases activity but results in larger reductions in MW.[3] The T_m values of the PEs produced by **3b**, **4b** and **5b** (~ 131 °C) are consistent with highly-linear PEs in the observed MW range.[10–12] These PEs contain a mixture of terminal $RCH=CH_2$ (56 – 93%) and internal RCH=CHR (7 – 44%) olefins, and the ratio of unsaturated $RCH=CH_2$ to saturated RCH_2CH_3 chain ends is ca. 1/1.The observation of ethylene polymerization and a long catalyst lifetime for **4b** contrasts with the ethylene oligomerization and short catalyst lifetime reported for the ethylene-linked analogue **C** (Chart 2.1, Chapter Two).[13] This difference is ascribed to the stabilizing effect of rigidifying the phosphine-alkanesulfonate ligand by the incorporation of the cyclopentane linker in **4b**. However, **3b**, **4b** and **5b** are much less active and produce PE with lower MWs compared to ($P(Ph^{OMe})_2$-*p*-toluenesulfonate)PdMe(py) (entry 8, Table 3.1).

Table 3.1. Ethylene polymerization by **3b**, **4b**, **5b** and **3e**.[a]

Entry	Cat.	Pd loading (μmol)	$P_{ethylene}$ (psi)	Time (h)	Act. (kg mol_{Pd}^{-1} h^{-1})	M_n (Da)[d]	PDI[d]	T_m (°C)[e]
1[b]	**3b**	0.88	250	2	100	4480	1.9	131.8
2[b]	**4b**	0.88	250	2	210	4210	2.0	131.8
3[b]	**4b**	1.6	250	2	190	3610	1.8	131.2
4[b]	**4b**	0.88	250	1	190	5200	2.0	131.3
5[b]	**4b**	0.88	800	2	170	5250	1.6	131.4
6[b]	**5b**	0.88	250	2	34	2050	3.5	129.2
7[c]	[f]**3b** + 2 $B(C_6F_5)_3$	0.88	250	2	84	1950	2.2	128.8
8[c]	**3e**	0.88	250	2	1330	16400	1.9	135.2

[a]All entries are an average of at least two runs. [b]Non-injection protocol, 50 mL toluene, 80 °C. [c]Injection protocol, 40 mL toluene, 10 mL chlorobenzene catalyst solution, 80 °C. [d]Determined by GPC. [e]Determined by DSC. [f]*In situ* generation of **5b** from **3** + 2$B(C_6F_5)_3$.

Copolymerization of Ethylene with Methyl Acrylate by 3b and 4b. The results of ethylene/MA copolymerization by **3b** and **4b** (Eq. 3.1) are summarized in Table 3.2. At 400 psi ethylene, 1.2 M MA and 80 °C, **3b** and **4b** produce copolymers with low MWs and 3.3–3.8 mol % MA incorporation (entries 1, 2). Increasing the [MA]/$P_{ethylene}$ ratio results in an increase in MA incorporation as expected (Figure 3.1).[8,14–16] Under otherwise identical conditions, increasing the concentration of MA from 0.7 M to 1.2 M increases the MA incorporation from 1.8 to 3.3 mol %, lowers the catalyst activity, and slightly decreases the copolymer MW (entries 2, 3). Increasing the amount of MA in the copolymer significantly decreases the T_m value.

Eq. 3.1

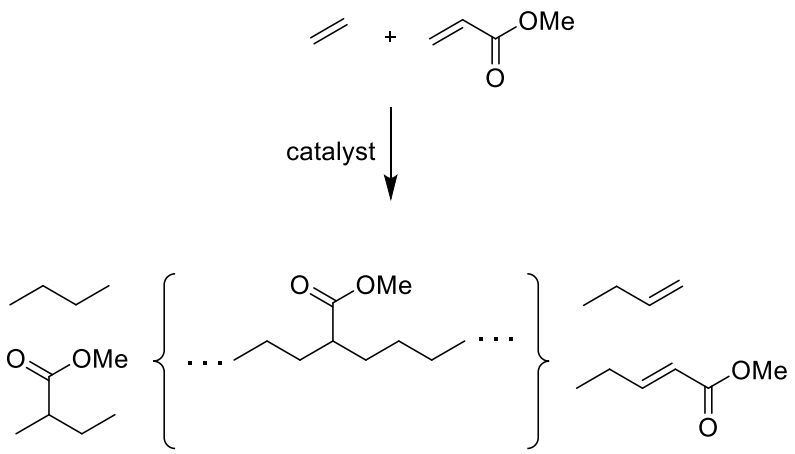

Table 3.2. Copolymerization of ethylene and methyl acrylate (MA) by **3b**, **3e**, **3f** and **4b**.[a]

Entry	Cat.	Pd loading (μmol)	$P_{ethylene}$ (psi)	[MA] (M)	Act. (kg mol_{Pd}^{-1} h^{-1})	M_n (Da)[f]	PDI[f]	MA incorp (mol %)[g]	T_m (°C)[h]
1[b]	**3b**	15	400	1.2	4.0	2230	2.0	3.8	110.5
2[c]	**4b**	15	400	1.2	23	2130	2.3	3.3	112.8
3[c]	**4b**	15	400	0.7	30	2520	2.6	1.8	121.7
4[d]	**4b**	13	300	1.2	15	1750	1.7	6.9	94.7
5[d]	**3e**	13	300	1.2	107	9800	–	6.3	–
6[e]	**4b**	20	73	0.6	5.0	1830	1.5	11.7	68.2
7[e]	**3f**	20	73	0.6	130	2500	2.3	9.4	–

[a]All entries were an average of two runs. [b]Conditions: injection procedure, 34.6 mL toluene, 10 mL chlorobenzene, 5.44 mL MA, and 0.1 g BHT, 80 °C, 2 h. [c]Conditions: non-injection procedure, 34.6 mL toluene, 10 mL chlorobenzene, 5.44 mL MA, 0.1 g BHT, 80 °C, 2 h. [d]Conditions:[17] 44.7 mL toluene, 5.3 mL MA, 1 mg BHT, 100 °C, 1 h. [e]Conditions:[8] 47.3 mL toluene, 2.7 mL MA, 1 mg BHT, 95 °C, 1 h.[f]Determined by GPC. [g]Determined by ^{1}H NMR; in all cases MA incorporated as $–CH_2CH(CO_2Me)CH_2–$ (80%), $– CH_2CH(CO_2Me)Me$ (8%) and $–CH_2CH=CH(CO_2Me)$ (12%)units. [h]Determined by DSC.

Figure 3.1. Dependence of MA incorporation on monomer feed ratio in ethylene/MA copolymerization by **4b** at 80 °C – 100 °C in toluene or toluene/chlorobenzene.

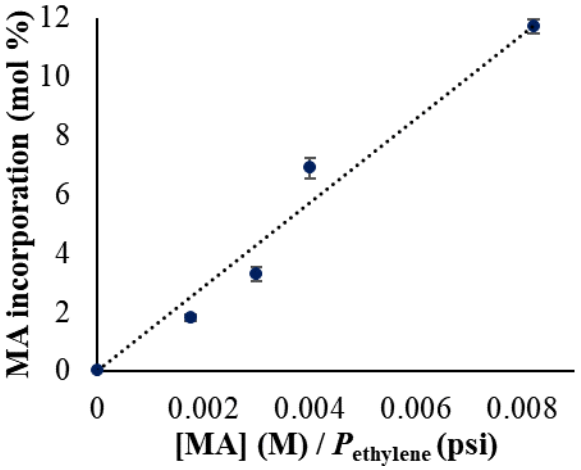

3b and **4b** incorporate MA mainly as $–CH_2CH(CO_2Me)CH_2–$ in-chain units (80%), with lower amounts of $–CH_2CH(CO_2Me)Me$ (8%) and $–CH=CHCO_2Me$ (12%) chain-end units observed (Eq. 3.1). These results imply that chain growth is favored over chain transfer following a MA insertion. The sum of saturated end groups is roughly equal to the sum of unsaturated end groups (see Table 3.7 in Experimental).

Interestingly, while **4b** is only ca. 2 times as active as **3b** in ethylene homopolymerization, it is ca. 6 times more active than **3b** in ethylene/MA copolymerization. A possible explanation for this difference is that pyridine competes more strongly with ethylene for coordination to Pd after a MA insertion than after an ethylene insertion, i.e. the K_{eq} value for Eq. 3.3 is greater than that for Eq. 3.2.

Eq. 3.2

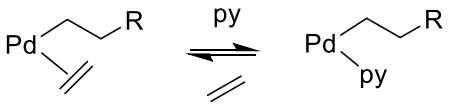

Eq. 3.3

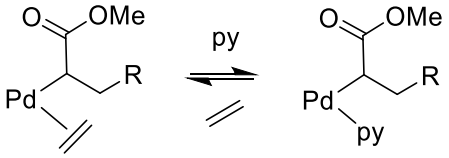

4b is less active in ethylene/MA copolymerization and produces copolymer with a lower MW, but incorporates a similar amount of MA (entries 4–7, Table 3.2), compared to the arenesulfonate analogues **3e**[17] and **3f**[8] (Chart 2.2, Chapter Two). Compounds **3b** and **3e** are both an order of magnitude less active in ethylene/MA copolymerization than in ethylene homopolymerization and produce copolymers with half the M_n value of their respective PEs, indicating that these *cyclopentane* and *arene*-linked (PO)PdR complexes suffer from a similar degree of inhibition in the presence of MA.

Copolymerization of Ethylene and Vinyl Fluoride by 3b and 4b. The results of ethylene/VF copolymerization by **3b** and **4b** are summarized in Table 3.3. At 80 °C, 220 psi ethylene and 80 psi VF, **3b** and **4b** incorporate ca. 0.1 mol % VF (entries 1–3). Under these conditions, the activity of each complex is severely depressed and the M_n value of the copolymer produced is similar relative to what is observed in ethylene homopolymerization. Increasing the

VF pressure to 160 psi increases the VF incorporation level to 0.4 mol % and decreases the copolymer M_n by half but does not strongly influence the activity (entry 4).

Table 3.3. Copolymerization of ethylene and vinyl fluoride (VF) with **3b**, **4b**, and **3e**.

Entry	Cat.	[Pd] (μmol)	E (psi)	VF (psi)	Act. (kg mol_{Pd}^{-1} h^{-1})	M_n (Da)[c]	PDI[c]	VF incorp (mol %)[d]	T_m (°C)[e]
1[a]	**3b**	0.88	220	80	5.7	4360[d]	n.d.	0.1	n.d.
2[a]	**3b**	8.8	220	80	2.6	4540	2.9	0.1	130.0
3[b,f]	**4b**	20	220	80	17	4180	1.6	0.1	131.1
4[b,f]	**4b**	20	220	160	15	1950	2.0	0.4	125.5
5[b]	**3e**	10	220	80	4.5	8100	1.9	0.5	n.d.

[a]Conditions: injection procedure, 40 mL toluene, 10 mL chlorobenzene, 80 °C, 2 h. [b]Conditions: non-injection procedure, 50 mL toluene, 10 mL chlorobenzene, 80 °C, 2 h. [c]Determined by GPC. [d]Determined by ^{1}H NMR. [e]Determined by DSC. [f]Average of two runs.

The microstructures of the ethylene/VF copolymers produced by **3b** and **4b** are summarized in Table 3.4. Approximately 80% of the VF is present as internal $–CH_2CHFCH_2–$ units, which arise from 1,2- or 2,1-insertion of VF into a growing (PO)PdR species followed by ethylene insertion. Three chain-end units are also observed: (i) $–CH_2CF_2H$, formed by 1,2-insertion of VF into a (PO)PdF species (generated by β-F elimination) followed by ethylene insertion, (ii) $–CH_2CHFCH_3$, formed by 2,1-insertion of VF into a (PO)PdH species followed by ethylene insertion, and (iii) $–CH_2CH_2F$, formed by 1,2-insertion of ethylene into a (PO)PdF species or 1,2-insertion of VF into a (PO)PdH species followed by ethylene insertion.[18,19] Unsaturated $–CH_2CH=CHF$ chain-end units, which can form by 2,1- VF insertion into a (PO)PdR species followed by β-H transfer, were not observed.[20]

3b and **4b** display similar activity for ethylene/VF copolymerization compared to phosphine-arenesulfonate complex **3e**, but produce copolymers with lower MWs and less VF incorporation (entry 5, Table 3.3). The microstructures of the E/VF copolymers produced by **3b** and **4b** and **3e** are also similar (Table 3.4).[18]

Table 3.4. Microstructures of E/VF copolymers produced by **3b**, **4b** and **3e**[18]

Catalyst	VF incorporation mode (%)[a]			
	$-CH_2CF_2H$	$-CH_2CH_2F$	$-CH_2CHFCH_2-$	$-CH_2CHFCH_3$
3b[b]	12	7	77	4
4b[b]	10	1	81	7
4b[c]	7	8	80	5
3e[b]	13	8	76	2

[a]Determined by ^{19}F NMR; values determined by ^{1}H NMR are similar. [b]Copolymerization in 4/1 toluene/chlorobenzene, 220 psi ethylene, 80 psi VF. [c]Copolymerization in 4/1 toluene/chlorobenzene, 220 psi ethylene, 160 psi VF.

3.3 Conclusion

Compounds **3b**, **4b**, and **5b** polymerize ethylene with low activity (up to 210 kg mol^{-1} h^{-1} at 250 psi and 80 °C) to linear polyethylene (M_n = 1950 – 5250 Da) with predominantly internal olefin placements. The ethylene polymerization activity is independent of ethylene pressure over the range 250 – 800 psi. **3b** and **4b** copolymerize ethylene with methyl acrylate to linear copolymers that contain up to 11.7 mol % methyl acrylate, which is incorporated as $-CH_2CH(CO_2Me)CH_2-$ (80%) in-chain units and $-CH_2CH(CO_2Me)Me$ (8%) and $-CH_2CH{=}CH(CO_2Me)$ (12%) chain-end units. **3b** and **4b** also copolymerize ethylene with vinyl fluoride to linear copolymers that contain up to 0.41 mol % vinyl fluoride, which is incorporated

as $–CH_2CHFCH_2–$ (~80%) in-chain units and $–CH_2CF_2H$ (7%), $–CH_2CHFCH_3$ (5%) and $–CH_2CH_2F$ (8%) chain-end units. Complexes **3b** and **4b** are more stable and active in ethylene polymerization than analogous (PAr_2-$CH_2CH_2SO_3$)PdR catalysts, but are less active than analogous (PAr_2-*arene*sulfonate)PdR catalysts.

3.4 Experimental Section

General Procedures. All experiments were performed using drybox or Schlenk techniques under a nitrogen atmosphere unless noted otherwise. Nitrogen was purified by passage through Q-5 oxygen scavenger and activated molecular sieves. Toluene was purified by passage through BASF R3-11 oxygen scavenger and activated alumina. CD_2Cl_2 was distilled from and stored over P_2O_5. Acetone was purchased from Sigma Aldrich and used without further purification. $B(C_6F_5)_3$ was donated by Boulder Scientific. Ethylene (polymer grade) and vinyl fluoride (VF) were purchased from Matheson. Methyl acrylate was dried over $CaCl_2$ and distilled before being stored at –40 °C under N_2.

NMR spectra were recorded on Bruker DMX-500 or DRX-400 spectrometers at ambient temperature unless otherwise indicated. ^1H and ^{13}C chemical shifts are reported relative to $SiMe_4$ and internally referenced to residual ^1H and ^{13}C solvent resonances. ^{31}P chemical shifts are externally referenced to 85% H_3PO_4 (δ 0.0).

Ethylene Homopolymerization. Polymerizations were performed in a 300 mL Parr stainless-steel autoclave fitted with a 200 mL glass autoclave liner and equipped with a mechanical stirrer, thermocouple, and water cooling loop and controlled by a Parr 4842 controller. Where

indicated, a 10 mL stainless steel injection tube with valves and Swagelok fittings on both ends was used to inject the catalyst solution into the autoclave after pressurization with ethylene. *Catalyst injection procedure:* A glass liner was charged with toluene (40 mL) and placed in the autoclave. The catalyst was dissolved in chlorobenzene (10 mL) and the solution was sealed in the injection tube. The autoclave and injection tube were sealed and removed from the glovebox. The autoclave was connected to an ethylene line, stirring was initiated at 170 rpm, and the autoclave was heated to 80 °C for 20 minutes. The autoclave was pressurized with ethylene (typically 240 psi). After 10 minutes, the ethylene line was closed. One end of the injection tube was attached to the autoclave and the other end was attached to a nitrogen line. The line between the nitrogen tank and the injection tube was evacuated and filled three times with N_2 at a pressure ca. 20 psi higher than the ethylene pressure (typically 260 psi). The catalyst solution was injected into the autoclave. The N_2 injection line was closed. The ethylene line was re-opened to the autoclave at a pressure ca. 10 psi higher than the N_2 pressure used (typically 270 psi). After the listed polymerization time (typically 2 h), the ethylene line was closed, and the autoclave was cooled to 25 °C by the cooling loop and an external ice bath and vented. The polymer was precipitated by addition of acetone (50 mL), collected by filtration, washed with acetone, and dried in a vacuum oven overnight. *Non-injection procedure*: The catalyst was weighed directly into a glass liner or added as a stock solution in dichloromethane (1 mL) and dried under vacuum. Toluene (50 mL) was added and the liner was placed in the autoclave. The autoclave was sealed and removed from the glovebox and attached to an ethylene line. Stirring was initiated at 160 rpm and the autoclave was heated to 80

°C. The autoclave was pressurized with ethylene. After the listed polymerization time (typically 2 h), the ethylene line was closed and the autoclave was cooled to 25 °C by the cooling loop and an external ice bath, and vented. The polymer was precipitated by addition of acetone (50 mL), collected by filtration, washed with acetone, and dried in a vacuum oven overnight. The complete ethylene polymerization data is shown in Table 3.5.

Table 3.5. Detailed ethylene homopolymerization data.

	Cat.	[Pd] (μmol)	$P_{ethylene}$ (psi)	Time (h)	Act. (kg mol^{-1} h^{-1})	M_n (Da)[c]	PDI[c]	T_m (°C)[d]
1[a]	**3b**	0.88	250	2	98	4783	1.9	131.6
2[b]	**3b**	0.88	250	2	103	4180	1.9	132.0
3[a]	**4b**	0.88	250	2	217	4750	1.9	131.8
4[a]	**4b**	0.88	250	2	211	4079	2.2	131.8
5[a]	**4b**	1.6	250	2	195	3341	1.8	131.1
6[a]	**4b**	1.6	250	2	189	3882	1.8	131.3
7[a]	**4b**	0.88	250	1	193	5202	2.0	131.3
8[a]	**4b**	0.88	800	2	168	5687	1.6	131.2
9[a]	**4b**	0.88	800	2	164	4815	1.6	131.6
10[a]	**5b**	0.88	250	2	34	2047	3.5	128.0
11[a]	**5b**	0.88	250	2	23	n.d.	n.d.	130.4
12[b]	**3b** + 2 BAr^F_3	0.88	250	2	94	1311	2.2	128
13[b]	**3b** + 2 BAr^F_3	0.88	250	2	74	2588	2.1	129.5
14[b]	**3e**	0.88	250	2	1333	16357	1.9	135.2

[a]Conditions: Non-injection protocol, 50 mL toluene, 80 °C, 250 psi ethylene, 2 h. [b]Conditions: Injection protocol, 40 mL toluene, 10 mL chlorobenzene catalyst solution, 80 °C, 250 psi ethylene, 2 h. [c]Determined by GPC. [d]Determined by DSC.

Copolymerization of Ethylene and Methyl Acrylate. *Injection procedure:* The injection procedure for ethylene homopolymerization described above was used with the following modifications: (i) The glass autoclave liner was charged with toluene, BHT (typically 100 mg), and methyl acrylate (total volume 40 mL), (ii) the contents of the autoclave were stirred at 160 rpm, (iii) the autoclave was pressurized with ethylene (380 psi), (iv) the solution of catalyst in 10 mL chlorobenzene was injected at 400 psi N_2, (v) the autoclave was pressurized with ethylene (420 psi), and (vi) MeOH (200 mL) was added to precipitate the polymer. *Non-injection procedure*: The non-injection procedure described above was used with the following modifications: (i) The glass liner was charged with the catalyst stock solution in chlorobenzene (10 mL), BHT (typically 100 mg), and toluene and methyl acrylate to give a total volume of 50 mL, (ii) the contents of the autoclave were stirred at 160 rpm, (iii) the autoclave was pressurized with ethylene (400 psi), and (iv) MeOH (200 mL) was added to precipitate the polymer. The complete ethylene/methyl acrylate copolymerization data is shown in Table 3.6.

Table 3.6. Detailed ethylene/methyl acrylate copolymerization data.

	Cat.	[Pd] (μmol)	$P_{ethylene}$ (psi)	[MA] (M)	Act. (kg mol^{-1} h^{-1})	M_n (Da)[f]	PDI[f]	MA incorp (mol %)[g]	T_m (°C)[h]
1[a]	**3b**	15	400	1.2	4.3	2138	2.0	n.d.	110.6
2[a]	**3b**	15	400	1.2	4.2	2311	1.9	3.84	110.3
3[b]	**4b**	15	400	1.2	23.4	2534	2.1	3.06	114.5
4[b]	**4b**	15	400	1.2	22.7	1720	2.5	3.56	111.1
5[b]	**4b**	15	400	0.7	29.2	2858	2.5	1.92	122.9
6[b]	**4b**	15	400	0.7	29.9	2180	2.7	1.68	120.4
7[c]	**4b**	13.1	300	1.2	15.2	1751	1.7	6.5	96.3
8[c]	**4b**	13.1	300	1.2	13.9	1740	1.7	7.2	93.0
9[c]	**3e**	13.1	300	1.2	106.7	9800	n.d	6.3	n.d.
10[d]	**4b**	20	73	2.5	trace	n.d.	n.d	n.d.	n.d.
11[d]	**3f**	20	73	2.5	37	3100	1.8	35	n.d.
12[e]	**4b**	20	73	0.6	4.1	1873	1.5	11.9	66.7
13[e]	**4b**	20	73	0.6	5.25	1779	15	11.4	69.6
14[e]	**3f**	20	73	0.6	128.5	2500	2.3	9.4	n.d.

[a]Conditions: injection procedure, 34.6 mL toluene, 5.44 mL MA, and 0.1 g BHT, 80 °C, 10 mL chlorobenzene (injected), 2 h. [b]Conditions: non-injection procedure, 34.6 mL toluene, 10 mL chlorobenzene, 5.44 mL MA and 0.1 g BHT, 80 °C, 2 h. [c]Conditions:[17] 44.7 mL toluene, 5.3 mL MA, 1 mg BHT, 100 °C, 1 h. [d]Conditions:[8] 38.7 mL toluene, 11.3 mL MA, 1 mg BHT, 95 °C, 1 h. [e]Conditions:[8] 47.3 mL toluene, 2.7 mL MA, 1 mg BHT, 95 °C, 1 h. [f]Determined by GPC. [g] Determined by ^{1}H NMR. [h] Determined by DSC.

Table 3.7. Analysis of saturated vs. unsaturated end-group determined by ^{1}H NMR. The proton assignments H_e, H_f, H_h, and H_a correspond to Figure **3.2**(b).

Table 3.2, entry 2					
		integral	#H	integral/#H	
saturated	sat. end	6.55	3	2.2	
	start MA (H_e)	0.41	1	0.4	
unsaturated	1-propenyl (H_f)	2.22	2	1.1	
	2-propenyl (H_h)	0.6	2	0.3	
	end MA (H_a)	1	1	1.0	
				sat/unsat =	1.1
Table 3.2, entry 3					
		integral	#H	integral/#H	
saturated	sat. end	8.68	3	2.89	
	start MA (H_e)	0.9	1	0.90	
unsaturated	1-propenyl (H_f)	2.23	2	1.12	
	2-propenyl (H_h)	1.68	2	0.84	
	end MA (H_a)	1	1	1.00	
				sat/unsat =	1.28
Table 3.2, entry 5					
		integral	#H	integral/#H	
saturated	sat. end	12.88	3	4.3	
	start MA (H_e)	0.58	1	0.6	
unsaturated	1-propenyl (H_f)	3.18	2	1.6	
	2-propenyl (H_h)	2.78	2	1.4	
	end MA (H_a)	1	1	1.0	
				sat/unsat =	1.2
Table 3.2, entry 7					
		integral	#H	integral/#H	
saturated	sat. end	5.97	3	2.0	
	start MA (H_e)	0.56	1	0.6	
unsaturated	1-propenyl (H_f)	1.77	2	0.9	
	2-propenyl (H_h)	1	2	0.5	
	end MA (H_a)	0.25	1	0.3	
				sat/unsat =	1.6

Copolymerization of Ethylene and Vinyl Fluoride. *Injection procedure:* The injection procedure for ethylene homopolymerization was used with the following modifications: (i) the autoclave was pressurized with vinyl fluoride (80 psi) and ethylene (300 psi), (ii) the solution of catalyst in chlorobenzene (10 ml) was injected with N_2 (400 psi), (iii) the autoclave was pressurized with ethylene (410 psi). *Non-injection procedure*: The non-injection procedure for ethylene homopolymerization was used with the following modification: the autoclave was pressurized with vinyl fluoride (80 psi) and ethylene (300 psi). A complete table of ethylene/vinyl fluoride copolymerizations is shown in Table 3.8.

Table 3.8. Complete ethylene/vinyl fluoride copolymerization data table.

entry	complex	[Pd] (μmol)	$P_{ethylene}$ (psi)	P_{VF} (psi)	activity (kg mol^{-1} h^{-1})	M_n (Da)[c]	PDI[c]	VF incorp (mol %)[d]	T_m (°C)[e]
1[a]	**3b**	0.88	220	80	5.7	4360[d]	n.d.	0.13	n.d.
2[a]	**3b**	8.8	220	80	2.6	4538	2.9	0.13	130.0
3[b]	**4b**	20	220	80	18.1	4416	1.6	0.09	130.7
4[b]	**4b**	20	220	80	16.7	3949	1.6	n.d.	131.5
5[b]	**4b**	20	220	160	16.3	2347	2.0	0.6	126.7
6[b]	**4b**	20	220	160	14.4	1561	1.9	0.2	125.5
7[a,f]	**3e**	10	220	80	4.5	8100	1.85	0.51	n.d.

[a]Conditions: injection procedure, 40 mL toluene, 10 mL chlorobenzene, 80 °C, 2 h. [b]Conditions: non-injection procedure, 50 mL toluene, 10 mL chlorobenzene (injected), 80 °C, 2 h. [c]Determined by GPC. [d]Determined by ^{1}H NMR. [e]Determined by DSC. [f]Results from ref. [18].

Polymer Characterization. Gel permeation chromatography (GPC) was performed on a Polymer Laboratories PL–GPC 200 instrument at 150 °C with 1,2,4-trichlorobenzene (stabilized with 125 ppm BHT) as the mobile phase. Three PLgel 10 μm Mixed-B LS columns were used. The molecular weights were calibrated using narrow polystyrene standards with a ten-point calibration of M_n from 570 Da to 5670 kDa, and are corrected for linear polyethylene by universal calibration by using the following Mark-Houwink parameters: polystyrene, $K = 1.75 \times 10^{-2}$ cm^3 g^{-1}, $\alpha = 0.67$; polyethylene, $K = 5.90 \times 10^{-2}$ cm^3 g^{-1}, $\alpha = 0.69$.[21] DSC measurements were performed on a TA Instruments 2920 differential scanning calorimeter. Samples (5 mg) were annealed by heating to 180 °C at 15 C/min, cooled to 50 °C at 15 °C/min, and analyzed by heating to 180 °C at 15 °C/min. NMR assignments for polymers and copolymers are based on literature sources.[4,18,22–26] Representative NMR spectra of PE, E/MA, and E/VF copolymers are shown in Figure 3.2.

Figure 3.2. NMR spectra of polymers.

(a) ^{1}H NMR spectrum of polyethylene produced by **4b**, Table 3.5, Entry 7 (393 K, dichlorobenzene-d_4, 500 MHz).

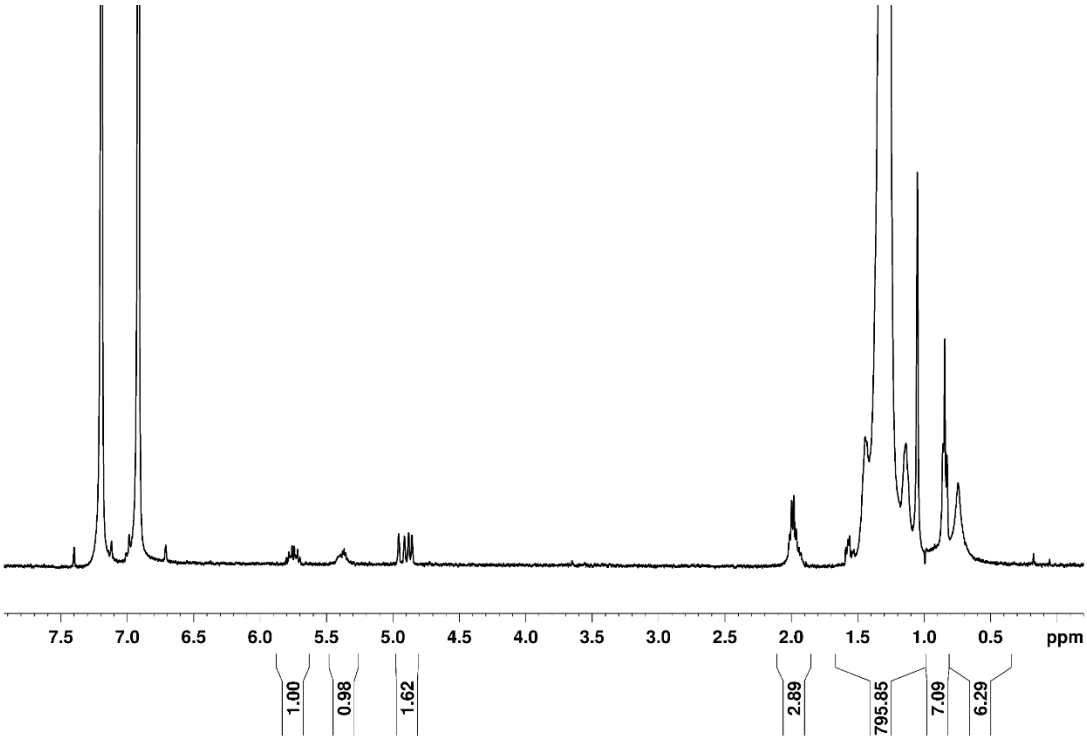

(b) ^{1}H NMR spectrum of ethylene/methyl acrylate copolymer produced by **4b**, Table 3.2, Entry 8 (393 K, $CDCl_2CDCl_2$, 500 MHz).

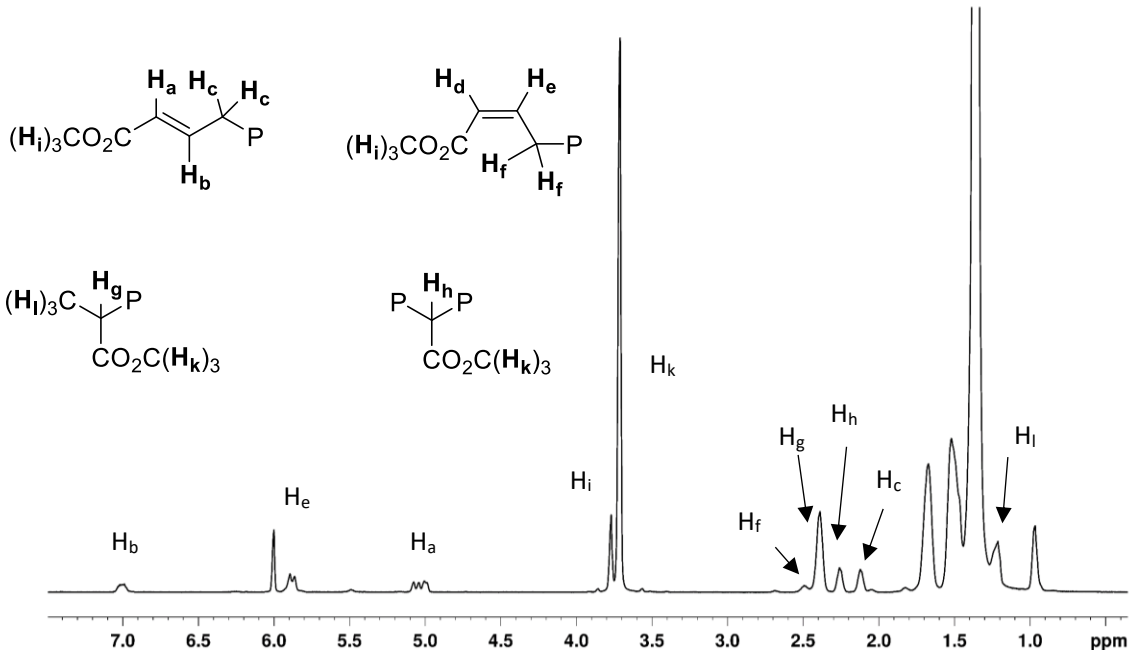

Figure 3.2, continued.

(c) ^{1}H NMR spectrum of ethylene/vinyl fluoride copolymer produced by **4b**, Table 3.3, Entry 3 (373 K, $CDCl_2CDCl_2$, 500 MHz).

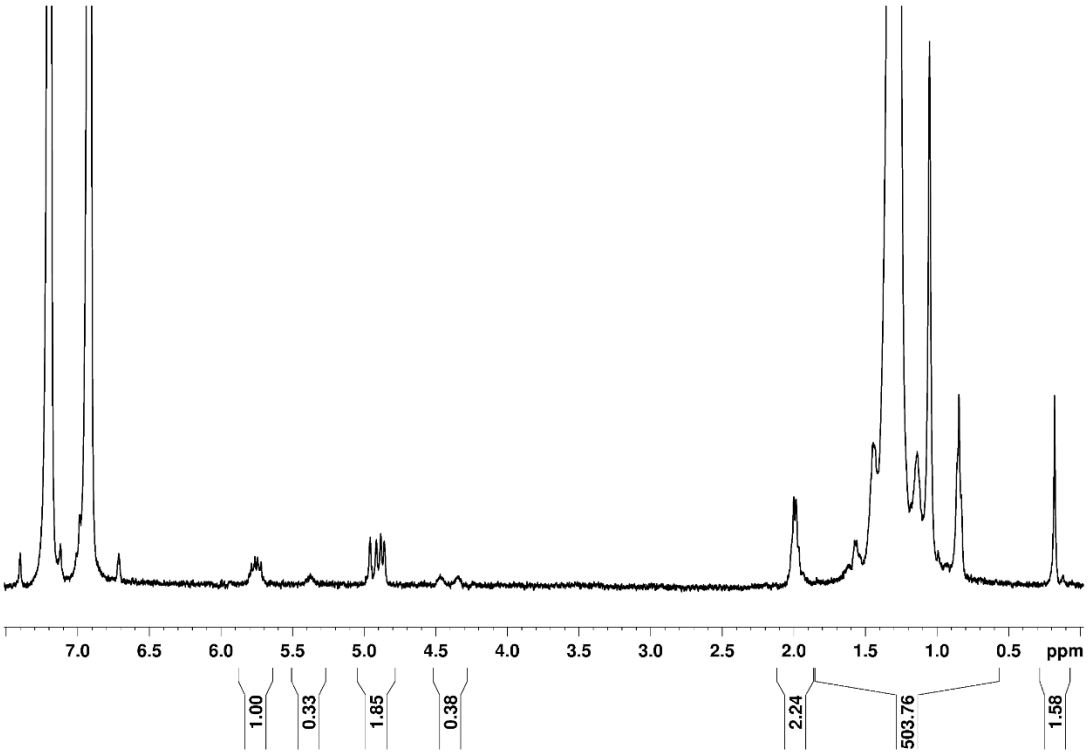

(d) ^{19}F NMR spectrum of ethylene/vinyl fluoride copolymer produced by **4b**, Table 3.2, Entry 3 (373 K, $CDCl_2CDCl_2$, 470 MHz)

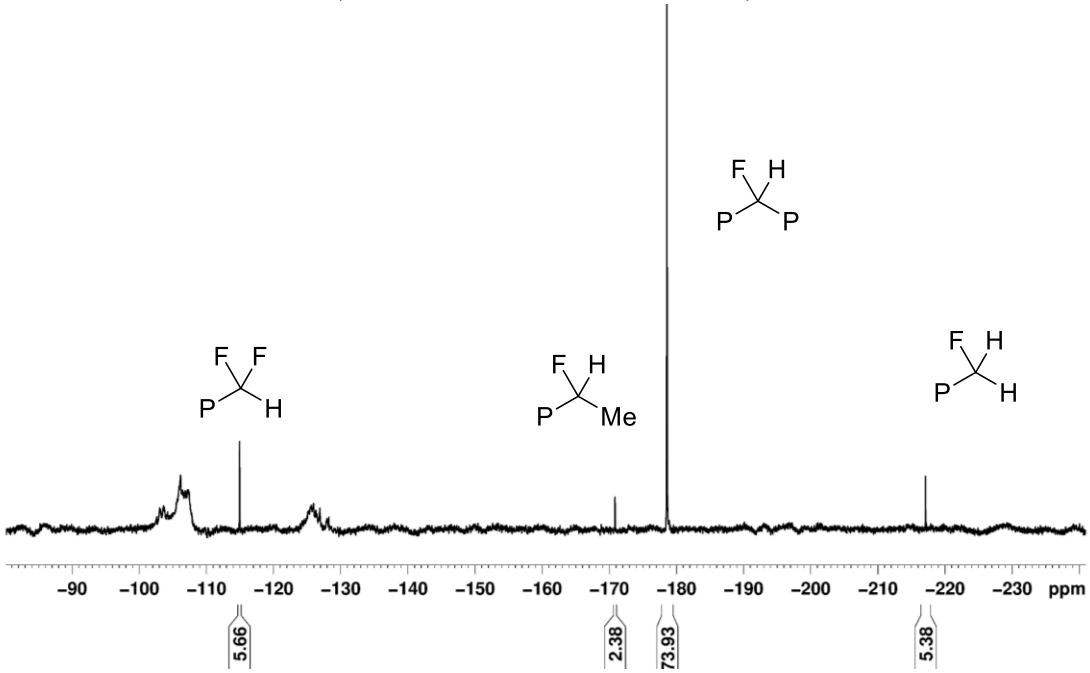

3.5 References and Notes

(1) Bettucci, L.; Bianchini, C.; Claver, C.; Suarez, E. J. G.; Ruiz, A.; Meli, A.; Oberhauser, W. *Dalton Trans.* **2007**, 5590.

(2) Compound **3a** generates only a trace amount of PE at 80 °C, consistent with the low thermal stability of this complex.

(3) Cai, Z.; Shen, Z.; Zhou, X.; Jordan, R. F. *ACS Catal.* **2012**, *2*, 1187.

(4) Vela, J.; Lief, G. R.; Shen, Z.; Jordan, R. F. *Organometallics* **2007**, *26*, 6624.

(5) Skupov, K. M.; Marella, P. R.; Simard, M.; Yap, G. P. A.; Allen, N.; Conner, D.; Goodall, B. L.; Claverie, J. P. *Macromol. Rapid Commun.* **2007**, *28*, 2033.

(6) Berkefeld, A.; Mecking, S. *Angew. Chem. Int. Ed.* **2008**, *47*, 2538.

(7) Luo, S.; Vela, J.; Lief, G. R.; Jordan, R. F. *J. Am. Chem. Soc.* **2007**, *129*, 8946.

(8) Guironnet, D.; Roesle, P.; Rünzi, T.; Göttker-Schnetmann, I.; Mecking, S. *J. Am. Chem. Soc.* **2009**, *131*, 422.

(9) Nakano, R.; Chung, L. W.; Watanabe, Y.; Okuno, Y.; Okumura, Y.; Ito, S.; Morokuma, K.; Nozaki, K. *ACS Catal.* **2016**, *6*, 6101.

(10) Stack, G. M.; Mandelkern, L.; Voigt-Martin, I. G. *Macromolecules* **1984**, *17*, 321.

(11) Mandelkern, L.; Prasad, A.; Alamo, R. G.; Stack, G. M. *Macromolecules* **1990**, *23*, 3696.

(12) Prasad, A.; Mandelkern, L. *Macromolecules* **1989**, *22*, 914.

(13) Lu, J.; Ye, J.; Duan, W.-L. *Org. Lett.* **2013**, *15*, 5016.

(14) Neuwald, B.; Falivene, L.; Caporaso, L.; Cavallo, L.; Mecking, S. *Chem. Eur. J.* **2013**, *19*, 17773.

(15) Neuwald, B.; Caporaso, L.; Cavallo, L.; Mecking, S. *J. Am. Chem. Soc.* **2013**, *135*, 1026.

(16) Wucher, P.; Goldbach, V.; Mecking, S. *Organometallics* **2013**, *32*, 4516.

(17) Skupov, K. M.; Hobbs, J.; Marella, P.; Conner, D.; Golisz, S.; Goodall, B. L.; Claverie, J. P. *Macromolecules* **2009**, *42*, 6953.

(18) Wada, S.; Jordan, R. F. *Angew. Chem. Int. Ed.* **2017**, *56*, 1820.

(19) Weng, W.; Shen, Z.; Jordan, R. F. *J. Am. Chem. Soc.* **2007**, *129*, 15450.

(20) Shen, Z.; Jordan, R. F. *Macromolecules* **2010**, *43*, 8706.

(21) Grinshpun, V.; Rudin, A. *Macromol. Rapid Commun.* **1985**, 219.

(22) Contrella, N. D.; Sampson, J. R.; Jordan, R. F. *Organometallics* **2014**, *33*, 3546.

(23) Drent, E.; van Dijk, R.; van Ginkel, R.; van Oort, B.; Pugh, R. I. *Chem. Commun.* **2002**, 744.

(24) Rünzi, T.; Guironnet, D.; Göttker-Schnetmann, I.; Mecking, S. *J. Am. Chem. Soc.* **2010**, *132*, 16623.

(25) Daigle, J.-C.; Piche, L.; Claverie, J. P. *Macromolecules* **2011**, *44*, 1760.

(26) Galland, G. B.; de Souza, R. F.; Mauler, R. S.; Nunes, F. F. *Macromolecules* **1999**, *32*, 1620.

Chapter Four

Experimental and Computational Mechanistic Studies of Olefin Polymerization by Palladium(II) Alkyl Complexes Bearing Phosphine-cyclopentanesulfonate Ligands

4.1 Introduction

(PO)PdRL and $[(PO)PdR]_2$ complexes bearing P(2-OMe-Ph)$_2$-cyclopentanesulfonate ligands are more stable and active in ethylene polymerization than analogous (PAr$_2$-*CH$_2$*-*CH$_2$*SO$_3$)PdR catalysts, but are less active than analogous (PAr$_2$-*arene*sulfonate)PdR catalysts (Chapter Three). This chapter describes low-temperature NMR studies and Density Functional Theory (DFT) calculations that were undertaken to probe the olefin polymerization mechanism by new (phopshine-alkanesulfonate)Pd(II) alkyl complexes and to investigate the reason for the lower activity of these complexes relative to their (phosphine-arenesulfonate)Pd(II)RL analogues.

4.2 Results and Discussion

Ethylene Insertion of (2b)PdMe(C$_2$H$_4$). As noted above, the observation that the activity of **4b** is independent of ethylene pressure (over the range 250–800 psi) suggests that the catalyst resting state is the ethylene adduct (**2b**)PdR(ethylene). Low-temperature NMR studies were pursued to probe the properties and ethylene insertion of such species. The reaction of base-free dimer **4b** with excess ethylene (12 equiv vs. Pd) at low temperature (below 0 °C) results in quantitative formation of (**2b**)PdMe(ethylene) (**7b**, Scheme 4.1). The ^{31}P NMR resonance of **7b** (δ 36.2), which contains a soft ethylene ligand *trans* to the phosphine, is shifted upfield by 10 – 15 ppm from those of **3b** (δ 46.3), **4b** (δ 50.9), **5b** (δ 51.1) and **6b** (δ 49.9), which contain hard nitrogen

or oxygen ligands *trans* to the phosphine. A similar chemical shift difference was observed between {*o*-P(3,5-^{t}Bu$_2$-Ph)$_2$-*p*-toluenesulfonate}PdMe(ethylene) (δ 15.9) and {*o*-P(3,5-^{t}Bu$_2$-Ph)$_2$-*p*-toluenesulfonate}PdMe(py) (δ 30.5) and [{*o*-P(3,5-^{t}Bu$_2$-Ph)$_2$-*p*-toluenesulfonate}PdMe]$_2$ (*δ* 33.0).[1] The ^{13}C{^{1}H} NMR spectrum of **7b** contains a singlet at δ 1.02 for the Pd-*Me* group. The absence of observable ^{31}P-^{13}C coupling establishes that the Me ligand is *cis* to the phosphine. Exchange of free and coordinated ethylene is fast on the NMR time scale for **7b** even at –35 °C, and one exchange-averaged ethylene signal is observed in the ^{1}H and ^{13}C NMR spectra.[2] A correlation between the Pd–C*H*$_3$ resonance and the exchange-averaged ethylene resonance is present in the ^{1}H-^{1}H NOESY spectrum, which provides conclusive evidence that **7b** contains an ethylene ligand.

Scheme 4.1. Reaction of **4b** with ethylene

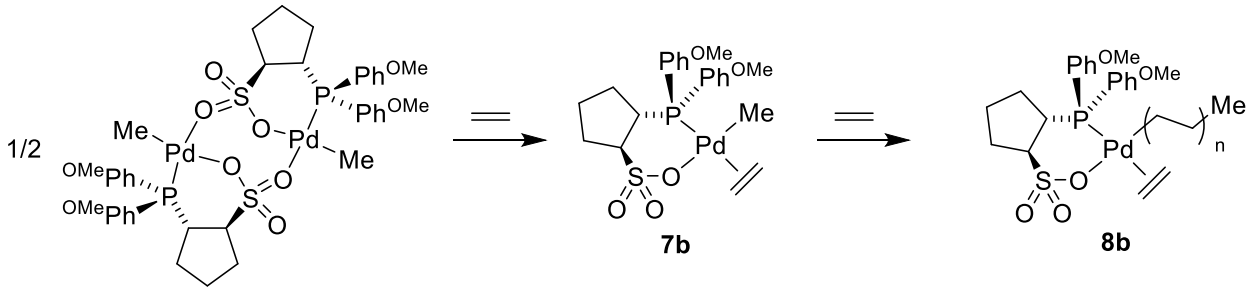

Complex **7b** undergoes multiple ethylene insertions at 5 °C to generate a mixture of (**2b**)Pd{(CH$_2$CH$_2$)$_n$Me}(ethylene) higher-alkyl species (Figure 4.5 in Experimental section). The ^{1}H NMR resonances for the **2b**$^-$ ligand do not change significantly as chain growth proceeds, but broad peaks in the *δ* 1.3–0.4 region grow in due to the Pd-alkyl chains. These alkyl resonances are

similar to those observed for {P(2-OMe-Ph)$_2$-benzenesulfonate}Pd(CH_2CH_2R)(2,6-lutidine) species with long alkyl chains.[1,3] After 65 min, ca. 9 equiv of ethylene were consumed and a white precipitate (PE or long-chain (**2b**)Pd(CH_2CH_2R)(ethylene) species) was present.

In a previous study of polyethylene chain growth by {*o*-P(3,5-^{t}Bu$_2$-Ph)$_2$-*p*-toluenesulfonate}PdMe(ethylene), the rate constant for ethylene insertion was determined by tracking the disappearance of the Pd*Me* resonance by ^{1}H NMR.[36] This approach is not possible for **7b**, because chain growth is accompanied by the growth of a resonance (δ 0.09) in the same region as the Pd*Me* resonance of **7b** (δ 0.07). Therefore, an apparent rate constant $k_{insert,PdR(ethylene)}$, which is a composite rate constant for insertion of all (**2b**)PdR(ethylene) species (R = Me, CH_2CH_2R, H) was determined by monitoring the disappearance of the ethylene resonance. Ethylene consumption was found to be zero-order in ethylene (Figure 4.1), consistent with the rate law in Eq. 4.1,

$$\frac{-d[ethylene]}{dt} = k_{insert,PdR(ethylene)}[Pd] \qquad \textbf{Eq. 4.1}$$

where $k_{insert,PdR(ethylene)}$ = 3.0 x 10^{-3} s^{-1} (5 °C, [Pd] = 0.067 M). The corresponding insertion barrier, $\Delta G^{\neq}_{insert}$ = 19.5 kcal/mol, agrees well with the value estimated from the apparent polymerization activity (20 kcal/mol)).[4]

Figure 4.1. Plot of [ethylene] versus time for the reaction of (**2b**)PdMe(C_2H_4) (**7b**) with ethylene at 5 °C in $CDCl_2CDCl_2$ solvent.

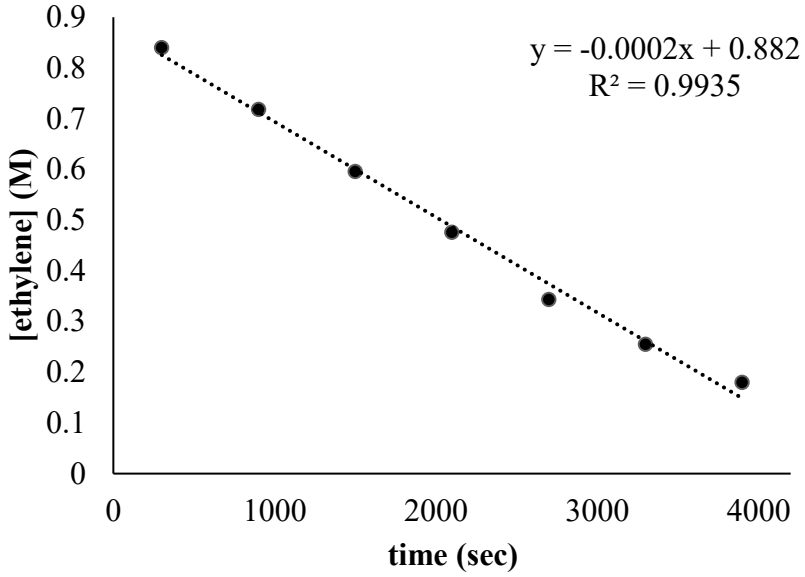

DFT Analysis of Ethylene Insertion of 7b and Comparison with Arene-linked Analogues. As noted above, **3b** and **4b** are approximately an order of magnitude less active than the phosphine-arenesulfonate analogue **3e**. DFT computations (B3LYP/6-31G* and LanL2dz) for the rate-limiting ethylene insertion of the corresponding (PO)Pd(R)(ethylene) species were carried out to probe the origin of this difference.

The ethylene polymerization mechanism by *arene*-linked (PO)PdMeL complexes has been thoroughly explored by DFT by Ziegler and co-workers[5,6] and Nozaki, Morokuma, and co-workers.[3,7,8] Their results show that *cis-P,R*-(PO)Pd(R)(ethylene) species are more stable than the corresponding *trans-P,R* isomers and that the lowest-barrier insertion pathway comprises isomerization of the *cis-P,R* isomer to the *trans-P,R* isomer followed by migratory insertion, rather than direct insertion of the *cis-P,R* isomer. Nozaki, Morokuma and coworkers found that the *cis-*

P,R/*trans*-*P,R* isomerization proceeds via a five-coordinate transition state in which the sulfonate group is bound in a κ^2 fashion.[3,9–11]

The model system (2-PMe_2-*cyclopentane*sulfonate)Pd(Pr)(ethylene) (**8-C5-PMe_2-Pr**, Chart 4.1) was first examined to enable comparison with earlier results for (2-PMe_2-*benzene*sulfonate)Pd(Pr)(ethylene) (**8-benzene-PMe_2-Pr**) system.[3] The processes examined include the isomerization of the *cis*-*P,C*-isomers **8** to *trans*-*P,C*-isomers **8'** and the insertion of each of these species. The results are shown in Figure 4.2, in which the free energies (*G*, kcal/mol) at 353 K are expressed relative to complexes **8-C5-PMe_2-Pr** and **8-benzene-PMe_2-Pr**. Consistent with earlier findings, in both model complexes, the *cis*-*P,R* isomers are more stable than the *trans*-*P,R* isomers, and the lowest-barrier insertion pathway involves *cis*/*trans* isomerization followed by migratory insertion of the *trans*-*P,R* isomer. Interestingly, the *cis*/*trans* isomerization is less endergonic and has a lower barrier for **8-C5-PMe_2-Pr** than for **8-benzene-PMe_2-Pr**, but the barrier to insertion of the *trans*-*P,R* isomer is slightly higher in the former case. These results show that the chain growth rate is controlled by the barrier to insertion of the *trans*-*P,R* isomer in both systems. Accordingly, this barrier was calculated for {2-P(2-OMe-Ph)$_2$-*cyclopentane*sulfonate)Pd(Pr)(ethylene) (**8b-Pr**, Chart 4.1) and the benzene-linked analogue **8d-Pr**. As shown in Figure 4.2, the barrier for insertion of the *trans*-*P,R* isomer is 1.6 kcal/mol higher for **8b-Pr** than **8d-Pr**. This result implies that the lower ethylene polymerization activity of **3b** and **4b** compared to analogous (phosphine-arenesulfonate)PdR catalysts is due to a slower ethylene insertion rate. However, due to the similarity of the insertion barriers, it is not possible to identify the structural/electronic origin of this difference.

Chart 4.1. Model compounds studied by DFT

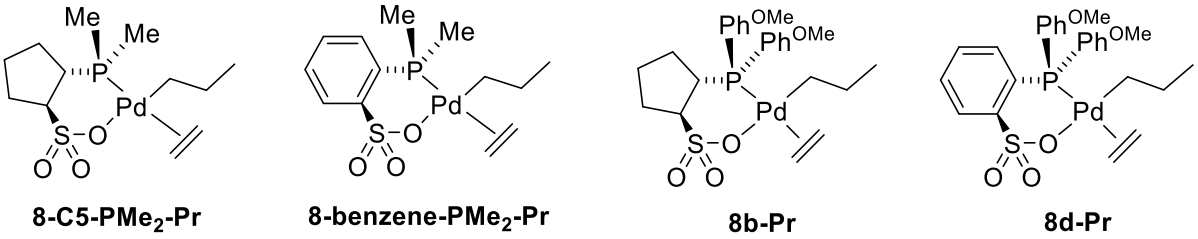

Figure 4.2. Computed free energy profile for chain growth of model complexes **8-C5-PMe$_2$-Pr** (red) and **8-benzene-PMe$_2$-Pr** (blue), and complexes **8b-Pr** (black) and **8d-Pr** (green). Free energies evaluated at 353 K are given in kcal/mol relative to those for starting complexes **8**. Starting at complex **8**, the direct insertion pathway is shown on the left and the indirect isomerization/insertion pathway is shown on the right.

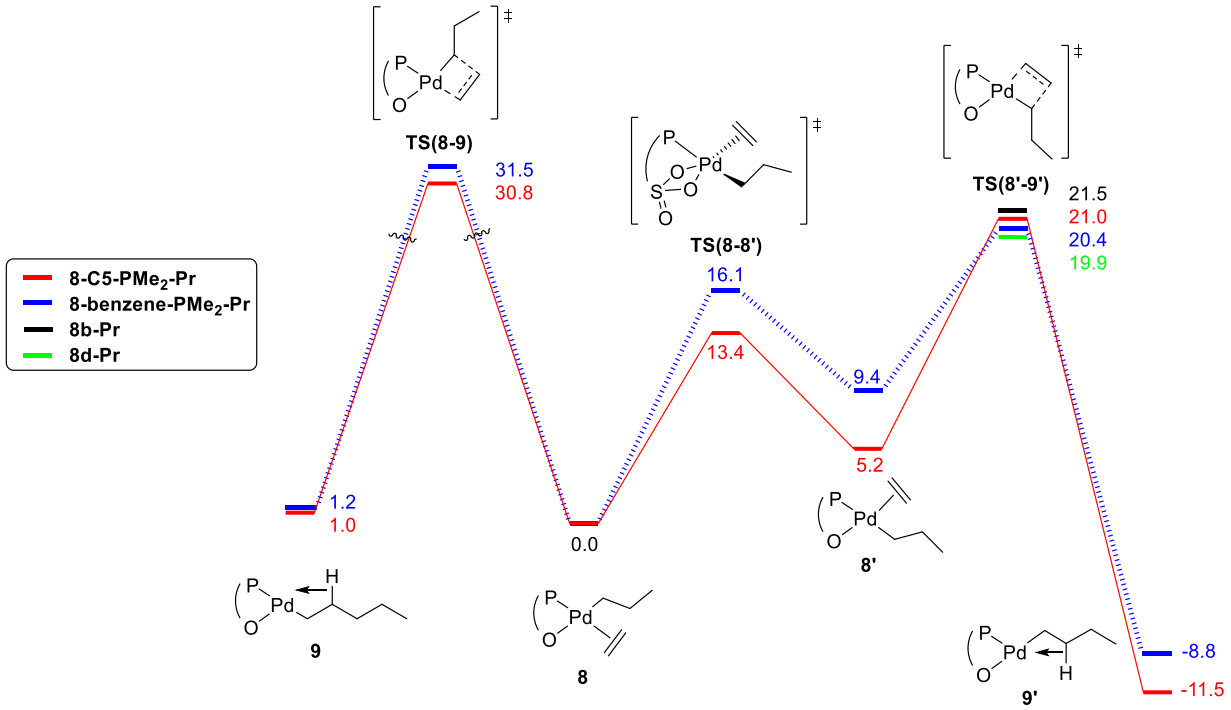

4.3 Conclusion

Low-temperature NMR studies and Density Functional Theory (DFT) calculations were performed to probe the ethylene polymerization mechanism by (phospine-

cyclopentanesulfonate)Pd(II) alkyl complexes. Base-free dimer [{P(2-OMe-Ph)$_2$-cyclopentanesulfonate}PdMe]$_2$ **4b** reacts with ethylene at low temperature to form the ethylene adduct *cis-P,R*-{P(2-OMe-Ph)$_2$-cyclopentanesulfonate}PdMe(ethylene) (**7b**), which undergoes insertion at 5 °C. These results show that ethylene polymerization by **4b** proceeds by rate-limiting insertion of {P(2-OMe-Ph)$_2$-cyclopentanesulfonate}PdR(ethylene) species. **3b** and **4b** are much more active and robust than the analogous {P(2-OMe-Ph)$_2$CH$_2$CH$_2$SO$_3$)PdR catalyst, which is ascribed to the enhanced molecular rigidity imparted by the cyclopentane linker (see Introduction of Chapter Two). However, **3b** and **4b** are less active and produce PE with lower MWs compared to analogous phosphine-arenesulfonate catalysts (see Chapter Three). DFT calculations show that this difference in activity results from a higher ethylene insertion barrier for the {P(2-OMe-Ph)$_2$-cyclopentanesulfonate}PdR system.

4.4 Experimental Section

General Procedures. All experiments were performed using drybox or Schlenk techniques under a nitrogen atmosphere unless noted otherwise. Nitrogen was purified by passage through Q-5 oxygen scavenger and activated molecular sieves. CD_2Cl_2 was distilled from and stored over P_2O_5. Ethylene (polymer grade) was purchased from Matheson.

NMR spectra were recorded on Bruker DMX-500 or DRX-400 spectrometers at ambient temperature unless otherwise indicated. ^{1}H and ^{13}C chemical shifts are reported relative to $SiMe_4$ and internally referenced to residual ^{1}H and ^{13}C solvent resonances. ^{31}P chemical shifts are externally referenced to 85% H_3PO_4 (δ 0.0).

Reaction of 4b with Excess Ethylene. An NMR tube was charged with **4b** (15 mg, 0.030 mmol Pd_1), ferrocene (6.0 mg, 0.030 mmol, internal standard), and $CDCl_2CDCl_2$ (0.5 mL). Ethylene (12 equiv vs Pd) was added by vacuum transfer at −78 °C. The tube was shaken to form a yellow solution of (**2b**)PdMe(C_2H_4) (**7b**). NMR spectra were recorded at −10 °C. The numbering scheme for **7b** is shown in .Figure 4.3. A ^{1}H-^{1}H NOESY spectrum showed a thru-space correlation between the Pd-CH_3 resonance and the broad ethylene signal (Figure 4.4). ^{1}H NMR ($CDCl_2CDCl_2$): δ 7.60–6.60 (br, 8H), 5.44 (br s, free and coordinated C_2H_4), 3.90 (br s, 4H, -OCH_3 and H^{13}), 3.70 (br s, 3H, -OCH_3), 3.00 (br s, 1H, H^{14}), 2.40–1.80 (6H, $H^{15\text{-}17}$), 0.090 (br s, 3H, PdCH_3). ^{13}C{^{1}H} NMR ($CDCl_2CDCl_2$): δ 160.2 (C^3 or C^8), 159.2 (C^3 or C^8), 140.0-135.0 (C^6 and C^{12}), 134.6 (C^{10}), 133.0 (C^4), 123.2 (br, coordinated and free C_2H_4), 121.2 (C^5 and C^{11}), 116.1 (C^1 or C^7), 113.2 (C^1 or C^7), 110.9 (C^3 or C^9), 110.2 (C^3 or C^9), 66.2 (C^{14}), 55.6 (C^{18}), 55.2 (C^{19}), 40.1 ($^1J_{PC}$ = 28 Hz, C^{13}), 30.6 (C^{17}), 29.7 (C^{15}), 26.1 (C^{16}), 1.02 (s, PdCH_3). ^{31}P{^{1}H} NMR ($CDCl_2CDCl_2$): δ 36.2 (s). The tube was warmed to 5 °C, and ethylene insertion was observed by ^{1}H NMR (Figure 4.5). After 65 min, a white precipitate had formed.

Figure 4.3. Numbering scheme for **7b**.

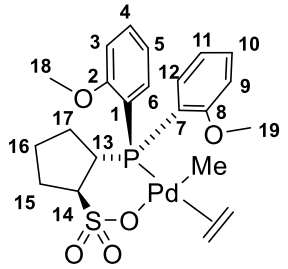

Figure 4.4. ^{1}H–^{1}H NOESY spectrum of **7b** (263 K in $CDCl_2CDCl_2$, 500 MHz).

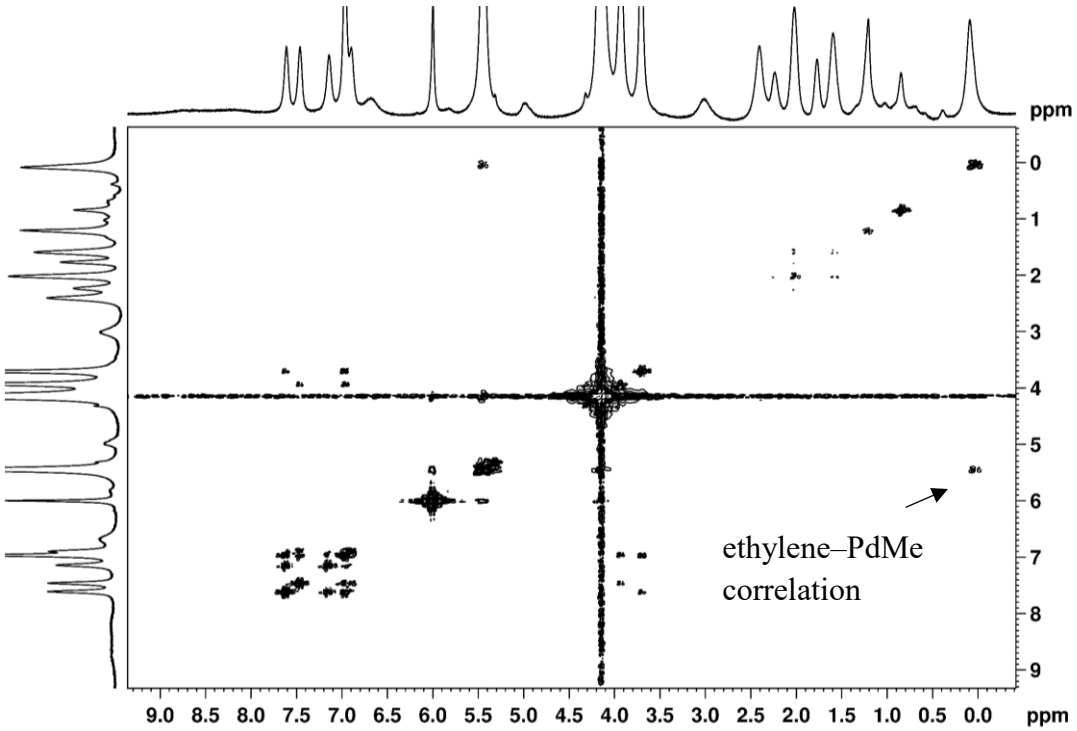

Figure 4.5. ^{1}H NMR spectrum of **7b** over time (278 K in $CDCl_2CDCl_2$, 500 MHz); insertion products (dotted lines) grow in as ethylene is consumed.

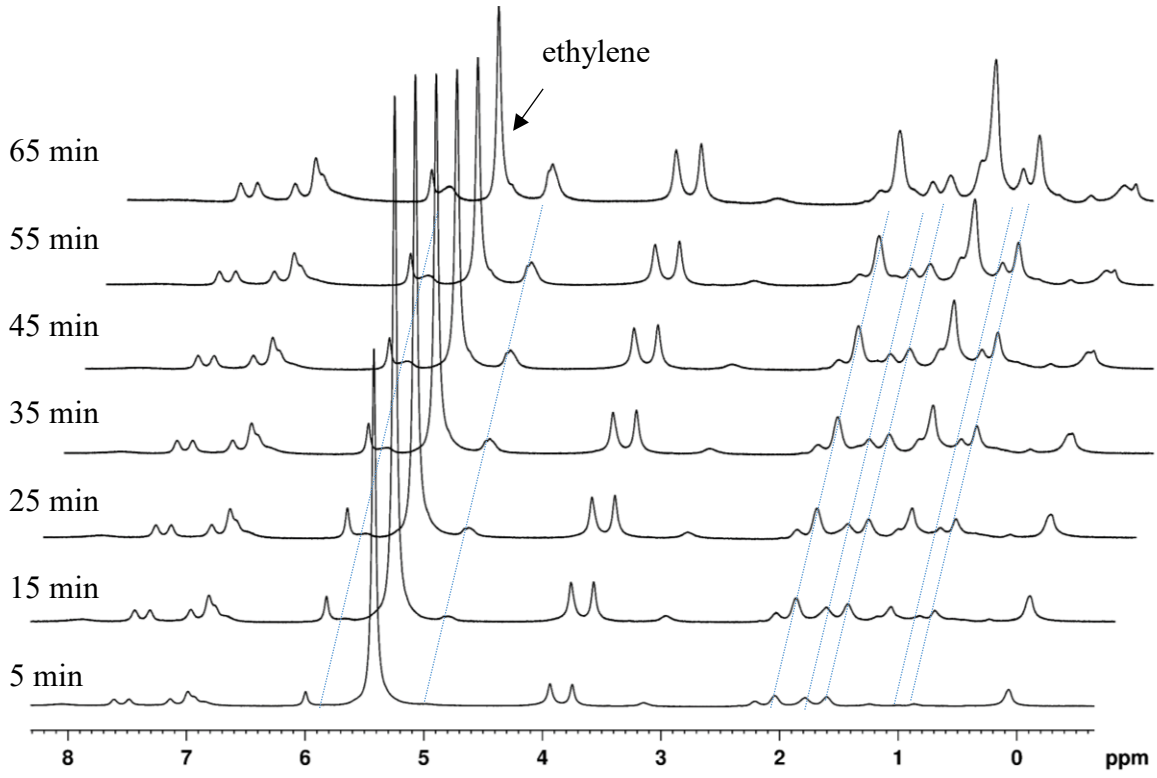

DFT Calculations. Geometry optimization and frequency calculations were completed using Gaussian09.[86] All calculations were done using the B3LYP functional with the LANL2DZ effective core potential on Pd and the 6-31G(d) basis set on all other atoms. All energy differences were calculated from the sum of the electronic and thermal free energies (ε 0 + G corr) for each respective species.

Figure 4.6. Optimized structures of all intermediates starting from **8-C5-PMe$_2$-Pr**.

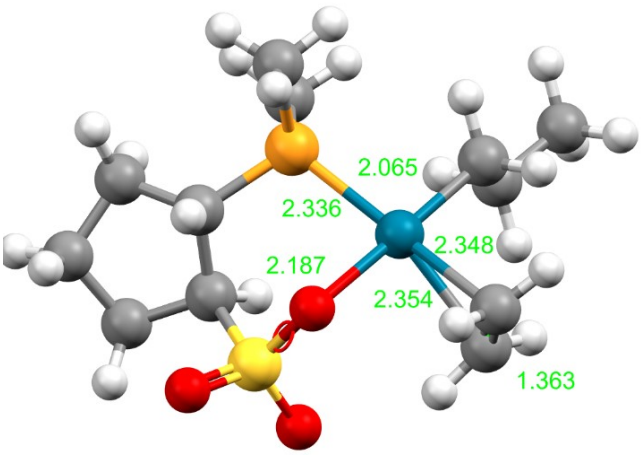

8

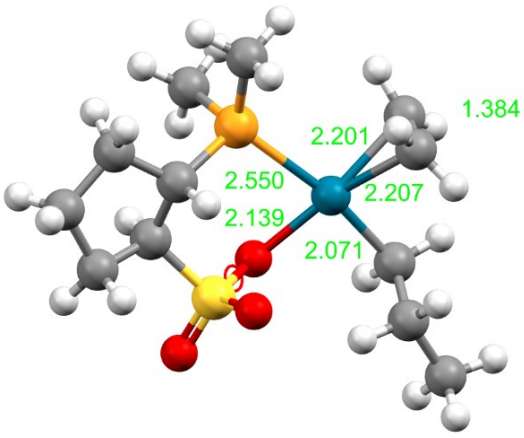

8'

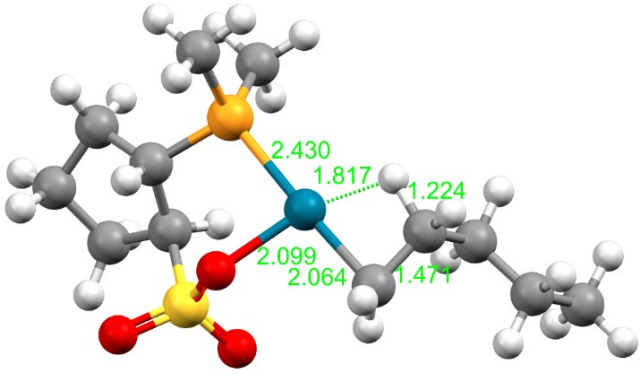

9

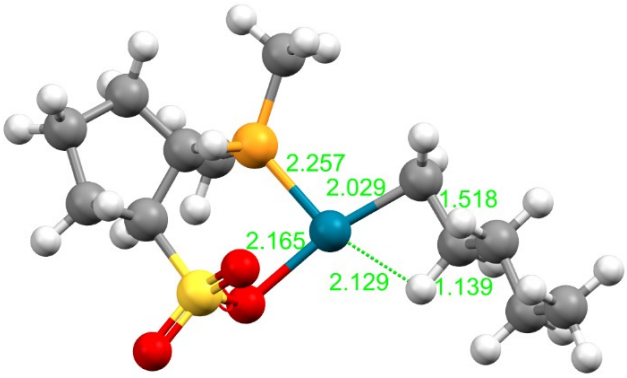

9'

Figure 4.7. Optimized structures of all transition states starting from **8-C5-PMe$_2$-Pr**.

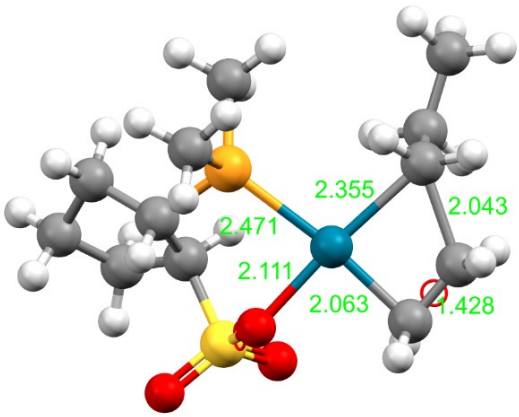

TS(8-9)

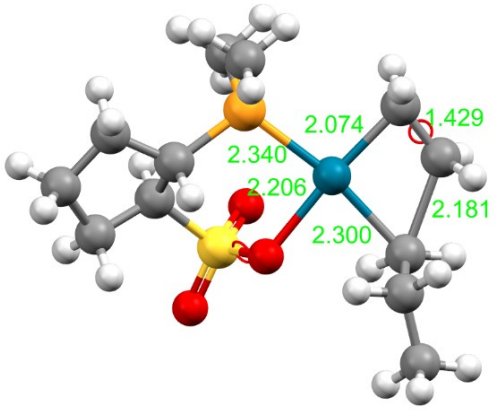

TS(8'-9')

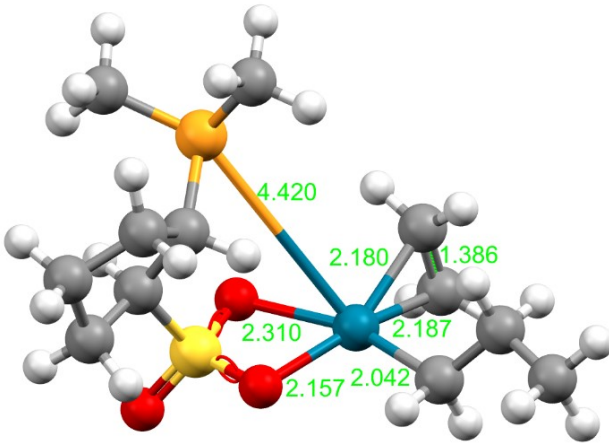

TS(8-8')

Figure 4.8. Optimized structures of all intermediates and transition states with full ligands.

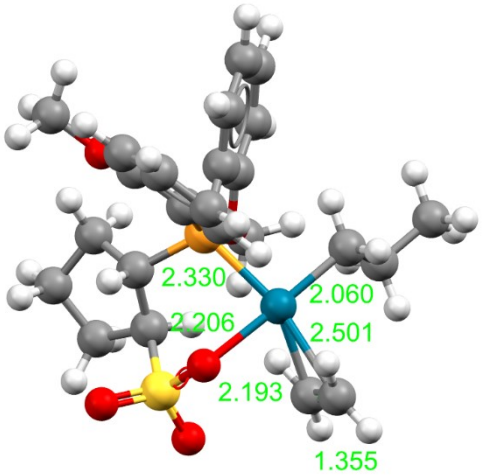

8b-Pr

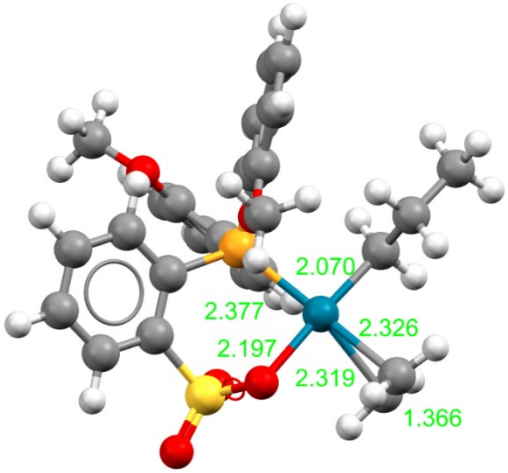

8d-Pr

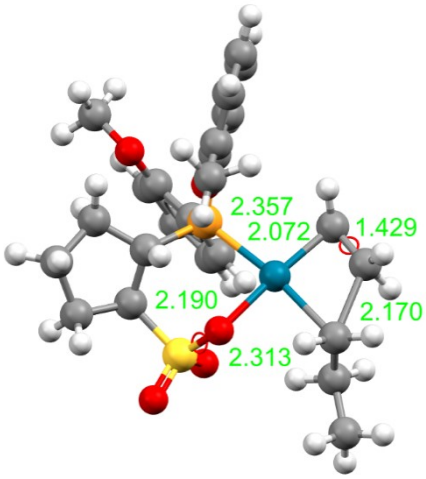

TS(8'-9') for **8b-Pr**

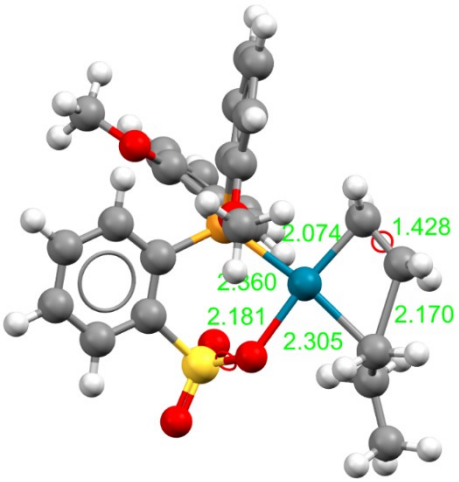

TS(8'-9') for **8d-Pr**

Table 4.1. Computed free energies (hartrees, kcal/mol) of all optimized species.

Species	T (K)	G (hartree)	G (kcal/mol)
8-C5-PMe$_2$-Pr	298.15	-1563.943457	-981388.5947586
9-C5-PMe$_2$-Pr	298.15	-1563.941702	-981387.493480
8'-C5-PMe$_2$-Pr	298.15	-1563.934950	-981383.256539
9'-C5-PMe$_2$-Pr	298.15	-1563.961856	-981400.140296
TS(8-C5-PMe$_2$-Pr to 9-C5-PMe$_2$-Pr)	298.15	-1563.894554	-981357.907686
TS(8'-C5-PMe$_2$-Pr to 9'-C5-PMe$_2$-Pr)	298.15	-1563.910156	-981367.698081
TS(8-C5-PMe$_2$-Pr to 8'-C5-PMe$_2$-Pr)	298.15	-1563.922029	-981375.148495
8-C5-PMe$_2$-Pr	353.15	-1563.958396	-981397.969115
9-C5-PMe$_2$-Pr	353.15	-1563.956837	-981396.990829
8'-C5-PMe$_2$-Pr	353.15	-1563.950148	-981392.793421
9'-C5-PMe$_2$-Pr	353.15	-1563.977112	-981409.713574
TS(8-C5-PMe$_2$-Pr to 9-C5-PMe$_2$-Pr)	353.15	-1563.909384	-981367.213644
TS(8'-C5-PMe$_2$-Pr to 9'-C5-PMe$_2$-Pr)	353.15	-1563.924872	-981376.932503
TS(8-C5-PMe$_2$-Pr to 8'-C5-PMe$_2$-Pr)	353.15	-1563.937079	-981384.592506
8-benzene-PMe$_2$-Pr	353.15	-1599.690218	-1003820.009007
9-benzene-PMe$_2$-Pr	353.15	-1599.688310	-1003818.811719
8'-benzene-PMe$_2$-Pr	353.15	-1599.675232	-1003810.605157
9'-benzene-PMe$_2$-Pr	353.15	-1599.704141	-1003828.745814
TS(8-benzene-PMe$_2$-Pr to 9-benzene-PMe$_2$-Pr)	353.15	-1599.639981	-1003788.484837
TS(8'-benzene-PMe$_2$-Pr to 9'-benzene-PMe$_2$-Pr)	353.15	-1599.657730	-1003799.622494
TS(8-benzene-PMe$_2$-Pr to 8'-benzene-PMe$_2$-Pr)	353.15	-1599.664505	-1003803.873868
8b-Pr	298.15	-2176.284208	-1365637.927078
TS(8'b-Pr to 9'b-Pr)	298.15	-2176.250277	-1365616.635070
8b-Pr	353.15	-2176.304626	-1365650.739557
TS(8'b-Pr to 9'b-Pr)	353.15	-2176.270294	-1365629.195918
8d-Pr	298.15	-2212.013500	-1388058.379372
TS(8'd-Pr to 9'd-Pr)	298.15	-2211.982180	-1388038.725790
8d-Pr	353.15	-2212.033672	-1388071.037483
TS(8'd-Pr to 9'd-Pr)	353.15	-2212.001913	-1388051.108425

4.5 References and Notes

(1) Cai, Z.; Shen, Z.; Zhou, X.; Jordan, R. F. *ACS Catal.* **2012**, *2*, 1187.

(2) Solubility limitations for **4b** limited experiments to $CDCl_2CDCl_2$, which freezes at −44 °C, precluding studies at lower temperatures.

(3) Noda, S.; Nakamura, A.; Kochi, T.; Chung, L. W.; Morokuma, K.; Nozaki, K. *J. Am. Chem. Soc.* **2009**, *131*, 14088.

(4) The observed activity of ca. 200 kg $molPd^{-1}$ h^{-1} at 80 °C corresponds to a turnover frequency of 2 s^{-1} and a free energy barrier of $\Delta G^{\ddagger}_{insert}$ = 20 kcal/mol. The $\Delta G^{\ddagger}_{insert}$ values estimated by NMR at 5 °C and from the polymerization activity at 80 °C are expected to be similar, as $\Delta S^{\ddagger}_{insert}$ is likely to be small for this unimolecular process.

(5) Haras, A.; Michalak, A.; Rieger, B.; Ziegler, T. *Organometallics* **2006**, *25*, 946.

(6) Haras, A.; Anderson, G. D. W.; Michalak, A.; Rieger, B.; Ziegler, T. *Organometallics* **2006**, *25*, 4491.

(7) Nozaki, K.; Kusumoto, S.; Noda, S.; Kochi, T.; Chung, L. W.; Morokuma, K. *J. Am. Chem. Soc.* **2010**, *132*, 16030.

(8) Nakano, R.; Chung, L. W.; Watanabe, Y.; Okuno, Y.; Okumura, Y.; Ito, S.; Morokuma, K.; Nozaki, K. *ACS Catal.* **2016**, *6*, 6101.

(9) Conley, M. P.; Jordan, R. F. *Angew. Chem. Int. Ed. Engl.* **2011**, *50*, 3744.

(10) Zhou, X.; Lau, K.-C.; Petro, B. J.; Jordan, R. F. *Organometallics* **2014**, *33*, 7209.

(11) For other cases in which cis/trans isomerization or equivalent exchange processes are mediated by intramolecular coordination of hemilabile ligands, see: Rotondo, E.; Battaglia, G.; Arena, C. G.; Faraone, F. J. *Organomet. Chem.* **1991**, *419*, 399−402. Imhoff, P.; van Asselt, R.; Ernsting, J. M.; Vrieze, K.; Elsevier, C. J.; Smeets, W. J. J.; Spek, A. L.; Kentgens, A. P. M. Organometallics **1993**, *12*, 1523−1536.Casares, J. A.; Espinet, P. *Inorg. Chem.* **1997**, *36*, 5428.

Chapter Five

Olefin Insertion Reactivity of a (Phosphine-arenesulfonate)Palladium(II) Fluoride Complex

5.1 Introduction

The tunable, direct copolymerization of ethylene (E) and vinyl fluoride (VF) using transition-metal catalysts would be an attractive way to produce new copolymers with intermediate properties between polyethylene (PE) and polytetrafluoroethylene (PTFE, Teflon). However, to date, the only transition metal complexes that have been shown to catalyze this reaction are the (PO)PdMe(py) catalysts shown in Chart 5.1 and those introduced in Chapter Two, which copolymerize E and VF to linear copolymers.[1–3] Catalysts **A-Et**, **A-OMe**, and **A-H** produce E/VF copolymers that contain up to 0.45 mol% VF as internal $–CH_2CHFCH_2–$ and chain-end $–CH_2CHFCH_3$ units.[1] Phosphine-bis-sulfonate catalyst **A-cage** produces E/VF copolymers that contain up to 3.6 mol% VF, including previously unobserved unsaturated $–CH_2CH{=}CHF$ chain ends.[2] Catalyst **B** produces E/V copolymer with the highest MW but the lowest VF content.[3] Interestingly, Wada and Jordan found that the E/VF copolymers produced by **C** and **D** contain significant amounts of $–CH_2CH_2CHF_2$ and $–CH_2CH_2CH_2F$ chain-end units, in contrast to the low levels observed in the copolymers formed by **A-OMe** and **B** (Figure 5.1). Interestingly, as the $PO^–$ ligand size increases from **A-OMe** < **D** < **C**, the selectivity for internal $–CH_2CHFCH_2–$ units decreases and chain-end $–CH_2CH_2CHF_2$ units increases.

Chart 5.1. (PO)PdR catalysts tests in E/VF copolymerization

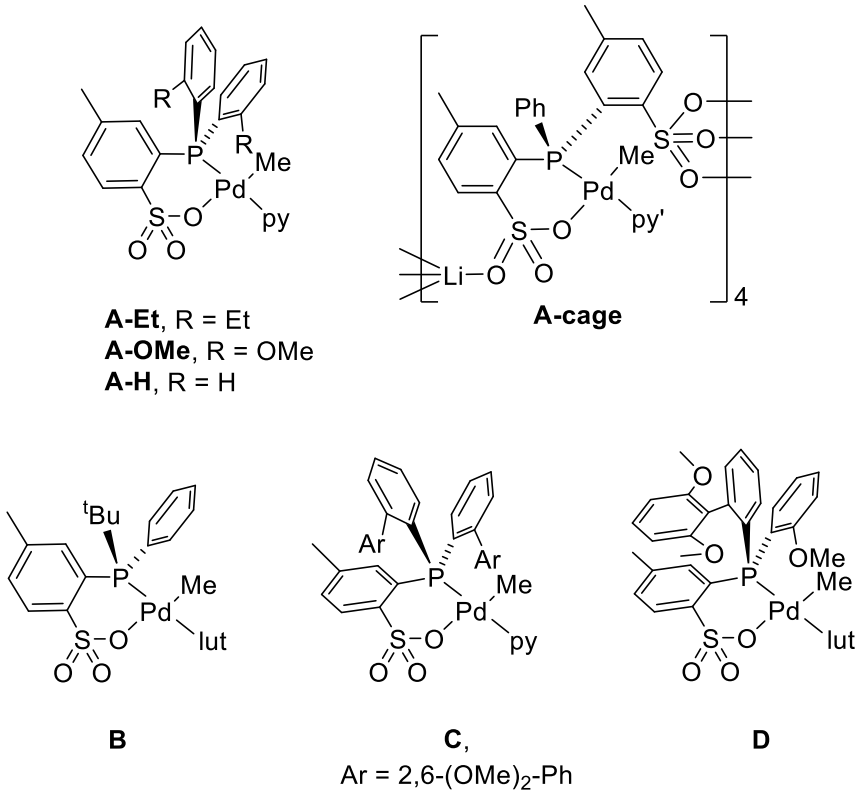

Figure 5.1. Microstructure of E/VF copolymers produced by **A-OMe**, **B**, **C**, and **D**. The VF incorporation mode (%) was identified by ^{1}H and ^{19}F NMR and quantified by ^{1}H NMR integration; P = Polymer.

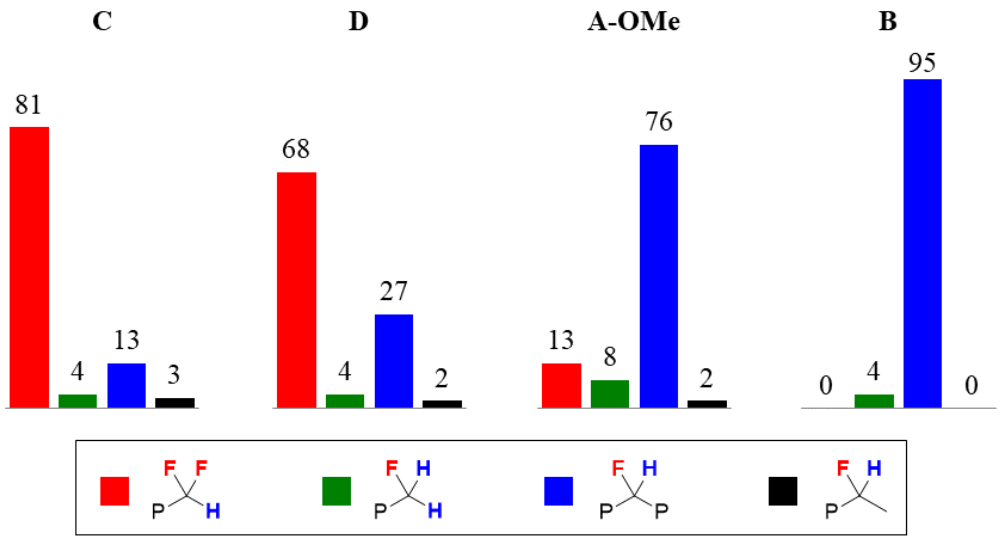

A summary of how these different VF units are generated by (PO)PdR species in E/VF copolymerization is shown in Scheme 5.1. Internal –CH_2CHFCH_2– units arise by 1,2- or 2,1-VF insertion into (PO)PdR species followed by E insertion, chain-end –CH_2CHFCH_3 units arise by 2,1-VF insertion into (PO)PdH species followed by E insertion, and chain-end –CH_2CH=CHF units arise by 2,1-VF insertion into (PO)PdR species followed by *β*-H elimination. The –$CH_2CH_2CHF_2$ and –$CH_2CH_2CH_2F$ chain-end units arise by *β*-F elimination from (PO)PdCH_2CHFR or (PO)Pd$CH(CH_2F)R$ species to generate a (PO)PdF species, which undergoes 1,2-VF or E insertion to form (PO)PdCH_2CHF_2 and (PO)PdCH_2CH_2F followed by subsequent chain growth. The apparent correlation observed between PO^- ligand size and selectivity for chain-end –$CH_2CH_2CHF_2$ units over internal –CH_2CHFCH_2– units suggests that increasing steric crowding at the metal center favors *β*-F elimination over chain growth. This correlation is intuitive as chain growth proceeds by associative E coordination, Berry pseudorotation via a five-coordinate intermediate, and insertion. This trend should be taken into account when designing new catalysts for E/VF copolymerization, as E/VF copolymers with F atoms incorporated along the polymer backbone likely have more interesting material properties than PE chains capped with -CF_2H units.

Scheme 5.1. E/VF copolymerization

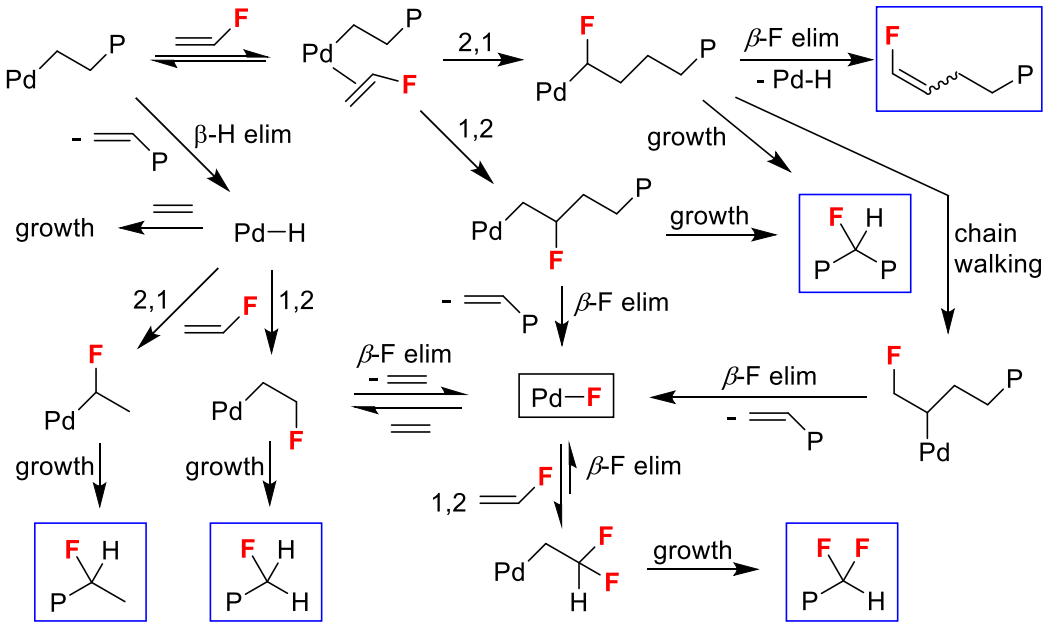

Wada and Jordan provided strong support for the proposal that the $–CH_2CH_2CHF_2$ and $–CH_2CH_2CH_2F$ chain-end units arise by VF or E insertion into a (PO)PdF species by independently synthesizing a palladium-fluoride complex, (PO-Bp/Ph^{OMe})PdF(lut) (**F**, Scheme 5.2), and demonstrating that this compound undergoes VF and E insertion under mild conditions (Scheme 5.3). Compound **F** was synthesized by the reaction of the PdBr complex (PO-Bp/Ph^{OMe})PdBr(lut) (**E**) with AgF, a typical route used previously in the literature.[4–11] Compound **F** reacts with VF to yield $PdCH_2CHF_2$ complex **G**, which was characterized by NMR spectroscopy and single-crystal X-ray crystallography. Compounds **F** and **G** both react with E at room temperature to give PEs with $–CH_2CH_2F$ and $–CH_2CHF_2$ units, respectively.

Scheme 5.2. Synthesis of (PO-BP/Ph^{OMe})PdF(lut)

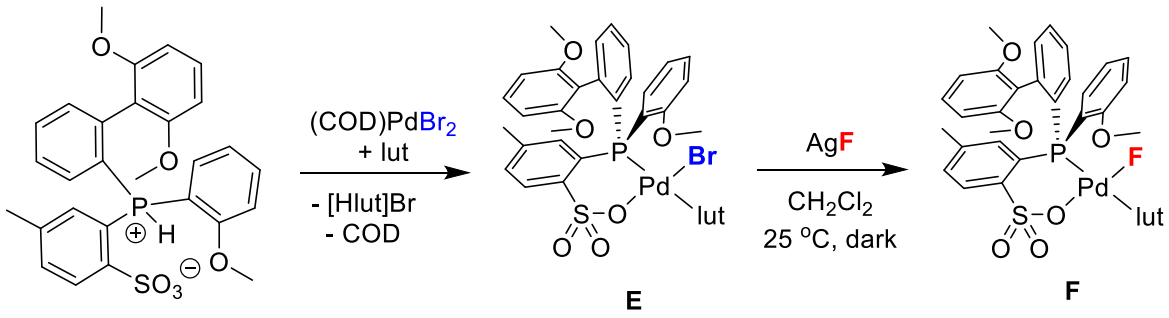

Scheme 5.3. E and VF reactivity with **F**

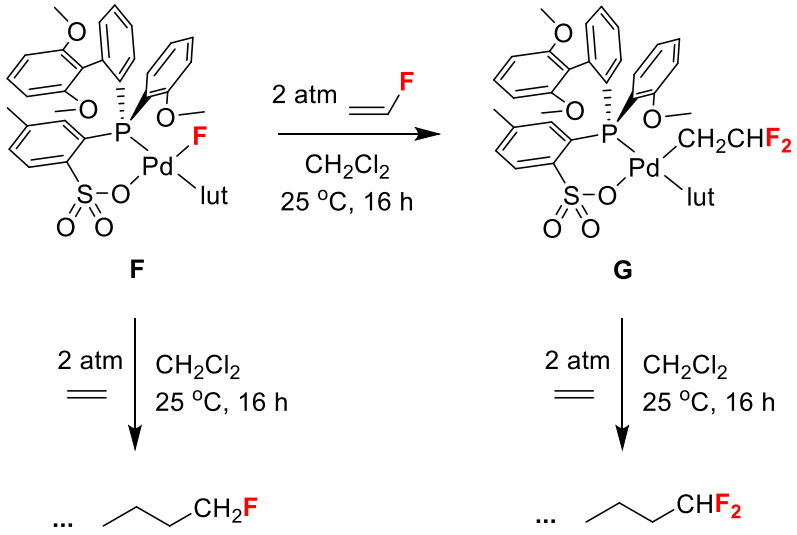

The fluoropalladation of E and VF by Pd–F complex **F** could occur either by a migratory insertion mechanism, which is expected to result in *cis* addition, or by *exo* attack of F^- on a bound olefin as in Wacker chemistry, which is expected to result in *trans* addition. Evidence for both of these mechanisms has been reported in other fluoropalladation studies.[12–15] However, DFT calculations show that the interconversion of the model complexes (P^P)PdF(CH_2=CH_2)$^+$ and (P^P)Pd$CH_2CH_2F^+$ (P^P = $H_2PCH_2CH_2PH_2$) occurs by migratory insertion and *β*-F elimination with low barriers, suggesting that a *cis*-addition mechanism may be operative in the (PO)Pd

system.[16] Determination of which fluoropalladation mechanism is operative in the (PO)PdF system may inform future efforts to design improved E/VF copolymerization catalysts and to develop new fluorination methods for organic synthesis.[17–26]

Wada synthesized **F** by standard synthetic protocols for Pd(II) complexes using borosilicate Schlenk glassware or vials under an inert atmosphere. However, this approach yielded recrystallized material described by Wada as "brown crystals and brown powder." Repetition of Wada's procedure for the synthesis of **F** by the author also resulted in brown crystals and brown powder, which were physically separated and analyzed by NMR. While the ^{1}H and ^{31}P NMR spectra for each sample were nearly identical, the ^{19}F NMR spectrum of the brown powder was enriched in signals ca. δ –129 and δ –153, which are characteristic of free fluoride[27,28] and fluorosilicate species,[29–31] respectively. Close examination of the ^{19}F NMR spectra taken by Wada for all samples of **F** in CD_2Cl_2 solution also contained these signals. The fluorosilicates likely arise from the reaction of HF with the glass of the Schlenk flasks, J-Young tubes, or storage vials used in the synthesis and manipulation of **F**. The HF is likely generated by the reaction of **F** with trace water or the reaction of F^- generated by the reaction of **F** with Si-OH groups on the surface of the borosilicate glass. Similar glass etching by other palladium fluoride complexes has been reported.[32] It is unknown what role, if any, the free F^- and/or fluorosilicate contaminants in samples of **F** played in the E and VF fluoropalladation reactions reported by Wada.

The objectives of this Chapter were to (i) improve the synthetic protocols for (PO)PdF compounds in order to avoid the presence of free F^- and fluorosilicate contaminants, (ii) use these improved protocols to expand the scope of (PO)PdF complexes that can be made, (iii) expand the set of olefins that react with (PO)PdF complexes, and (iv) devise a way to determine whether fluoropalladation occurs by *cis* or *trans* addition.

5.2 Results and Discussion

Synthesis of (PO-OMe)PdF(lut) Complex. The unusual chemistry of transition-metal fluoride complexes can be rationalized in terms of destabilizing electron-electron repulsion between the filled d orbitals on the metal and a lone electron pair on fluorine.[33] This filled-filled effect weakens the M–F bond below that of an ordinary single bond, making the fluoride highly basic/nucleophilic and a locus for H bonding. To avoid the formation of HF, free fluoride and fluorosilicate species in this work, polypropylene (PP) vials, beakers, funnels, and Erlenmeyer flasks, Teflon filtration flasks and Teflon NMR tube liners were used for the synthesis, storage, and reactions of all palladium fluoride compounds described below. The reaction of pro-ligand H[PO-OMe] with (COD)$PdBr_2$ followed by addition of lutidine yielded (PO-OMe)PdBr(lut) (**1**) and lutidinium bromide, the latter of which was removed by a water wash (Scheme 5.4). **1** was recrystallized to give orange crystals that were dried under vacuum overnight (Yield: 77.0%, 3.28 g). X-ray quality crystals of **1**•CH_2Cl_2 were grown from a concentrated methylene chloride solution of **1** (Figure 5.2). The bond lengths and angles in **1** are very similar to those in (PO-Bp/Ph^{OMe})PdBr(lut) reported by Wada and Jordan.[3] The reaction of **1** with AgF in CH_2Cl_2 in a foil-wrapped polypropylene vial afforded **2** as a mixture of *cis-P,F* and *trans-P,F* isomers (Yield 95.0%, 0.338 g).

Scheme 5.4. Synthesis of (PO-OMe)PdF(lut)

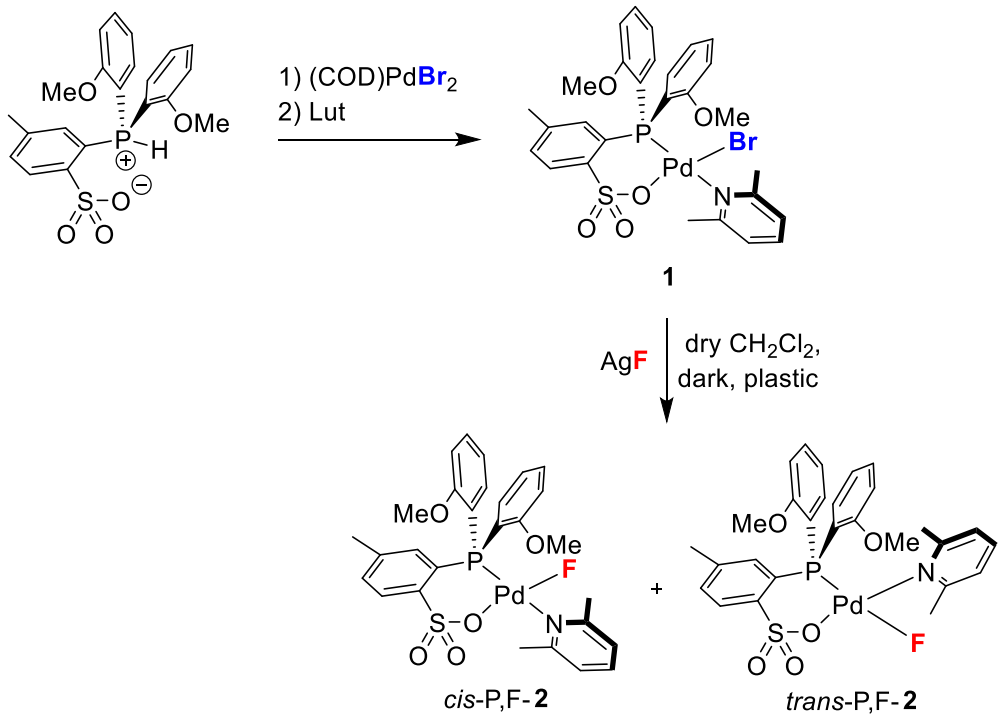

Figure 5.2. Molecular structure of **1**•CH_2Cl_2. Hydrogen atoms and a CH_2Cl_2 solvent molecule are omitted. Bond lengths (Å) and angles (°): Pd1–Br1 2.3903(4), Pd1–N1 2.113(3), Pd1–O1 2.069(2), Pd1–P1 2.2483(9), Br1–Pd1–N1 88.26(7), N1–Pd1–O1 87.84(9), Br1–Pd1–P1 88.40(2), O1–Pd1–P1 95.51(6).

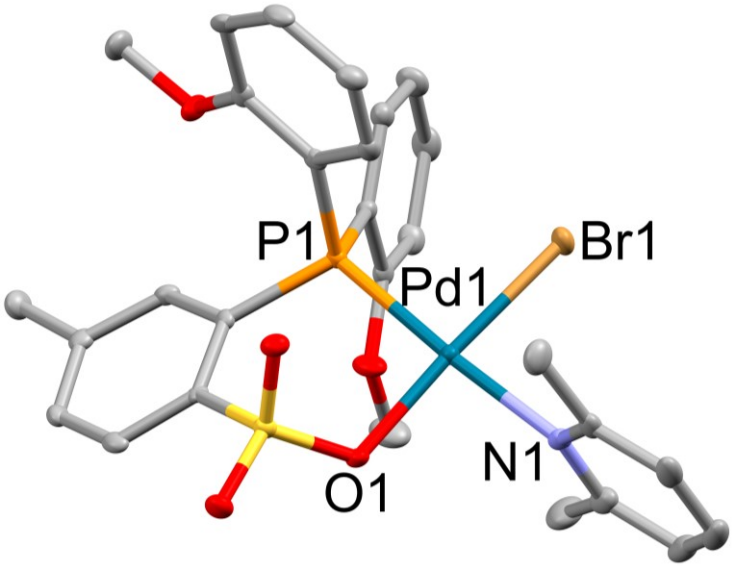

Solution structure and dynamics of *cis*/*trans*-*P,F*-(PO-OMe)PdF(lut) (2). Interestingly, **2** was first isolated as a ca. 82:18 *cis*-*P,F*:*trans*-*P,F* mixture, but isomerized in the solid-state at –40 °C under N_2 over 3 weeks to a 44:56 *cis*-*P,F*:*trans*-*P,F* mixture and in CD_2Cl_2 at room temperature over 1 month to a 1:2 *cis*-*P,F*:*trans*-*P,F* equilibrium mixture. The rate of equilibration of *cis*-*P,F*-**2** and *trans*-*P,F*-**2** (Eq. 5.1) was estimated by periodic NMR assaying of a non-equilibrium mixture of *cis*-/*trans*-*P,F*-**2** in CD_2Cl_2 at room temperature. The concentrations of [*cis*-*P,F*-**2**] and [*trans*-*P,F*-**2**] were measured by ^{1}H NMR integration of their *p*-tolyl-CH_3 resonances (Figure 5.3). These concentration data were treated using first-order approach-to-equilibrium kinetics by Eqs. 5.2 and 5.3:

$$\textit{cis}\text{-}P,F\text{-}\mathbf{2} \underset{k_{-1}}{\overset{k_1}{\rightleftharpoons}} \textit{trans}\text{-}P,F\text{-}\mathbf{2} \qquad \textbf{Eq. 5.1}$$

$$\ln\left(\frac{[cis] - [cis]_\infty}{[cis]_0 - [cis]_\infty}\right) = -k_{\text{obs}}t \qquad \textbf{Eq. 5.2}$$

$$K_{eq} = \frac{[trans]_\infty}{[cis]_\infty} = \frac{k_1}{k_{-1}} = 2.0 \qquad \textbf{Eq. 5.3}$$

$$k_{\text{obs}} = k_1 + k_{-1} \qquad \textbf{Eq. 5.4}$$

where k_{obs} is the observed first-order rate constant for approach to equilibrium, which is equal to the sum of the forward (k_1) and reverse (k_{-1}) first-order rate constants (Eq. 5.4) and K_{eq} is the equilibrium constant for Eq. 5.1, which was determined to equal 2.0. The linear least-squares fit and rate constants obtained based on data for *cis*-*P,F*-**2** are shown in Figure 5.4. From the slope of

this plot, k_{obs} was found to be 5.0 x 10 $^{-6}$ s^{-1}. The first-order rate constants k_1 (3.3 x 10 $^{-6}$ s^{-1}) and k_{-1} (1.7 x 10 $^{-6}$ s^{-1}) were calculated using Eqs. 5.3 and 5.4.

Figure 5.3. Time dependence concentrations of *cis-P,F*-**2** (red) and *trans-P,F*-**2** (blue) in CD_2Cl_2 at room temperature.

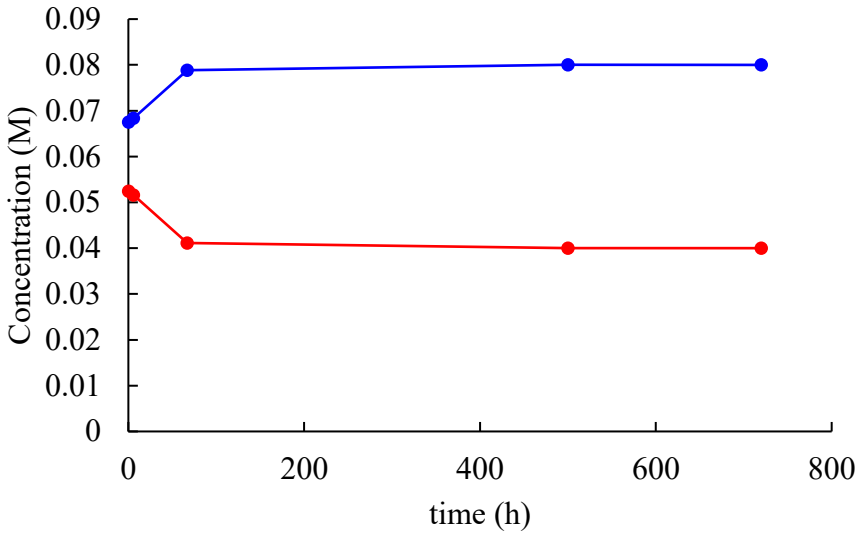

Figure 5.4. Plot of ln[([*cis-P,F*-**2**]-[*cis-P,F*-**2**]$_\infty$)/([*cis-P,F*-**2**]$_0$-[*cis-P,F*-**2**]$_\infty$)] vs time (min).

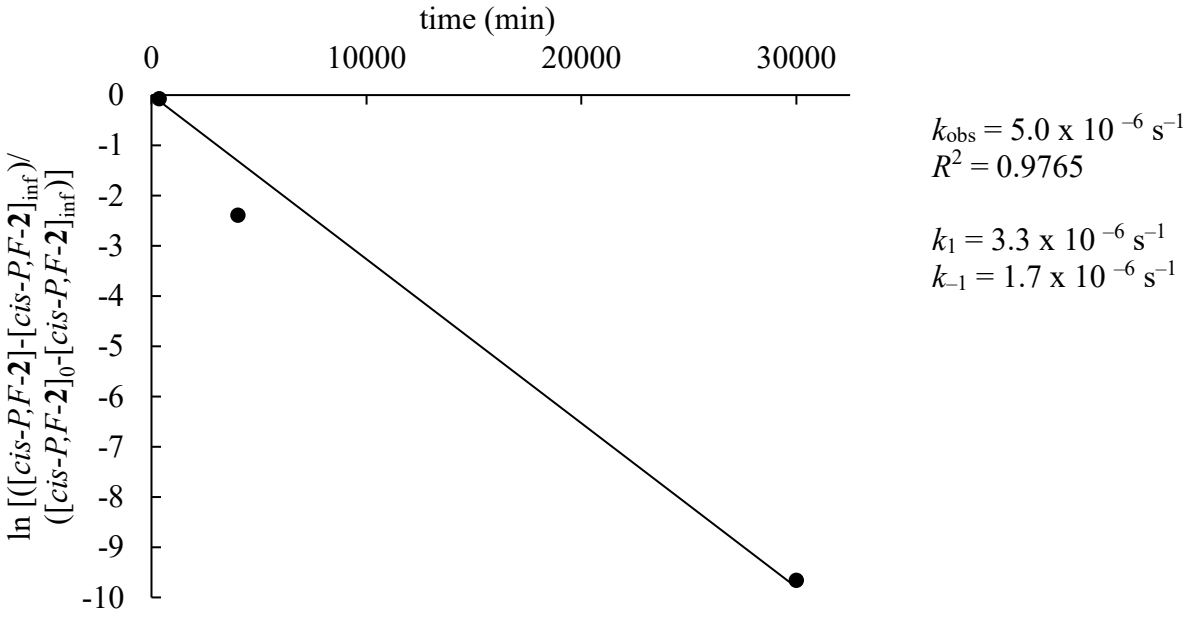

Square planar PdL_2X_2 (L = lut or other pyridines; X = Br, I, N_3, CNS) complexes are known to undergo *cis*/*trans* isomerization in the presence of traces of free ligand L.[34] This occurs by associative ligand coordination to generate a five-coordinate (PO)$PdXL_2$ intermediate, Berry pseudorotation, and release of L from the opposite axial position. Similarly, studies of $[(PO)Pd(py)_2]^+$ and of non-equilibrium *cis*/*trans* mixtures of the Pd-*Cl* species (PO)PdClP(O-*o*-tolyl)$_3$ indicate that an external ligand is necessary for *cis*/*trans* isomerization of these complexes.[35] It also has been shown that the isomerization of *trans-P,C*-(PO-OMe)PdMe(lut) *alkyl* species to the thermodynamically-favored *cis-P,C* isomers can occur either by a lutidine-catalyzed pathway or by a unimolecular pathway.[36] Based on these precedents, both ligand-catalyzed and unimolecular pathways are possible for **2**. The isomerization behavior of **2** stands in stark contrast to the behavior of (PO-Bp/Ar^{OMe})PdF(lut), for which only the *cis-P,F* isomer was observed.[3] Since the (PO-OMe) and (PO-Bp/Ar^{OMe}) ligands have similar electron donating abilities, *cis-P,F*-(PO-Bp/Ar^{OMe})PdF(lut) is likely preferred as this isomer avoids the steric pressure between the Bp unit and lutidine that is expected in *trans-P,F*-(PO-Bp/Ar^{OMe})PdF(lut) (see Chapter Six for an analysis of the solution conformations of (PO-Bp/Ar^{OMe})PdMeL, where L = pyridine and lutidine).

In the presence of added CsF (vide infra), the room temperature $^{31}P\{^1H\}$ NMR spectrum of **2** contains two doublets centered at δ 3 ($^1J_{PF}$ = 200 Hz) and δ –5 ($^1J_{PF}$ = 14 Hz, Figure 5.5(a)), which are assigned to the *trans-P,F* and *cis-P,F* isomers, respectively. Consistent with these results, the room temperature ^{19}F NMR spectrum (non-$\{^1H\}$) contains a doublet at δ –267 ($^1J_{PF}$ = 200) and a broad singlet at δ –436, which sharpens into a doublet ($^1J_{PF}$ = 14) at –15 °C, which are assigned to the *trans-P,F* and *cis-P,F* isomers, respectively (Figure 5.5(b)). These data are consistent with previous results for Pd(II) fluoride complexes bearing phosphine ligands *trans* to fluoride (^{19}F: δ –200 to –300; $J_{PF,trans}$ > 150 Hz)[6–11] and *cis* to fluoride (^{19}F: δ < –300; $J_{PF,cis}$ = 6–

18 Hz).[3,6,37–42] Representative Pd(II) fluoride complexes are shown in Chart 5.2 and their ^{19}F NMR chemical shifts and $^{2}J_{PF}$ values are shown in Table 5.1. The addition of excess [NBu4]Br to *cis*:*trans*-*P,F*-**2** (32:68 ratio) gives **1** quantitatively, which confirms that these species are isomers (Figure 5.6).

Figure 5.5. NMR spectra, including expansions, of **2** before (bottom) and after (top) addition of CsF (CD_2Cl_2, 25 °C).

(a) $^{31}P\{^1H\}$ NMR (202 MHz)

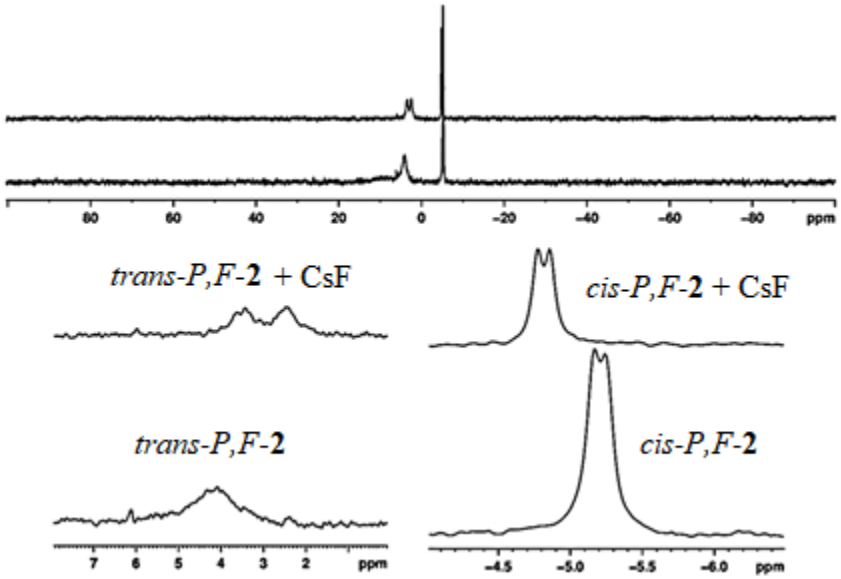

(b) ^{19}F NMR spectra (470 MHz)

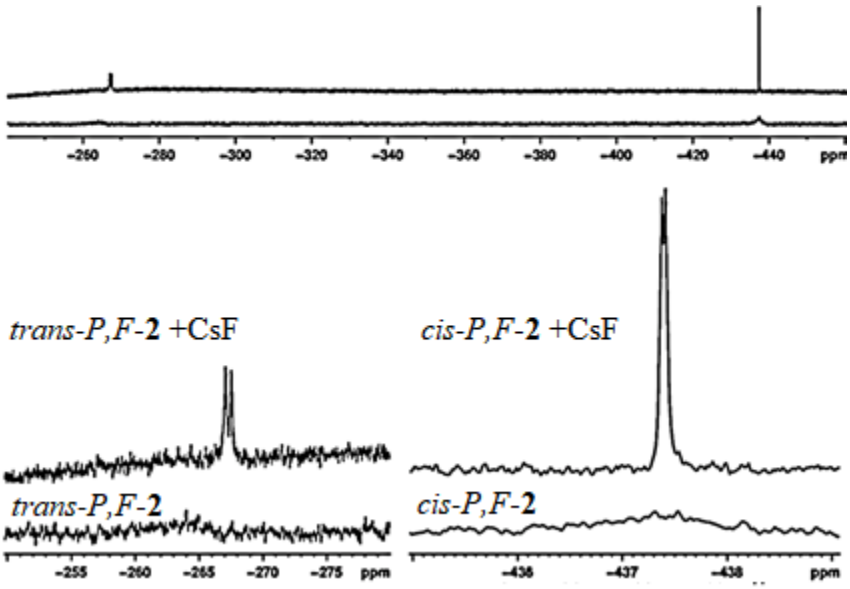

Chart 5.2. Representative examples of isolated Pd(II)–Fluoride complexes

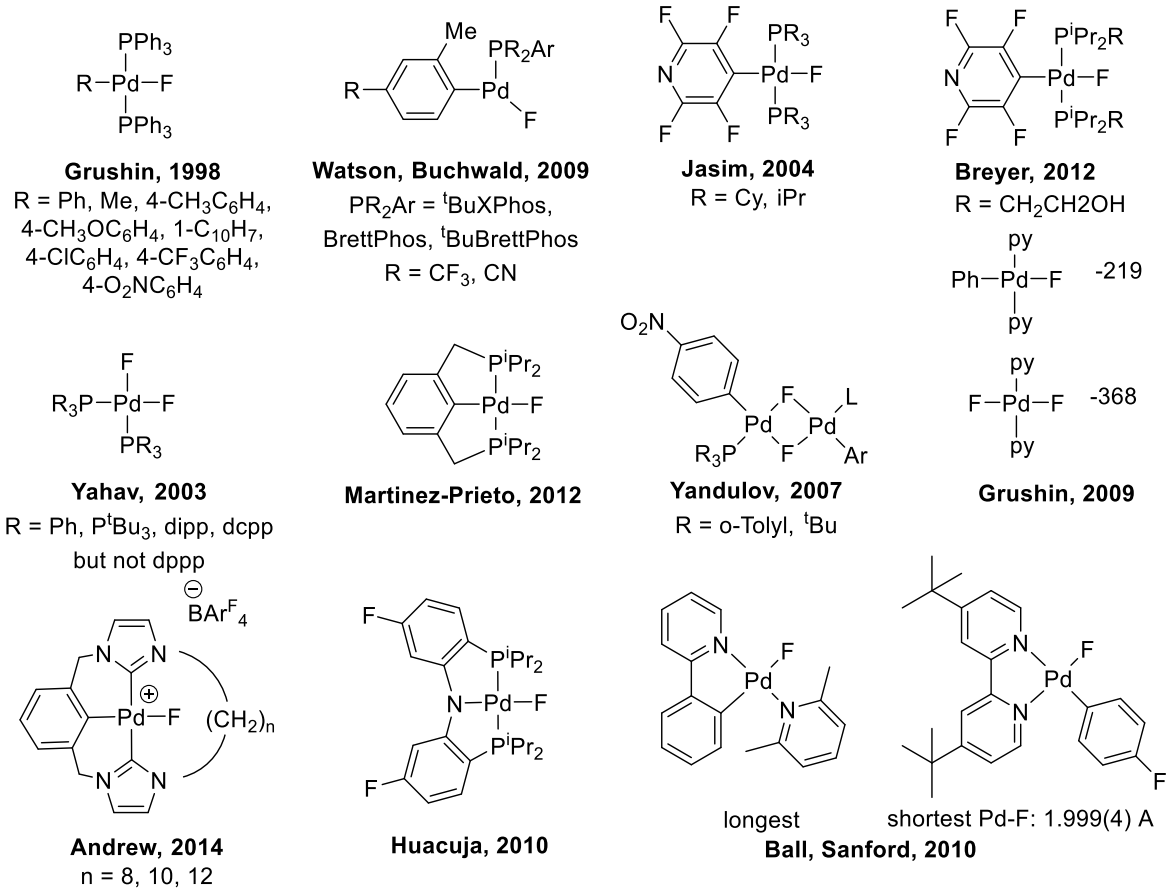

Table 5.1. ^{19}F NMR chemical shifts and $^{2}J_{PF}$ values for some Pd(II)–fluoride complexes

	Orientation of PR_3 and F ligands	^{19}F chemical shift (δ)	$^{2}J_{PF}$ (Hz) in ^{19}F NMR
$[(Ph_3P)_2Pd(R)F]$, R = Ph, Me[37]	cis	–274 and –268	13.3 and 12.5
PdF(BrettPhos)(Ar)[38]	trans	~ –207	~175 Hz, depending on Ar
$PdF(PR_3)(Ar^F)$[39]	cis	–322	14.1
$PdF(P^iPr_2R)(Ar^F)$[40]	cis	−316.5	17.4
L_2PdF_2, L_2 = dippp(a), dcpp (b), dppe (c)[43]	cis/trans	–251.7 (a), –251.7 (b), –238.7 (c)	"broadened"
(PCP)PdF[41]	cis	−245.3	"too broad"
$[Pd(PR_3)(Ar)(\mu\text{-}F)]_2$[42]	cis/trans	–292.7 and –286.9	167 and 154
$PdF(Ph)(py)_2$ and *trans*-$PdF_2(py)_2$[6]	trans	–219 and –368	N/A
$[(NHC,C,NHC)PdF][BAr^F_4]$[10]	N/A	ca. −400	N/A
(PNP)PdF[11]	cis	−414.3	N/A
(*o*-Ph-py)Pd(lut)F and others[7]	N/A	–340.7, –240, –350	N/A
$(PO\text{-}Bp/Ph^{OMe})PdF(lut)$[3]	cis	–429.3	17

Figure 5.6. NMR monitoring of the reaction of **2** and NBu_4Br (CD_2Cl_2, 25 °C).

(a) ^1H NMR spectra (500 MHz) (b)^{31}P NMR spectra (202 MHz)

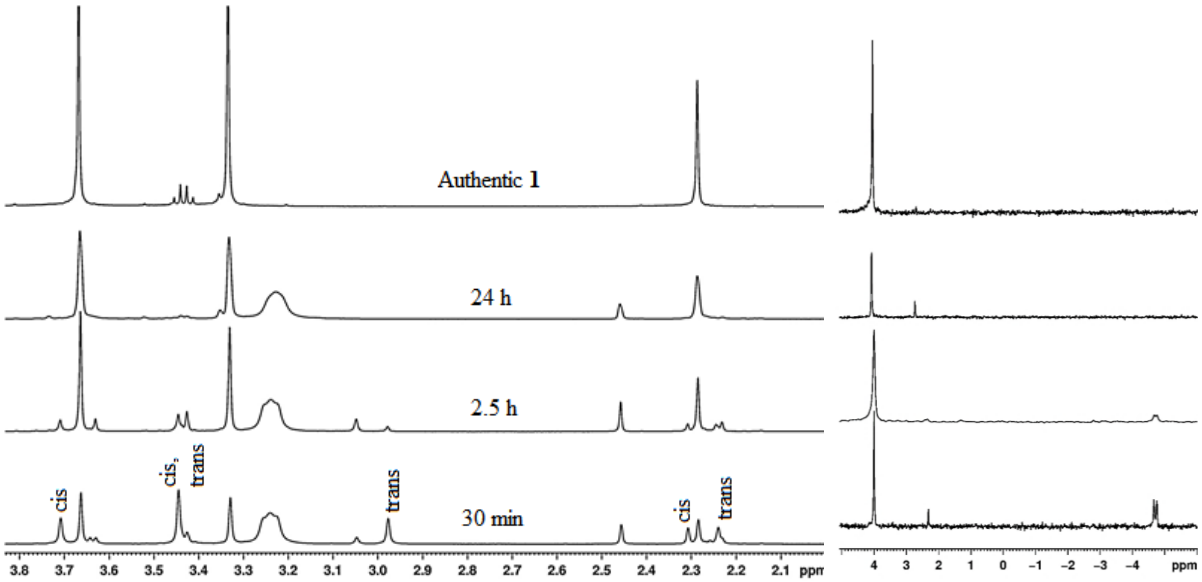

The addition of CsF was necessary to observe all of the ^{31}P and ^{19}F NMR couplings for *cis-P,F* and *trans-P,F*-**2**, which is typical for PdF complexes.[7,8,33,37] In the absence of added CsF in dry CD_2Cl_2, the P–F coupling is observed for the ^{31}P resonance of *cis-P,F*-**2**, but not for the ^{31}P resonance of *trans-P,F*-**2** or the ^{19}F resonances of either isomer. As shown in Figure 5.5, the $^{31}P\{^1H\}$ spectrum of **2** in dry CD_2Cl_2 comprises a broad signal in the range δ 5–3 (*trans-P,F*-**2**) and a doublet at δ –4.8 (J_{PF} = 16 Hz, *cis-P,F*-**2**) and the ^{19}F NMR spectrum comprises broad singlets at δ –258 ($\Delta\upsilon_{1/2}$ = 500–1,000 Hz, *trans-P,F*-**2**) and δ –437 ($\Delta\upsilon_{1/2}$ = 95–500 Hz, *cis-P,F*-**2**). The collapse of the P–F coupling is ascribed to hydrogen bonding with adventitious water or HF. Intermolecular fluoride exchange is unlikely because P–F coupling would not be observed for the ^{31}P resonance of *cis-P,F*-**2** (δ –4.8) if this were the case. Grushin[4] has investigated the interaction of a series of $(PPh_3)_2Pd(F)(R)$ complexes with water in solution, and has proposed that two processes are possible: Pd–F ionization (Eq. 5.5) and Pd–F•••HOH hydrogen bond formation (Eq.

5.6).[44] Of these, the latter process is likely for **2**. CsF sequesters adventitious water through hydrogen bonding.

$$(Ph_3P)_2Pd(Ph)F + H_2O \rightleftharpoons (Ph_3P)_2Pd(Ph)^+ + F^- \qquad \textbf{Eq. 5.5}$$

$$(Ph_3P)_2Pd(Ph)F + H_2O \rightleftharpoons (Ph_3P)_2Pd(Ph)F\bullet\bullet\bullet HOH \qquad \textbf{Eq. 5.6}$$

Synthesis and structure of (PO-OMe)Pd(FHF)(lut). As noted above, adventitious hydrolysis or decomposition of a (PO)PdFL complex may generate HF, leading to secondary chemistry that may complicate the reactivity of the (PO)PdFL species itself with olefins. For this reason, the reaction of **2** with HF was investigated briefly. Addition of the mild HF source $NEt_3(HF)_3$ to a solution of *cis:trans-P,F*-**2** (27:73) in CD_2Cl_2 gave a mixture the bifluoride complex (PO-OMe)Pd(FHF)(lut) as a mixture of *cis-P,F* and *trans-P,F* isomers (**3**, 27:73, Scheme 5.5) and other, as yet unidentified, species. A single crystal of *trans-P,F*-**3** suitable for X-ray diffraction was grown by layering pentane over the CD_2Cl_2. The structure of *trans-P,F*-**3** is shown in Figure 5.7.[45] The Pd–FHF bond length of 2.057(3) Å is slightly shorter than that in *trans*-$(Ph_3P)_2Pd(R)(FHF)$ (R = Ph: 2.098(2) Å; R = Me: 2.103(2) Å),[37] and $Pd(F)_2(HF_2)(Ar)(^t$Bu-bpy) (2.113(2) Å, Ar = *p*-F-Ph, ^{t}Bu-bpy = *tert*-butyl-bipyridine), in which the FHF ligand is *trans* to the Ar ligand.[8] These differences in Pd-FHF bond lengths reflect differences in the *trans* influence of the *trans* ligand and in coordination number. Notably, the Pd–FHF bond length in *trans-P,F*-**3** is within the range reported for palladium fluoride compounds (1.948-2.178 Å),[46,47] which indicates that the PdF---HF interaction does not strongly perturb the Pd–F bond.

Scheme 5.5. Formation of (PO-OMe)Pd(FHF)(lut)

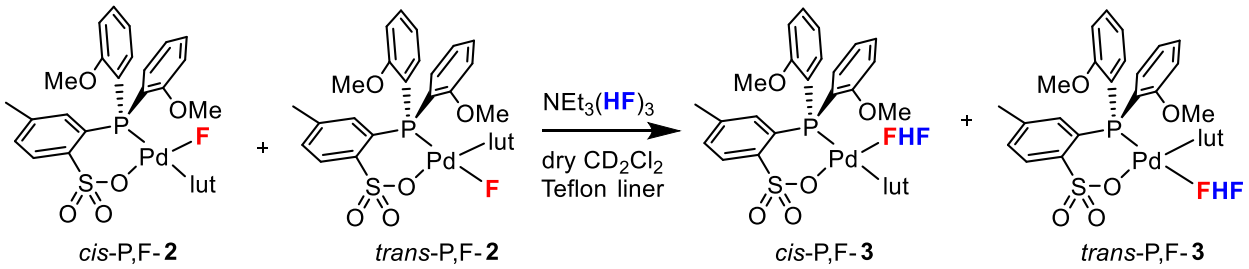

Figure 5.7. Molecular structure of *trans-P,F*-**3**. Hydrogen atoms except for F*H*F are omitted. Bond lengths (Å) and angles (°): Pd1–F1 2.057(3), Pd1–N1 2.014(4), Pd1–O1 2.047(4), Pd1–P1 2.2047(14), F1–Pd1–N1 89.49(15), F1–Pd1–O1 92.11(14), N1–Pd1–P1 95.18(12), O1–Pd1–P1 83.34(11).

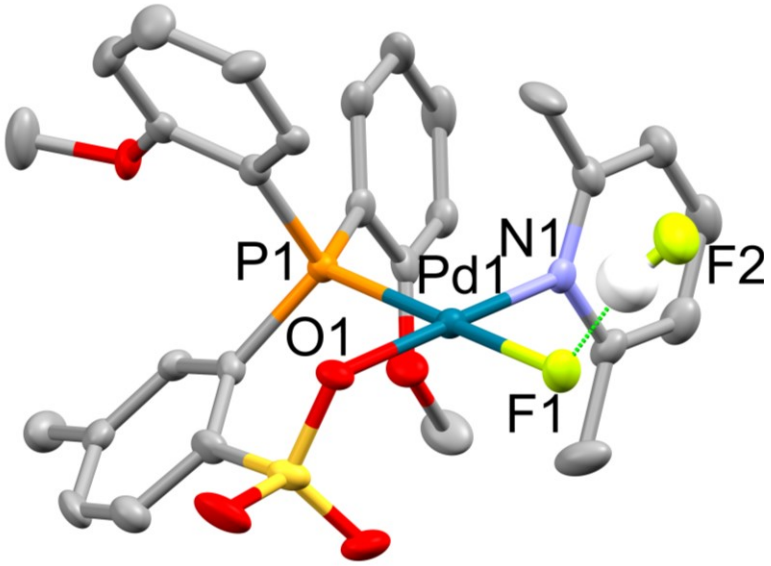

This is the first crystal structure of a (PO)PdXL complex with the neutral L ligand *trans* to the sulfonate moiety. The P-Pd-O angle (83.34(11)°) is on the small end of the spectrum observed for other (PO)Pd(II) complexes (e.g. 83.57(13)° in (PO-Bp/Ph^{OMe})PdMe(py) and 94.96(4)° in (PO-Bp/Ph^{OMe})PdMe(lut)). The small P-Pd-O angle leads to significant deviation from the typical boat conformation of the 6-membered chelate ring; in *trans-P,F*-**3**, the P-C-C-S-O atoms are nearly

coplanar whereas in typical (PO)PdXL complexes, the sulfonate oxygen atom is usually orientated out of the P-C-C-S plane.

The ^{19}F NMR spectrum of isolated *trans-P,F*-**3** comprises a broad singlet at δ –257, and the ^{31}P spectrum comprises a broad resonance at δ 5. These chemical shifts are almost indistinguishable from those of *trans-P,F*-**2,** which is typical for Pd(II)-FHF species. The ^{1}H NMR spectrum of the *cis:trans-P,F*-**3** mixture generated in situ in the presence of excess $NEt_3(HF)_3$ mixture is, as expected, very similar to that of **2**, except for the presence of a broad downfield resonance at δ 10.6 arising from the PdF*H*F ligand.[4] Attempts to resolve this broad signal into the expected multiplet (ddd) by low temperature NMR were unsuccessful, probably due to rapid exchange reactions involving the FHF unit.[48] The room temperature ^{31}P{^{1}H} NMR spectrum of *cis/trans*-P,F-**3** contains a broad resonance at δ 5 (*trans-P,F*) and a sharp resonance at δ –5.6 (*cis-P,F*), similar to the spectrum of *cis/trans-P,F*-**2**. The room temperature ^{19}F NMR spectrum contains free F^-,[49] and a broad signal at δ –171, which is the expected chemical shift for $NEt_3(HF)_3$ and the distal fluoride (M-FH*F*) of *cis/trans-P,F*-**3**.[32] Additional signals are observed at δ –331 and –396, which are unassigned, but likely arise due to the presence of excess $NEt_3(HF)_3$ in solution. Importantly, none of these ^{19}F signals were observed in the reactions between **2** and the olefins described below, indicating that bifluoride species **3** are not involved in those reactions.

Reaction of 2 with vinyl fluoride. Compound **2** (39:61 *cis*:*trans* mixture) reacts quantitatively with vinyl fluoride (VF) in CD_2Cl_2 solution to yield the net insertion product (PO-OMe)Pd(CH_2CF_2H)(lut) (**4**, Scheme 5.6). Complex **4** was characterized by NMR spectroscopy and HRMS. The ^{1}H and ^{19}F NMR spectra of **4** contain characteristic signals for the PdCH_2CF_2H unit (^{1}H NMR: δ 4.84 (tt, $^{2}J_{FH}$ = 57, $^{3}J_{HH}$ = 5, PdCH_2CHF_2, Figure 5.8) and δ 1.06 (tt, $^{3}J_{FH}$ = 21, $^{3}J_{HH}$ = 5, PdCH_2CHF_2); ^{19}F NMR: δ –98.3 (d, $^{2}J_{FH}$ = 57)) that are similar to those observed for the

analogous (PO-Bp/Ph^{OMe})Pd(CH_2CF_2H)(lut) complex **G** reported by Wada (^{1}H NMR: δ 4.94 (br t, $^2J_{FH}$ = 60), 1.06 (br s); ^{19}F NMR: δ –96.1 (br d, J_{FF} = 263), –99.3 (br d, J_{FF} = 263)).[3] Complex **4** exists as the *cis-P,C* isomer, as established by a room temperature NOESY correlation between the Pd$CH_2$$CHF_2$ hydrogens and H^6-PhOMe, the hydrogens *ortho* to P on the 2-OMe-Ph rings (Figure 5.9).

Scheme 5.6. Reaction of **2** and VF

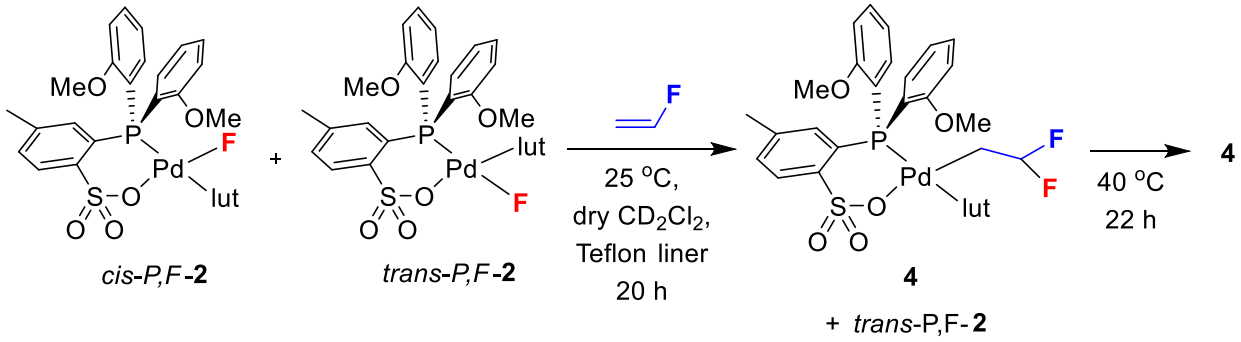

Figure 5.8. ^{1}H NMR spectrum showing Pd$CH_2$$CHF_2$ resonances in **4** (CD_2Cl_2, 500 MHz).

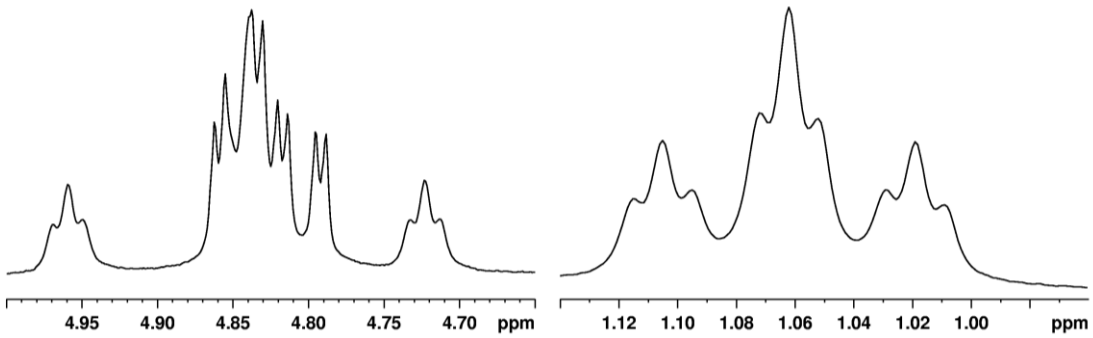

Figure 5.9. NOESY spectrum of **4** during the reaction of **2** and VF (CD_2Cl_2, 500 MHz, 25 °C).

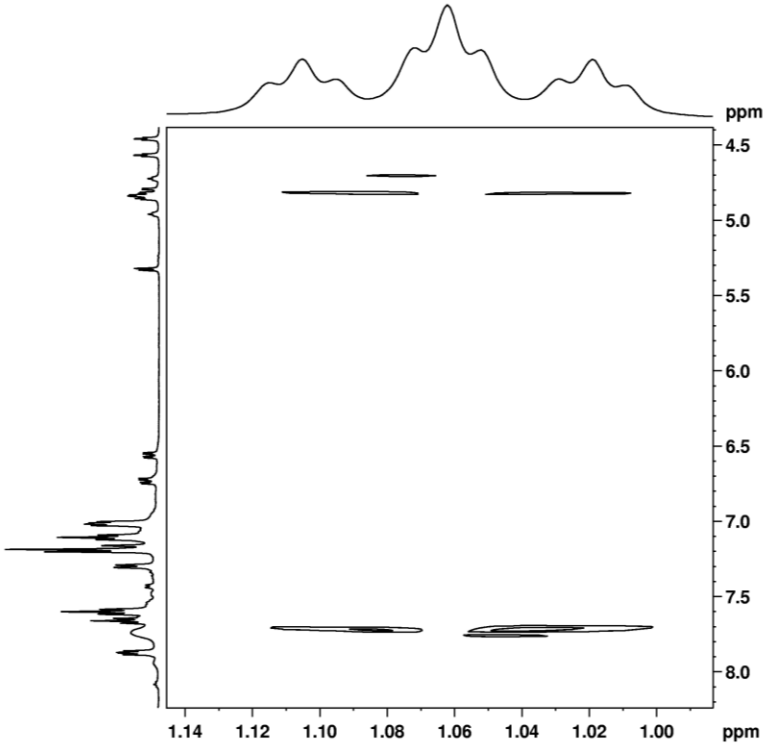

The reaction of **2** and VF was monitored by NMR (Figure 5.10), although a detailed kinetic analysis was not performed. The concentrations of [*cis*-*P*,*F*-**2**], [*trans*-*P*,*F*-**2**], and [**4**] were measured by ^{1}H NMR integration of one of their baseline-resolved –OMe resonances (Figure 5.11). The *cis*-*P*,*F*-**2** isomer reacts much faster than *trans*-*P*,*F*-**2**. The apparent first-order rate constants for the disappearance of *cis*-*P*,*F*-**2** and *trans*-*P*,*F*-**2**, determined by a first-order kinetic analysis of the data in Figure 5.11, are $k_{\text{disappear},cis} = -4.6 \times 10^{-5}$ and $k_{\text{disappear},trans} = -3.0 \times 10^{-6}$ (Figure 5.12). At room temperature, the sample contained a 49:51 mixture of **4** and *trans*-*P*,*F*-**2** at 20 h and a 61:39 mixture at 44 h. Heating the sample tube at 40 °C for an additional 22 h gave **4** in >95% yield.

Figure 5.10. ^{1}H NMR monitoring of the reaction of **2** and VF (CD_2Cl_2, 500 MHz, 25 °C). The atom numbering schemes for *cis-P,F* and *trans-P,F*-**2** (c,t) and **4** are given in Figure 5.16 and Figure 5.18.

(a) Expansion of aromatic region

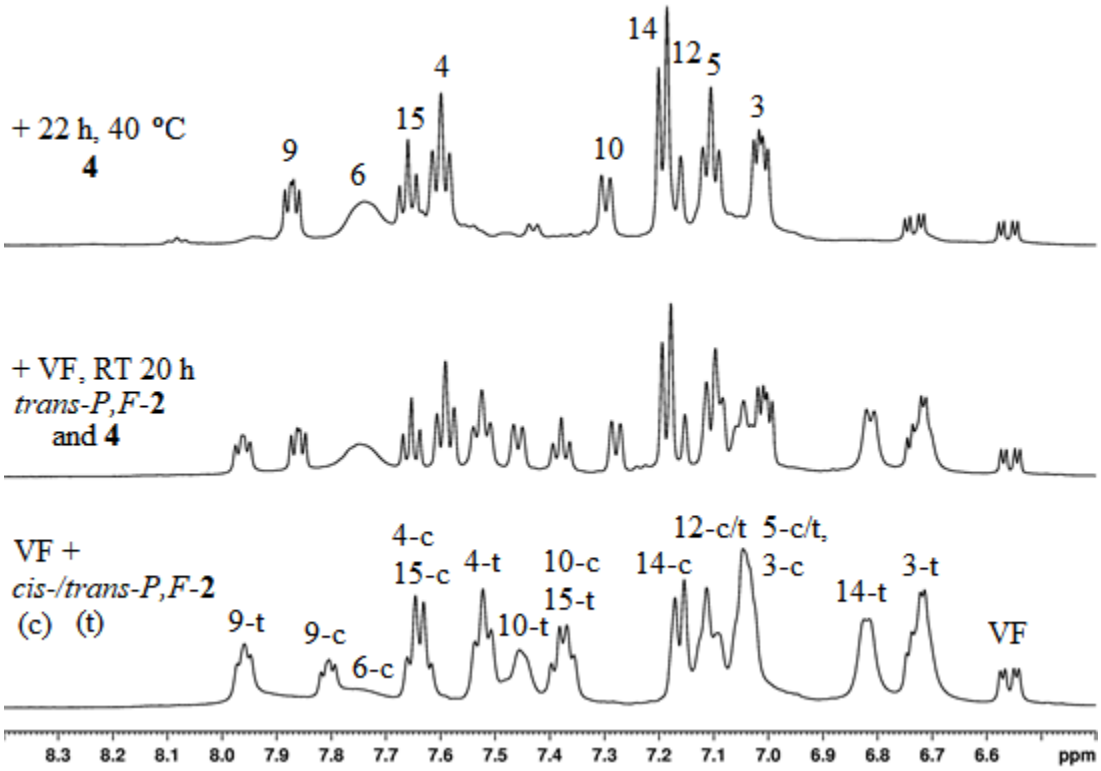

(b) Expansion of -OMe and Me region

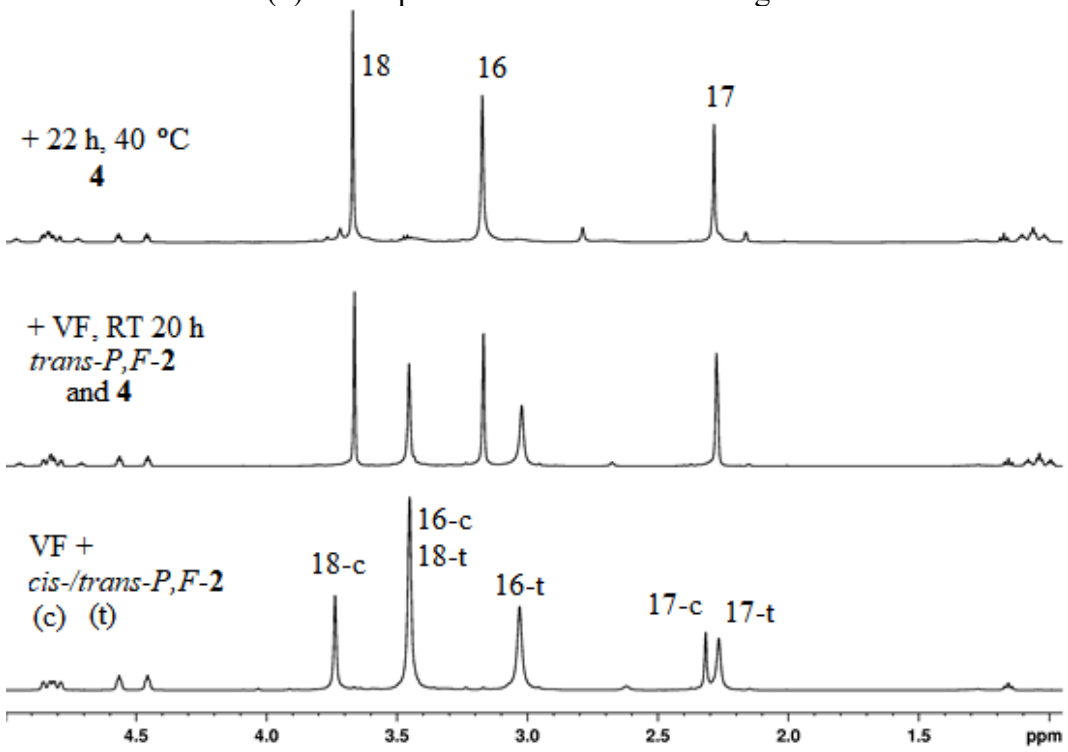

Figure 5.11. Time dependence concentrations of *cis-P,C*-**2** (red), *trans-P,C*-**2** (blue), and **4** (black) during the reaction of **2** and VF (CD_2Cl_2, room temperature).

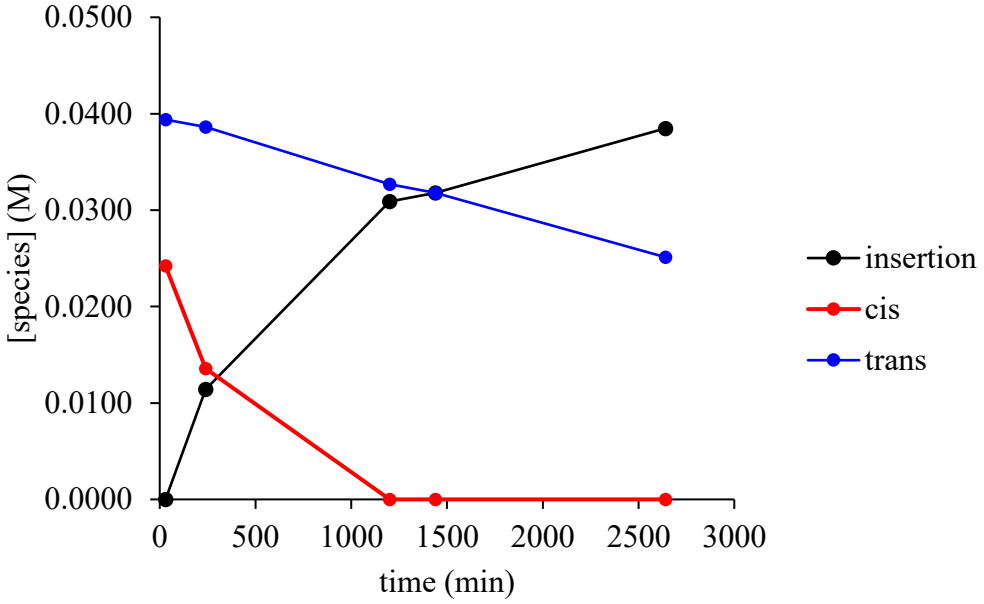

Figure 5.12. Plots of (a) ln[*cis-P,F*-**2**] vs. time (s) and (b) ln[*trans-P,F*-**2**] time (s).

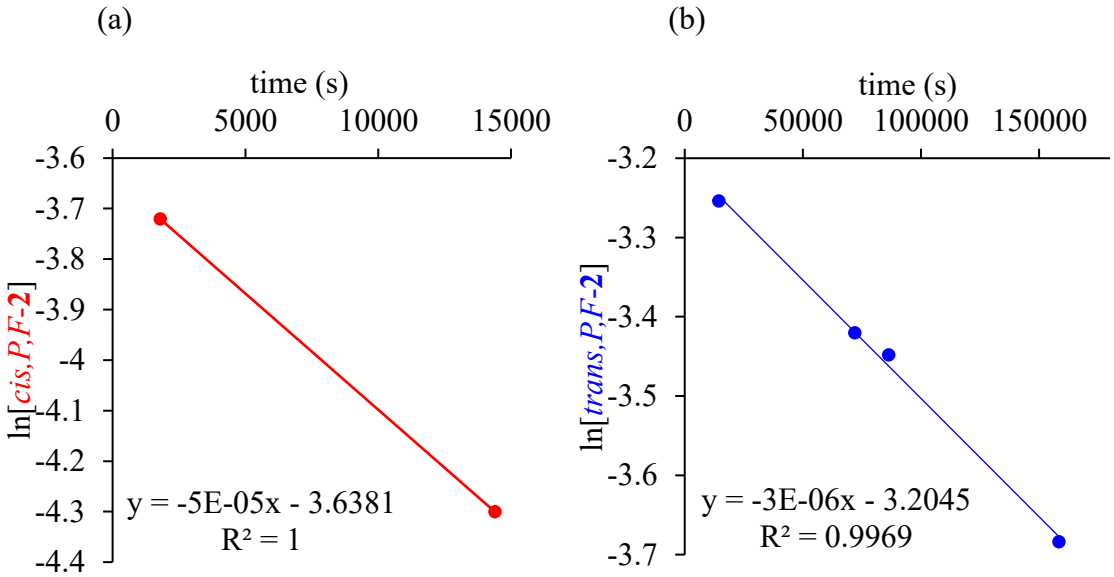

While the detailed mechanism for the reaction between **2** and VF is unknown, this process likely proceeds by initial ligand exchange to give (PO)Pd(F)(CH_2=CHF) species (Scheme 5.7). By analogy to insertion of E into (PO)Pd–Me bonds,[50] it is possible that *cis-P,F*-(PO)Pd(F)(CH_2=CHF) isomerizes to *trans-P,F*-(PO)Pd(F)(CH_2=CHF), which inserts and is trapped with lut to produce the observed *cis-P,C*-**4**. The apparent rate constant for the disappearance of *trans-P,F*-**2**, $k_{\text{disappear},trans}$, is similar or slightly lower than the rate constant for the isomerization of *trans-P,F*-**2** to *cis-P,F*-**2**, k_{-1}, which suggests that the major pathway for the reaction of *trans-P,F*-**2** with VF is isomerization to *cis-P,F*-**2**, followed by ligand exchange and subsequent insertion. The different rates of lut/VF ligand exchange from *cis-P,F*-**2** and *trans-P,F*-**2** can be explained based on differences in *trans* effects.

Scheme 5.7. Proposed mechanism for the reaction of *cis-P,F*-**2** and *trans-P,F*-**2** and VF

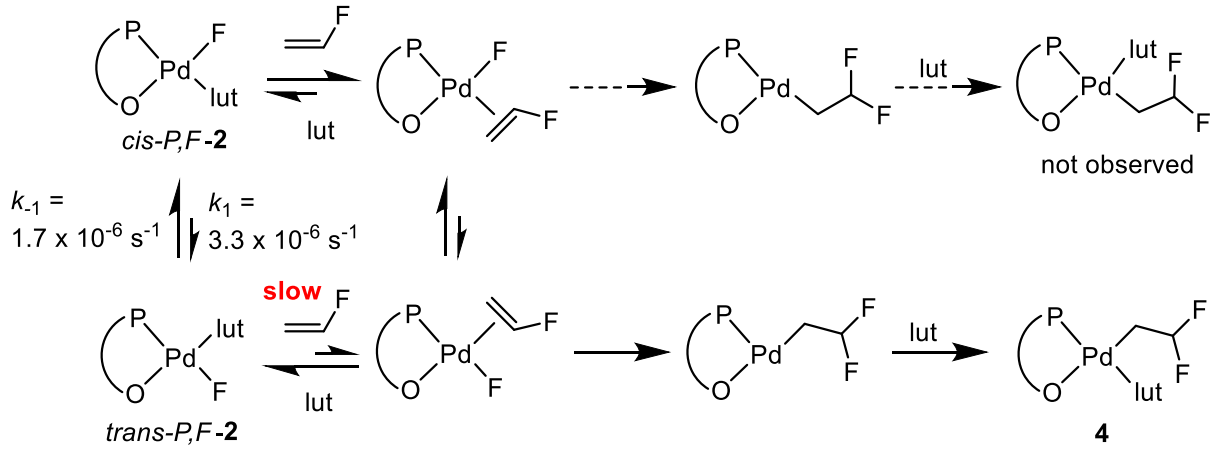

Unexpected aryl transfer by $B(C_6F_5)_3$ during attempted synthesis of $\{(PO\text{-}OMe)PdF\}_2$. Base-free dimer complexes of type $\{(PO)PdR\}_2$ are generated by abstraction of L from (PO)PdR(L) complexes with $B(C_6F_5)_3$ and typically undergo much faster olefin insertion than their (PO)PdR(L) analogues because the olefin monomer does not need to compete with the L ligand for coordination to Pd (see Chapter Three).[51–53] Accordingly, with the aim of enhancing the insertion reactivity of

2, attempts were made to generate the base-free dimer {(PO-OMe)PdF}$_2$. Addition of 1 equiv of B(C_6F_5)$_3$ to a solution of *cis/trans-P,F*-**2** in CD_2Cl_2 resulted in a color change from brown to yellow and the formation of a brown precipitate. This result was initially viewed as promising because most {(PO)PdR}$_2$ compounds are insoluble in CD_2Cl_2.[51] However, the ^{19}F NMR spectrum (between 30 and –50 °C) of a $CDCl_2CDCl_2$ solution of the brown precipitate contained no Pd–F signals, and addition of excess lutidine to this solution did not regenerate **2**, as would be expected for {(PO)PdF}$_2$ species. Furthermore, the ^{19}F NMR spectra of the original CD_2Cl_2 supernatant contained resonances for one major C_6F_5-containing species at δ –136 (s), –162 (t, 24 Hz), and –167 (t, 18 Hz), which are more similar to the signals for [FB(C_6F_5)$_3$]$^-$ (δ –135.6 (t, J = 13.0 Hz), –162.9 (t, J = 19.5 Hz), –167.1 (m)),[54] than those for lut-B(C_6F_5)$_3$ (δ –132.4 (s), –157.6 (t), and –166.7 (t)).[55]

Colorless crystals suitable for X-ray diffraction were grown from a methanol solution of the brown precipitate over several days at room temperature (5 mg, 65% yield). The crystals were identified as (PO-OMe)Pd(C_6F_5)(lut)•CH_2Cl_2 (**8**•CH_2Cl_2) by X-ray diffraction. The molecular structure and selected bond distances and angles are shown in Figure 5.13. The N1–Pd1–O1 bond angle (82.99(16) Å) is significantly smaller than those in (PO)PdMe(lut) complexes, likely because of the steric bulk of the C_6F_5 ring.

Figure 5.13. Molecular structure of **8**•CH_2Cl_2. Hydrogen atoms and the methylene chloride solvent molecular are omitted. Bond lengths (Å) and angles (°): Pd1–C29 2.015(6), Pd1–N1 2.132(5), Pd1–O1 2.084(4), Pd1–P1 2.2631(14), C29–Pd1–N1 94.8(2), N1–Pd1–O1 82.99(16), C29–Pd1–P1 88.41(16), O1–Pd1–P1 93.80(11).

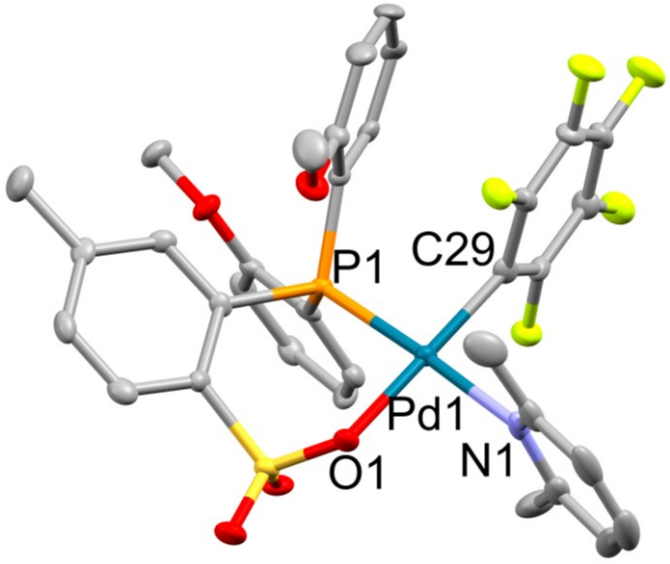

Collectively, these results suggest that the reaction of **2** with $B(C_6F_5)_3$ proceeds by initial fluoride abstraction to produce a (PO)Pd(lut)]$^+$ [$FB(C_6F_5)_3]^-$ ion pair followed by transfer of a C_6F_5 group back to Pd, as shown in Scheme 5.8. Similar R/C_6F_5 and H/C_6F_5 exchange reactions involving $B(C_6F_5)_3$ have been observed for metal alkyl and hydride complexes, including those of Zr,[56–58] Ti,[59,60] Al and Ga,[61,62] Zn,[63,64] Au,[65,66] Ni,[67–69] Fe,[70,71] and Pt,[72,73] and metal fluoride complexes, such as AgF[74,75] and an Ir-FPF_5 complex.[76] A representative example involving a Au(III) alkyl is shown in Scheme 5.9(a).[65] However, it should be noted these kinds of C_6F_5 exchange processes are very rare for Pd complexes, with only one example involving C_6F_5/acetate exchange reported in the literature (Scheme 5.9(b)).[77] NMR studies show that this reaction is complex due to secondary chemistry following the initial C_6F_5/acetate exchange.

Scheme 5.8. Reaction of **2** with $B(C_6F_5)_3$

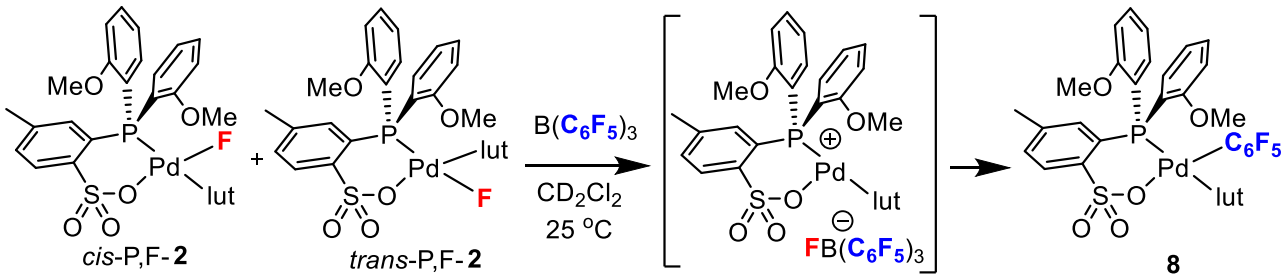

Scheme 5.9. Aryl transfer from $B(C_6F_5)_3$ to transition metal via an ion paired intermediate

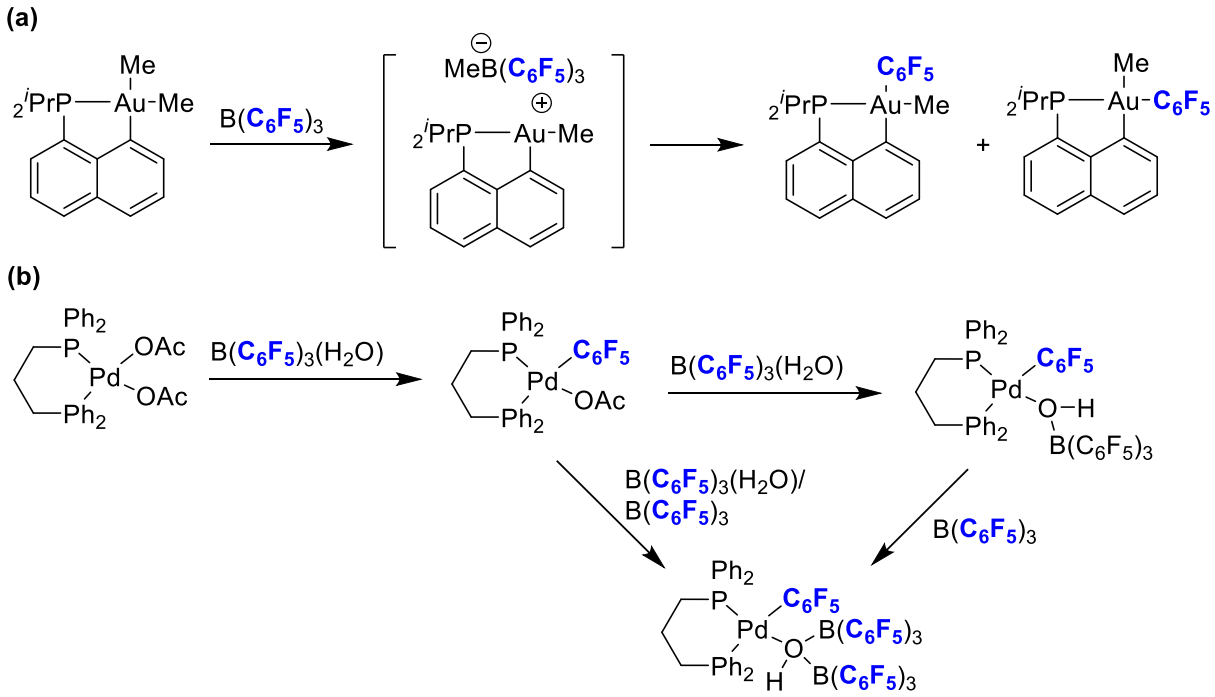

Reaction of 2 with vinyl acetate. Compound **2** (ca. 70:30 *cis-P,F*:*trans-P,F* mixture) reacts with vinyl acetate (VOAc) to yield the net insertion product (PO-OMe)Pd($CH_2CHF(OAc)$)(lut) (**5**, Scheme 5.10). The reaction was monitored by ^{1}H, ^{31}P, and ^{19}F NMR and proceeds slowly at room temperature. After 2.2 h at 50 °C, 100% of *cis-F,P*-**2** and 67% of *trans-F,P*-**2** had reacted, resulting in an overall 78% conversion to **5**. Complex **5** was identified

by comparison of its NMR spectra to those of **4** (the signals for the PO-OMe and lut ligands of the two complexes are nearly identical) and by 2D NMR spectroscopy. The ^{1}H NMR resonances for the methylene and methine hydrogens in the Pd(C*H*$_2$C*H*F(OAc)) ligand of **5** (δ 5.36 (dt, $^{2}J_{FH}$ = 58, $^{3}J_{HH}$ = 5.5, 1H, PdCH$_2$C*H*F(OAc), 1.06 (dt, $^{3}J_{FH}$ = 18, $^{3}J_{HH}$ = 5, 1H, PdC*H*$_2$CHF(OAc), Figure 5.25(d)) are similar to those for the Pd*CH*$_2$*CF*$_2$*H* hydrogens in **4** and the (PO-Bp/Ph^{OMe})Pd(CH$_2$CF$_2$H)(lut) complex reported by Wada.[3] The multiplicities and coupling constants are consistent with the presence of one fluorine atom in **5**.

Scheme 5.10. Reaction of **2** and VOAc

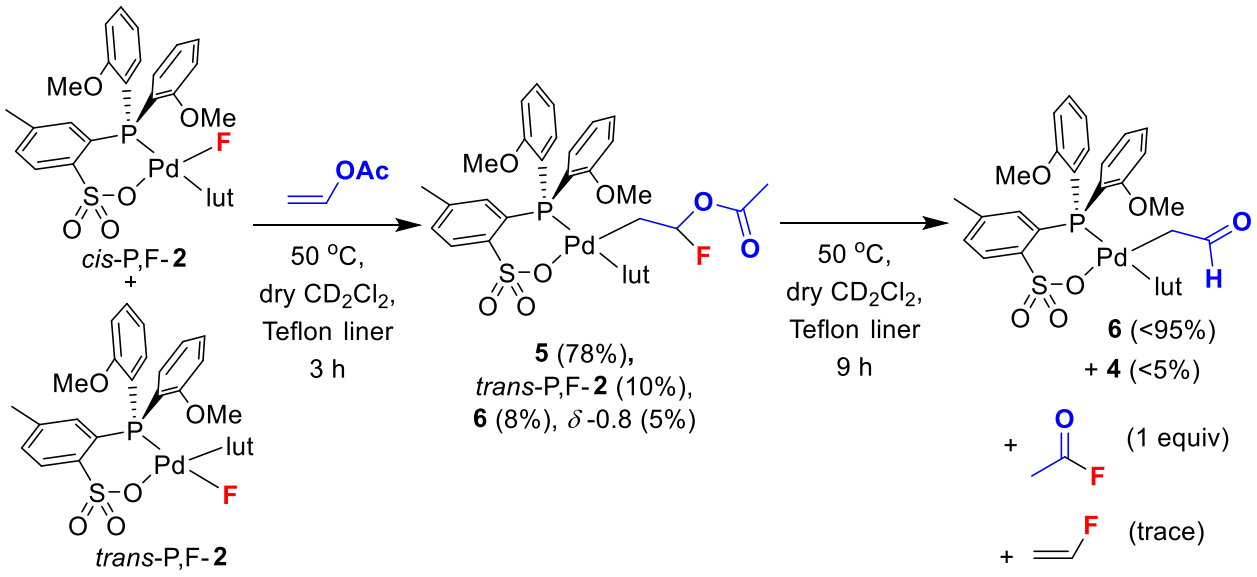

Upon continued heating at 50 °C over 10 h, **5** cleanly converted to C-bound Pd(II) enolate complex **6** (>95% by ^{31}P, Scheme 5.10), without observable intermediates. Small amounts of vinyl fluoride (<5% vs **6** by ^{19}F NMR and trace in ^{1}H NMR), **4** (<5% by ^{31}P NMR), and acetyl fluoride (^{19}F: δ 50.5; ^{1}H: δ 2.2 (d, $^{3}J_{FH}$ = 7 Hz), 1:1 equiv to **6**) were also observed. The ^{1}H NMR spectrum of **6** contains a low-field signal at δ 8.54 (t, $^{2}J_{HH}$ = 7 Hz) for the aldehyde hydrogen and a signal at

δ 1.84 (dd, $^{3}J_{PH}$ = 5 Hz, $^{2}J_{HH}$ = 4.7 Hz) for the PdCH_2C(=O)H hydrogens. The ^{1}H NMR resonances for the PO-OMe and lut ligand hydrogens are similar to those of *cis-P,F*-**2**, **3**, **4**, and **5**.

An analogous reaction of **2** (42:58% *cis-P,F*:*trans-P,F* mixture) and vinyl benzoate in CD_2Cl_2 solution produced **6** in high yield along with PhC(=O)F, which was observed by ^{19}F NMR (δ 17.4, Scheme 5.11), and a small amount of VF. After heating the reaction mixture at 60 °C for 3 h, the ^{31}P NMR spectrum contained resonances for the benzoate-analogue of **5** (41%), **6** (6%), *trans-P,F*-**2** (38%), and unidentified species. After an additional 22 h of heating, the ^{31}P NMR spectrum contained only resonances for Pd-enolate **6** (80%) and an unknown species (δ 0.1, 20%), which is most likely a decomposition product of **6**.

Scheme 5.11. Reaction of **2** with vinyl benzoate

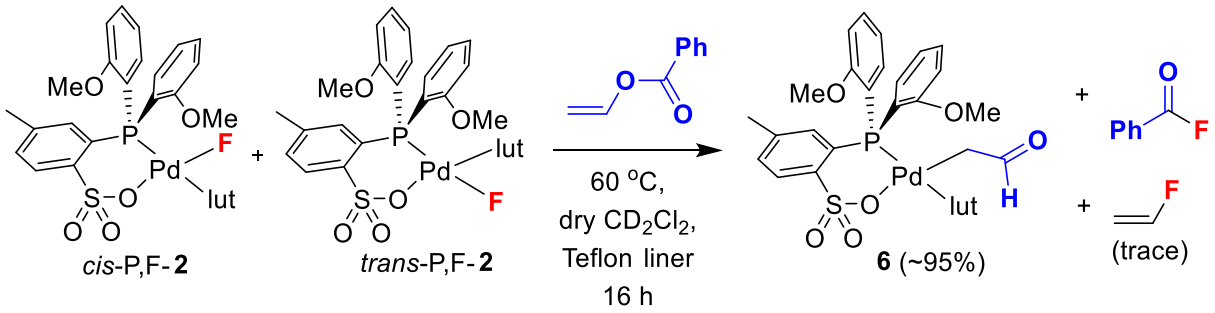

Crystals of **6**•1.5(CH_2Cl_2) (72% yield) were obtained by layering pentane over the CD_2Cl_2 solution at the end of the reaction shown in Scheme 5.10 and cooling the mixture at –40 °C. The molecular structure and selected metrical data are shown in Figure 5.14.

Figure 5.14. Molecular structure of **6**•1.5(CH_2Cl_2). Hydrogen atoms except those of the CH_2(C=O)H ligand are omitted. Bond lengths (Å) and angles (°): Pd1–C29 2.065(6), Pd1–N1 2.121(5), Pd1–O1 22.114(4), Pd1–P1 2.2391(16), C29–C30 1.468(9), O6–C30 1.216(8), C29–Pd1–N1 90.1(2), N1–Pd1–O1 86.45(17), C29–Pd1–P1 88.96(18), O1–Pd1–P1 94.56(12).

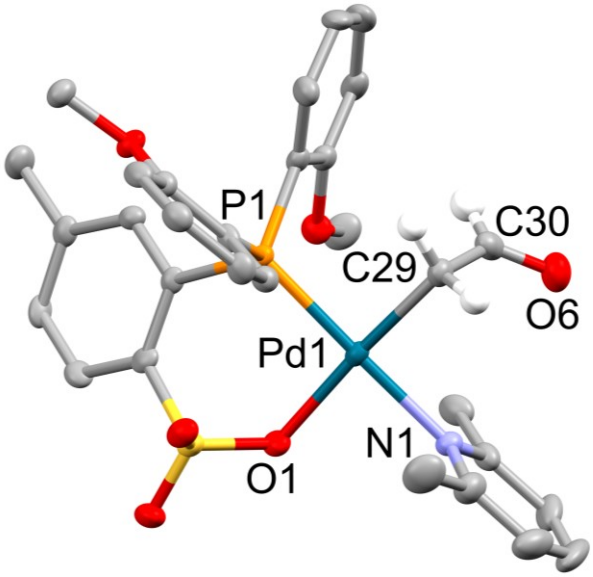

C-bonded enolate complexes of several metals, including Pd,[78] Ir(II),[79-80] Hg(II),[81] Au(III),[82] and Rh[80,83,84] have been prepared, and some have been characterized by X-ray crystallography. Notable examples are shown in Chart 5.3. The C−C (1.468 Å) and the C=O double bond (1.216 Å) distances in **6** are similar to those in aldehydes (1.510(8) and 1.192(5) Å),[85] as well as enolate complexes **J** (1.429(8) and 1.206(7)),[80] and **L** (1.468(3) and 1.212(3)).[82]

Chart 5.3. Representative examples of metal-enolates

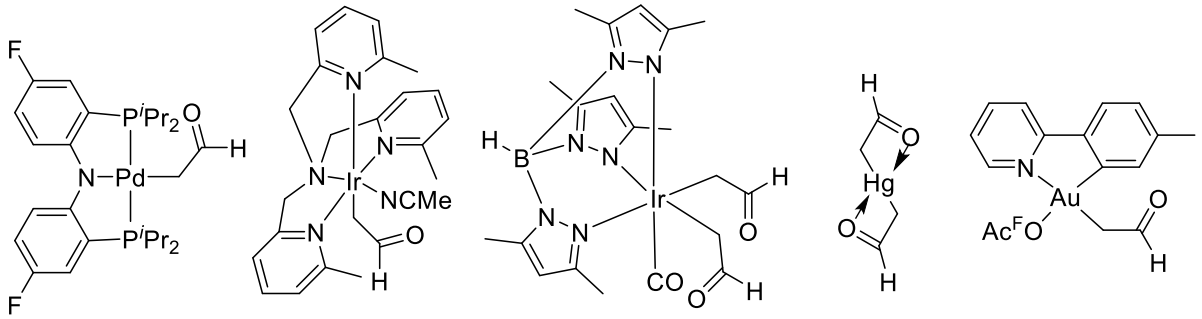

H **I** **J** **K** **L**

Several routes to C-bound enolate complexes have been discovered, including *β*-H elimination of M-OEt species to generate a M-H species and acetaldehyde followed by insertion (**H,** Chart 5.3) and ozonolysis of metallocyclopentanes (**J**, Chart 5.3). Most relevant to the present work, Nova and Tilset[82] generated Au(III) C-bonded enolate complex **L** (Scheme 5.12) by two methods: (i) the reaction of Au(tpy)$(OAc^F)_2$ (**M**, OAcF = $O(C{=}O)CF_3$) and $H_2C{=}CH_2OAc^F$ in $HOAc^F$ and (ii) the hydrolysis of Au-$CH{=}CHOAc^F$ complex **O** in the presence of $HOAc^F$. They proposed that insertion of $H_2C{=}CH_2OAc^F$ into the Au–OAc^F bond of **M** generates $AuCH_2CH(OAc^F)_2$ intermediate **N**, which undergoes elimination of trifluoroacetic anhydride. Intermediate **N** is also formed by addition of $HOAc^F$ across the C=C bond of **O**. Similar acid-catalyzed eliminations have been used to interconvert 1,1-diacetates and corresponding aldehydes and acetic anhydride,[86,87] as illustrated in Scheme 5.12.

Scheme 5.12. Synthesis of a Au-enolate via a proported 1,1-diacetate intermediate

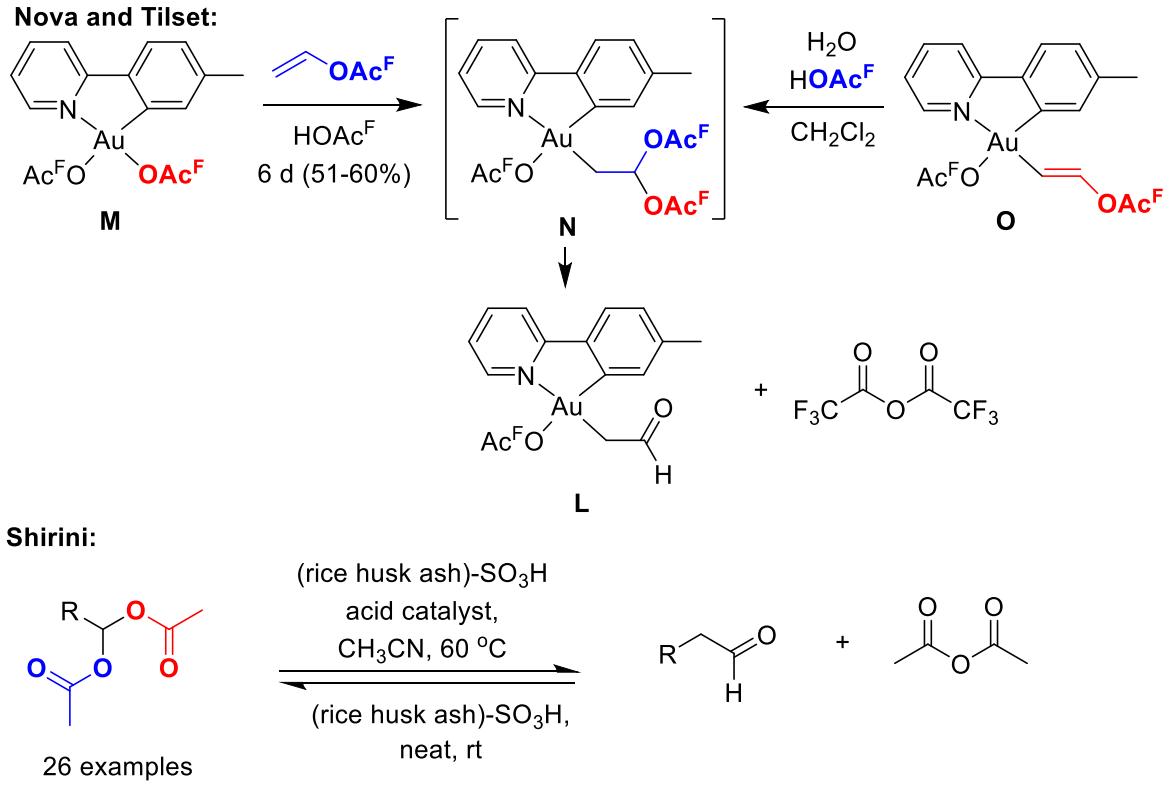

Based on these precedents, two mechanisms for the conversion of **5** to **6** in the presence of excess VOAc may be proposed. One possibility is direct elimination of acyl fluoride from **5** (*mechanism a*, Scheme 5.13). A second possibility is initial *β*-OAc elimination of **5** to generate a PdOAc species, insertion of VOAc to yield a 1,1-diacetate $PdCH_2CH(OAc)_2$ species, and elimination of acetic anhydride and **6** (*mechanism b*, Scheme 5.13). Both of these routes generate 1 equiv of acetyl fluoride, which was observed by ^{1}H and ^{19}P NMR (vide supra). However, *mechanism b* would also produce a full equiv of VF and acetic acid. Since only small amounts of VF and complex **4** were observed by NMR and acetic acid was not detected, this reaction most likely operates by *mechanism a*. Furthermore, DFT calculations performed on $[L_2PdCH_2CH_2X]^+$ species (L_2 = $H_2PCH_2CH_2PH_2$, X = Cl, Br, I, F, OAc, etc.) show that the barrier to *β*-OAc elimination for thermodynamically and kinetically stable $L_2Pd(\kappa^2\text{-}CH_2CH_2OC(O)Me)^+$ complexes is high (25.7 kcal/mol).[16]

Scheme 5.13. Possible mechanisms for the formation of **6**

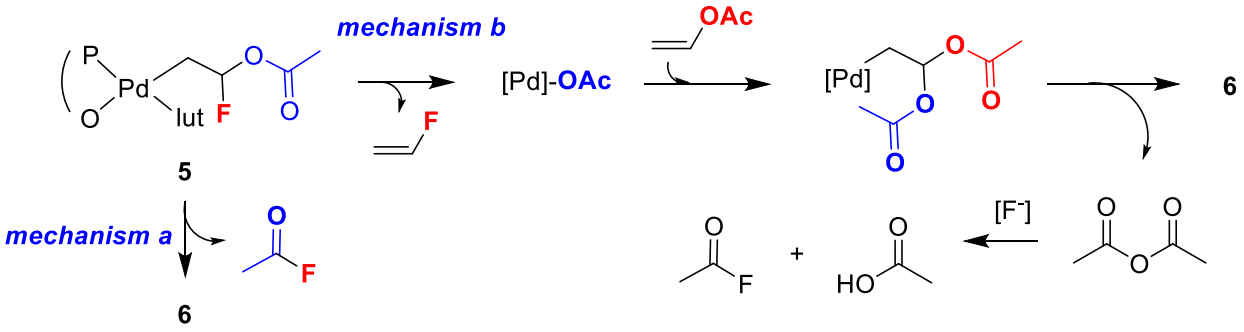

Reaction of 2 with vinyl bromide. Complex **2** (ca. 1:1 *cis-P,F*:*trans-P,F* mixture) reacts with vinyl bromide (VBr) to give PdBr compound **1** and VF (Scheme 5.14). Unlike the reactions with VF and VOAc, the (PO-OMe)Pd(CH_2CHBrF)(Lut) insertion product is not observed by NMR, which establishes that *β*-Br elimination is faster than the initial fluoropalladation step. This is consistent with DFT calculations of $[L_2PdCH_2CH_2X]^+$ species (L_2 = $H_2PCH_2CH_2PH_2$, X = Cl, Br, I, F, OAc, etc.) which indicate that *β*-Br elimination from $PdCH_2CH_2Br$ is a kinetically and thermodynamically favorable process and proceeds with a small barrier of 1.9 kcal/mol.[16] After 13 h at 50 °C, the sample tube contained PdBr compound **1** (73% by ^{31}P NMR), $PdCH_2CHF_2$ compound **4** (11%), an unidentified compound (9%, ^{31}P: *δ* 16), and *cis-P,F*-**2** (7%). The presence of **4** indicates that VF and VBr react with **2** at comparable rates. As was the case with VF, it is likely that *cis-P,F*-**2** reacts faster with VBr than does *trans-P,F*-**2**. Therefore, the presence of a small amount of *cis-P,F*-**2** at the end of the reaction is most likely due to *β*-F elimination from **4**. For comparison to the calculated *β*-Br elimination barrier given above, $[L_2PdCH_2CH_2F]^+$ undergoes *β*-F elimination with a higher barrier of 14.0 kcal/mol, and this process is endothermic due to the strong C–F bond and relatively weak Pd–F bond in the *β*-F elimination product.[16] The presence of another electron-withdrawing fluorine atom in $PdCH_2CF_2H$ **4** should further raise the barrier for *β*-F elimination from **4**.

Scheme 5.14. Reaction of **2** with VBr

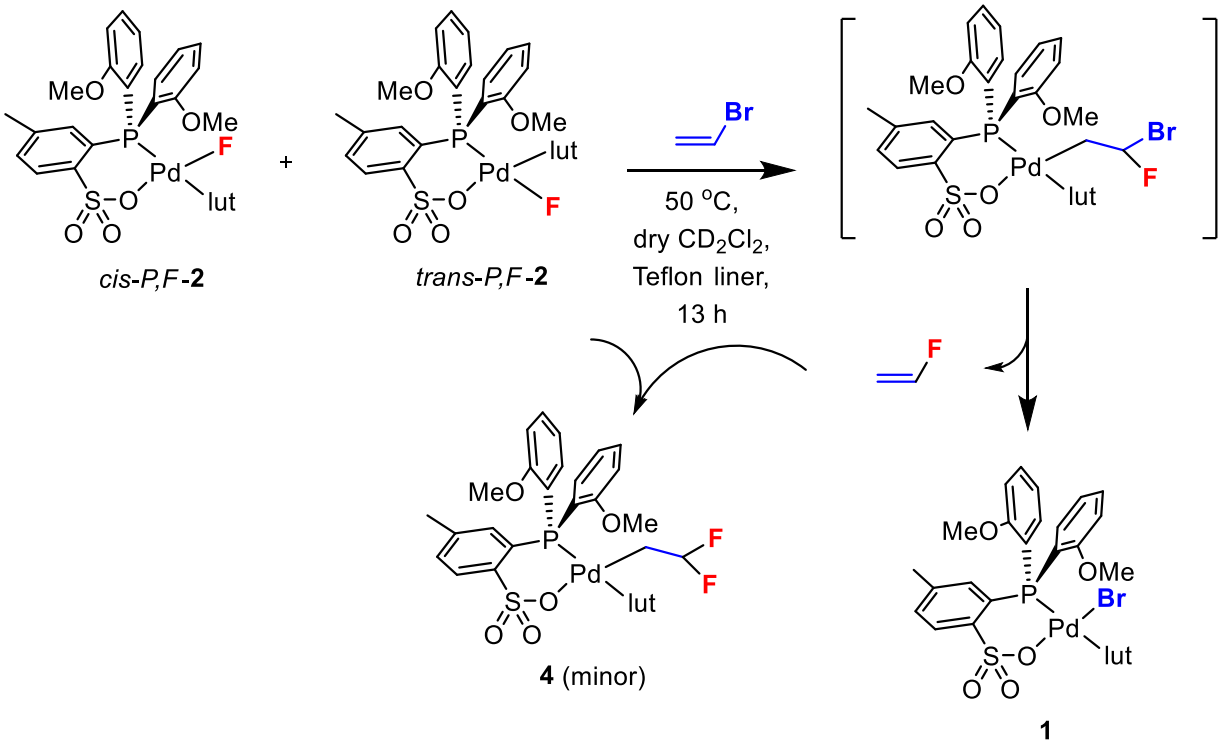

Reaction of 2 with 1,5-hexadiene. Compound **2** (67:33% *cis-P,F*:*trans-P,F* mixture) reacts with 1,5-hexadiene in CD_2Cl_2 solution to yield cyclopentylmethyl complex **7** as a 42/58 mixture of diastereomers. This reaction proceeds via insertion of one C=C bond of hexadiene inserts into the Pd–F bond followed by coordination and insertion of the other end of the diene, resulting in cyclization (Scheme 5.15). NMR monitoring of the reaction showed that ~100% of *cis-P,F*-**2** and 33% of *trans-P,F*-**2** (by ^{31}P NMR) had converted to **7** after 88 h at room temperature. The remaining *trans-P,F*-**2** was converted to **7** by heating the sample to 60 °C for 6 h. Complex **7** was identified by 2D NMR spectroscopy. The ^{19}F NMR spectrum contains two multiplets centered at δ –166.0 and –167.7 in a 42/58 intensity ratio. These signals are diagnostic for secondary alkyl fluorides (cf. 2-fluoropropane δ –166.0, 2-fluoropentane δ –173).[88] Consistent with the ^{19}F NMR data, the ^{31}P{^{1}H} NMR spectrum contains two major signals at δ 22.4 and 22.2 in a 42/58 intensity

ratio (70% total by ^{31}P NMR). The ^{31}P spectrum also contains minor resonances at δ 22.4 (~10%) and in the range δ 2–8 (<5% each) due to unidentified species. The two diastereomers result from competing coordination/insertion of the *re* and *si* faces of the pendant olefin in the second insertion/cyclization step (Scheme 5.15). Signals in the ESI-MS and HRMS are consistent with the proposed composition of **7**.

Scheme 5.15. Reaction of **2** with 1,5-hexadiene

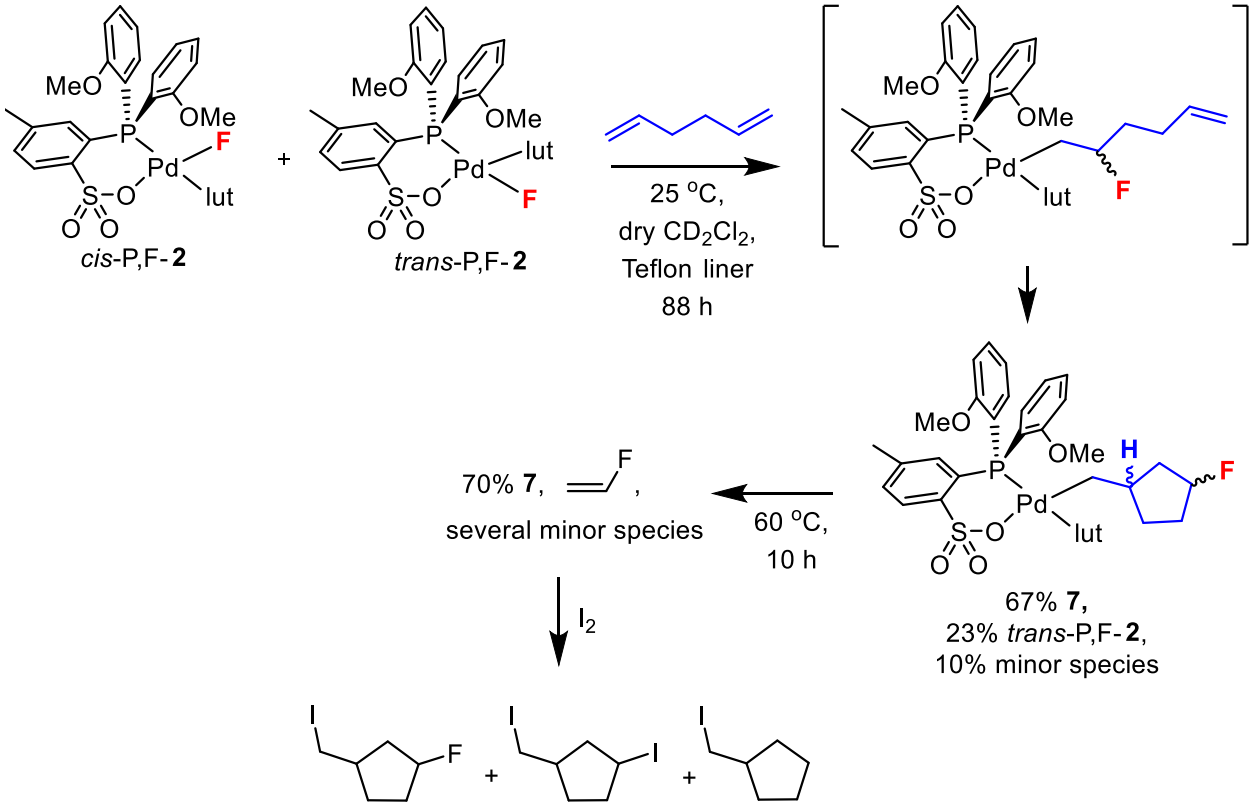

The reaction between **2** and *trans*,*trans*-*D*,*D*-1,5-hexadiene could be used to determine whether fluoropalladation occurs by *cis* addition (i.e. migratory insertion) or *trans* addition (i.e. *exo* attack of F^- on a bound olefin as in Wacker chemistry), since these processes would give *syn*-*F,D* and *anti*-*F,D* products, respectively (Scheme 5.16). However, it is first necessary to obtain a single diastereomer and assign the ^{1}H resonances for the cyclopentane ring. This would be most

easily accomplished by cleaving the Pd–C bonds in **7** and using chiral HPLC or distillation to separate the diastereomeric organic products. Quantitative NOESY NMR could then be used, as in Chapter Two, to determine the *syn* and *anti*-orientation of hydrogens on the cyclopentane ring.

To this end, attempts were made to cleanly cleave the Pd–C bonds of **7**. As shown in Scheme 5.15, addition of I_2 to a CD_2Cl_2 solution of **7** produced a mixture of 1-fluoro-, 1-iodo-, and 1-hydro- 3-iodomethyl-cyclopentane in a 13:71:16 ratio as determined by GCMS (assuming equal response factors). The 1-iodo and 1-hydro products likely result from secondary chemistry involving the Pd–I species generated by the iodinolysis step. Another typical Pd–C bond cleavage protocol comprises successive reaction with CO and MeOH, which proceeds by CO insertion to give a PdC(=O)R complex, followed by addition of MeOH to give a PdH species and an ester. Addition of CO (1.5 equiv) to a CD_2Cl_2 solution of **7** and *trans-P,F*-**2** (4:1 ratio) gave a new species as shown by ^{19}F and ^{31}P NMR (75% conversion from **7**) over 16 h at room temperature, during which time the solution turned from dark brown to yellow. However, addition of MeOH and heating did not significantly change the NMR spectra and no ester products were observed by GCMS. Another typical Pd–C bond cleavage protocol is addition of $HSiEt_3$, which is reported to give hydrogenated chain ends and various Pd species. Addition of $HSiEt_3$ (1 equiv) to a CD_2Cl_2 solution of **7** and *trans-P,F*-**2** (4:1 ratio) resulted in a color change from dark brown to yellow with concomitant Pd black formation. Heating at 45 °C for 16 h resulted in a mixture of products. The ^{31}P NMR spectrum showed the presence of many phosphorous-containing species and a ^{19}F NMR spectrum showed the presence of free fluoride (singlet at δ –151) and HF (singlet at δ –176). Further efforts will be required to develop a clean P–C cleavage protocol in order to establish the stereochemical course of the reaction of **2** and hexadiene.

Scheme 5.16. Proposed route to determine mechanism of fluoropalladation

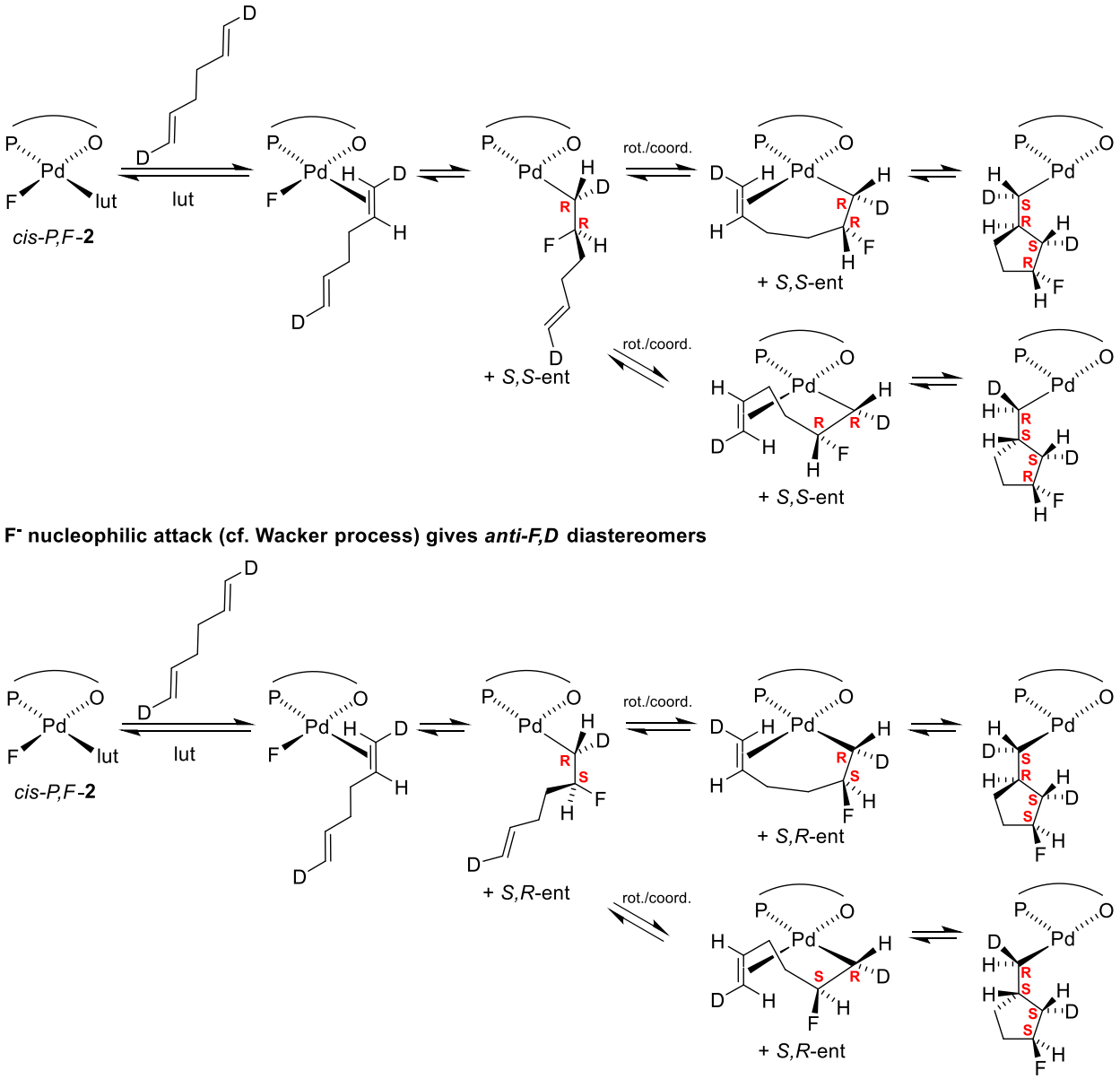

5.3 Conclusion

(PO-OMe)PdF(lut) complex **2** was synthesized in pure form without contamination by fluoride or fluorosilicate species using rigorously dried solvents, plastic ware, and Teflon NMR tube liners. Compound **2** exists as a mixture of *cis-/trans-P,F* isomers that interconvert both in solution and in the solid state. Compound **2** reacts cleanly with a variety of polar vinyl monomers to give net insertion products, including $PdCH_2CHF_2$ complex **4** by insertion of VF, analogous to **G** reported by Wada,[3] and $PdCH_2CHF(OAc)$ complex **5** by insertion of VOAc. Complex **5** reacts further to give the unusual C-bound Pd-enolate complex **6**, which was identified by NMR and X-ray crystallography. Reaction of **2** with VBr yields (PO-OMe)PdBr(lut) **1** and VF by initial fluoropalladation to form a transient $PdCH_2CHBrF$ species that undergoes fast *β*-Br elimination. Compound **2** reacts with 1,5-hexadiene by insertion and cyclization to give Pd-fluoro-cyclopentylmethyl compound **7**. The analogous reaction with selectively deuterium-labeled 1,5-hexadiene may provide a means of determining whether fluoropalladation occurs by *cis*-addition via migratory insertion or *trans*-addition via *exo*- nucleophilic attack by fluoride (cf. Wacker chemistry).

5.4 Experimental Section

General Procedures. All experiments were performed using dry box or Schlenk techniques under a nitrogen atmosphere unless noted otherwise. Nitrogen was purified by passage through Q-5 oxygen scavenger and activated molecular sieves. CH_2Cl_2, Et_2O, and THF were dried by passage through activated alumina. Pentane and hexanes were purified by passage through BASF R3-11 oxygen scavenger and activated alumina. CD_2Cl_2 and $CDCl_2CDCl_2$ were distilled from and stored over P_2O_5. Toluene-d_8 and THF-d_8 were distilled from Na/benzophenone. ^{n}BuLi solution (1.6 M or 2.5 M in hexanes), 2-bromoanisole, $(COD)PdBr_2$, 2,6-lutidine (99+%), CsF,

VBr (1 M, THF), VOAc, and NBu_4Br were purchased from Sigma Aldrich. NBu_4Br was recrystallized from hot toluene and VOAc was distilled from $CaCl_2$ before being stored in a glove box. Other materials were used without further purification. Vinyl fluoride was purchased from Synquest Laboratories and used as received.

NMR spectra were recorded on Bruker Avance II+ 500 or DRX400 spectrometers at ambient temperature unless otherwise indicated. ^{1}H and ^{13}C chemical shifts are reported relative to $SiMe_4$ and internally referenced to residual ^{1}H and ^{13}C solvent resonances. ^{31}P chemical shifts are externally referenced to 85% H_3PO_4 (δ 0.0). ^{11}B and ^{19}F chemical shifts are externally referenced to $BF_3(OEt_2)$ (δ 0.0 for ^{11}B and δ –153 for ^{19}F).

Electrospray mass spectra (ESI-MS) and atmospheric pressure chemical ionization mass spectra (APCI-MS) were recorded using Agilent 6224 TOF–MS (high resolution) or 6130 LCMS (low resolution) instruments. The observed isotope patterns closely matched calculated isotope patterns. The listed *m/z* value corresponds to the most intense peak in the isotope pattern.

{P(2-OMe-Ph)$_2$(2-SO$_3$-5-Me-Ph)}PdBr(2,6-lutidine) (1, (PO-OMe)PdBr(lut)). A solution of $HP^{+}(2\text{-OMe-Ph})_2(2\text{-}SO_3^{-}\text{-5-Me-Ph})$ (2.41 g, 5.80 mmol) in CH_2Cl_2 (60 mL) was added dropwise to a solution of $(COD)PdBr_2$ (2.16 g, 5.80 mmol) in CH_2Cl_2 (30 mL). The solution was stirred for 1.5 h at room temperature. Lut (1.34 mL, 11.6 mmol) was added dropwise and the mixture was stirred for 30 min at room temperature. Pentane (600 mL) was added and an orange precipitate formed. The orange powder was collected by filtration, washed with pentane, and recrystallized from CH_2Cl_2/Et_2O (100 mL/300 mL) at –40 °C to afford orange crystals, which were identified as (PO-OMe)PdBr(lut)•CH_2Cl_2 (**1**•CH_2Cl_2) by X-ray crystallography. X-ray quality crystals could also be grown from a concentrated CH_2Cl_2 solution of **1** at room temperature. X-ray data and structure refinement for **1**•CH_2Cl_2 can be found in Table 5.2. The crystals were collected

by filtration and dried under vacuum to afford **1**. Yield 3.62 g (86.2% based on (COD)$PdBr_2$). The atom numbering scheme used in the NMR assignments of **1** is shown in Figure 5.15. ^{1}H NMR (CD_2Cl_2): δ 8.03 (br s, 2H, H^6), 7.83 (dd, $^3J_{HH}$ = 8, J_{PH} = 5, 1H, H^9), 7.62 (t, $^3J_{HH}$ = 7.5, 1H, H^{15}), 7.60 (t, $^3J_{HH}$ = 7.5, 2H, H^4), 7.32 (d, $^3J_{HH}$ = 7.5, 1H, H^{10}), 7.16 (d, $^3J_{HH}$ = 8, 2H, H^{14}), 7.12 (d, $^3J_{PH}$ = 14, 1H, H^{12}), 7.11 (t, $^3J_{HH}$ = 7.5, 1H, H^5), 6.97 (dd, $^3J_{HH}$ = 8, $^3J_{PH}$ = 5, 2H, H^3), 3.67 (s, 6H, H^{18}), 3.51 (s, 6H, H^{16}), 2.29 (s, 3H, H^{17}). ^{13}C{^{1}H} NMR (CD_2Cl_2): δ 160.6 (C^2), 159.4 (C^{13}), 143.9 (C^8), 139.6 (C^{11}), 139.3 (C^{15}),138.8 (C^6), 135.4 (C^{12}), 134.4 (C^4), 131.7 (C^{10}), 127.2 (C^9), 126.6 (d, J_{PC} = 53, C^7), 123.4 (C^{14}), 120.7 (d, J_{PC} = 12, C^5), 115.0 (d, J_{PC} = 64, C^1), 111.8 (C^3), 55.5 (C^{18}), 26.0 (C^{16}), 21.4 (C^{17}). ^{31}P{^{1}H} NMR (CD_2Cl_2): δ 4.6 (s). HRMS (ESI, positive mode; *m/z*): Calcd. for $[C_{28}H_{29}BrNO_5PPdS+H]^+$: 702.9744; Found: 702.9747.

Figure 5.15. Atom numbering scheme for **1**.

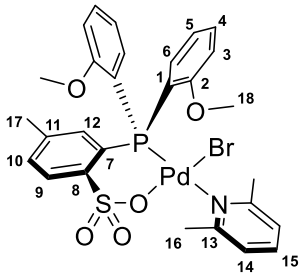

{P(2-OMe-Ph)$_2$(2-SO$_3$-5-Me-Ph)}PdF(2,6-lutidine) (2, (PO-OMe)PdF(lut)). Note: No glassware was used and all solvents and plastic ware were rigorously dried before use to avoid formation of fluorosilicates. In a dark glove box, AgF (0.208 g, 1.64 mmol) was added to an orange solution of **1** (0.397 g, 0.548 mmol) in CH_2Cl_2 (15 mL) in a foil-wrapped PP vial. An excess of AgF was used because AgF is only sparingly soluble in CH_2Cl_2. The mixture was stirred for 20 h at room temperature. The dark brown slurry was gravity filtered over filter paper into a Teflon filtration flask to remove the brown-black AgX powder. The volatiles were removed under vacuum

and the light brown solid was transferred to a PP vial and stored at –40 °C. Yield: 0.338 g, 95.3%. The crude material was enriched in *cis-P,F*-**2** (82:18 *cis*-:*trans-P,F*), but a 44:56 *cis*-:*trans-P,F* mixture formed over 1 month while the solid was stored at –40 °C. The atom numbering scheme used in the NMR assignments of **1** is shown in Figure 5.16. NMR data for *cis-P,F*-**2**: ^{1}H NMR (CD_2Cl_2): δ 7.81 (dd, $^{3}J_{HH}$ = 8, J_{PH} = 5, 1H, H^{9}), 7.75 (br s, 1H, H^{6}), 7.65 (t, $^{3}J_{HH}$ = 7.5, 1H, H^{4}), 7.63 (t, $^{3}J_{HH}$ = 7.5, 1H, H^{15}), 7.37 (t, $^{3}J_{HH}$ = 7.5, 1H, H^{10}), 7.16 (d, $^{3}J_{HH}$ = 8, 2H, H^{14}), 7.11 (d, $^{3}J_{HH}$ = 6.5, 1H, H^{12}), 7.06 (t, $^{3}J_{HH}$ = 8, 2H, H^{5}), 7.03 (d, $^{3}J_{HH}$ = 8, 2H, H^{3}), 3.71 (s, 6H, H^{18}), 3.45 (s, 6H, H^{16}), 2.32 (s, 3H, H^{17}). $^{13}C\{^{1}H\}$ NMR (CD_2Cl_2): δ 161.0 (C^{2}), 159.6 (C^{13}), 143.5 (br s, C^{8}), 140.1 (C^{11}), 139.4 (C^{15}), 137.5 (C^{6}), 136.3 (C^{12}), 134.6 (C^{4}), 132.0 (C^{10}), 127.3 (C^{9}), 126.7 (d, J_{PC} = 52, C^{7}), 123.2 (C^{14}), 121.4 (d, J_{PC} = 11, C^{5}), 114.7 (d, J_{PC} = 56, C^{1}), 111.8 (C^{3}), 55.8 (C^{18}), 24.0 (C^{16}), 21.4 (C^{17}). $^{31}P\{^{1}H\}$ NMR (CD_2Cl_2): δ –4.7 (d, $^{1}J_{PF}$ = 16). ^{19}F NMR (CD_2Cl_2, –15 °C): δ –436 (d, $^{1}J_{PF}$ = 12). NMR data for *trans-P,F*-**2**: ^{1}H NMR (CD_2Cl_2): δ 7.96 (dd, $^{3}J_{HH}$ = 8, J_{PH} = 5, 1H, H^{9}), 7.52 (t, $^{3}J_{HH}$ = 8, 2H, H^{4}), 7.46 (d, $^{3}J_{HH}$ = 8, 1H, H^{10}), 7.36 (d, $^{3}J_{HH}$ = 7, H^{15}), 7.11 (d, 1H, H^{12}), 7.06 (t, $^{3}J_{HH}$ = 8, 2H, H^{5}), 6.81 (d, $^{3}J_{HH}$ = 7, 2H, H^{14}), 6.74 (d, $^{3}J_{HH}$ = 6.5, 2H, H^{3}), 3.43 (s, 6H, H^{18}), 3.06 (s, 6H, H^{16}), 2.24 (s, 3H, H^{17}). $^{13}C\{^{1}H\}$ NMR (CD_2Cl_2): δ 161.2 (C^{13}), 160.4 (C^{2}), 145.6 (d, J_{PC} = 14, C^{8}), 140.4 (C^{11}), 139.5 (C^{15}), 137.5 (C^{6}), 135.4 (C^{4}), 133.9 (C^{12}), 133.5 (C^{10}), 128.0 (C^{9}), 128.0 (d, J_{PC} = 52, C^{7}), 122.9 (C^{14}), 121.8 (d, J_{PC} = 7, C^{5}), 114.7 (d, J_{PC} = 56, C^{1}), 111.8 (C^{3}), 55.4 (C^{18}), 27.1 (C^{16}), 21.3 (C^{17}). $^{31}P\{^{1}H\}$ NMR (CD_2Cl_2): δ 3.0 (d, $^{1}J_{PF}$ = 195). ^{19}F NMR (CD_2Cl): δ –267 (d, $^{1}J_{PF}$ = 210). HRMS (ESI mode; *m/z*): Calcd. for $[C_{28}H_{29}FNO5PPdS+H]^{+}$: 647.0523; Found: 647.0533.

Figure 5.16. Atom numbering scheme for *cis*/*trans*-*P,F*-**2**.

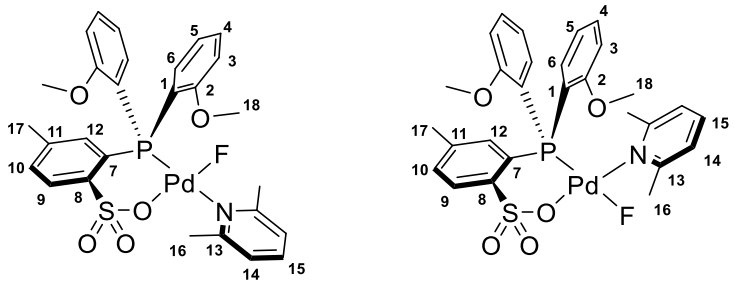

cis-P,F-**2** *trans-P,F*-**2**

Conversion of *cis*/*trans*-*P,F*-(PO-OMe)PdF(lut) (2) to (PO-OMe)PdBr(lut) (1). A Teflon NMR tube liner was charged with *cis*/*trans*-*P,F*-**2** (8.9 mg, 0.014 mmol), NBu_4Br (4.4 mg, 0.014 mmol), and 0.3 mL CD_2Cl_2. The sample was tracked by ^1H, ^{31}P, and ^{19}F NMR (see **Error! Reference source not found.**). Quantitative conversion to (PO)PdBr(lut) **1** was complete by 28 h.

{P(2-OMe-Ph)(2-{2,6-(OMe)$_2$}-Ph)(2-SO$_3$-5-Me-Ph)}PdBr(2,6-lutidine), (PO-Bp/Ph^{OMe})PdBr(lut), E. A solution of HP^+(2-OMe-Ph)(2-{2,6-(OMe)$_2$-Ph}-Ph)(2-SO3-5-Me-Ph) (1.40 g, 2.67 mmol) in CH_2Cl_2 (40 mL) was added to a solution of (COD)$PdBr_2$ (1.00 g, 2.67 mmol) in CH_2Cl_2 (40 mL). The solution was stirred for 1 h at room temperature. Lut (0.62 mL, 5.3 mmol) was added and the mixture was stirred at room temperature for 1 h. Pentane (800 mL) was added resulting in the formation of an orange precipitate. The orange powder was collected by filtration, and dissolved in CH_2Cl_2 (20 mL). The solution was washed with water (3 x 200 mL), dried over $MgSO_4$, and the volatiles were removed under vacuum to yield a light orange powder of **E**. Yield 2.06 g (94.5% based on (COD)$PdBr_2$). ^1H and ^{13}C NMR assignments are consistent with those reported by Wada, et al.[3] $^{31}P\{^1H\}$ (CD_2Cl_2): δ 10.7 (s).

{P(2-OMe-Ph)(2-{2,6-(OMe)$_2$}-Ph)(2-SO$_3$-5-Me-Ph)}PdF(2,6-lutidine), ((PO-Bp/Ph^{OMe})PdF(lut), F). In a foil-wrapped Teflon Erlenmeyer flask (with Teflon cap), AgF (0.584 g, 4.60 mmol) was added to a solution of **E** (1.876 g, 2.30 mmol) in CH_2Cl_2 (125 mL) and stirred

at room temperature for 16 h. The mixture was gravity filtered over pre-dried filter paper using a plastic funnel. The solution was collected in a Teflon filtration flask and dried under vacuum. The residue was recrystallized from CH_2Cl_2/Et_2O (1/3 *v*/*v*) at –40 °C to afford brown crystals and brown powder. The crystals and powder were collected by filtration and dried under vacuum to afford **F**. ^{1}H, ^{13}C, and ^{19}F NMR assignments are consistent with those reported by Wada.[3] $^{31}P\{^{1}H\}$ (CD_2Cl_2): δ –3.4 (d, J_{PF} = 17).

{P(2-OMe-Ph)$_2$(2-SO$_3$-5-Me-Ph)}Pd(FHF)(2,6-lutidine) (3, (PO-OMe)Pd(FHF)(lut)). *cis/trans*-PdF(lut) (0.015 g) was added to a CD_2Cl_2 solution of $NEt_3(HF)_3$. NMR experiments were taken at various temperatures (see below). The atom numbering scheme for **3** is shown in Figure 5.17. NMR signals attributed to *cis-P,F*-**3**: ^{1}H NMR (CD_2Cl_2): δ 12.58 (PdF*H*F), 7.80 (dd, $^{3}J_{HH}$ = 8, J_{PH} = 5, 1H, H^9), 7.73 (br s, 1H, H^6), 7.64 (t, $^{3}J_{HH}$ = 7.5, 1H, H^4), 7.62 (t, $^{3}J_{HH}$ = 7.5, 1H, H^{15}), 7.41 (t, $^{3}J_{HH}$ = 7.5, 1H, H^{10}), 7.15 (d, $^{3}J_{HH}$ = 8, 2H, H^{14}), 7.14 (d, $^{3}J_{HH}$ = 6.5, 1H, H^{12}), 7.04 (br m, $^{3}J_{HH}$ = 8, 2H, H^5), 7.04 (d, $^{3}J_{HH}$ = 8, 2H, H^3), 3.75 (s, 6H, H^{18}), 3.44 (s, 6H, H^{16}), 2.32 (s, 3H, H^{17}). $^{13}C\{^{1}H\}$ NMR (CD_2Cl_2): δ 160.9 (C^2), 159.4 (C^{13}), 143.3 (C^8), 139.5 (C^{11}), 139.4 (C^{15}), 137.0 (C^6), 135.3 (C^4), 134.7 (C^{12}), 132.1 (C^{10}), 127.3 (C^9), 125.4 (d, J_{PC} = 57, C^7), 123.2 (C^{14}), 121.4 (C^5), 112.5 (d, J_{PC} = 66, C^1), 111.8 (C^3), 55.9 (C^{18}), 24.7 (C^{16}), 21.3 (C^{17}). $^{31}P\{^{1}H\}$ NMR (CD_2Cl_2): δ –5 (br s). ^{19}F NMR (CD_2Cl_2): δ –171 (br s, PdFH*F*), –425 (br s, Pd*F*HF). NMR signals attributed to *trans-P,F*-**3**: ^{1}H NMR (CD_2Cl_2,): δ 12.58 (PdF*H*F), 7.94 (dd, J_{PH} = 5, 1H, H^9), 7.53 (t, $^{3}J_{HH}$ = 8, 2H, H^4), 7.45 (d, $^{3}J_{HH}$ = 8, 1H, H^{10}), 7.37 (d, $^{3}J_{HH}$ = 7, H^{15}), 7.09 (m, 1H, H^{12}), 7.04 (m, 2H, H^5), 6.85 (br s, 2H, H^{14}), 6.74 (br s, 2H, H^3), 3.45 (s, 6H, H^{18}), 3.01 (s, 6H, H^{16}), 2.26 (s, 3H, H^{17}). $^{13}C\{^{1}H\}$ NMR (CD_2Cl_2): δ 160.9 (C^{13}), 160.3 (C^2), 145.0 (C^8), 140.4 (C^{11}), 139.5 (C^{15}), 137.0 (C^6), 135.9 (C^4), 133.9 (C^{12}), 133.4 (C^{10}), 127.8 (C^9), 125.4 (d, J_{PC} = 57, C^7), 123.0 (C^{14}), 121.7 (d, J_{PC} = 7, C^5), 112.5 (d, J_{PC} = 66, C^1), 111.8 (C^3), 55.4 (C^{18}), 26.9 (C^{16}), 21.3 (C^{17}). $^{31}P\{^{1}H\}$

NMR (CD_2Cl_2): δ 6 (br s), 5 (br s). $^{31}P\{^1H\}$ NMR (CD_2Cl_2, –60 °C): δ 17.1 (dd, $^1J_{PF}$ = 202), 15.2 (dd, $^1J_{PF}$ = 202). ^{19}F NMR (CD_2Cl_2): δ –171 (br s, PdFH*F*), –253 (br s, Pd*F*HF). X-ray quality crystals were obtained by layering pentane on this CH_2Cl_2 solution in the Teflon NMR tube liner and storage at –40 °C. X-ray data and structure refinement for *trans-P,F*-**3** can be found in Table 5.2.

Figure 5.17. Atom numbering scheme for *cis*/*trans-P,F*-**3**.

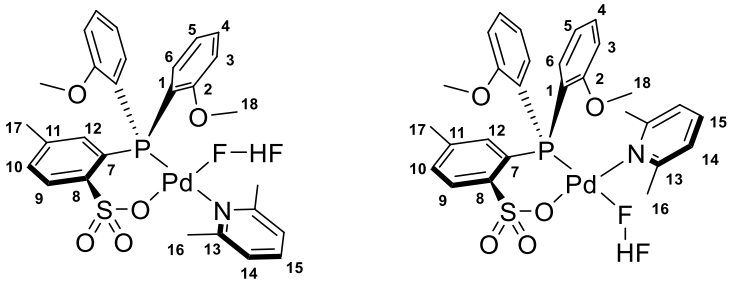

{P(2-OMe-Ph)$_2$(2-SO$_3$-5-Me-Ph)}Pd(CH$_2$CF$_2$H)(2,6-lutidine) (4, (PO-OMe)PdCH$_2$CF$_2$H(lut)). A Teflon NMR tube liner was charged with **2** (10 mg, 0.015 mmol, 39:61 *cis*:*trans*) and 0.3 mL CD_2Cl_2. The uncapped liner was sealed in a J-Young tube. On a Schlenk line, 1 atm of vinyl fluoride (VF) was condensed into the frozen sample tube (20 mL gas bulb, 129 mm Hg of VF, 1.5 equiv). Conversion from *cis-P,F*-**2** to **4** was complete in 20 h to give a ~54:46 mixture of *trans-P,F*-**2** and a new species, which was identified as **4** by COSY, NOESY, HMQC, and HMBC NMR spectroscopy. The sample tube was heated at 40 °C for 22.5 h, during which time *trans-P,F*-**2** converted to **4**. The atom numbering scheme for **4** is shown in Figure 5.18. Figure 5.23 shows NMR monitoring over the course of the reaction. NMR spectra used to characterize **4** are shown in Figure 5.24. ^1H NMR (CD_2Cl_2,): δ 7.87 (dd, $^3J_{HH}$ = 8, $^4J_{PH}$ = 5, 1H, H^9), 7.74 (br s, 2H, H^6), 7.66 (t, $^3J_{HH}$ = 7.5, 1H, H^{15}), 7.60 (t, $^3J_{HH}$ = 7.5, 2H, H^4), 7.30 (d, $^3J_{HH}$ = 7.5, 1H, H^{10}),

7.19 (d, $^{3}J_{HH}$ = 8, 2H, H^{14}), 7.17 (d, $^{3}J_{PH}$ = 12.5, 1H, H^{12}), 7.11 (t, $^{3}J_{HH}$ = 7.5, 2H, H^{5}), 7.01 (dd, $^{3}J_{HH}$ = 8, $^{4}J_{PH}$ = 4.5, 2H, H^{3}), 4.84 (tt, $^{2}J_{FH}$ = 57, $^{3}J_{HH}$ = 5, 1H, $PdCH_2CHF_2$), 3.66 (s, 6H, H^{18}), 3.25 (s, 6H, H^{16}), 2.28 (s, 3H, H^{17}), 1.06 (tt, $^{3}J_{FH}$ = 22, $^{3}J_{HH}$ = 5, 1H, $PdCH_2CHF_2$). $^{13}C\{^{1}H\}$ NMR (CD_2Cl_2): δ 160.8 (C^{2}), 159.5 (C^{13}), 145.2 (d, J_{PC} = 15, C^{8}), 139.2 (C^{11}), 139.1 (C^{15}),138.0 (C^{6}), 135.4 (C^{12}), 134.2 (C^{4}), 131.3 (C^{10}), 127.7 (C^{9}), 126.7 (d, J_{PC} = 52, C^{7}), 123.2 (C^{14}), 121.1 (d, J_{PC} = 11, C^{5}), 120.1 (t, J_{FC} = 237, $PdCH_2CHF_2$), 114.7 (d, J_{PC} = 56, C^{1}), 111.6 (C^{3}), 55.4 (C^{18}), 26.0 (C^{16}), 21.4 (C^{17}), 12.7 ($PdCH_2CHF_2$). $^{31}P\{^{1}H\}$ NMR (CD_2Cl_2): δ 15.8 (s). ^{19}F NMR (CD_2Cl_2): δ –98.3 (d, $^{2}J_{FH}$ = 57). HRMS (ESI mode; *m/z*): Calcd. for $[C_{30}H_{32}F_2NO_5PPdS+H]^{+}$: 693.0742; Found: 693.0751.

Figure 5.18. Atom numbering scheme for **4**.

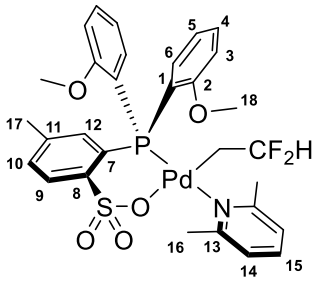

{P(2-OMe-Ph)$_2$(2-SO$_3$-5-Me-Ph)}Pd(CH$_2$CF(OAc)H)(2,6-lutidine) (5, (PO-OMe)Pd(CH$_2$CF(OAc)H)(lut)). A Teflon NMR tube liner was charged with **2** (21 mg, 0.033 mmol, 70:30 *cis*-/*trans*-*P,F*) and 0.25 mL CD_2Cl_2. VOAc (46 μL, 0.49 mmol) was added to the solution via microsyringe and the Teflon liner was sealed. The sample tube was heated in a 50 °C water bath for 2.3 h, during which time, <78% **2** converted to **5** by ^{31}P NMR. NMR assignments of **5** were made using 1D and 2D NMR experiments of this mixture (Figure 5.25). The numbering scheme for **5** is shown in Figure 5.19. ^{1}H NMR (CD_2Cl_2): δ 7.86 (dd, $^{3}J_{HH}$ = 8, $^{4}J_{PH}$ = 5, 1H, H^{9}), 7.73 (br s, 2H, H^{6}), 7.65 (t, $^{3}J_{HH}$ = 8, 1H, H^{15}), 7.57 (t, $^{3}J_{HH}$ = 8, 2H, H^{4}), 7.30 (d, $^{3}J_{HH}$ = 8, 1H,

H^{10}), 7.17 (overlapping, 2H, H^{14}), 7.16 (d, $^{3}J_{PH}$ = 11.5, 1H, H^{12}), 7.09 (t, $^{3}J_{HH}$ = 7.5, 2H, H^{5}), 7.00 (dd, $^{3}J_{HH}$ = 8, $^{4}J_{PH}$ = 4.5, 2H, H^{3}), 5.36 (dt, $^{2}J_{FH}$ = 58, $^{3}J_{HH}$ = 5.5, 1H, $PdCH_2C\mathit{H}F(OAc)$), 3.66 (s, 3H, H^{18}), 3.65 (s, 3H, H^{18}), 3.17 (s, 3H, H^{16}), 3.16 (s, 3H, H^{16}), 2.26 (s, 3H, H^{17}), 2.26 (s, 3H, $PdCH_2CHF(OC(O)C\mathit{H_3})$), 1.06 (dt, $^{3}J_{FH}$ = 18, $^{3}J_{HH}$ = 5, 1H, $PdC\mathit{H_2}CHF(OAc)$). $^{13}C\{^{1}H\}$ NMR (CD_2Cl_2): δ 160.9 (C^{2}), 159.4 (C^{13}), 145.8 (d, C^{8}), 139.0 (C^{11}), 138.9 (C^{15}),138.2 (C^{6}), 135.4 (C^{12}), 134.1 (C^{4}), 131.3 (C^{10}), 127.7 (C^{9}), 126.8 (d, $^{1}J_{PC}$ = 51, C^{7}), 123.2 (C^{14}), 121.0 (d, J_{PC} = 9.5, C^{5}), 114.8 (d, $^{1}J_{PC}$ = 54, C^{1}), 111.7 (C^{3}), 105.6 (d, $^{1}J_{FC}$ = 220, $PdCH_2\mathit{C}HF(OAc)$), 55.4 (C^{18}), 30.1 ($PdCH_2CHF(OC(O)\mathit{C}H_3)$), 26.1 ($C^{16}$), 21.3 ($C^{17}$), 12.4 (d, $^{2}J_{FC}$ = 17, $Pd\mathit{C}H_2CHF(OAc)$). $^{31}P\{^{1}H\}$ NMR (CD_2Cl_2): δ 16.7 (s). ^{19}F NMR (CD_2Cl_2): δ –108 (s).

Figure 5.19. Atom numbering scheme for **5**.

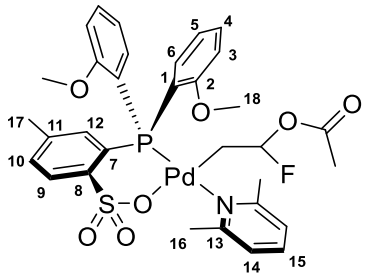

{P(2-OMe-Ph)$_2$(2-SO$_3$-5-Me-Ph)}Pd(CH$_2$C(=O)H)(2,6-lutidine) (6, (PO-OMe)Pd(CH$_2$C(=O)H)(lut)). A Teflon NMR tube liner was charged with *cis*/*trans*-*P,F*-**2** (21 mg, 0.033 mmol) and 0.25 mL CD_2Cl_2. VOAc (46 μL, 0.49 mmol) was added to the solution via plastic microsyringe and the Teflon liner was sealed. The sample tube was heated in a 60 °C water bath for 12 h. X-ray quality crystals of **6**•1.5(CH_2Cl_2) were isolated (72% yield) by layering pentane over this reaction mixture and storage at –40 °C. The numbering scheme for **6** is shown in Figure 5.20. NMR spectra used to characterize **6** are shown in Figure 5.26. ^{1}H NMR (CD_2Cl_2): δ 8.54 (dd, $^{3}J_{HH}$ = 6.5, $PdCH_2C(=O)\mathit{H}$), 7.86 (t, $^{3}J_{HH}$ = 8, $^{4}J_{PH}$ = 5, 1H, H^{9}), 7.71 (br s, 2H, H^{6}), 7.66 (t, $^{3}J_{HH}$

= 8, 1H, H^{15}), 7.57 (t, $^{3}J_{HH}$ = 8, 2H, H^{4}), 7.29 (d, $^{3}J_{HH}$ = 8, 1H, H^{10}), 7.18 (overlapping, 2H, H^{14}), 7.12 (d, $^{3}J_{PH}$ = 9, 1H, H^{12}), 7.10 (t, $^{3}J_{HH}$ = 7.5, 2H, H^{5}), 7.01 (dd, $^{3}J_{HH}$ = 8, $^{4}J_{PH}$ = 4.5, 2H, H^{3}), 3.69 (s, 3H, H^{18}), 3.14 (s, 3H, H^{16}), 2.28 (s, 3H, H^{17}), 1.84 (dd, $^{3}J_{HH}$ = 5, $^{4}J_{PH}$ = 4.7, 2H, PdC*H*$_2$C(=O)H). $^{13}C\{^{1}H\}$ NMR (CD_2Cl_2): δ 208.8 (PdCH$_2$*C*(=O)H), 160.9 (C^{2}), 159.4 (C^{13}), 145.8 (d, C^{8}), 139.1 (C^{11}), 137.8 (C^{15}, C^{6}), 135.1 (C^{12}), 134.2 (C^{4}), 131.5 (C^{10}), 128.2 (C^{9}), 127.8 (d, $^{1}J_{PC}$ = 50, C^{7}), 123.4 (C^{14}), 121.1 (d, J_{PC} = 10, C^{5}), 114.8 (d, $^{1}J_{PC}$ = 52, C^{1}), 111.7 (C^{3}), 55.5 (C^{18}), 25.8 (C^{16}), 25.1 (C^{17}), 21.4 (Pd*C*H$_2$C(=O)H). $^{31}P\{^{1}H\}$ NMR (CD_2Cl_2): δ 13.1 (s).

Figure 5.20. Atom numbering scheme of **6**.

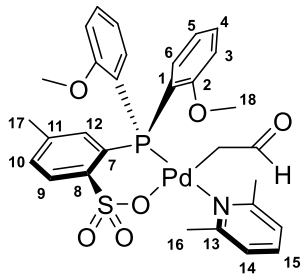

{P(2-OMe-Ph)$_2$(2-SO$_3$-5-Me-Ph)}Pd(CH$_2$-(3-F-cyclopentanyl))(2,6-lutidine) (7, (PO-OMe)Pd(CH$_2$-(3-F-cyclopentanyl))(lut)). A Teflon NMR tube liner was charged with *cis*/*trans*-*P,F*-**2** (15 mg, 0.023 mmol, 67:33 *cis*-:*trans*-*P,F*) and 0.25 mL CD_2Cl_2. 1,5-hexadiene (2.7 µL, 0.023 mmol) was added to the solution via microsyringe and the Teflon liner was sealed. The sample tube was kept at room temperature for 80 h, during which time, the ^{31}P NMR showed 67% of **2** was converted to **7**, with no *cis*-*P,F*-**2** and 66% of the original *trans*-*P,F*-**2** remaining. The sample tube was heated at 60 °C for 6 h to yield **7** (>95%). NMR assignments of **6** were made using 1D and 2D NMR experiments of this mixture. The atom numbering using for NMR assignments of **7** are shown in Figure 5.21. ^{1}H NMR (CD_2Cl_2): δ 7.87 (br s, 2H, H^{6}), 7.83 (dd, $^{3}J_{HH}$ = 7.5, J_{PH} = 5.5, 1H, H^{9}), 7.65 (t, $^{3}J_{HH}$ = 7, 1H, H^{15}), 7.55 (t, $^{3}J_{HH}$ = 7.5, 2H, H^{4}), 7.26 (dd, $^{3}J_{HH}$

= 7.5, J_{PH} = 12.5, 1H, H^{10}), 7.19 (d, $^3J_{HH}$ = 8.5, 2H, H^{14}), 7.09 (d, $^3J_{HH}$ = 7, 1H, H^{12}), 7.08 (t, $^3J_{HH}$ = 7.5, 2H, H^5), 6.97 (dd, $^3J_{HH}$ = 8, $^3J_{PH}$ = 4, 2H, H^3), 4.66 (doublet of multiplets, 1H, H^e), 3.62 (s, 6H, H^{18}), 3.22 (s or t, 6H, H^{16}), 2.27 (s, 3H, H^{17}), overlapping multiplets in the range 1.65 – 0.40. $^{13}C\{^1H\}$ NMR (CD_2Cl_2): δ 161.2 (C^2), 160.9 (C^2), 160.4 (C^{13}), 159.3 (C^{13}), 138.7 (C^{11}), 138.6 (C^{15}),138.6 (C^6), 135.2 (C^{12}), 133.6 (C^4), 130.7 (C^{10}), 128.0 (C^9), 127.4 (C^7), 123.0 (C^{14}), 120.6 (br s, C^5), 115.0 (d, J_{PC} = 64, C^1), 111.7, 111.4 (C^3), 55.2 (C^{18}), 26.4 (C^{16}), 21.3 (C^{17}). $^{31}P\{^1H\}$ NMR (CD_2Cl_2): δ 22.4 (s), 22.2 (s), $^{19}F\{^1H\}$ NMR (CD_2Cl_2): δ –166 (7-tet, 30 Hz, $\Delta_{½}$ = 150 Hz), –168 (7-tet, 30 Hz, $\Delta_{½}$ = 150 Hz). HRMS (ESI mode; *m/z*): Calcd. for $[C_{34}H_{39}FNO_5PPdS\text{-lut}+Li]^+$: 628.0652; Found: 628.0635.

Figure 5.21. Atom numbering scheme for **7**.

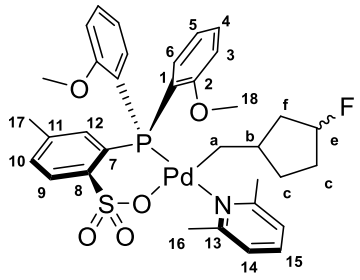

Figure 5.22. NMR spectra of **2** (CD_2Cl_2, with added CsF).

(a) ^{1}H NMR (500 MHz)

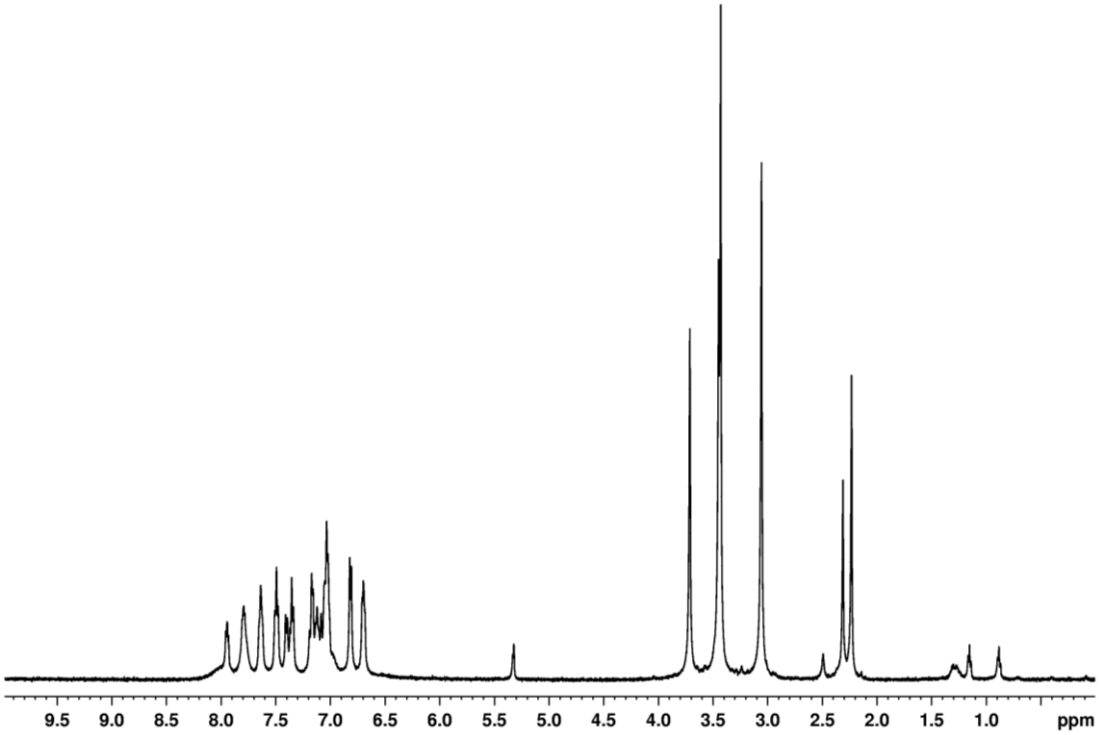

(b) ^{1}H NMR of aromatic region (500 MHz)

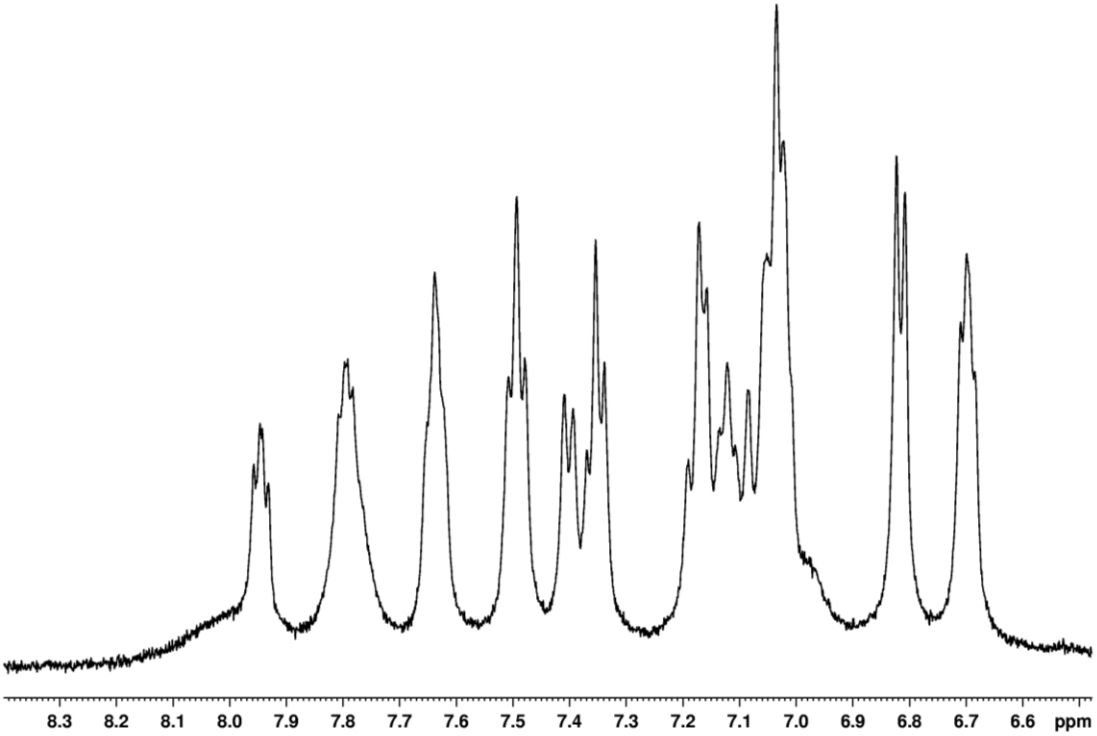

Figure 5.22, continued.

(c) ^{1}H NMR of aliphatic region (500 MHz)

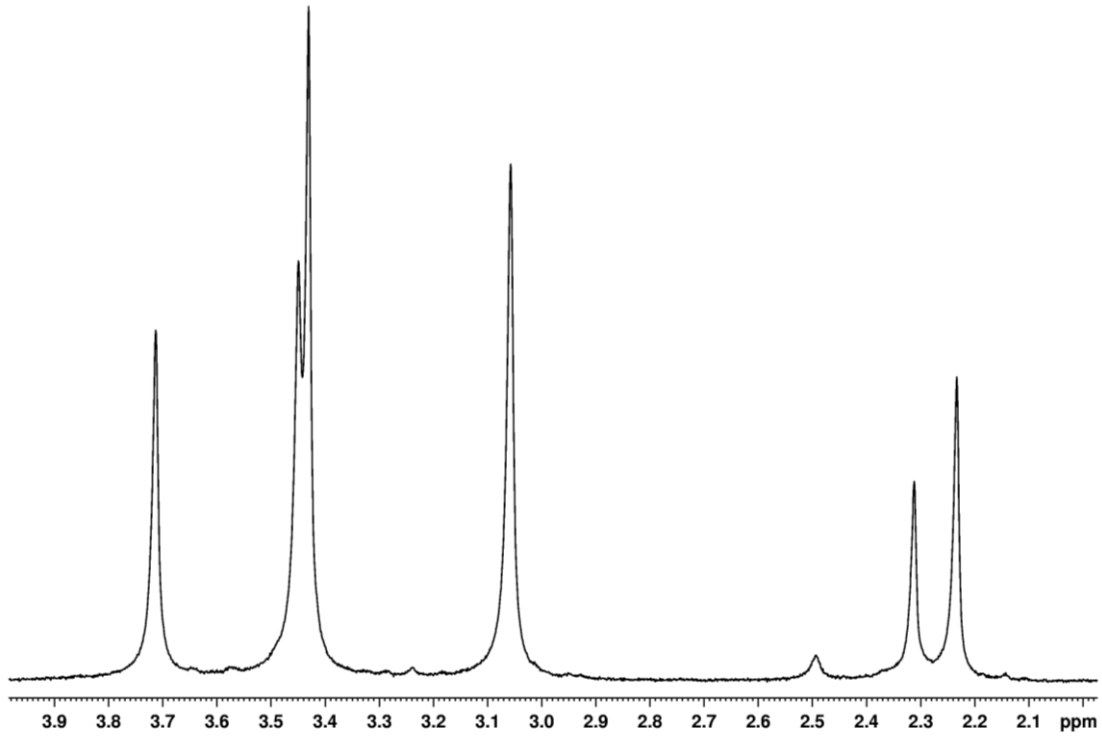

(d) ^{31}P NMR (202 MHz)

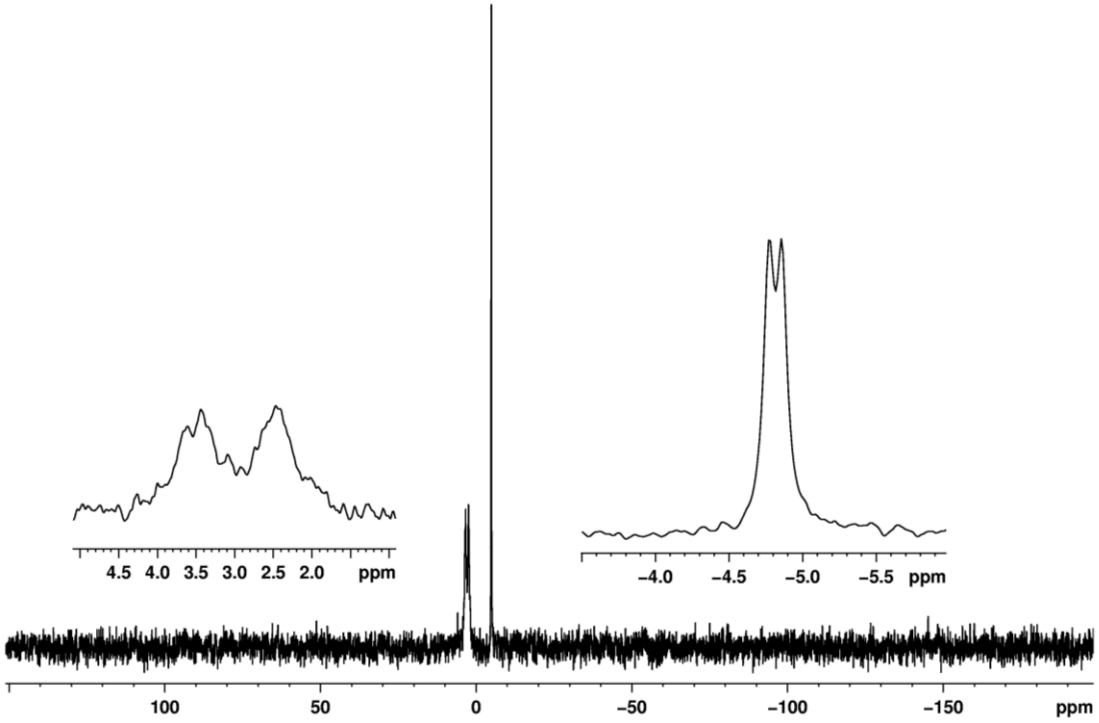

Figure 5.22, continued.

(e) ^{19}F NMR (470 MHz)

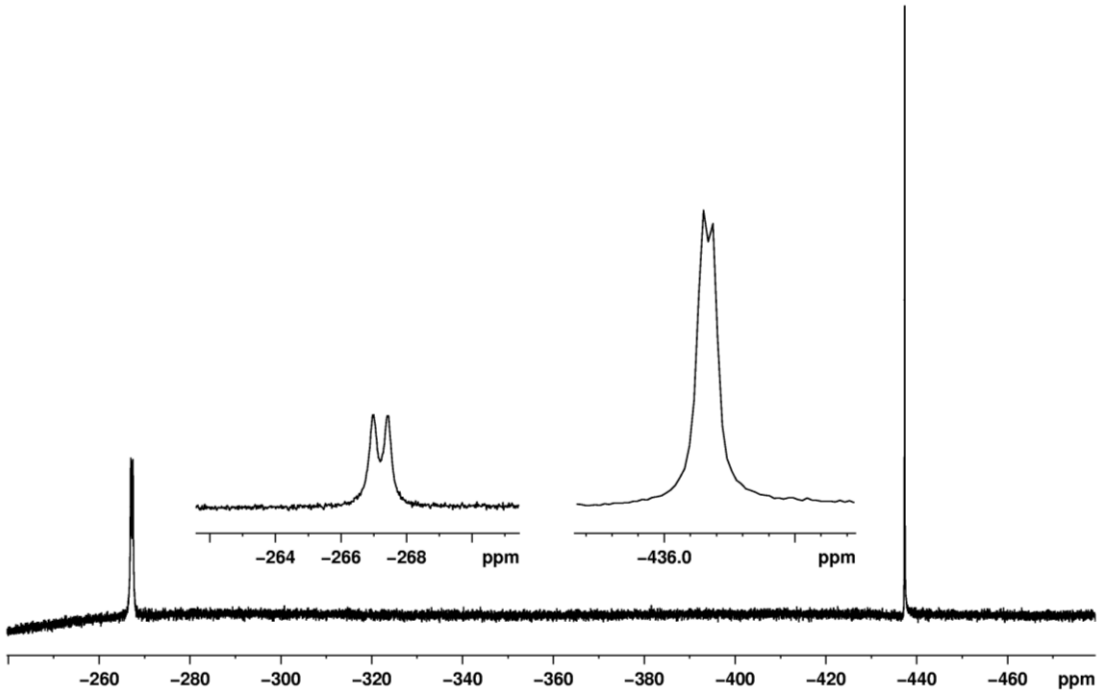

Figure 5.23 Stacked NMR spectra of reaction progress of **2** and vinyl fluoride (CD_2Cl_2),

(a) ^{1}H NMR of aliphatic region (500 MHz)

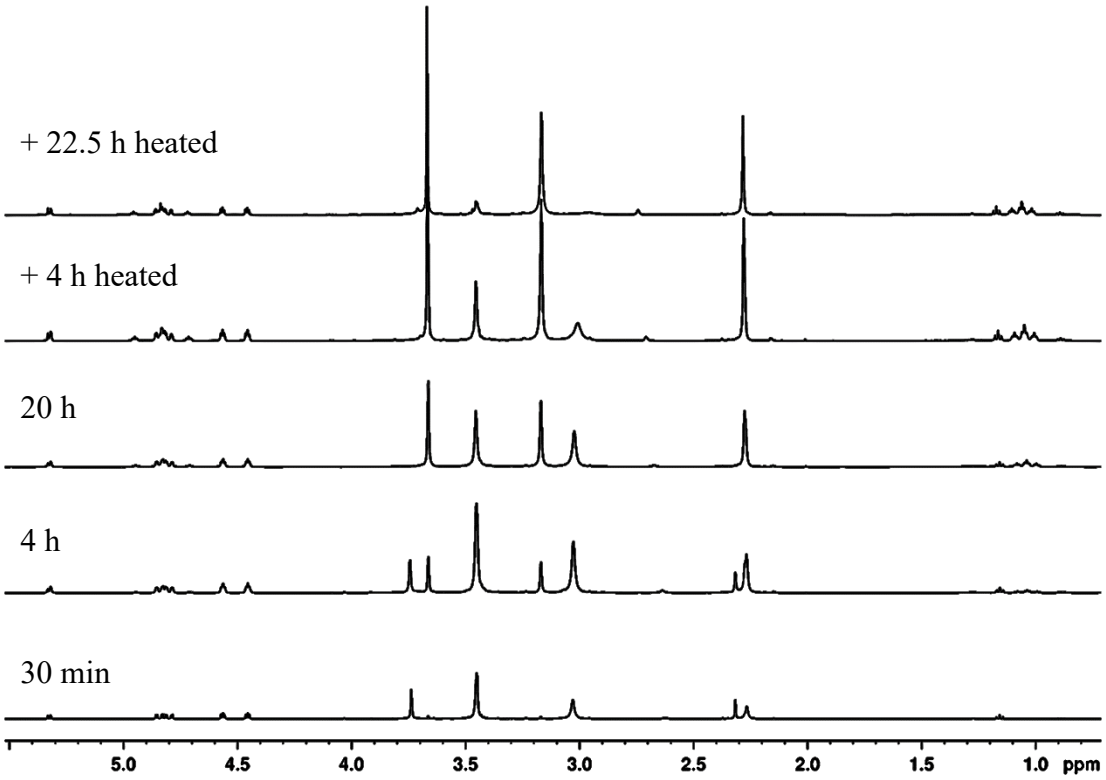

Figure 5.23, continued.

(b) ^{1}H NMR of aromatic region (500 MHz)

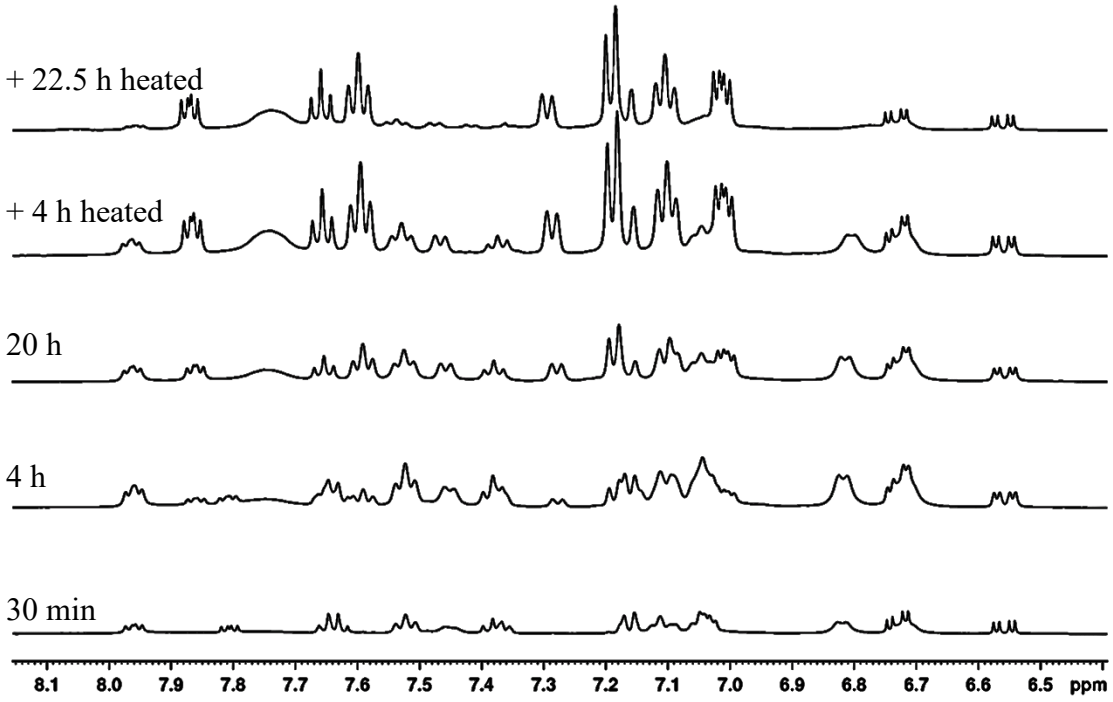

(c) ^{1}H NMR showing the peaks corresponding to PdC*H*$_2$CF$_2$*H* (500 MHz). VF: dq at δ 4.82.

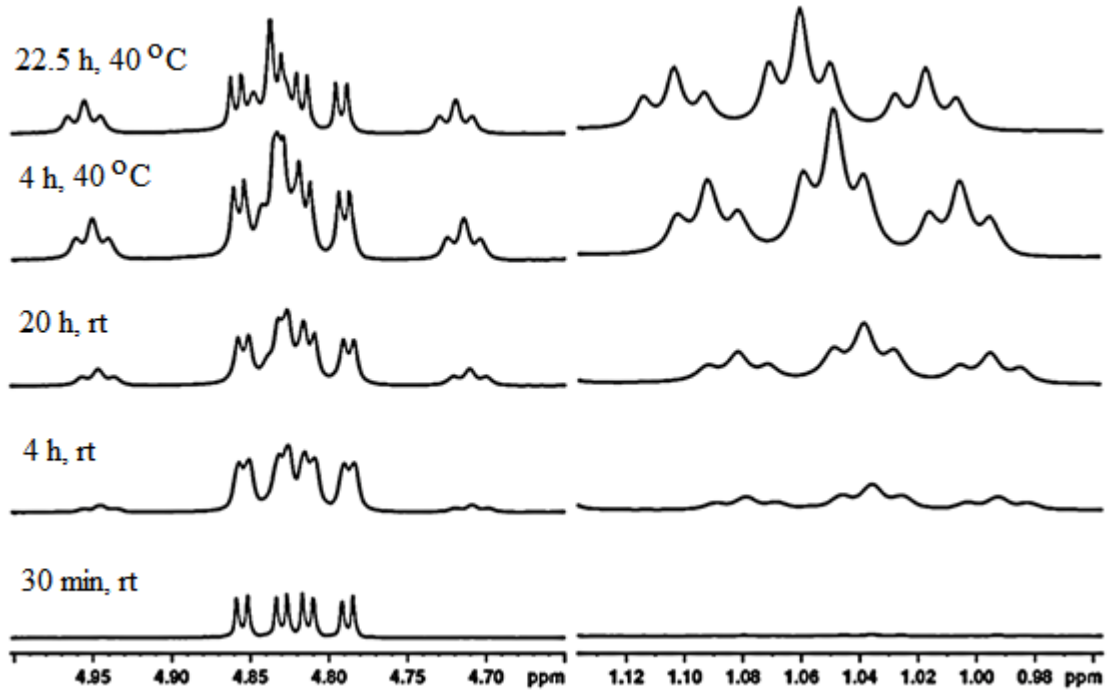

Figure 5.23, continued.

(d) left: ^{31}P NMR (202 MHz), right: ^{19}F NMR (470 MHz)

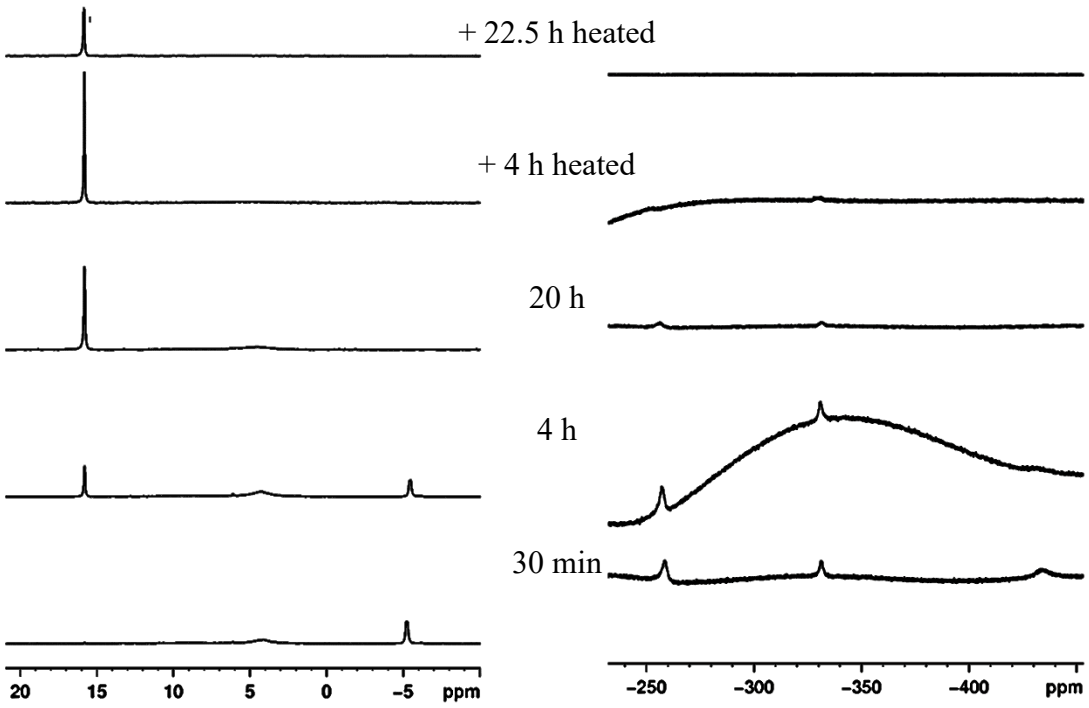

(e) ^{19}F NMR (470 MHz), VF at δ –117.

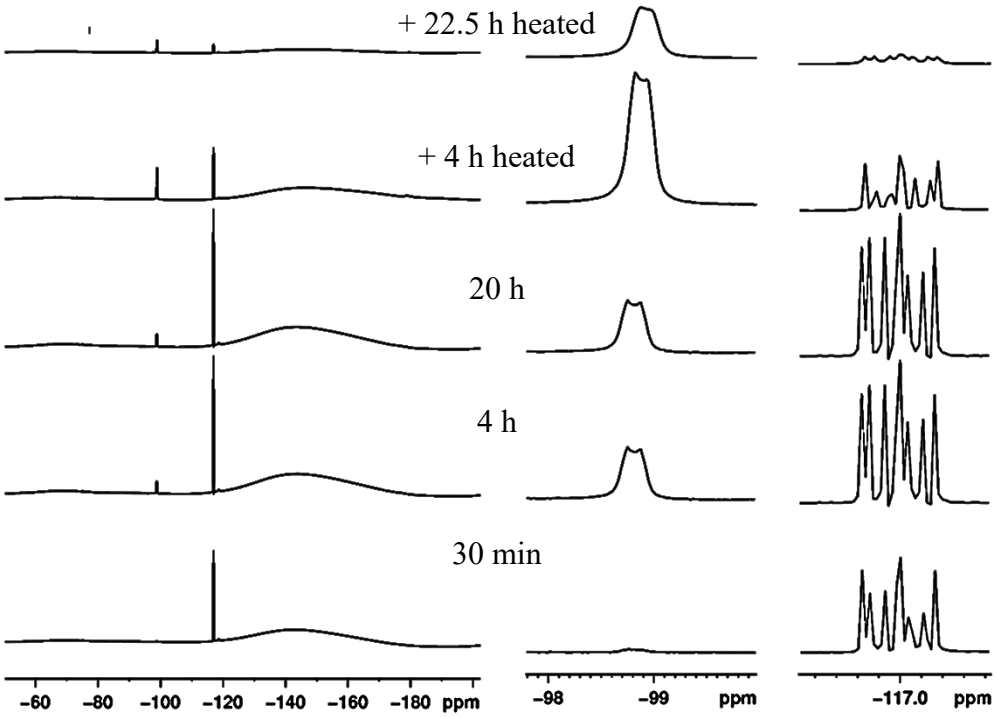

Figure 5.24. NMR spectra of **4** (>90% from the reaction between **2** and VF, CD_2Cl_2).

(a) ^{1}H NMR (500 MHz)

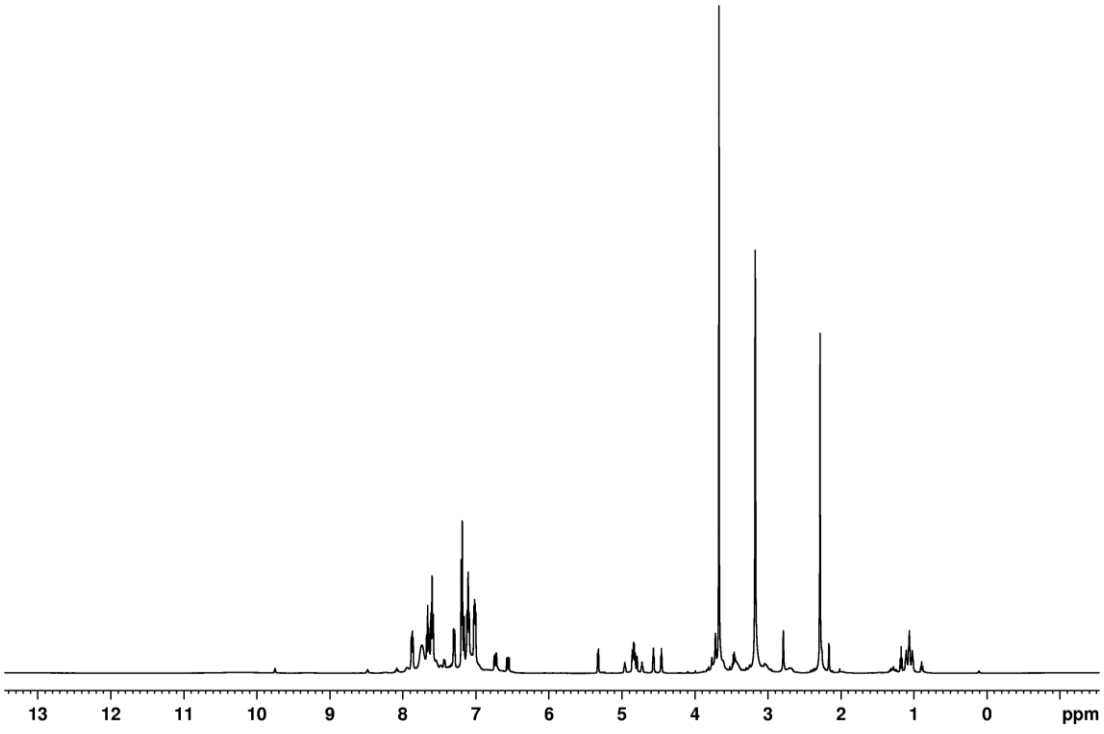

(b) ^{1}H NMR spectrum expansion from δ 6.4–8.6 (500 MHz)

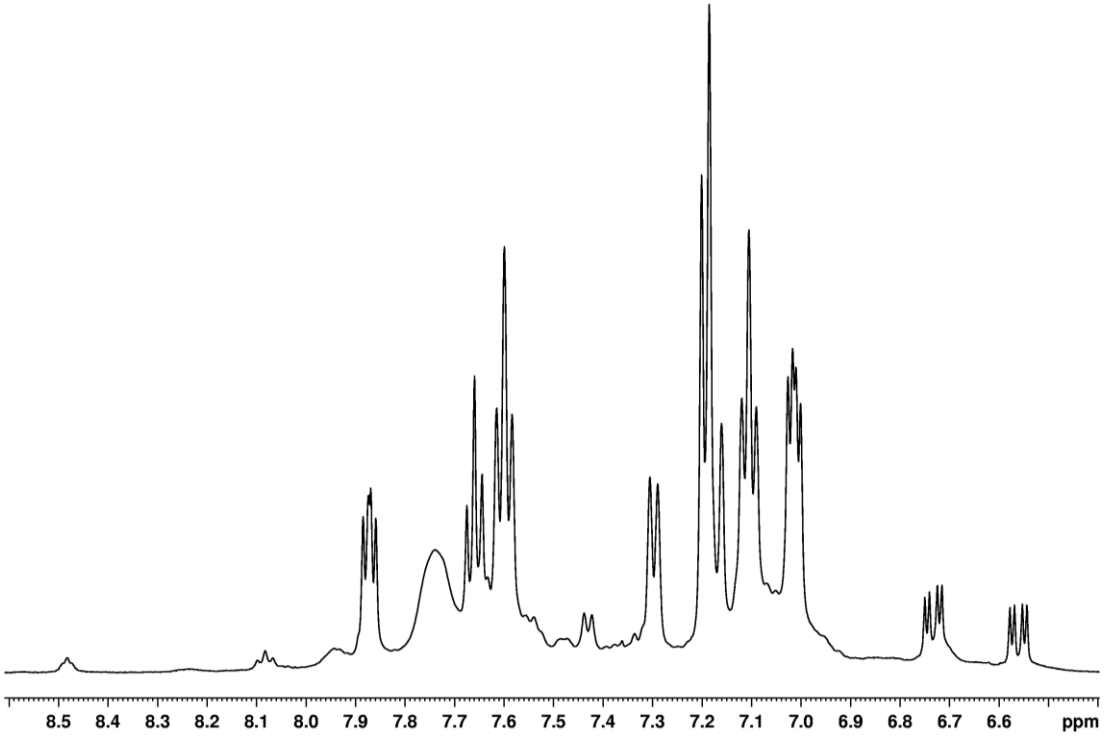

Figure 5.24, continued.

(c) ^{1}H NMR spectrum expansion from δ 0.5–5.5 (500 MHz)

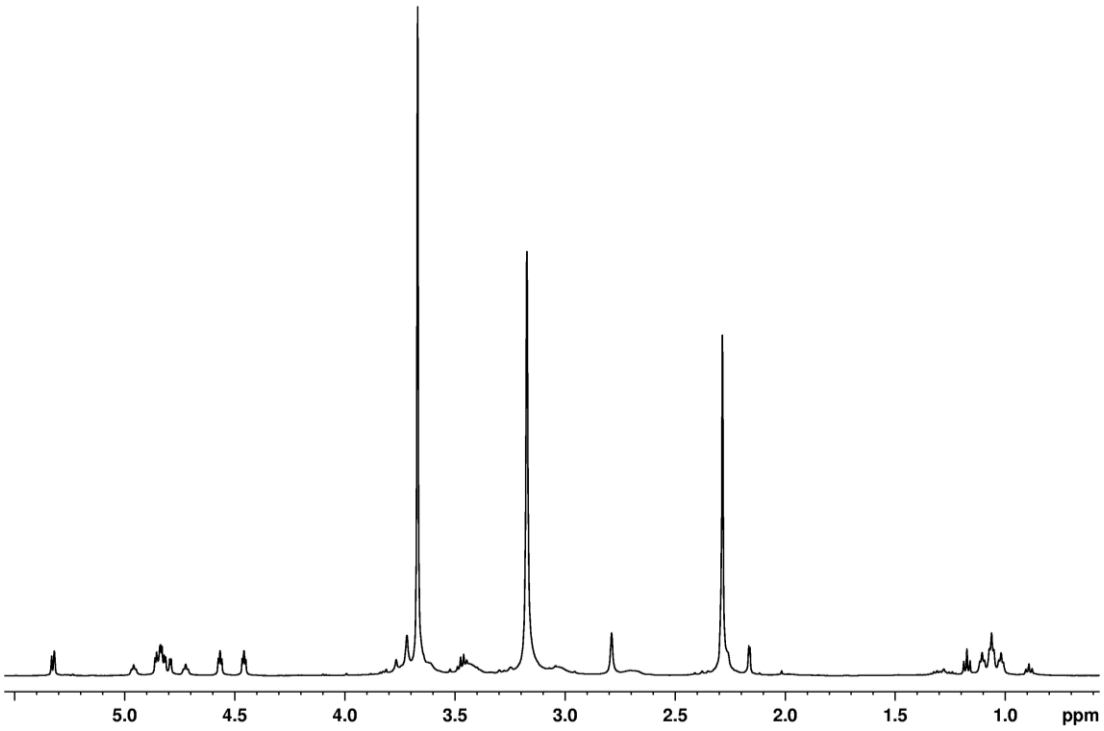

(d) ^{31}P NMR (202 MHz)

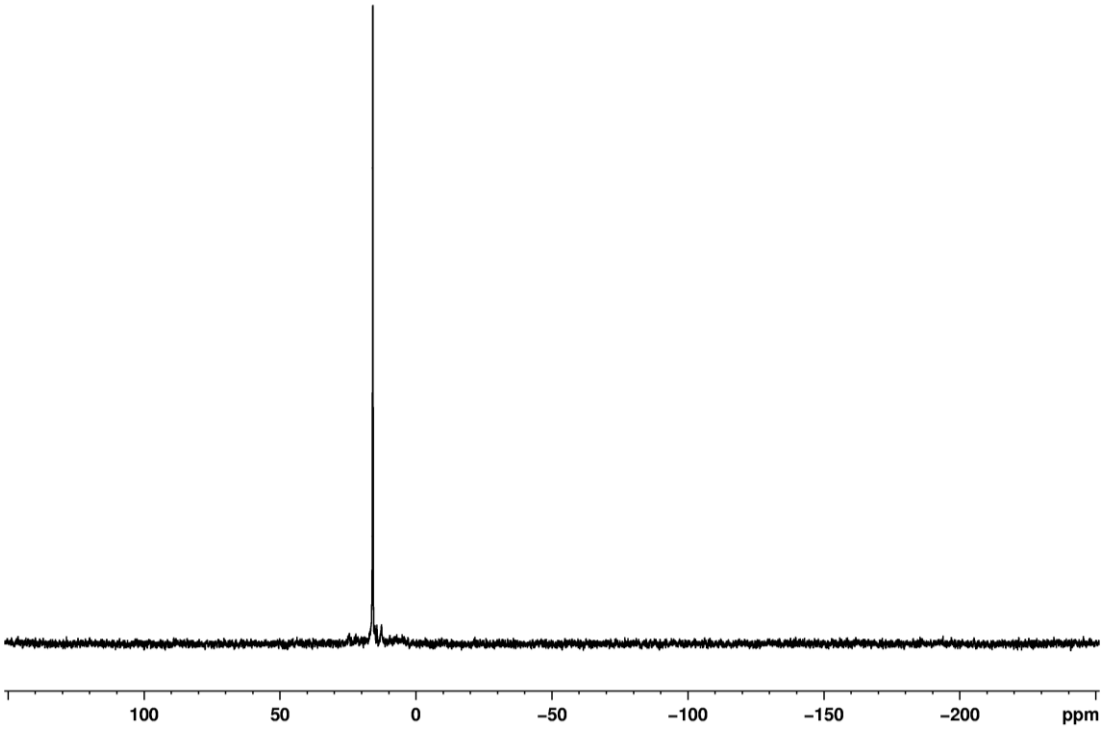

Figure 5.24, continued.

(e) ^{19}F NMR (470 MHz), VF at δ –117.

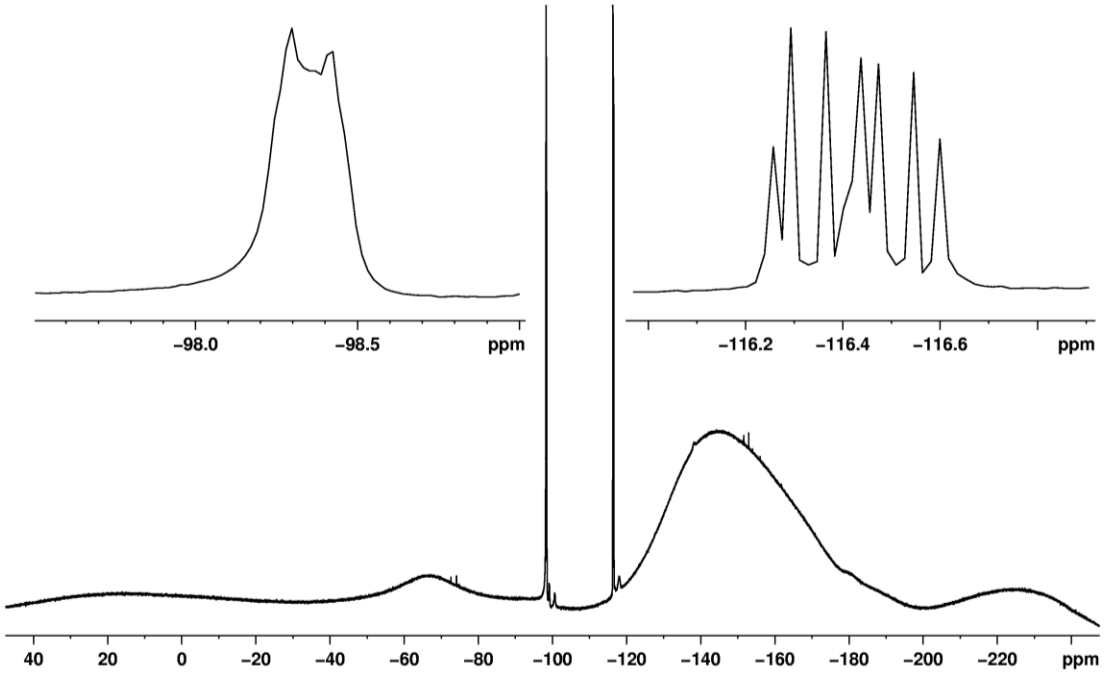

(f) ^{13}C NMR (125 MHz)

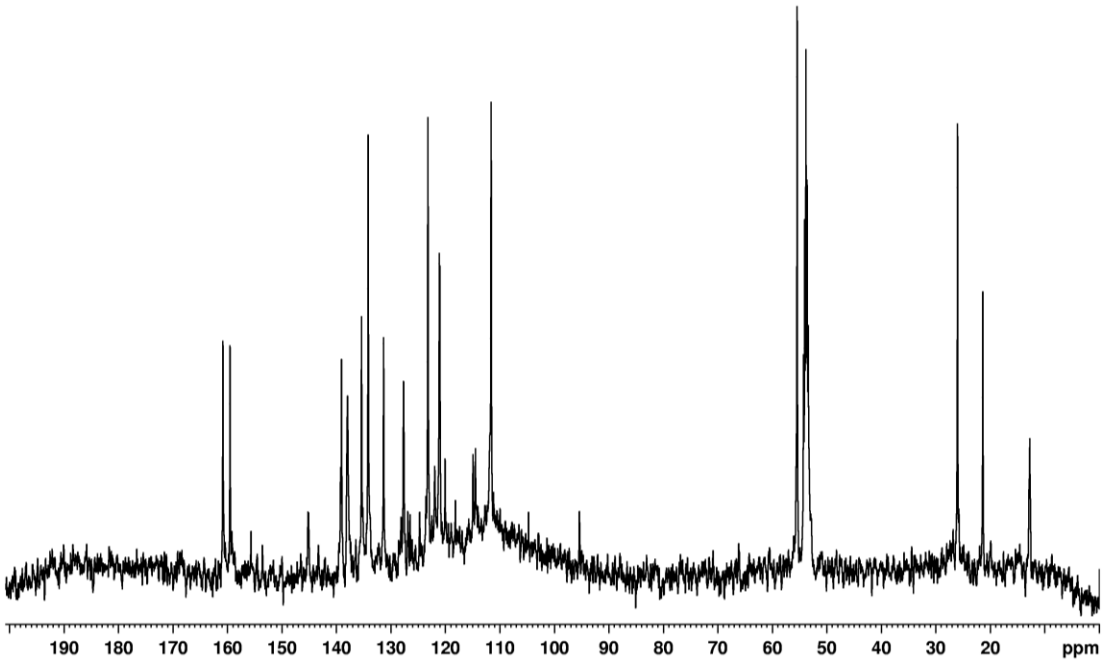

Figure 5.24, continued.

(g) ^{13}C NMR spectrum expansion from δ 90–165 (125 MHz)

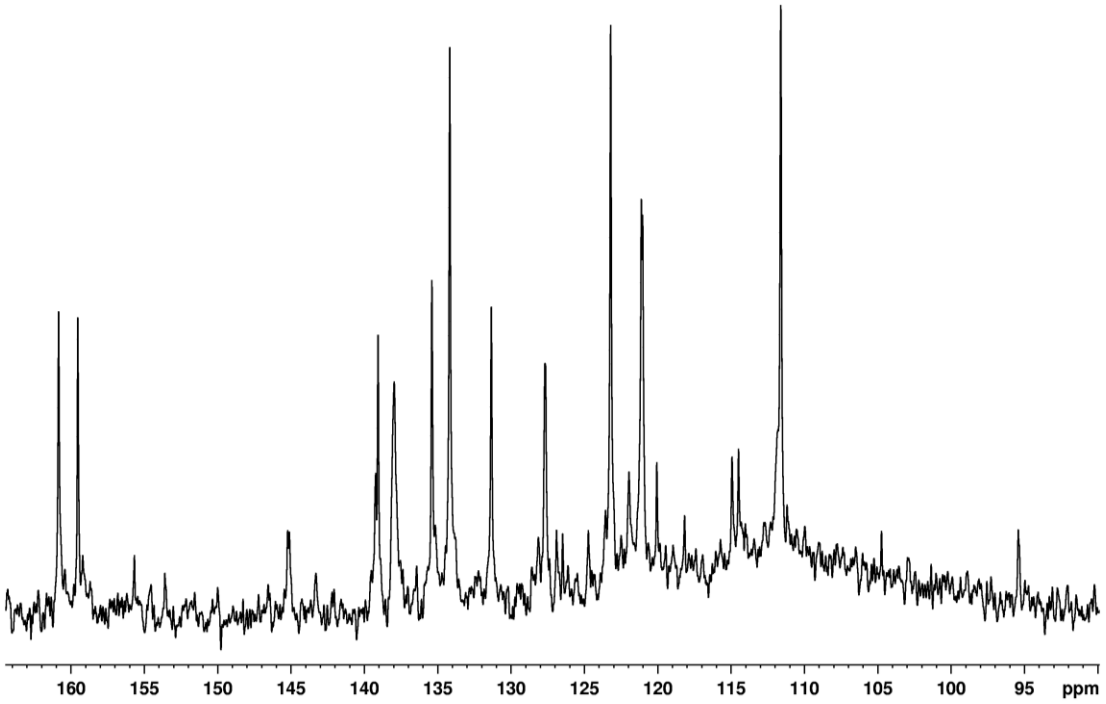

(h) COSY NMR (500 MHz)

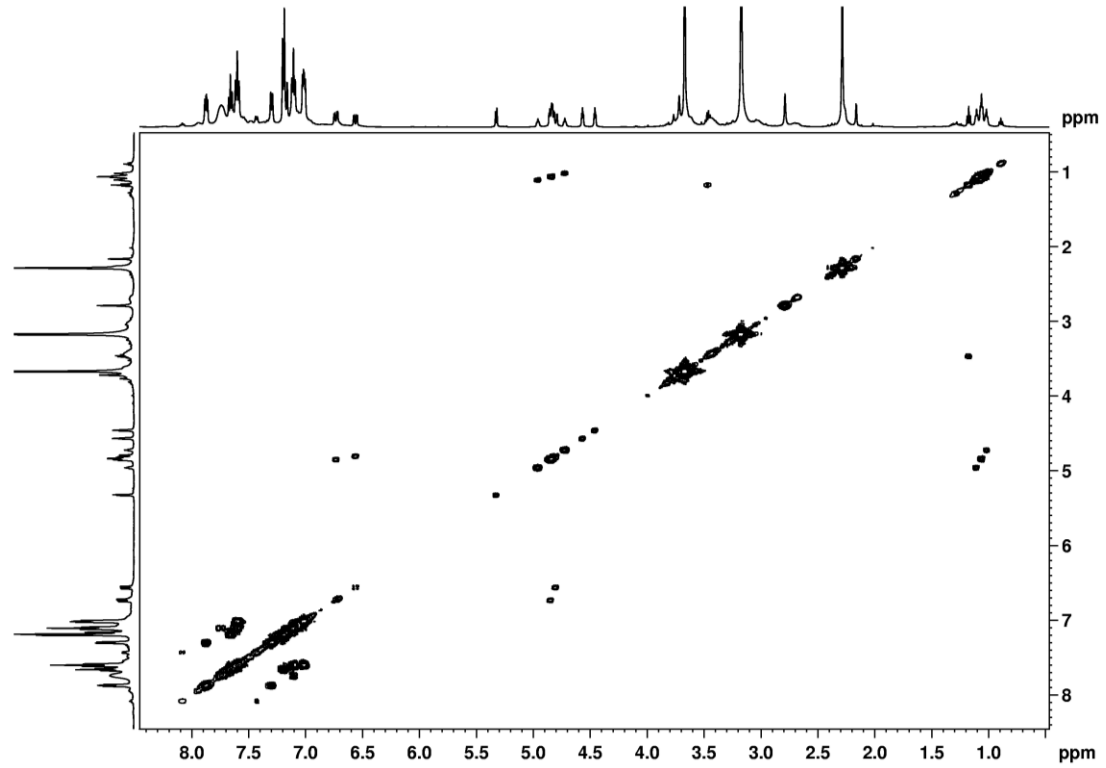

Figure 5.24, continued.

(i) COSY NMR spectrum expansion (500 MHz)

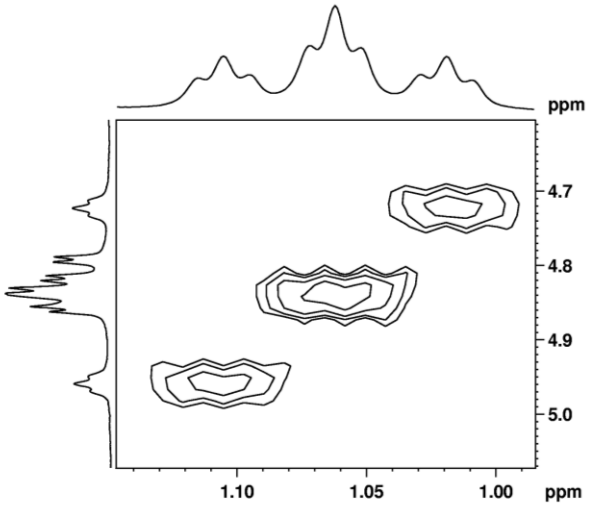

Figure 5.25. NMR spectra for **5** from the reaction of **2** and VOAc (CD_2Cl_2).

(a) ^1H NMR spectrum (500 MHz). VOAc: δ 7.25, 4.85, 4.54, and 2.09.

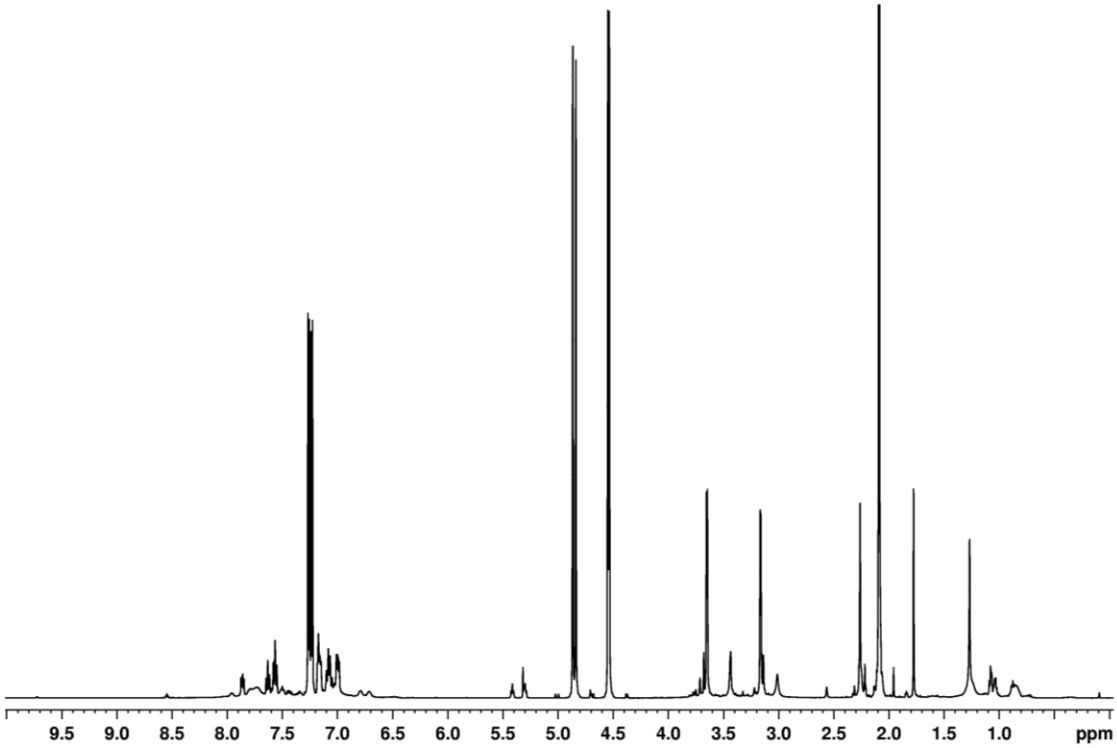

Figure 5.25, continued.

(b) ^{1}H NMR spectrum expansion from δ 6.4–8.6 (500 MHz)

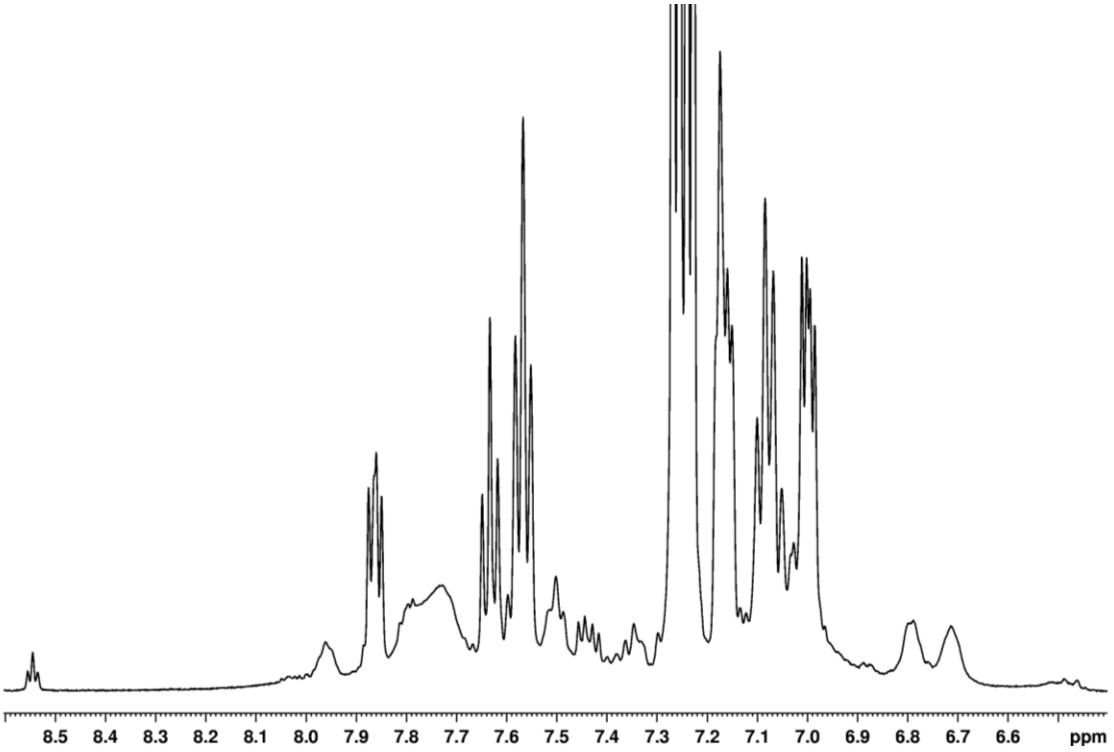

(c) ^{1}H NMR spectrum expansion from δ 0.0–6.2 (500 MHz)

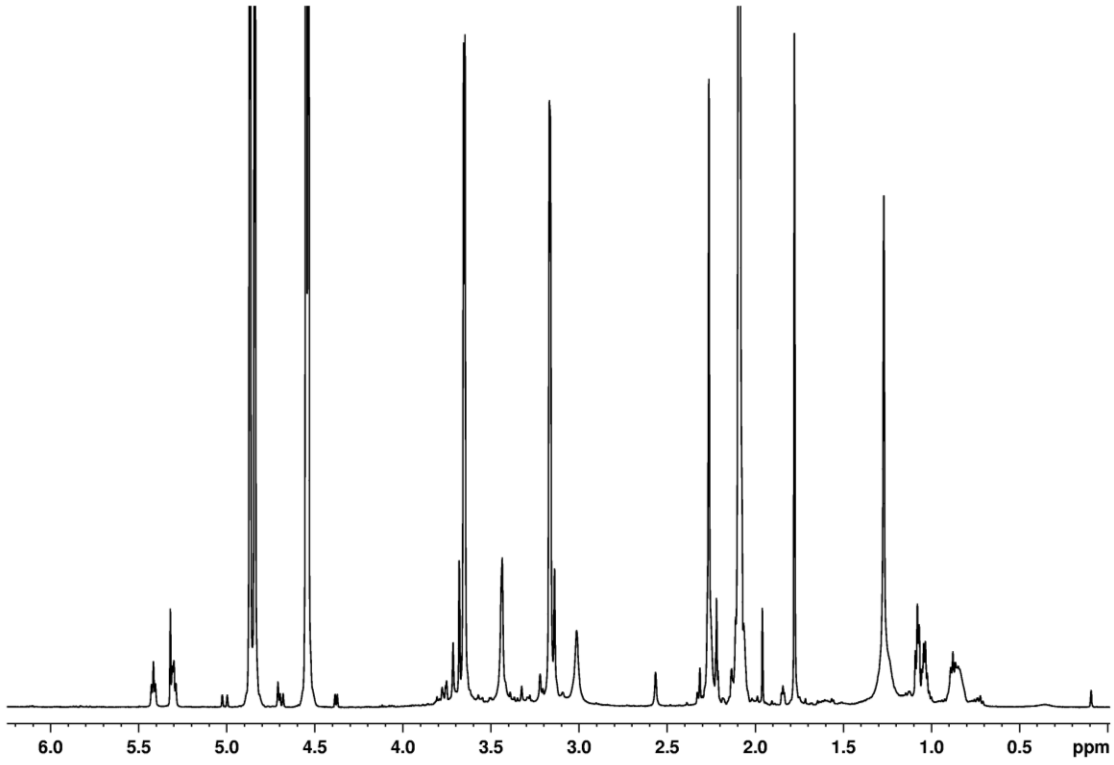

Figure 5.25, continued.

(d) ^{1}H NMR spectrum showing PdCH_2CHF(OAc) signals (500 MHz)

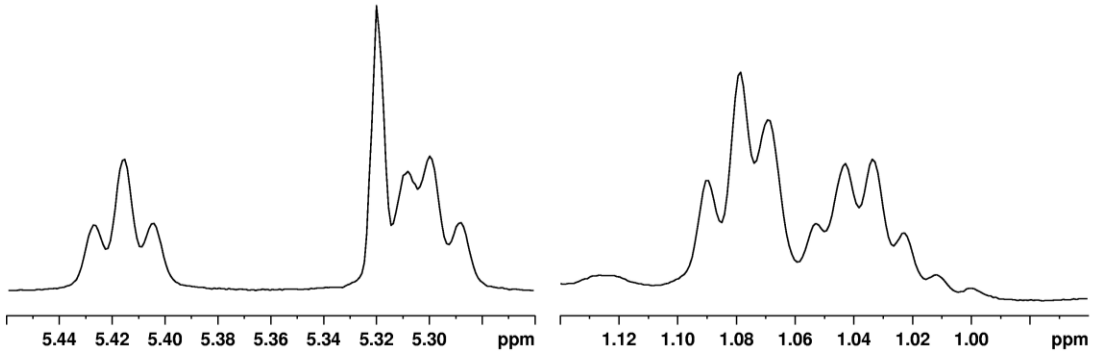

(e) ^{13}C NMR spectrum, including expansions (125 MHz)

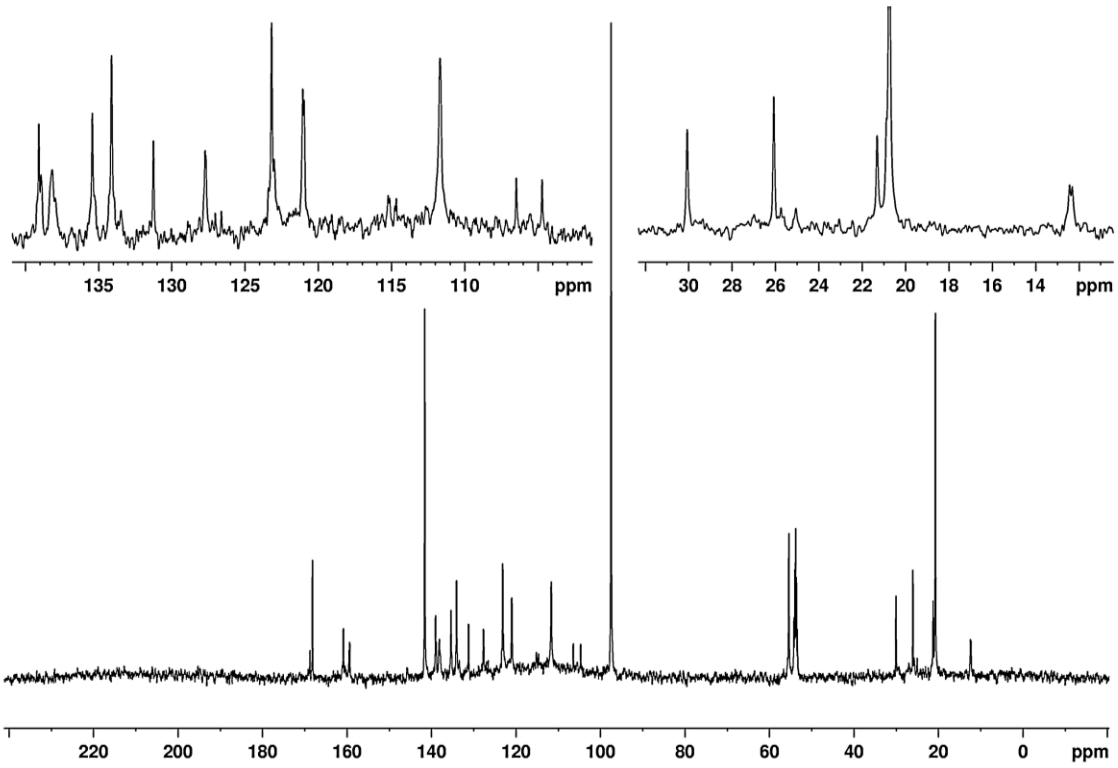

Figure 5.25, continued.

(f) ^{31}P NMR spectrum (202 MHz)

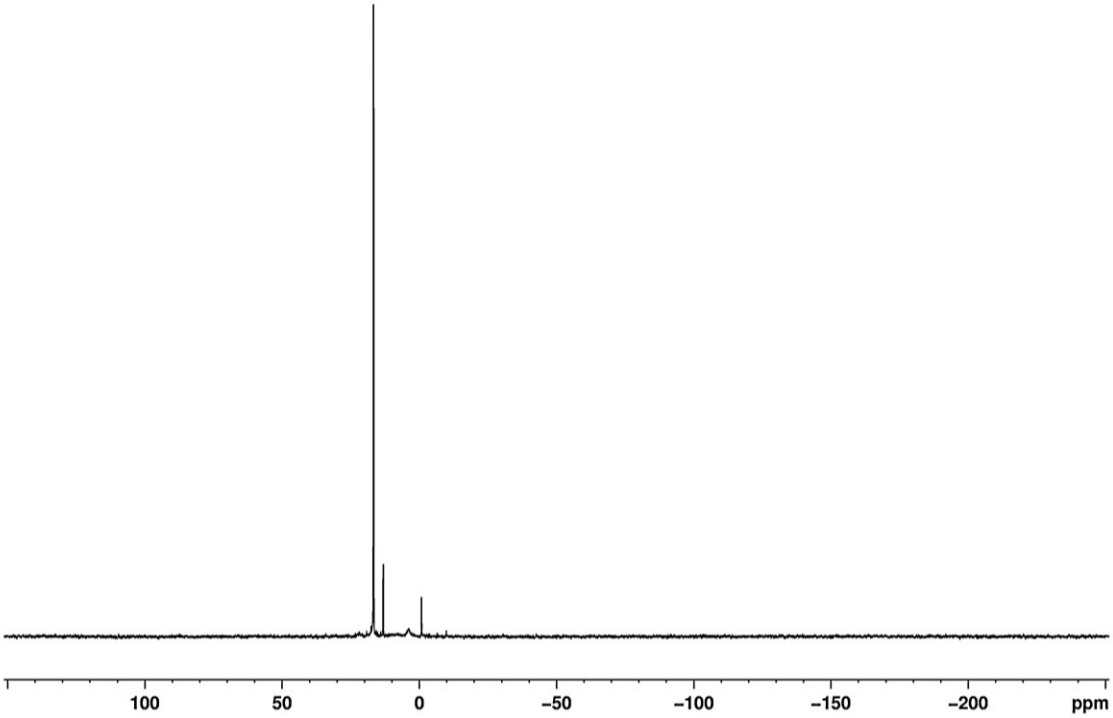

(g) ^{19}F NMR spectrum (470 MHz)

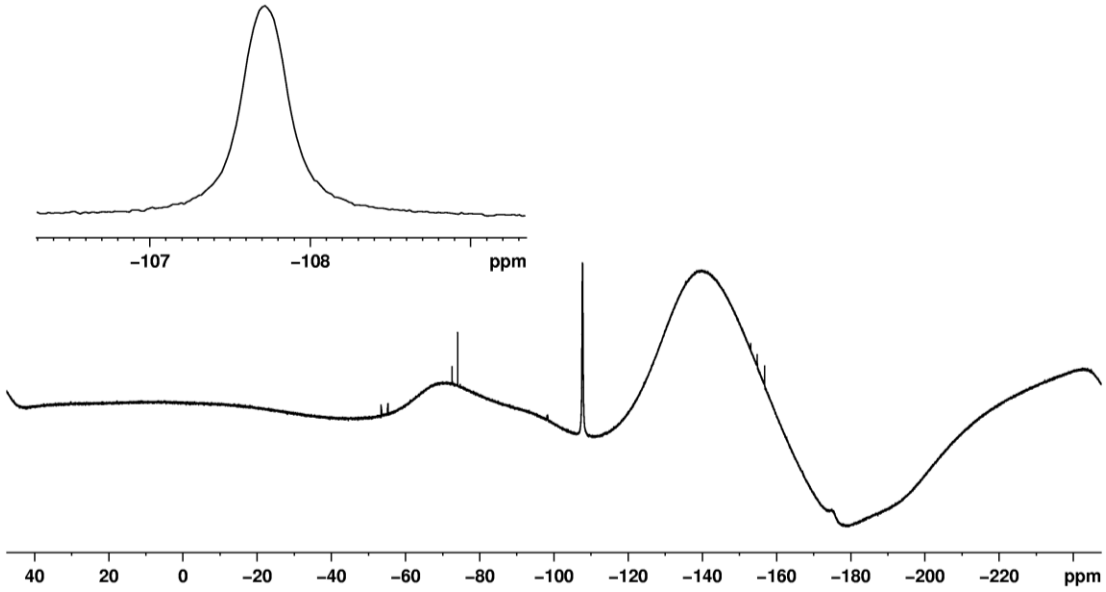

Figure 5.25, continued.

(h) COSY NMR spectrum (500 MHz)

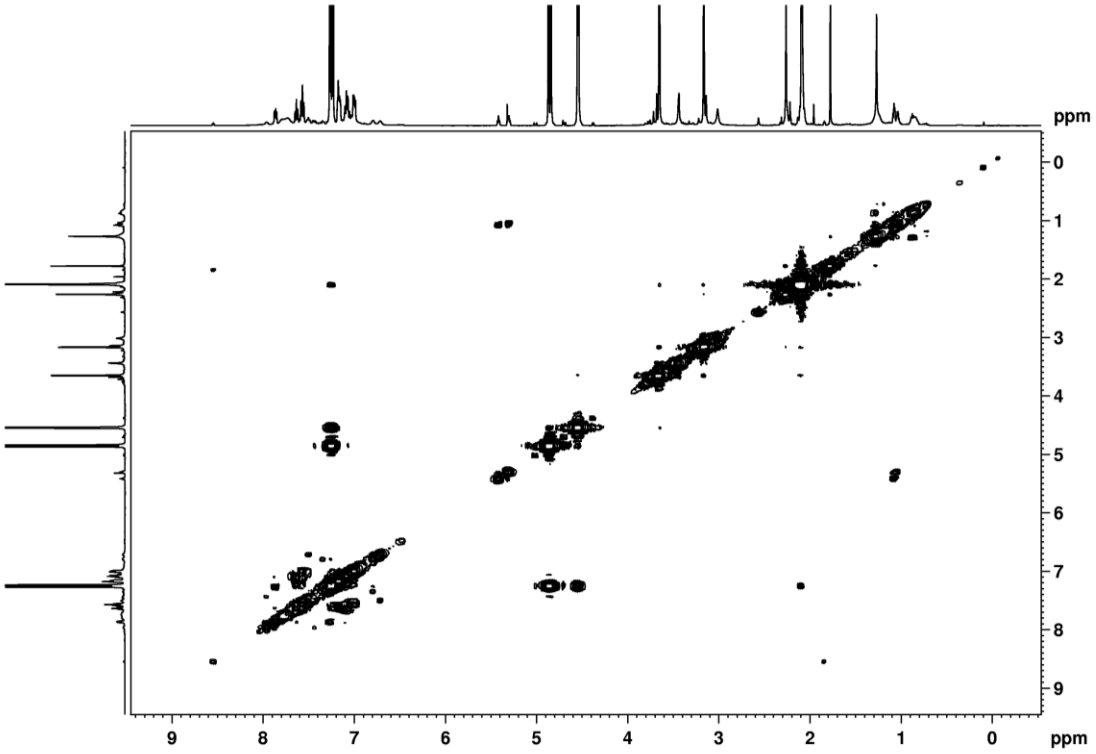

(i) COSY NMR spectrum expansion showing PdCH_2CHF(OAc) signals (500 MHz)

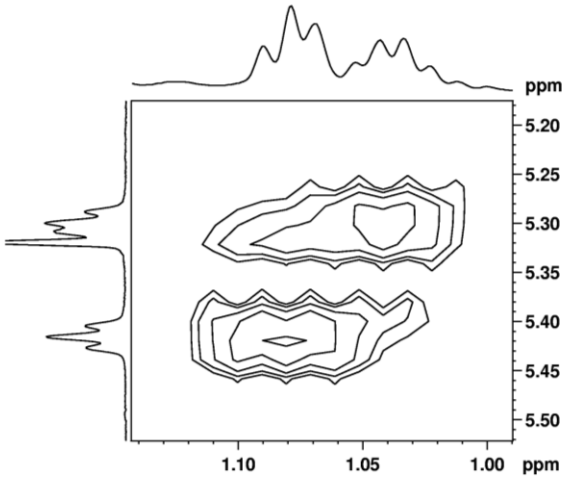

Figure 5.26. NMR spectra for Pd-enolate **6** (CD_2Cl_2)

(a) ^{1}H NMR spectrum expansion from δ 6.4–8.6 (500 MHz)

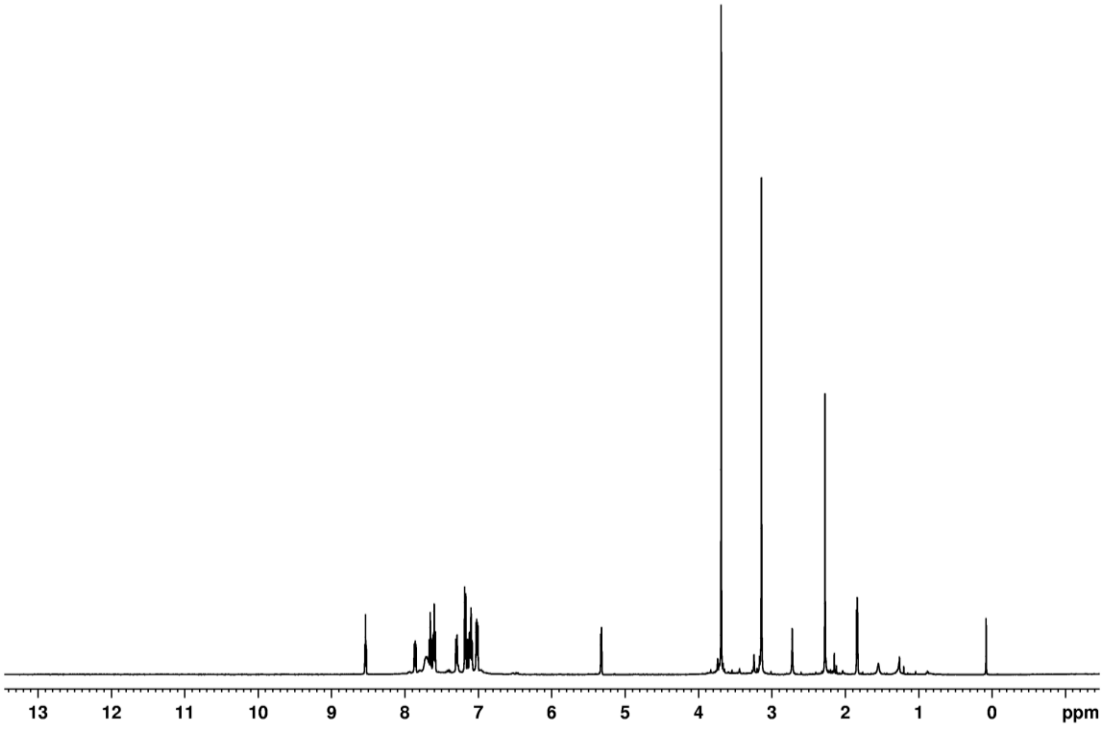

(b) ^{1}H NMR spectrum expansion from δ 6.4–8.6 (500 MHz)

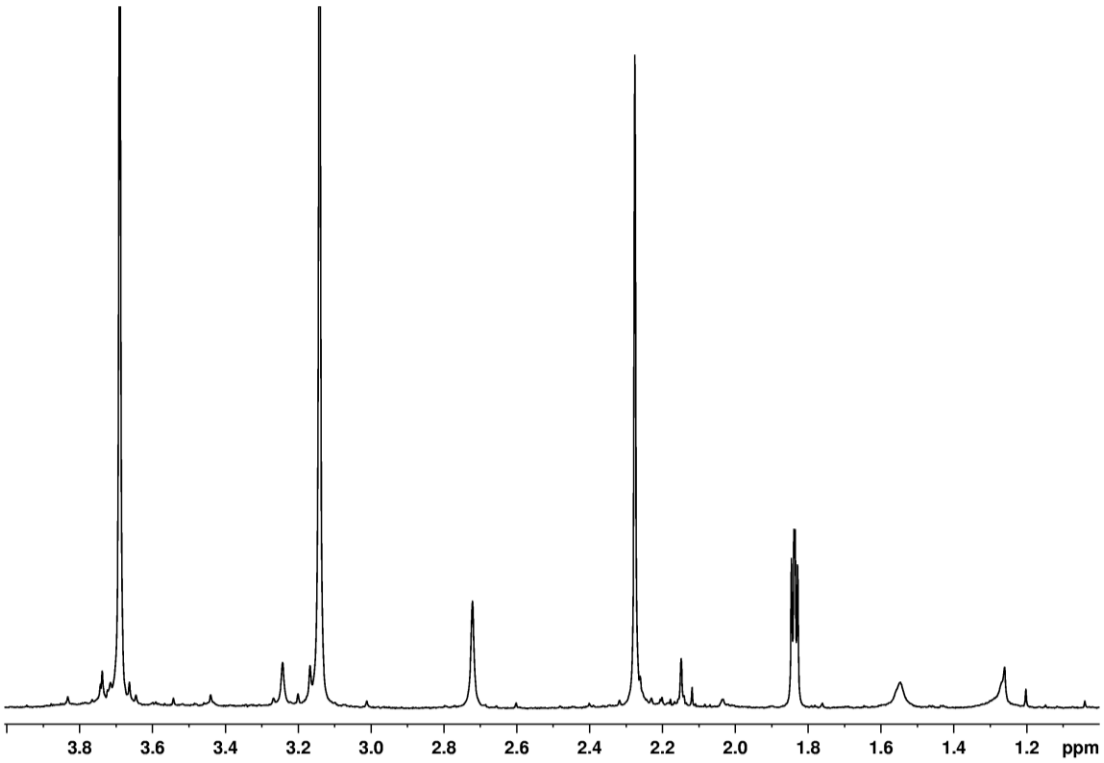

Figure 5.26, continued.

(c) ^{1}H NMR spectrum expansion from δ 6.4–8.6 (500 MHz)

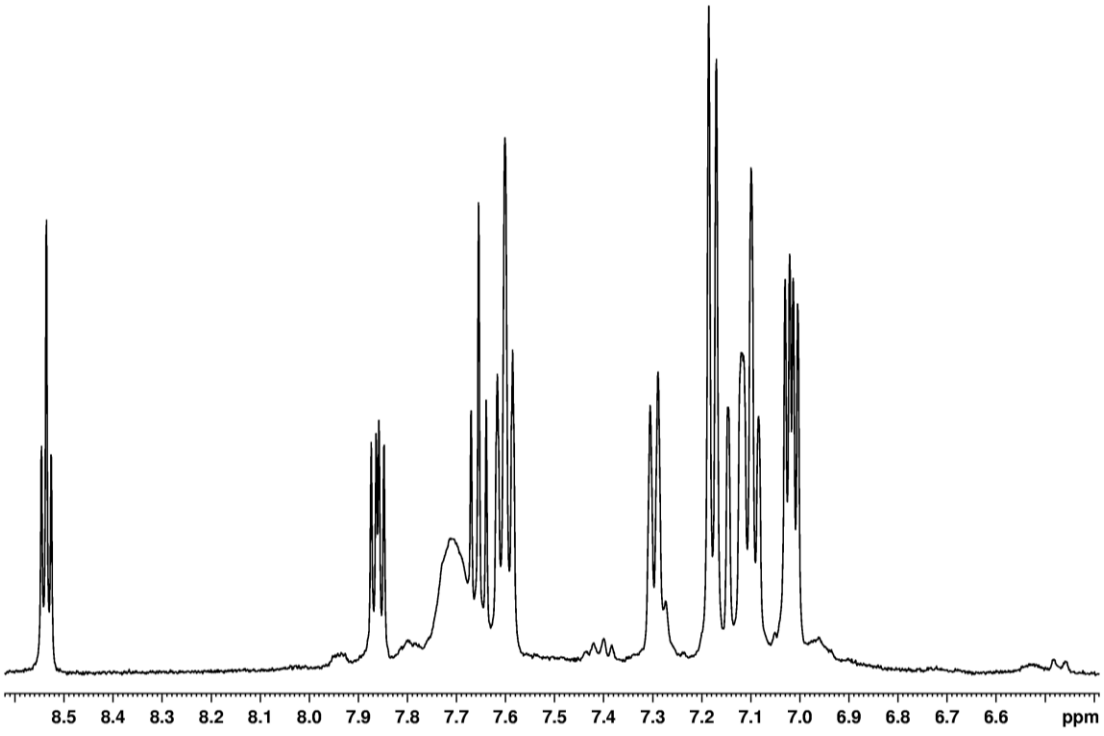

(d) ^{31}P NMR spectrum (202 MHz)

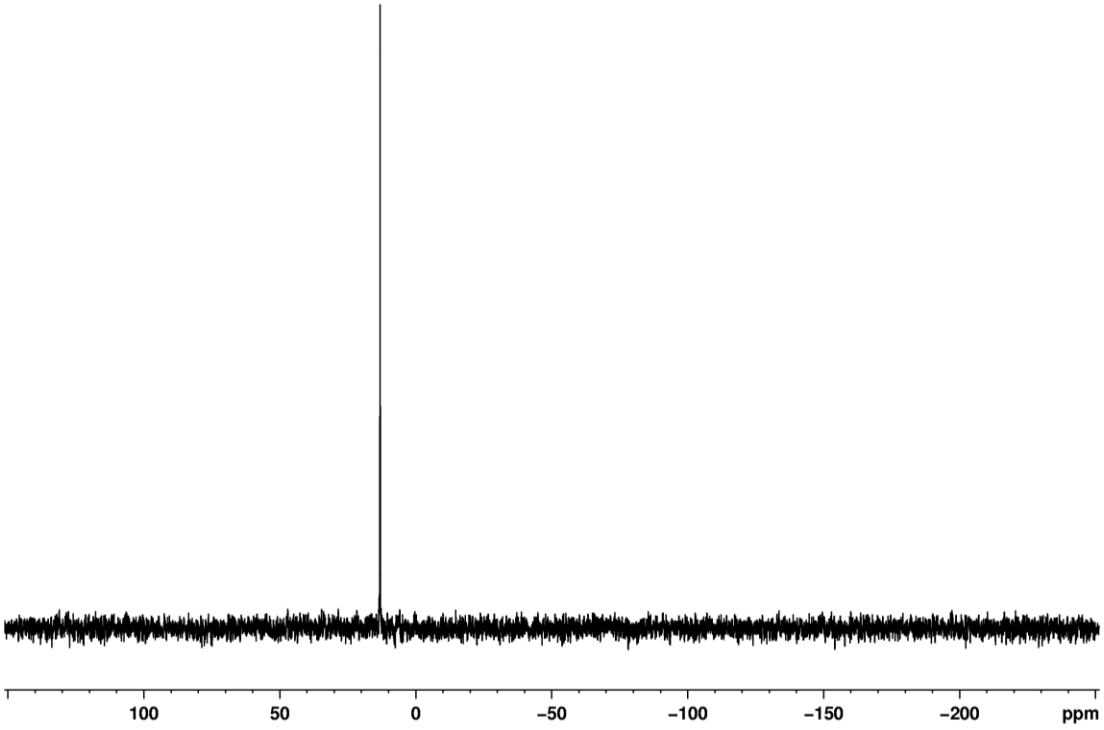

Figure 5.26, continued.

(e) ^{13}C NMR spectrum, including expansions (125 MHz)

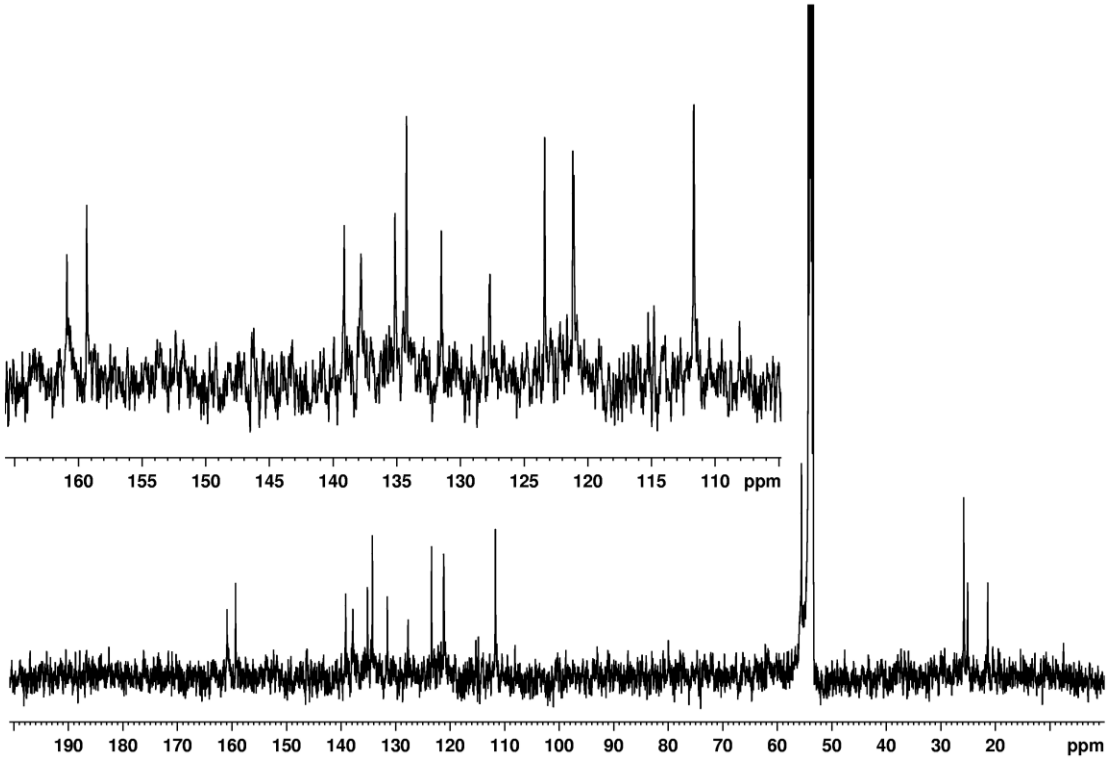

Table 5.2. Crystal data and structure refinement for **1**•CH_2Cl_2, *trans-P,F*-**3**, **6**•1.5CH_2Cl_2, and **8**•CH_2Cl_2

	(PO-OMe)PdBr(lut)•CH_2Cl_2, **1**•CH_2Cl_2	*trans-P,F*,-(PO-OMe)Pd(FHF)(lut), *trans-P,F*-**3**	(PO-OMe)Pd($CH_2C(=O)H$)(lut)•CH_2Cl_2, **6**•1.5CH_2Cl_2	(PO-OMe)Pd(C_6F_5)(lut)•CH_2Cl_2, **8**•CH_2Cl_2
Identification code	0492_black	0566_black	tw4	0594_black
Empirical formula	$C_{29}H_{31}BrCl_2NO_5PPdS$	$C_{28}H_{30}F_2NO_5PPdS$	$C_{31.5}H_{35}Cl_3NO_6PPdS$	$C_{35}H_{31}Cl_2F_5NO_5PPdS$
Formula weight	793.79	667.96	799.38	880.94
Temperature (K)	100(2)	100(2)	100(2)	100(2)
Crystal system	monoclinic	monoclinic	triclinic	triclinic
Space group	$P2_1/c$	$P2_1/n$	P-1	P-1
a (Å)	16.0520(9)	9.3091(5)	11.4841(6)	10.8683(7)
b (Å)	12.0213(7)	21.6742(10)	12.3043(7)	11.6088(8)
c (Å)	17.3935(10)	15.2790(8)	13.3303(8)	14.3442(10)
α (°)	90	90	85.405(2)	90.655(2)
β (°)	111.076(2)	93.884(2)	68.589(2)	104.881(2)
γ (°)	90	90	88.673(2)	91.856(2)
Volume ($Å^3$)	3131.8(3)	3075.7(3)	1747.95(17)	1747.8(2)
Z	4	4	2	2
Density (calculated) **(**Mg/m3)	1.684	1.442	1.519	1.674
Absorption coefficient (mm^{-1})	2.196	0.771	0.908	0.860
F(000)	1592.0	1360.0	814.0	888.0

Table 5.2, continued.

Crystal size (mm^3)	0.25 × 0.09 × 0.05	0.19 × 0.16 × 0.14	0.31 × 0.16 × 0.12	0.34 × 0.22 × 0.16
Radiation	MoKα (λ = 0.71073)	MoKα (λ = 0.71073)	MoKα (λ = 0.71073)	MoKα (λ = 0.71073)
Theta range for data collection (°)	4.344 to 54.362	4.612 to 54.276	4.854 to 52.756	4.222 to 54.276
Index ranges	$-20 \leq h \leq 20$, $-15 \leq k \leq 14$, $-18 \leq l \leq 20$	$-11 \leq h \leq 10$, $-25 \leq k \leq 26$, $-18 \leq l \leq 18$	$-13 \leq h \leq 14$, $-14 \leq k \leq 14$, $0 \leq l \leq 16$	$-13 \leq h \leq 13$, $-14 \leq k \leq 13$, $-18 \leq l \leq 18$
Reflections collected	42822	30229	6647	35778
Independent reflections	6751 [R_{int} = 0.0733, R_{sigma} = 0.0688]	6401 [R_{int} = 0.0708, R_{sigma} = 0.0827]	6647 [R_{int} = 0.0611, R_{sigma} = 0.0708]	7469 [R_{int} = 0.0898, R_{sigma} = 0.1007]
Data / restraints / parameters	6751/0/375	6401/1/360	6647/0/421	7469/7/465
Goodness-of-fit on F^2	1.013	1.079	1.058	1.053
Final R indices [I>2sigma(I)]	R_1 = 0.0386, wR_2 = 0.0724	R_1 = 0.0573, wR_2 = 0.1161	R_1 = 0.0637, wR_2 = 0.1233	R_1 = 0.0628, wR_2 = 0.1355
R indices (all data)	R_1 = 0.0764, wR_2 = 0.0822	R_1 = 0.0920, wR_2 = 0.1243	R_1 = 0.0962, wR_2 = 0.1363	R_1 = 0.1151, wR_2 = 0.1557
Largest diff. peak and hole ($e.Å^{-3}$)	0.99/-0.80	0.61/-0.68	1.21/-0.88	1.88/-2.04

5.5 References and Notes

(1) Weng, W.; Shen, Z.; Jordan, R. F. *J. Am. Chem. Soc.* **2007**, *129*, 15450.

(2) Shen, Z.; Jordan, R. F. *Macromolecules* **2010**, *43*, 8706.

(3) Wada, S.; Jordan, R. F. *Angew. Chem. Int. Ed. Engl.* **2017**, *56*, 1820.

(4) Pilon, M. C.; Grushin, V. V. *Organometallics* **1998**, *17*, 1774.

(5) Flemming, J. P.; Pilon, M. C.; Borbulevitch, O. Y.; Antipin, M. Y.; Grushin, V. V. *Inorganica Chim. Acta* **1998**, *280*, 87.

(6) Grushin, V. V.; Marshall, W. J. *J. Am. Chem. Soc.* **2009**, *131*, 918.

(7) Ball, N. D.; Kampf, J. W.; Sanford, M. S. *Dalton Trans.* **2010**, 632.

(8) Ball, N. D.; Sanford, M. S. *J. Am. Chem. Soc.* **2009**, *131*, 3796.

(9) Furuya, T.; Benitez, D.; Tkatchouk, E.; Strom, A. E.; Tang, P.; Goddard, W. A.; Ritter, T. *J. Am. Chem. Soc.* **2010**, *132*, 3793.

(10) Andrew, R. E.; Chaplin, A. B. *Dalton Trans.* **2014**, *43*, 1413.

(11) Huacuja, R.; Herbert, D. E.; Fafard, C. M.; Ozerov, O. V. *J. Fluor. Chem.* **2010**, *131*, 1257.

(12) Peng, H.; Liu, G. *Org. Lett.* **2011**, *13*, 772.

(13) Henry, P. M. *Acc. Chem. Res.* **1973**, *6*, 16.

(14) Zhu, G.; Lu, X. *Organometallics* **1995**, *14*, 4899.

(15) Kilyanek, S. M.; Stoebenau, E. J.; Vinayavekhin, N.; Jordan, R. F. *Organometallics* **2010**, *29*, 1750.

(16) Zhao, H.; Ariafard, A.; Lin, Z. *Organometallics* **2006**, *25*, 812.

(17) Ahrens, T.; Kohlmann, J.; Ahrens, M.; Braun, T. *Chem. Rev.* **2015**, *115*, 931.

(18) Liu, G. *Org. Biomol. Chem.* **2012**, *10*, 6243.

(19) Ohashi, M.; Ogoshi, S. In *Organometallic Fluorine Chemistry*; Braun, T.; Hughes, R. P., Eds.; Topics in organometallic chemistry; Springer International Publishing: Cham, 2015; Vol. 52, pp. 197–215.

(20) Orsi, D. L.; Altman, R. A. *Chem. Commun.* **2017**, *53*, 7168.

(21) Katcher, M. H.; Sha, A.; Doyle, A. G. *J. Am. Chem. Soc.* **2011**, *133*, 15902.

(22) Henne, A. L.; Midgley, T. *J. Am. Chem. Soc.* **1936**, *58*, 882.

(23) Mennie, K. M.; Banik, S. M.; Reichert, E. C.; Jacobsen, E. N. *J. Am. Chem. Soc.* **2018**, *140*, 4797.

(24) Landelle, G.; Bergeron, M.; Turcotte-Savard, M.-O.; Paquin, J.-F. *Chem. Soc. Rev.* **2011**, *40*, 2867.

(25) Grushin, V. V. *Acc. Chem. Res.* **2010**, *43*, 160.

(26) Ohashi, M.; Saijo, H.; Shibata, M.; Ogoshi, S. *Eur. J. Org. Chem.* **2013**, *2013*, 443.

(27) Christe, K. O.; Wilson, W. W. *J. Fluor. Chem.* **1990**, *47*, 117.

(28) Christe, K. O.; Wilson, W. W. *J. Fluor. Chem.* **1990**, *46*, 339.

(29) Gel'mbol'dt, V. O.; Ennan, A. A. *Russ. Chem. Rev.* **1989**, *58*, 371.

(30) Pevec, A.; Demšar, A. *J. Fluor. Chem.* **2008**, *129*, 707.

(31) Conley, B. D.; Yearwood, B. C.; Parkin, S.; Atwood, D. A. *J Fluor Chem* **2002**, *115*, 155.

(32) Nahra, F.; Brill, M.; Gómez-Herrera, A.; Cazin, C. S. J.; Nolan, S. P. *Coord. Chem. Rev.* **2016**, *307*, 65.

(33) Grushin, V. V. *Chem. Eur. J.* **2002**, *8*, 1006.

(34) Cattalini, L.; Martelli, M. *J. Am. Chem. Soc.* **1969**, *91*, 312.

(35) Conley, M. P.; Jordan, R. F. *Angew. Chem. Int. Ed.* **2011**, *50*, 3744.

(36) Zhou, X.; Lau, K.-C.; Petro, B. J.; Jordan, R. F. *Organometallics* **2014**, *33*, 7209.

(37) Fraser, S. L.; Antipin, M. Y.; Khroustalyov, V. N.; Grushin, V. V. *J. Am. Chem. Soc.* **1997**, *119*, 4769.

(38) Watson, D. A.; Su, M.; Teverovskiy, G.; Zhang, Y.; García-Fortanet, J.; Kinzel, T.; Buchwald, S. L. *Science* **2009**, *325*, 1661.

(39) Jasim, N. A.; Perutz, R. N.; Whitwood, A. C.; Braun, T.; Izundu, J.; Neumann, B.; Rothfeld, S.; Stammler, H.-G. *Organometallics* **2004**, *23*, 6140.

(40) Breyer, D.; Braun, T.; Kläring, P. *Organometallics* **2012**, *31*, 1417.

(41) Martínez-Prieto, L. M.; Melero, C.; del Río, D.; Palma, P.; Cámpora, J.; Álvarez, E. *Organometallics* **2012**, *31*, 1425.

(42) Yandulov, D. V.; Tran, N. T. *J. Am. Chem. Soc.* **2007**, *129*, 1342.

(43) Yahav, A.; Goldberg, I.; Vigalok, A. *J. Am. Chem. Soc.* **2003**, *125*, 13634.

(44) Chierotti, M. R.; Rossin, A.; Gobetto, R.; Peruzzini, M. *Inorg. Chem.* **2013**, *52*, 12616.

(45) A second X-ray quality crystal of *trans-P,F*-**3** was obtained by layering pentane onto a toluene/DCM solution of **2** in a glass vial and storage at –40 °C for several weeks, indicating that small amounts of HF are formed upon decomposition or reaction of **2** with the silicates or borates in glass. This underscores the importance of using plastic ware while synthesizing and handling **2**.

(46) Müller, B. G. *Angew. Chem. Int. Ed.* **1987**, *26*, 1081.

(47) Tressaud, A.; Soubeyroux, J. L.; Touhara, H.; Demazeau, G.; Langlais, F. *Mater. Res. Bull.* **1981**, *16*, 207.

(48) Roe, D. C.; Marshall, W. J.; Davidson, F.; Soper, P. D.; Grushin, V. V. *Organometallics* **2000**, *19*, 4575.

(49) Hudlicky, M. *J. Fluor. Chem.* **1985**, *28*, 461.

(50) Noda, S.; Nakamura, A.; Kochi, T.; Chung, L. W.; Morokuma, K.; Nozaki, K. *J. Am. Chem. Soc.* **2009**, *131*, 14088.

(51) Cai, Z.; Shen, Z.; Zhou, X.; Jordan, R. F. *ACS Catal.* **2012**, *2*, 1187.

(52) Black, R. E.; Jordan, R. F. *Organometallics* **2017**, *36*, 3415.

(53) Johnson, A. M.; Contrella, N. D.; Sampson, J. R.; Zheng, M.; Jordan, R. F. *Organometallics* **2017**, *36*, 4990.

(54) Alcarazo, M.; Gomez, C.; Holle, S.; Goddard, R. *Angew. Chem. Int. Ed.* **2010**, *49*, 5788.

(55) Geier, S. J.; Stephan, D. W. *J. Am. Chem. Soc.* **2009**, *131*, 3476.

(56) Yang, X.; Stern, C. L.; Marks, T. J. *J. Am. Chem. Soc.* **1994**, *116*, 10015.

(57) Pindado, G. J.; Lancaster, S. J.; Thornton-Pett, M.; Bochmann, M. *J. Am. Chem. Soc.* **1998**, *120*, 6816.

(58) Woodman, T. J.; Bochmann, M.; Thornton-Pett, M. *Chem. Commun.* **2001**, 329.

(59) Krempner, C.; Köckerling, M.; Reinke, H.; Weichert, K. *Inorg. Chem.* **2006**, *45*, 3203.

(60) Scollard, J. D.; McConville, D. H.; Rettig, S. J. *Organometallics* **1997**, *16*, 1810.

(61) Klosin, J.; Roof, G. R.; Chen, E. Y.-X.; Abboud, K. A. *Organometallics* **2000**, *19*, 4684.

(62) Hair, G. S.; Cowley, A. H.; Gorden, J. D.; Jones, J. N.; Jones, R. A.; Macdonald, C. L. B. *Chem. Commun.* **2003**, 424.

(63) Sarazin, Y.; Wright, J. A.; Harding, D. A. J.; Martin, E.; Woodman, T. J.; Hughes, D. L.; Bochmann, M. *J. Organomet. Chem.* **2008**, *693*, 1494.

(64) Krempner, C.; Reinke, H.; Weichert, K. *Eur. J. Inorg. Chem.* **2007**, *2007*, 1067.

(65) Rekhroukh, F.; Brousses, R.; Amgoune, A.; Bourissou, D. *Angew. Chem. Int. Ed.* **2015**, *54*, 1266.

(66) Roşca, D.-A.; Smith, D. A.; Bochmann, M. *Chem. Commun.* **2012**, *48*, 7247.

(67) Liang, L.-C.; Chien, P.-S.; Huang, Y.-L. *J. Am. Chem. Soc.* **2006**, *128*, 15562.

(68) Kalamarides, H. A.; Iyer, S.; Lipian, J.; Rhodes, L. F.; Day, C. *Organometallics* **2000**, *19*, 3983.

(69) Yamamoto, T.; Shikada, C.; Kaita, S.; Olivier, T.; Maruyama, Y.; Wakatsuki, Y. *J. Mol. Catal. A: Chem.* **2009**, *300*, 1.

(70) Bart, S. C.; Hawrelak, E. J.; Schmisseur, A. K.; Lobkovsky, E.; Chirik, P. J. *Organometallics* **2004**, *23*, 237.

(71) Volbeda, J.; Meetsma, A.; Bouwkamp, M. W. *Organometallics* **2009**, *28*, 209.

(72) Mitton, S. J.; McDonald, R.; Turculet, L. *Organometallics* **2009**, *28*, 5122.

(73) Driver, T. G.; Day, M. W.; Labinger, J. A.; Bercaw, J. E. *Organometallics* **2005**, *24*, 3644.

(74) Kuprat, M.; Lehmann, M.; Schulz, A.; Villinger, A. *Organometallics* **2010**, *29*, 1421.

(75) Ibad, M. F.; Schulz, A.; Villinger, A. *Organometallics* **2015**, *34*, 3893.

(76) Maity, A.; Kölsch, J. C.; Na, H.; Teets, T. S. *Dalton Trans.* **2017**, *46*, 11757.

(77) Barlow, G. K.; Boyle, J. D.; Cooley, N. A.; Ghaffar, T.; Wass, D. F. *Organometallics* **2000**, *19*, 1470.

(78) Fafard, C. M.; Ozerov, O. V. *Inorganica Chim. Acta* **2007**, *360*, 286.

(79) Hetterscheid, D. G. H.; Bens, M.; de Bruin, B. *Dalton Trans.* **2005**, 979.

(80) Gómez, M.; Rendón, N.; Álvarez, E.; Mereiter, K.; Poveda, M. L.; Paneque, M. *Chem. Eur. J.* **2017**, *23*, 16346.

(81) Murahashi, S.; Nozakura, S.; Fuji, S. *Bull. Chem. Soc. Jpn.* **1965**, *38*, 1840.

(82) Holmsen, M. S. M.; Nova, A.; Balcells, D.; Langseth, E.; Øien-Ødegaard, S.; Heyn, R. H.; Tilset, M.; Laurenczy, G. *ACS Catal.* **2017**, *7*, 5023.

(83) Krom, M.; Peters, T.; Coumans, R.; Sciarone, T.; Hoogboom, J.; ter Beek, S.; Schlebos, P.; Smits, J.; de Gelder, R.; Gal, A. *Eur. J. Inorg. Chem.* **2003**, *2003*, 1072.

(84) Poveda and Paneque synthesized and reported thecrystal structure of an Ir(II) complex bearing two C-bonded enolate ligands, a CO ligand, and a tridentate hydrotris(3,5-dimethylpyrazolyl)borate ligand by ozonolysis of a parent iridacyclepentane.

(85) Allen, F. H.; Kennard, O.; Watson, D. G.; Brammer, L.; Orpen, A. G.; Taylor, R. *Perkin Trans. 2* **1987**, S1.

(86) Shirini, F.; Mamaghani, M.; Seddighi, M. *Catal. Commun.* **2013**, *36*, 31.

(87) Deka, N.; Kalita, D. J.; Borah, R.; Sarma, J. C. *J. Org. Chem.* **1997**, *62*, 1563.

(88) Dolbier, W. R. *Guide to fluorine NMR for organic chemists*; John Wiley & Sons, Inc.: Hoboken, NJ, USA, 2009.

Chapter Six

Solution Structures of Pd(II)-Alkyl Ethylene Polymerization Catalysts that Contain a (2',6'-Dimethoxy-biphenyl)(*o*-methoxyphenyl)phosphine-arenesulfonate Ligand

6.1 Introduction

Palladium alkyl complexes that bear phosphine-sulfonate (PO^-) ligands polymerize ethylene (E) to linear polyethylene (PE) and copolymerize E with a wide range of polar vinyl comonomers (H_2C=CHX) to functionalized, linear PEs with functional groups incorporated at both in-chain and chain-end positions (see Chapter One).[1–5] However, the benchmark complex, (PO)PdMe(py) (**a-py,** Chart 6.1), exhibits low activity and produces PE with low to moderate molecular weight (MW, M_n = 10,000–20,000 Da) compared with early transition metal catalysts,[6,7] and the catalyst activity and MW of the polymer is further reduced by addition of polar monomers in copolymerizations.

Many (PO)PdRL complexes with a wide range of structurally diverse -PR_2 units have been synthesized and their behavior in E polymerization and E/H_2C=CHX copolymerization has been extensively studied.[8–13] These investigations provide insight to how the steric and electronic properties of the -PR_2 unit influence catalyst performance. It has been found that catalysts that contain more strongly electron-donating and sterically-crowded phosphines produce PE with higher MW and exhibit higher activity in some cases. For example, Claverie[8] and Nozaki[12] found that blocking a Pd axial site by a 2-(2',6'-dimethoxyphenyl)phenyl (**b**) or menthyl (**d**) group led to a dramatic increase in PE MW (Chart 6.1). However, increasing the steric bulk of the PO^- ligand

can lower comonomer incorporation in copolymerizations, since H_2C=CHX olefins are larger than ethylene.

Chart 6.1. Examples of (PO)Pd alkyl catalysts

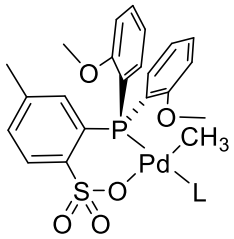

a-lut, L = lutidine
a-py, L = pyridine

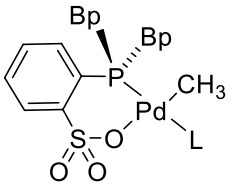

b-CD_3OD, L = CD_3OD
b-lut, L = lutidine
b-py, L = pyridine

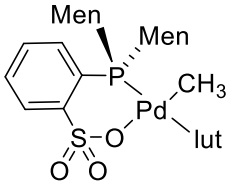

c-lut

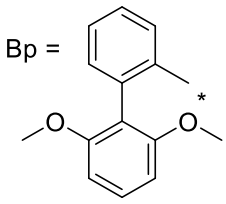

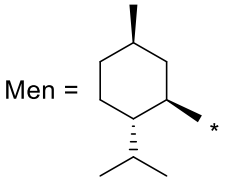

Dr. Jacqueline Defoe, a previous Jordan group member, developed a catalyst that was able to overcome this drawback. Defoe synthesized the zwitterionic proligand 2-{PH(2-{2,6-$(OMe)_2$-Ph}-Ph)(2-OMe-Ph))}-4-Me-benzefnesulfonate (H[PO-Bp/Ph^{OMe}], H[**1**]) and the corresponding (PO-Bp/Ph^{OMe})PdMeL catalysts **2-py** and **2-lut** (Chart 6.2).[14] Under identical E polymerization conditions (0.88 μmol catalyst, 80 °C, 250 psi E, 50 mL toluene, 2 h), **2-lut** is more active (2.0 kg mol^{-1} h^{-1}) and produces PE with higher MW (M_n = 86,700) compared with **a-lut** (0.66 kg mol^{-1} h^{-1}, M_n = 13,200). Following Johnson and Jordan's method for determining the rates of chain growth (R_{growth}, R'_{growth}) and chain transfer ($R_{transfer}$, $R'_{transfer}$) for a pair of ethylene polymerization catalysts (cat, cat′),[15] these data show that chain growth is three-times faster and chain transfer is

two-times slower for **2-lut** compared to **a-lut**. Most importantly, under identical E/^{n}Bu-vinyl ether (^{n}BuVE) copolymerization conditions (0.44 μmol catalyst, 80 °C, 80 psi E, 19 mmol ^{n}BuVE, 50 mL toluene, 21 h), **2-lut** is more active (0.04 vs 0.01 kg mol^{-1} h^{-1}) and produces copolymer with higher MW (Mn = 21,100 vs. 4,600) *and* a higher level of ^{n}BuVE incorporation (1.7 vs. 0.64 mol%) compared to **a-lut**.

Chart 6.2. H(PO-Bp/Ph^{OMe}) and (PO)PdR(L) complexes

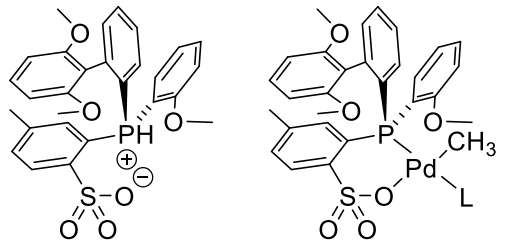

H[**1**] **2-lut**: L = lutidine **2-py**: L = pyridine

Defoe attributed the increased rate of chain propagation and decreased rate of chain transfer of **2-lut** relative to **a-lut** to steric crowding in **2-lut**, since increased steric crowding at the catalyst center typically hinders associative chain transfer. Space-filling models of the solid-state structures of **a-lut**[16] and **2-lut**[14] can be used to assess differences in steric crowding by these (PO)$^{-}$ ligands (Figure 6.1(a)). However, steric maps of the structures of **a-lut** and **2-lut** using SambVca 2[17] show that the degree of steric blockage of the Pd axial sites in **a-lut** and **2-lut** is nearly identical (Figure 6.1(b,c)). Therefore, it is not obvious that associative chain transfer should be inhibited for **2-lut**. A striking feature of the solid-state structure of **2-lut** is a classic π stacking interaction between the electron-poor Ar^{SO3} ring and the electron-rich *endo* 2,6-dimethoxyphenyl (Ar^{2}Bp) ring (Figure 6.2).

These rings are offset slightly to enable an attractive interaction of the quadrupoles of the rings. As a result, the *meta*-H on $Ar^{2}Bp$ and the *ortho*-H on Ar^{SO3} sit in the shielding cone of the other ring. An alternative explanation for the enhanced polymerization performance by **2-lut** is that this π stacking interaction rigidifies the (PO)Pd complex during polymerization, inhibiting changes in coordination number and ligand conformations required for associative chain transfer. However, the NMR assignments of **H[1]** and **2-lut** are incorrect in Defoe's thesis, which precludes the determination of whether a similar π stacking interaction is present in solution for **2-lut** or active (PO)PdR(ethylene) species derived thereof.

Figure 6.1. Molecular structures of **a-lut**[16] and **2-lut**[14]: (a) Space-fill style with the lut ring shown in wireframe style, (b) top-down SambVca 2 steric profile map of the Pd square plane, (c) bottom-up SambVca 2 steric profile map of the Pd square plane.

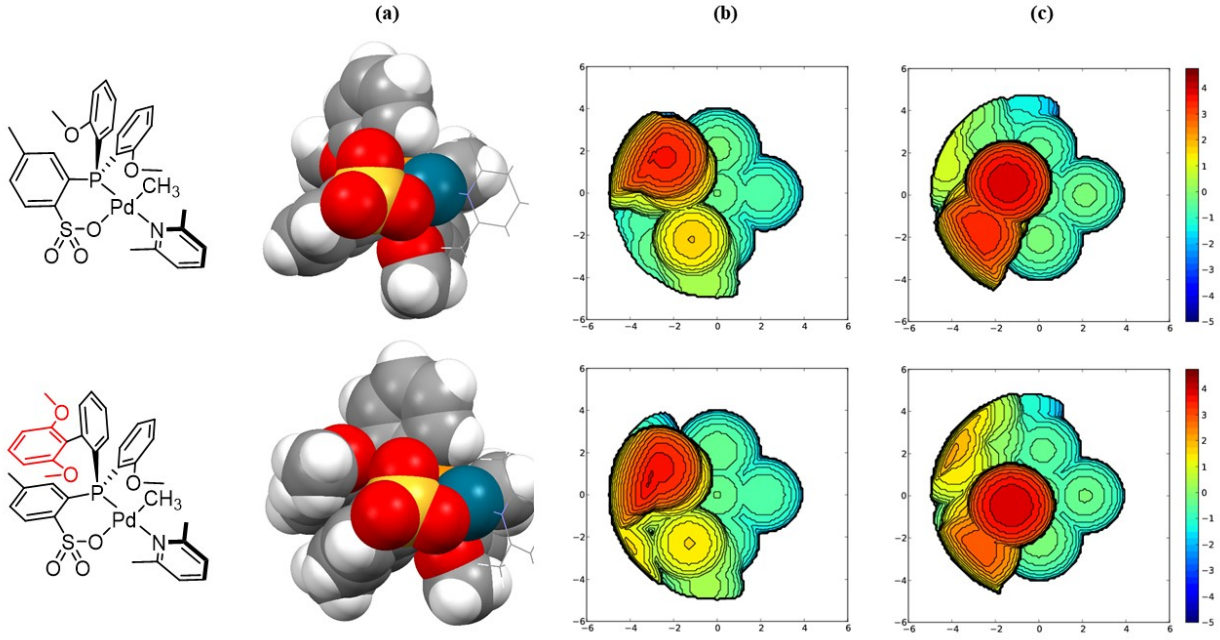

Figure 6.2. The solid-state structure of **2-lut** highlighting the π stacking interaction of the Ar^2Bp and Ar^{SO3} rings: (a) the full structure of **2-lut** shown without hydrogens and (b) the Ar^2Bp and Ar^{SO3} rings are shown in ellipsoid style and the rest of the structure is shown in wire-frame style. The two hydrogens shown sit in the shielding cone of the other ring.

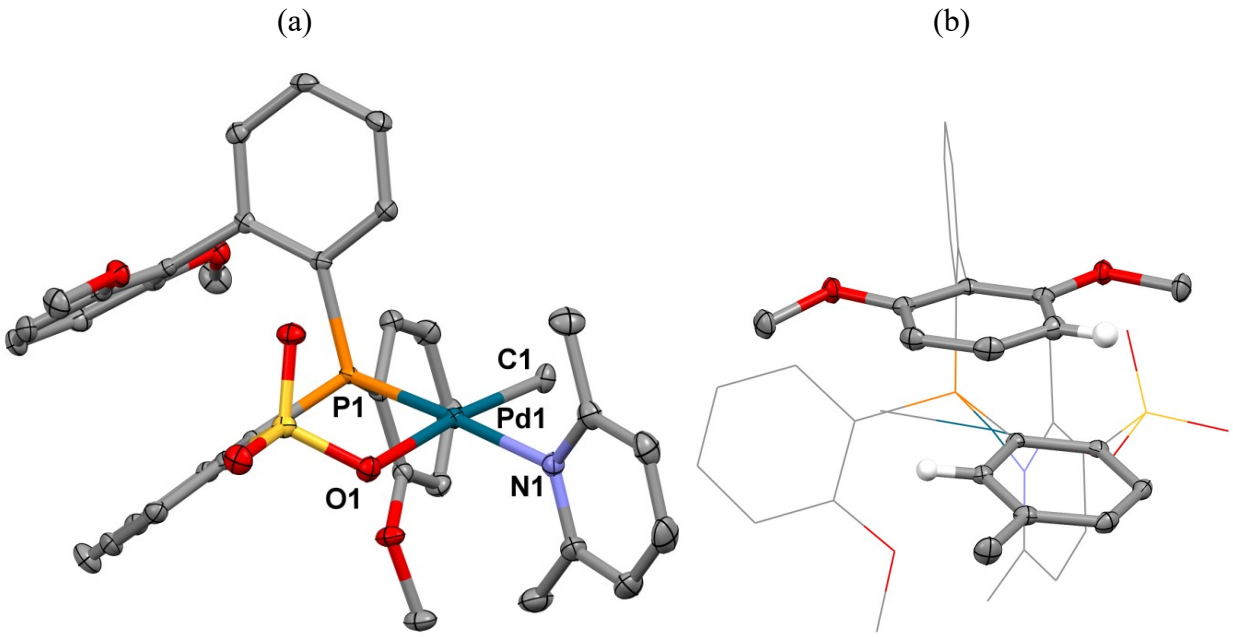

Interestingly, through low temperature ^{1}H NMR studies, Defoe found that **2-py** exists as two isomers in solution in a ca. 1:1 ratio. The barrier for interconversion of the isomers, determined from the coalescence of the Pd–Me ^{1}H NMR resonances, is $\Delta G^{\neq}$ = 13.2 kcal/mol at –20 °C.[14] Defoe did not characterize the structures of the two isomers. However, understanding the solution behavior of **2-py** may provide insight into the origin of the enhanced polymerization performance of **2-lut** and related species relative to **a-lut**.

The objective of this Chapter was to synthesize H[**1**], **2-py**, and **2-lut** and to determine the solution structures of these compounds. The key questions of interest were: (i) is the solution-structure of **2-lut** similar to the solid-state structure and, in particular, is a π stacking interaction

present?, (ii) what is the structure of **2-py** and why are two isomers observed in solution?, and (iii) what implications does this have for polymerization? The systematic process by which the NMR spectra for H[**1**] and **2-lut** were assigned and these assignments exploited in NOESY studies to probe the solution structures is described. The solid-state structure of one isomer of **2-py** was determined by X-ray diffraction and compared to that of **2-lut**. The solution-behavior of **2-py**, reported by Defoe,[14] is re-analyzed based on these structural studies.

6.2 Results and Discussion

Synthesis of (PO)PdMe(L) complexes. Proligand 2-{PH(2-{2,6-(OMe)$_2$-Ph}-Ph)(2-OMe-Ph))}-4-Me-benzenesulfonate (H[**PO-Bp/Ph^{OMe}**], H[**1**]) was synthesized according to Scheme 6.1. Defoe developed the synthetic route,[14] and it has been further optimized and scaled-up by Hannah Yi, a summer-rotation graduate student in the Jordan lab, and Kelsey Brown, an undergraduate in the Jordan lab, both of whom I supervised. In one pot, the aryllithium reagents (1 equiv each) were sequentially added to a cooled solution of triphenylphosphite. ^{31}P NMR was used to assay the reaction mixture throughout the reaction to ensure that the major species in solution was P(OPh)$_2$Bp, P(OPh)BpAr^{SO3}, or PBpAr^{SO3}Ph^{OMe} after each aryllithium reagent was added. Acidification of the reaction mixture with excess HCl (solution in Et$_2$O) quenched the LiOPh generated by the arylation steps and converted the phosphine arylsulfonate salt to zwitterion H[**1**] (yield: 61.4% from P(OPh)$_3$, 7.27 g). Care was taken to remove all of the phenol byproduct from H[**1**] to avoid formation of (TMEDA)PdMe(OPh) during metalation (see Defoe[14] for alternative syntheses). The reaction of H[**1**] with (TMEDA)PdMe$_2$, followed by addition of 5 equiv of L (pyridine or lutidine) afforded (PO-Bp/Ph^{OMe})PdMe(L) in 73% (**2-py**) and 84% yield (**2-lut**).

Scheme 6.1. Synthesis of H[**1**], **2-py**, and **2-lut**

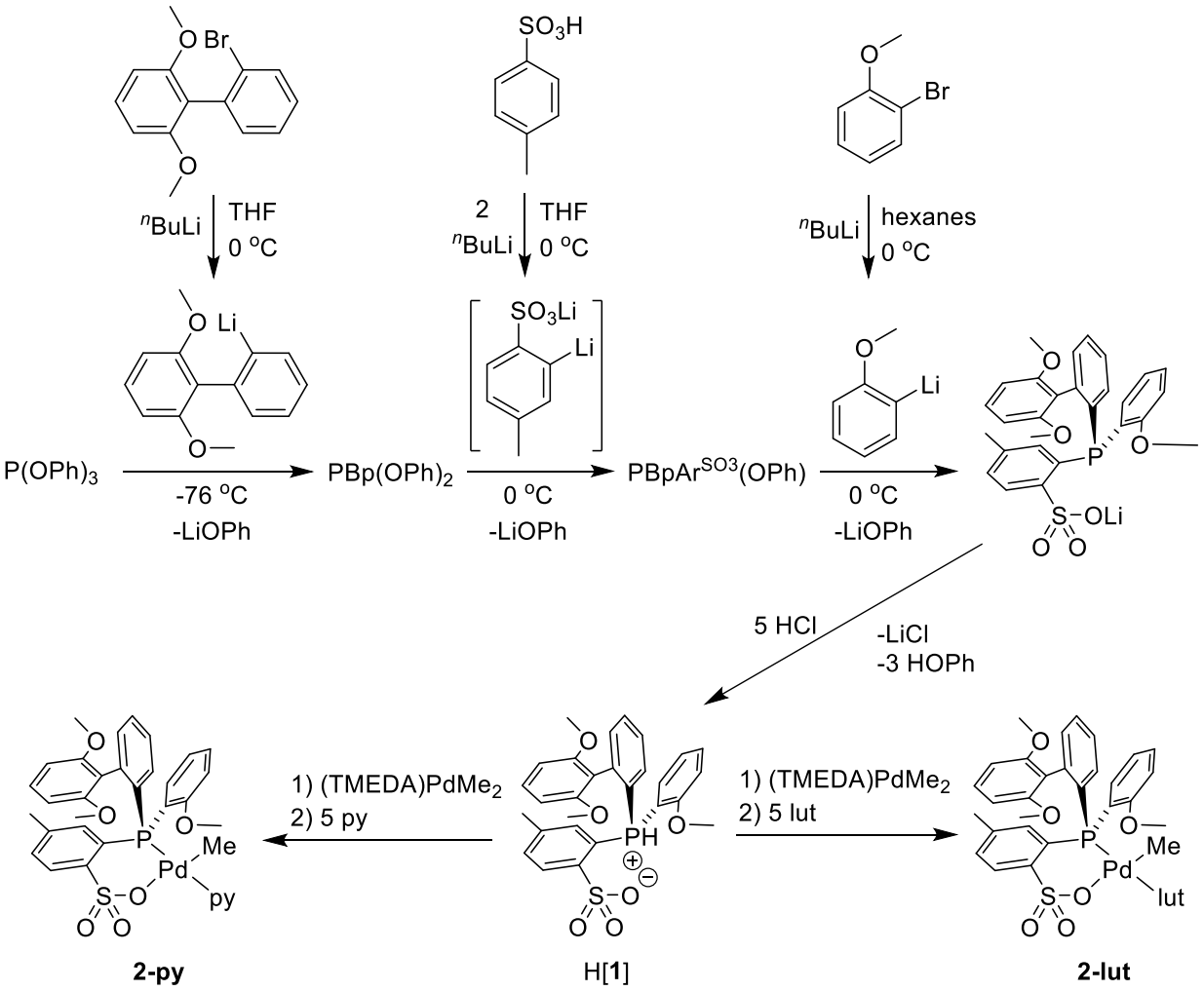

Assignment of the NMR spectra of H[1]. The NMR spectra of H[1] were assigned by exhaustive 2D NMR experiments, including ^{1}H-^{1}H COSY, ^{1}H-^{1}H NOESY, ^{1}H-^{13}C HMQC, and ^{1}H-^{13}C HMBC, in order to assist in the NMR assignments of **2-lut** and **2-py**. The atom numbering scheme for H[**1**] is shown in Figure 6.3. The P-bound ring of the biphenyl unit ($Ar^{1}Bp$) contains four hydrogens that generate three COSY correlations (H^{3}–H^{4}, H^{4}–H^{5}, and H^{5}–H^{6}), the Ar^{OMe2} ring of the biphenyl unit ($Ar^{2}Bp$) contains three inequivalent protons that generate two COSY

correlations (H^3–H^4 and H^4–H^5), and the p-tolyl ring (Ar^{SO3}) contains three protons that generate only one COSY correlation (H^3–H^4). Three of the ^1H signals for the anisolyl (Ph^{OMe}) ring hydrogens overlap (H^3, H^4, and H^5), so the expected COSY signals between H^2–H^3, H^3–H^4, and H^4–H^5 for this ring appear as a single, intense cross peak. HMQC and HMBC experiments were further used to assign the ^1H and ^{13}C NMR resonances. The final assignments agree well with those reported for similar compounds (Table 6.1). The ^{13}C assignments of the Ar^{SO3} ring are nearly identical to those of the Ar^{SO3} ring in the benchmark complex, (PO-OMe)PdMe(lut).[18] The ^{13}C assignments of the anisolyl ring are very similar to those of phenol. The ^{13}C NMR assignments of the Ar^1Bp and Ar^2Bp rings are nearly identical to those for the biphenyl substituent in H[P(Bp)(Ph^{OMe2})(benzenesulfonate)] and H[$P(Bp)_2$(benzenesulfonate)], reported by Mecking.[19]

Figure 6.3. Atom numbering for H[**1**].

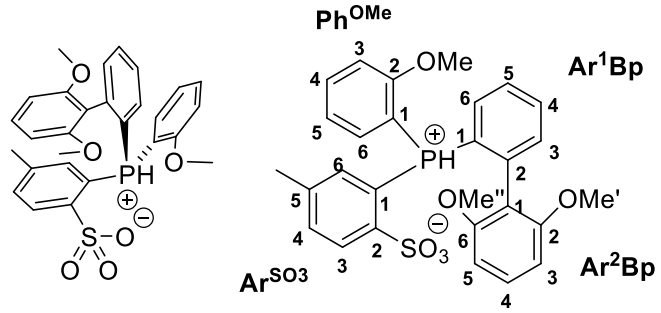

Table 6.1. ^{13}C NMR assignments of H[**1**] and similar compounds.

	H[**1**] (δ)	H[P(Ph^{OMe})$_2$ (benzenesulfonate)][18] (δ)	H[P(Bp)(Ph^{OMe2}) (benzenesulfonate)][19] (δ)	H[P(Bp)$_2$ (benzenesulfonate)][19] (δ)	Phenol (δ)
C^1-Ar^{SO3}	113 (97 Hz)	113.1, (99 Hz	121.1 (98.4 Hz)	115.2 (95.4 Hz)	
C^2-Ar^{SO3}	150.4 (9 Hz)	151.0, (10 Hz	152.8 (9.8 Hz)	152.9 (9.2 Hz)	
C^3-Ar^{SO3}	129.2 (10 Hz)	129.4, (10 Hz	129 (9.5 Hz)	128.6 (9.3 Hz)	
C^4-Ar^{SO3}	135.4 (3 Hz)	135.8, (2 Hz	133.8	133.9 (3 Hz)	
C^5-Ar^{SO3}	140.4 (12 Hz)	140.5, (14 Hz	128.9 (13 Hz)	129.0 (12.7 Hz)	
C^6-Ar^{SO3}	135.2 (11 Hz)	134.4, (12 Hz	135.1 (11 Hz)	134.6–134.3	
C^1-Ph^{OMe}	109.2 (98 Hz)				
C^2-Ph^{OMe}	161.2				155.02
C^3-Ph^{OMe}	112.3 (6 Hz)				115.5 (ortho)
C^4-Ph^{OMe}	136.5 (2 Hz)				130 (meta)
C^5-Ph^{OMe}	122 (13 Hz)				121 (para)
C^6-Ph^{OMe}	134.9 (8 Hz)				
C^1-Ar^1Bp	120.7		121.1 (97 Hz)	120.1 (91.1 Hz)	
C^2-Ar^1Bp	141.3		138.9 (10.6 Hz)	141.2 (8.4 Hz)	
C^3-Ar^1Bp	134.2 (10 Hz)		133.0 (11.1 Hz)	134.6–134.3	
C^4-Ar^1Bp	134 (3 Hz)		132.8 (2.8 Hz)	133.7	
C^5-Ar^1Bp	128.2 (13 Hz)		127.6 (13.4 Hz)	128.1–127.2	
C^6-Ar^1Bp	134.5 (10 Hz)		134.4 (10.6 Hz)	135.6	
C^1-Ar^2Bp	114.5		114.7 (5.2 Hz)	115.3–113.5	
C^2-Ar^2Bp	157.6 or 157.5		157.1, 156.9	158.2–156.8	
C^3-Ar^2Bp	104.3 or 104.7		103.7	105.7–103.0	
C^4-Ar^2Bp	131.8		130.8	131.4	
C^5-Ar^2Bp	104.3 or 104.7		114.7 (5.2 Hz)	115.3–113.5	
C^6-Ar^2Bp	157.6 or 157.5		157.1, 156.9	158.2–156.8	

Complete assignment of NMR spectra of 2-lut. The solution-structure of **2-lut** was determined by a thorough NMR analysis, including ^{1}H, ^{13}C-^{1}H, $^{13}C\{^{1}H\}$, $^{13}C\{^{1}H,^{31}P\}$, ^{1}H-^{1}H COSY, ^{1}H-^{13}C HMQC, ^{1}H-^{13}C HMBC, and ^{1}H-^{1}H NOESY NMR, performed at various temperatures (–80 °C, 25 °C, 35 °C, 80 °C). The atom labeling scheme for **2-lut** is shown in Figure 6.4. All ^{1}H and ^{13}C assignments for **2-lut**, and some assignments of similar compounds for comparison, are shown in Table 6.2. There are five groups of aryl ^{1}H NMR resonances, which were grouped according to Ar-H resonances by COSY, and were further assigned within each ring by ^{1}H-^{13}C HMQC and HMBC experiments.

Figure 6.4. Labeling scheme for **2-lut**.

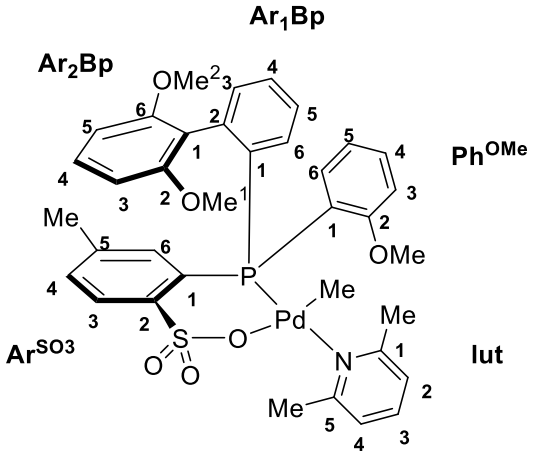

Table 6.2. ^{1}H and ^{13}C NMR assignments for **2-lut**.

	^{13}C chemical shift (δ)	^{1}H chemical shift (δ)	P(Bp)$_2$(Ar^{SO3})[19] (^{13}C or ^{1}H NMR, δ)	(PO-OMe)PdMePy[8] (^{13}C or ^{1}H NMR, δ)
CH$_3$^{1}-lut	26.8 (J_{CH} = 127 Hz)	3.24 (s)		
C^{1}-lut	159.5 (s)			
H^{2}/C^{2}-lut	122.8 (J_{PC} = 2 Hz, J_{CH} = 164 Hz)	7.19 (d, 7.6 Hz)		
H^{3}/C^{3}-lut	138.6 (J_{CH} = 162 Hz)	7.61 (t, 3.8 Hz)		
H^{4}/C^{4}-lut	122.7 (J_{PC} = 2 Hz, J_{CH} = 165 Hz)	7.11 (d, 7.2 Hz)		
C^{5}-lut	159.0 (s)			
CH$_3$^{5}-lut	26.1, J_{CH} = 127 Hz	2.93 (s)		
C^{1}-Ar^{2}Bp	117.9 (d, J_{PC} = 14 Hz)		^{13}C: 115.3-113.5	
C^{2}-Ar^{2}Bp	158.3 (s)		^{13}C: 158.2-156.8	
O*CH*$_3$^{1}-Ar^{2}Bp	55.1, (d, J_{CH} = 143 Hz)	3.45 (s)	^{13}C: 57.25-54.55	
H^{3}/C^{3}-Ar^{2}Bp	103.1, (d, J_{CH} = 167 Hz)	6.24 (br @ rt, d @ low T)	^{13}C: 105.7-103.0	
H^{4}/C^{4}-Ar^{2}Bp	129.6 (d, J_{CH} = 158 Hz)	6.9	^{13}C: 131.4	
H^{5}/C^{5}-Ar^{2}Bp	102.0, (d, J_{CH} = 158 Hz)	5.8 (br rt, d @ low T)		
C^{6}-Ar^{2}Bp	157.5 (s)			
O*CH*$_3$^{2}-Ar^{2}Bp	54.9, (d, J_{CH} = 143 Hz)	3.15 (s)		
O*CH*$_3$-Ph^{OMe}	55.2 (J_{CH} = 143 Hz)	3.6 (s)	^{1}H: 3.66	^{1}H: 3.67
C^{1}-Ph^{OMe}	121.0 (J_{PC} = 80 Hz)			^{13}C: 116.84
C^{2}-Ph^{OMe}	159.9			^{13}C: 161.17
H^{3}/C^{3}-Ph^{OMe}	110.4 (J_{CH} = 158 Hz)	6.82 (br)	^{1}H: 6.97	^{13}C: 111.99, J_{PC} = 5 Hz, ^{1}H: 6.97
H^{4}/C^{4}-Ph^{OMe}	132.5 (J_{CH} = 158 Hz)	7.40 (br t)	^{1}H: 7.55	^{13}C: 133.74, ^{1}H: 7.7-7.57

Table 6.2, continued.

H^5/C^5-Ph^{OMe}	119.7 (J_{PC} = 9 Hz, J_{CH} = 170 Hz)	6.88 (m)	^{1}H: 7.03	^{13}C: 121.02, J_{PC} = 12 Hz, ^{1}H: 7.04
H^6/C^6-Ph^{OMe}	136.5 (J_{PC} = 9 Hz, J_{CH} = 173 Hz)	6.9-7	^{1}H: 7.48	^{13}C: 130.66, ^{1}H: 7.51-7.44
CH_3-Ar^{SO3}	21.4 (J_{CH} = 126 Hz)	1.98 (s)		
C^1-Ar^{SO3}	129.6 (J_{PC} = 10 Hz)			^{13}C: 127.5
C^2-Ar^{SO3}	146.3			^{13}C: 146.3, J_{PC}=16
H^3/C^3-Ar^{SO3}	126.9 (J_{CH}= 164 Hz)	7.81 (br)		^{13}C: 138.9, J_{PC}= 8, ^{1}H: 7.94
H^4/C^4-Ar^{SO3}	130.6 (J_{CH} = 161 Hz)	7.05 (br m)		^{13}C: 131.1, ^{1}H: 7.27
C^5-Ar^{SO3}	138.6			127.8
H^6/C^6-Ar^{SO3}	129.1 (J_{PC} = 22 Hz, J_{CH} = 178 Hz)	7.52 (br m)		^{13}C: 138.6, ^{1}H: 7.11-6.97
C^1-Ar^1Bp	140.5 (est. J_{PC} = 60 Hz)			
C^2-Ar^1Bp	140.9			
C^3-Ar^1Bp	134.7 (J_{CH} = 171 Hz)	6.24		
C^4-Ar^1Bp	134.1 (J_{PC} = 6 Hz, J_{CH} = 161 Hz)	7.05 (m)		
C^5-Ar^1Bp	131 (J_{CH} = 165 Hz)	7.6 (m)		
C^6-Ar^1Bp	127.3 (J_{PC} = 17.5 Hz, J_{CH} = 171 Hz)	8.83 (dd at low T)		

The ^{1}H and ^{13}C resonances of the lutidine ring were assigned first. There are five singlets in the δ 2–4 methoxy- and lutidine-methyl region of the ^{1}H NMR spectrum, consistent with the presence of three methoxy and two lutidine methyl groups in **2-lut** due to slow rotation around the Pd–N bond on the NMR time scale. Two of these singlets (δ 3.24 and 2.93) have two HMBC correlations each, so these resonances were assigned to the lutidine -CH_3 groups. The other methyl resonances have only one or no HMBC correlations and were therefore assigned to the methoxy groups. The two lutidine methyl ^{1}H signals each have NOESY correlations to the Pd-CH_3 resonance, indicating that lutidine is oriented perpendicular to the square plane. The two lut-Me resonances each have a COSY correlation with an aromatic resonance at either δ 7.19 or 7.11, which were therefore assigned as H^2-lut and H^4-lut, respectively. HMQC correlations between H^2-lut and H^4-lut and ^{13}C signals at δ 122.8 and δ 122.7, respectively, allow for these signals to be assigned as C^2- and C^4-lut. H^3-lut (δ 7.61) was assigned by the presence of COSY correlations to resonances H^2-lut and H^4-lut. C^3-lut (δ 138.6) was assigned by the presence of an HMQC correlation to H^3-lut.

After the assignment of the lutidine ring, the Ar^2Bp ring was assigned. The ^{1}H NMR spectrum contains a set of three COSY-correlated aromatic resonances, which is unique to the Ar^2Bp ring in **2-lut** (notwithstanding the lutidine ring, which was assigned as described above). δ 5.8–δ 6.9 and δ 6.9–δ 6.24 COSY correlations enable the assignment of H^3-, H^4-, and H^5-Ar^2Bp. The signals for H^3, H^4, H^5 are broad at room temperature. The H^3 and H^5 resonances resolve into the expected doublets at –40 °C. The H^4 resonance overlaps with other resonances at –40 °C so its

multiplicity could not be determined. The H^3-Ar^2Bp and H^4-Ar^2Bp resonances each have a NOESY correlation to a singlet in the methyl region, which enables assignment of OCH_3^1-Ar^2-Bp (δ 3.15) and OCH_3^2-Ar^2-Bp (δ 3.45), respectively. Once all of the ^{1}H signals were assigned, the corresponding ^{13}C signals were assigned based on HMQC correlations. The upfield shifts of the signals corresponding to C^3-Ar^2Bp (δ 103.1) and C^5- Ar^2Bp (δ 102.0) are consistent with the *ortho* position relative to the methoxy groups in the Ar^{OMe2} ring (c.f. δ 103.5 in both PPh_2(Bp) and $P(Ph^{OMe})_2$(Bp)).[19,20] The ^{13}C NMR resonances at δ 158.3 and 157.5 each have an HMBC correlation with a methoxy methyl signal and an HMBC correlation with H^4-Ar^2Bp and were assigned as ^{2}C-Ar^2Bp and ^{6}C-Ar^2Bp, respectively. The *ipso*-C ^{1}C-Ar^2Bp resonance (δ 118) was assigned by HMBC correlation to H^3- and H^5-Ar^2Bp. These ^{13}C NMR assignments are consistent with those reported in the literature for the Ar^2Bp rings in $P(ArSO_3)(Bp)_2$.[19]

The Ph^{OMe} ring was assigned next. The last unassigned ^{1}H NMR signal in the -OMe/-Me region was assigned as OCH_3-Ph^{OMe}. HMQC shows that these Hs are attached to the carbon at δ 55.2 (OCH$_3$-Ph^{OMe}). COSY and NOESY experiments enabled assignment of the rest of the ring. There is a NOESY correlation between the OCH_3-Ph^{OMe} resonance and a resonance at δ 6.82, which was assigned as H^3-Ph^{OMe}. Strong COSY and NOESY cross peaks at room temperature between the H^3-Ph^{OMe} and δ 7.40 resonances as well as between the δ 7.40 and δ 6.88 resonances enabled the assignment of H^4-Ph^{OMe} and H^5-Ph^{OMe}. The ^{1}H resonance at δ 7.0 was assigned as H^6-Ph^{OMe} because of an 80 °C COSY correlation to H^5-Ph^{OMe} and a NOESY correlation to OCH_3^2-Ar^2Bp (see discussion of solution structure at end of this section). C^3-, C^4-, and C^5-Ph^{OMe} were

assigned based on HMQC correlations to their connected ^{1}H resonances. The ^{13}C resonance at δ 159.9 was assigned as ^{2}C-Ph^{OMe} because of its HMBC correlation to OCH_3-Ph^{OMe}. There were no room temperature-, high T-, or low T- HMBC correlations observed for any of the C^{1} (*ipso*) resonances in **2-lut**. Therefore, C^{1}-Ph^{OMe} was assigned as δ 121.0 because it has a J_{PC} = 80 Hz, which is typical for the corresponding *ipso*-C in the benchmark (PO-OMe)PdMe(py) complex.[8]

For the p-toluene-sulfonate ring (Ar^{SO3}), all Ar-H resonances are broad between room temperature and –80 °C. The ^{1}H signal at δ 1.94 integrates for 3H and is in the characteristic range for the *para*-Me groups of other p-toluenesulfonate ligands, and was therefore assigned to the Ar^{SO3} methyl group. The CH$_3$-Ar^{SO3} ^{13}C resonance was identified at δ 21.5 by HMQC. The ^{1}H resonance at δ 7.05 was assigned as H^{4}-Ar^{SO3} due to a strong NOESY correlation with CH_3-Ar^{SO3} and a COSY correlation to another ^{1}H resonance (δ 7.81). This latter resonance was assigned as H^{3}-Ar^{SO3} on the basis of this COSY correlation and the low-field chemical shift, which is typical for H^{3}-Ar^{SO3} resonances.[18,19] The assignment of H^{3}-Ar^{SO3} was confirmed based on this precedent. The ^{1}H resonance at δ 7.52 is assigned as H^{6}-Ar^{SO3} because of its HMBC correlation to C^{4}-Ar^{SO3}. The resonances at δ 126.9, δ 130.7, and δ 127.4 were assigned as C^{3}-Ar^{SO3}, C^{4}-Ar^{SO3}, C^{6}-Ar^{SO3}, respectively, based on HMQC respective correlations to their attached proton. The resonance at δ 129.6 was assigned as C^{1}-Ar^{SO3} based on an HMBC correlation with H^{4}-Ar^{SO3} and because its chemical shift (~ δ 120) and J_{PC} (~60-80 Hz) values are typical for a P-C^{Ar} carbon. The signal at δ 138.5 (J_{CH} = 162 Hz) was assigned as C^{5}-Ar^{SO3} due to an HMBC correlation with H^{3}-Ar^{SO3}. Finally, the signal at δ 146.0 was assigned as C^{2}-Ar^{SO3} on the basis of its chemical shift, which is

typical for aryl sulfonates. There are no HMBC correlations with this resonance.

The remaining ^{1}H resonances are assigned to the Ar^{1}Bp ring by process of elimination. The resonance at δ 8.83 was assigned as H^{6}-Ar^{1}Bp based on the NOESY correlation between the Pd-*CH*$_3$ and one *CH*$_3$-lut. These NOESY correlations and the downfield chemical shift of this resonance are consistent with a conformation in which H^{6}-Ar^{1}Bp is positioned close to the Pd center in an axial site, where it is anisotropically shielded. The resonance at δ 7.6 was assigned as H^{5}-Ar^{1}Bp because of its COSY and NOESY correlations with H^{6}-Ar^{1}Bp. The resonances at δ 7.05 and δ 6.24 were assigned as H^{4}-Ar^{1}Bp and H^{3}-Ar^{1}Bp, respectively, based on COSY correlations. C^{4}-Ar^{1}Bp and C^{5}-Ar^{1}Bp were assigned based on HMQC correlations with their attached Hs. The resonance at δ 129.1 was assigned as C^{6}-Ar^{1}Bp based on its low T HMBC correlations with H^{4}-Ar^{1}Bp and H^{6}-Ar^{1}Bp. The resonance at δ 141.0 was assigned as C^{2}-Ar^{1}Bp by its HMBC correlation with H^{6}-Ar^{1}Bp. The δ 134.7 resonance was assigned as C^{3}-Ar^{1}Bp based on chemical shift and the fact that it is one of the last unassigned carbon signals. The δ 140.5 resonance was assigned as ^{1}C-Ar^{1}Bp based on 25 °C and –40 °C HMBC correlations with H^{5}-Ar^{1}Bp and its large J_{PC} value (60 Hz, identified from HMBC).

Solution structure of 2-lut. The solution structure of **2-lut** was determined by NOESY NMR experiments performed at 25 °C, –40 °C, and 80 °C, taking advantage of the rigorous peak assignments determined as described above. There is a NOESY correlation between OC*H*$_3$-Ph^{OMe} and Pd-C*H*$_3$, indicating that the methoxy group of the anisolyl ring is pointed toward the Pd-C*H*$_3$ in an *exo* orientation (see Chapter Two for a discussion of *exo*/*endo* conformations of P-Ar groups

in phosphine compounds). This implies that H^6-Ph^{OMe} must point away from Pd, which is corroborated by a NOESY correlation between H^6-Ph^{OMe} and OCH_3^2-Ar^2Bp. NOESY correlations between H^3-Ar^{SO3} and OCH_3-Ar^2Bp and between CH_3-Ar^{SO3} and H^4-Ar^2Bp *definitively show that the Ar^2Bp and Ar^{SO3} rings are π stacked in solution between –40 °C and 80 °C*. The key NOESY correlations that elucidate the *π stack* are shown in Figure 6.5.

Figure 6.5. Solid-state structure of **2-lut** showing key NOESY correlations (shown in blue) that establishes the presence of π stacking in solution

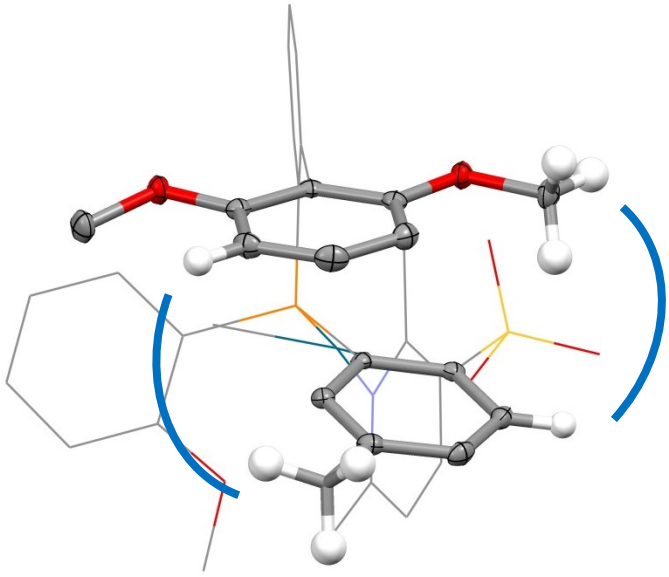

Solid-state structure of 2-py. X-ray quality crystals of **2-py** were grown from a CH_2Cl_2 solution of crude **2-py** layered with Et_2O (1 g/60mL CH_2Cl_2/200 mL Et_2O) and stored at –40 °C (Figure 6.6). Unlike the solid-state structure of **2-lut**[14] (Figure 6.7) which contains a π stacking interaction between the Ar^{SO3} and *endo* Ar^2Bp rings, the structure of **2-py** has the Ar^2Bp ring in an *exo* orientation and positioned above the Pd square plane. The 6-membered (PO)Pd chelate ring,

which typically adopts a boat-conformation as in **2-lut**, is significantly puckered. Also, the Pd–Me bond distance in **2-py** is significantly shorter (2.008(8) Å) than that in **2-lut** (2.060(2) Å). A comparison of other structural features between **2-py** and **2-lut** is shown in Table 6.3.

Figure 6.6. Molecular structure of **2-py**. Hydrogen atoms, disordered lut ring and Ar^2Bp ring are omitted. Bond lengths (Å) and angles (deg): Pd1–C34 2.008(8), Pd1–N1 2.10(4), Pd1–O1 2.168(5), Pd1–P1 2.2195(19), C34–Pd1–P1 95.1(3), O1–Pd1–P1 83.57(13), N1–Pd1–C34 87.8(14), O1–Pd1–N1 93.6(14).

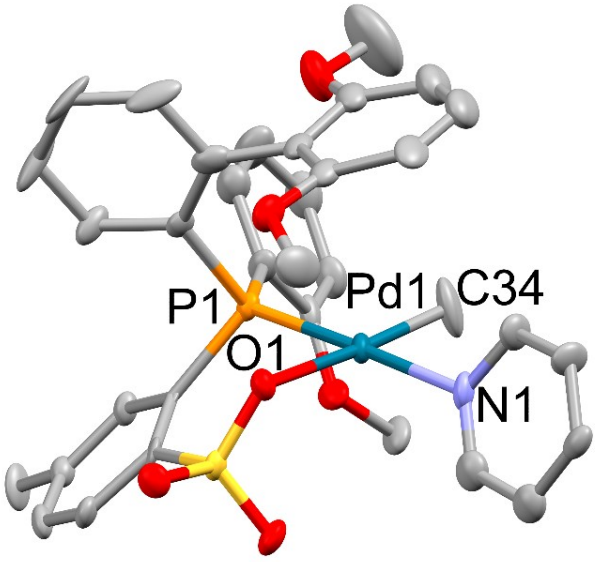

Figure 6.7. Molecular structure of **2-lut**•2(THF), reported by Defoe.[14] Hydrogen atoms and THF molecules are omitted. Bond lengths (Å) and angles (deg): Pd1–C1 2.060(2), Pd1–N1 2.121(2), Pd1–O1 2.165(2), Pd1–P1 2.253(7), C1–Pd1–P1 90.67(6), O1–Pd1–P1 94.96(4), N1–Pd1–C1 89.10(8), O1–Pd1–N1 85.13(6).

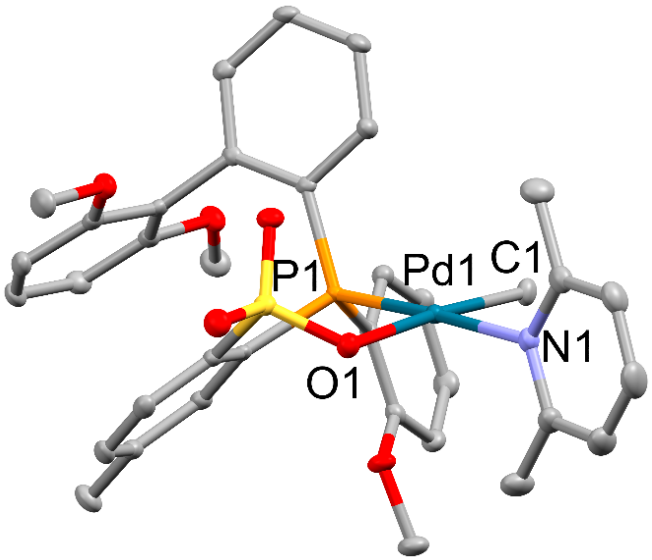

Table 6.3. Comparison of crystal structures of **2-lut** and **2-py**.

	2-lut	**2-py**
Pd–O(S) (Å)	2.165(2)	2.168(5)
Pd–P (Å)	2.2525(7)	2.2195(19)
Pd–C (Å)	2.060(2)	2.008(8)
Pd–N (Å)	2.121(2)	2.10(4)
(PO)Pd conformation	Boat	5 atoms ~planar, 1 atom puckered
Angle between square plane and plane of anisole ring (P-C-C-O)	75.49°	57.51°

Reconciling the solution behavior and solid-state structure of 2-py. As noted above, variable temperature ^{1}H NMR studies of **2-py** by Defoe[14] show the presence of two sets of resonances below 0 °C that are fully resolved at –60 °C, which were proposed to be due to a pair

of isomers that "probably differ in the conformation of the [PO]Pd chelate ring." It is likely that the two isomers observed for **2-py** in solution at low temperatures differ in the rotational conformation of the Bp unit. In one isomer, the Ar^2Bp ring is in an *endo* orientation and is π-stacked with the Ar^{SO3} ring (as observed for **2**-lut in the solid state and solution) and, in the other isomer, the Ar^2Bp ring is in an *exo* orientation and is positioned over an axial site of the Pd square plane (as observed for **2**-py in the solid state). The latter isomer is disfavored for **2-lut** due to steric bulk from the *ortho*-Me substituents of the lutidine ligand.

Two possible explanations for the slow chain transfer rate and resulting high MW of the PE produced in ethylene polymerization by **2-lut** are (i) axial blockage by the PO^- ligand, which would disfavor associative chain transfer, and (ii) enhanced rigidity due to the presence of a *π stacking* interaction. While **2-lut** and **2-py** are useful, isolable models to help us rationalize polymerization results, it would useful to study the active (PO)PdR(ethylene) active species directly. Investigations into whether π stacking is present in (PO)PdR(ethylene) is ongoing in the Jordan lab by Kelsey Brown. The proposal is to synthesize the base-free $\{(PO)PdR\}_2$ dimer by abstraction of pyridine with $B(C_6F_5)_3$ and to generate the ethylene-adduct at low temperature and fully characterize it by NMR.

6.3 Conclusion

The phosphine-sulfonate proligand H[**1**] and the corresponding (PO)PdMe(L) complexes **2-py** and **2-lut** were synthesized. A thorough NMR investigation enabled the complete assignment of all ^{1}H and ^{13}C resonances for H[**1**] and **2-lut**. ^{1}H-^{1}H NOESY NMR experiments establish that

the solution-state structure of **2-lut** is similar to the solid-state structure and *contains a π stacking interaction between the Ar^2Bp and Ar^{SO3} rings of the PO^- ligand*. **2-py** exists as a mixture of two isomers in solution. The solid-state structure of one isomer was determined by single crystal X-ray crystallography and, interestingly, the Ar^2Bp ring is positioned in an *exo* orientation and lies over the Pd square plane. It is most likely that the two species seen in solution at low temperature differ in the rotational conformation of the Bp unit. In one isomer, the Ar^2Bp ring is in an *endo* orientation and is π-stacked with the Ar^{SO3} ring (as observed for **2**-lut in the solid state and solution) and, in the other isomer, the Ar^2Bp ring is in an *exo* orientation and is positioned over an axial site of the Pd square plane (as observed for **2**-py in the solid state). The latter isomer is disfavored for **2-lut** due to steric bulk from the *ortho*-Me substituents of the lutidine ligand.

6.4 Experimental Section

General Procedures. All experiments were performed using drybox or Schlenk techniques under a nitrogen atmosphere unless noted otherwise. Nitrogen was purified by passage through Q-5 oxygen scavenger and activated molecular sieves. CH_2Cl_2 and Et_2O were dried by passage through activated alumina. Pentane and hexanes were purified by passage through BASF R3-11 oxygen scavenger and activated alumina. CD_2Cl_2 was distilled from and stored over P_2O_5. ^{n}BuLi solution (1.6 M or 2.5 M in hexanes), 2-bromoanisole, HCl solution (2.0 M in Et_2O), pyridine (Fisher), and 2,6-lutidine (99+%) were purchased from Sigma Aldrich and used without further purification. $LiP(2\text{-}OMe\text{-}Ph)_2$,[21–24] $(TMEDA)PdMe_2$ (TMEDA = tetramethylethylene diamine),[25] and 2-lithio-2',6'-dimethoxy-biphenyl were prepared according to the literature.

NMR spectra were recorded on Bruker Advance II+ or DRX 400 spectrometers at ambient temperature unless otherwise indicated. ^{1}H and ^{13}C chemical shifts are reported relative to $SiMe_4$ and internally referenced to residual ^{1}H and ^{13}C solvent resonances. ^{31}P chemical shifts are externally referenced to 85% H_3PO_4 (δ 0.0). Coupling constants are reported in Hertz (Hz). NMR assignments are based on COSY, NOESY, and HMQC experiments.

Electrospray mass spectra (ESI-MS) and atmospheric pressure chemical ionization mass spectra (APCI-MS) were recorded using Agilent 6224 TOF–MS (high resolution) or 6130 LCMS (low resolution) instruments. The observed isotope patterns closely matched calculated isotope patterns. The listed *m/z* value corresponds to the highest % abundance in the isotope pattern.

2-lithio-2',6'-dimethoxy-biphenyl (LiBp). 2-bromo-2',6'-dimethoxy-biphenyl (20.00 g, 0.068 mol) was dissolved in Et_2O (350 mL) and cooled with an ice bath. An ^{n}BuLi solution (2.5 M in hexane, 30.0 mL, 0.075 mol) was added dropwise over 15 min. The white precipitate was collected on a swivel frit, washed with Et_2O, dried, and stored in a ground-glass storage tube under N_2 at -40 C. Yield: 15.0 g, 99.9%.

***in situ*-generated dilithiated *p*-toluenesulfonate ($LiAr^{SO3}$).** *p*-toluenesulfonic acid (3.90 g, 0.023 mol) was dissolved in THF (50 mL) and cooled in an ice bath. An ^{n}BuLi solution (2.5 M in hexane, 20.0 mL, 0.050 mol) was added dropwise via syringe, during which time a white precipitate appeared. The reaction was stirred for 30 min at 0 °C, the cold bath was removed, and the suspension was allowed to come to room temperature over 2 h. This solution was used in the synthesis of $P(Bp)(Ar^{SO3})(OPh)$ below.

2-lithioanisole (LiPh^{OMe}). 2-bromoanisole (23.4 mL, 0.188 mol) was dissolved in hexane (50 mL) and cooled with an ice bath. An ^{n}BuLi solution (2.5 M in hexane, 82.5 mL, 0.206 mol) was added dropwise over 15 min. The white precipitate was collected on a swivel frit, washed with Et_2O, dried, and stored in a ground-glass storage tube under N_2. Yield: 21.2 g, 98.9%.

P(Bp)(OPh)$_2$. LiBp (5.00 g, 0.023 mol) and THF (75 mL) were added to a flask to give a white suspension. $P(OPh)_3$ (7.04 g, 0.023 mol) and THF (50 mL) were added to another flask to give a colorless solution. Both flasks were cooled to –78 °C and the LiBp solution was added dropwise via syringe to the $P(OPh)_3$ solution. The cold bath was removed after the addition and the white suspension was allowed to come to room temperature. Below 0 °C and over the course of 15 min, the white solid dissolved to give a yellow solution. The reaction progress was assayed by taking a 0.5 mL aliquot for analysis by ^{31}P NMR. Three more portions of LiBp (1.20 g, 0.24 equiv in 20 mL THF; 0.565 g, 0.113 equiv in 10 mL THF; 0.200 g, 0.04 equiv in 5 mL THF) were added to fully convert the $P(OPh)_3$. Before each addition, the reaction mixture was cooled to –78 °C and then the reaction mixture was brought to room temperature over 1 h before assaying by ^{31}P NMR. This yellow solution was used for the synthesis of P(Bp)(Ar^{SO3})(OPh) below. ^{31}P NMR (THF): δ 157.1 (s). Less than 2% $P(Bp)_2(OPh)$ was observed at δ 106.8 (s).

P(Bp)(Ar^{SO3})(OPh). The flasks containing *in situ*-generated dilithiated *p*-toluenesulfonate (0.023 mol, 50 mL THF and 20 mL hexane) and $P(Bp)(OPh)_2$ (0.023 mol, ~155 mL THF) were cooled to 0 °C. The LiAr^{SO3} solution was added dropwise to the $P(Bp)(OPh)_2$ solution over 15 min. The cold bath was removed and the yellow slurry was allowed to come to room temperature. Over

1.5 h, the solid dissolved and the red-orange solution was assayed by ^{31}P NMR. This red-orange solution was used for the synthesis of H[P(Bp)(Ar^{SO3})(Ph^{OMe})] below. ^{31}P NMR (THF, hexane): δ 100.6 (s).

H[P(Bp)(Ar^{SO3})(Ph^{OMe})] (H[1]). A solution of LiPh^{OMe} (2.59 g, 0.023 mol) in THF (50 mL) was added dropwise to a flask containing P(Bp)(Ar^{SO3})(OPh) (0.023 mol, 225 mL THF and hexane). The solution was stirred for 12 h, and the dark red solution of Li[P(Bp)(Ar^{SO3})(Ph^{OMe})] was assayed by ^{31}P NMR. ^{31}P NMR (THF, hexane): δ –22.3 (s). The solution was acidified by addition of an HCl solution (2.0 M in Et_2O, 56.0 mL, 0.112 mol). The red color was quenched after ~5 mL HCl solution was added and a white precipitate persisted in solution after ~45 mL HCl solution was added. This white powder was collected by filtration and washed with Et_2O (1.8 g, 15% yield H[**1**]). The reaction mixture filtrate was stripped to give an orange oil, which was dissolved in CH_2Cl_2 (50 mL) and passed through a fine frit to remove LiCl. Et_2O (350 mL) was added and a white powder precipitated. This solid was collected by filtration and dried under vacuum overnight to give crude H[**1**] (total from two crops: 7.28 g, 61.4% yield). The numbering scheme for NMR assignments is shown in Figure 6.3 and the assignments are tabulated with some comparisons to literature compounds in Table 6.1. ^{1}H NMR (CD_2Cl_2, rt): δ 8.92 (d, J_{PH} = 595, 1H, P-*H*), 8.05 (dd, J_{HH} = 8, J_{PH} = 5, H^3-Ar^{SO3}), 7.74 (t, 1H, H^6-Ar^{1}Bp), 7.627 (m, 1H, H^6-Ph^{OMe}), 7.55 (d, J_{HH} = 8, 1H, H^4-Ar^{SO3}), 7.46–7.483 (m, 2H, H^5-Ar^{1}Bp and H^3-Ar^{1}Bp), 7.29–7.35 (m, 2H, H^4-Ar^{1}Bp and H^4-Ar^{2}Bp), 7.17 (m, 1H, H^6-Ar^{SO3}), 7.01–7.03 (m, 2H, H^4-Ph^{OMe} and H^5-Ph^{OMe}), 6.97 (t, 1H, H^3-Ph^{OMe}), 6.58 (d, J_{HH} = 8.5, 1H, H^5-Ar^{2}Bp), 6.47 (d, J_{HH} = 8, 1H, H^3-Ar^{2}Bp), 3.73 (s, 3H,

OC*H*$_3$''-Ar^{2}Bp), 3.67 (s, 3H, OC*H*$_3$-Ph^{OMe}), 3.24 (s, 3H, O C*H*$_3$'-Ar^{2}Bp), 2.35 (s, 3H, C*H*$_3$-Ar^{SO3}). ^{13}C{^{1}H} NMR (CD_2Cl_2): δ 161.2 (s, C^2-Ph^{OMe}), 157.6 (s, C$^{2\text{ or }6}$-Ar^{2}Bp), 157.5 (s, C$^{2\text{ or }6}$-Ar^{2}Bp), 150.4 (d, J_{PC} = 9, C^2-Ar^{SO3}), 141.3 (d, J_{PC} = 10, C^2-Ar^{1}Bp), 140.4 (d, J_{PC} = 12, C^5-Ar^{SO3}), 136.5 (d, J_{PC} = 2, C^6-Ph^{OMe}), 135.4 (d, J_{PC} = 3, C^4-Ar^{SO3}), 135.2 (d, J_{PC} = 11, C^6-Ar^{SO3}), 134.9 (d, J_{PC} = 8, C^4-Ph^{OMe}), 134.5 (d, J_{PC} = 10, C^4-Ar^{1}Bp), 134.2 (d, J_{PC} = 10, C^5-Ar^{1}Bp), 134 (d, J_{PC} = 3, C^6-Ar^{1}Bp), 131.8 (s, C^4-Ar^{2}Bp), 129.2 (d, J_{PC} = 10, C^3-Ar^{SO3}), 128.2 (d, J_{PC} = 13, C^3-Ar^{1}Bp), 122 (d, J_{PC} = 13, C^5-Ph^{OMe}), 120.7 (s, C^1-Ar^{1}Bp), 114.5 (s, C^1-Ar^{2}Bp), 113 (d, J_{PC} = 97, C^1-Ar^{SO3}), 112.3 □d, J_{PC} = 6, C^3-Ph^{OMe}), 109.2 (d, J_{PC} = 98, C^1-Ph^{OMe}), 104.7 (s, C^5-Ar^{2}Bp), 104.3 (s, C^3-Ar^{2}Bp), 56.7 (s, *Me*-Ph^{OMe}), 56.1 (s, O*C*H$_3$-Ar^{2}Bp'), 55.5 (s, O*C*H$_3$-Ar^{2}Bp), 21.4 (s, *C*H$_3$-Ar^{SO3}). ^{31}P{^{1}H} NMR (CD_2Cl_2): δ -7.3.

2-lut. The NMR labeling scheme for **2-lut** is shown in Figure 6.4 and the assignments are tabulated with some comparisons to literature compounds in Table 6.2. ^{1}H NMR (CD_2Cl_2, rt): δ 8.90 (br d, 1H, H^6-Ar^{1}Bp), 7.85 (t, 1H, H^3-Ar^{SO3}), 7.63 (t, 1H, H^3-lut), 7.56-7.646 (br m, 2H, H^6-Ar^{SO3} and H^5-Ar^{1}Bp), 7.45 (br t, 1H, H^4-Ph^{OMe}), 7.23 (d, 1H, H^2-lut), 7.15 (d, 1H, H^4-lut), 7.12–7.04 (br m, 2H, H^4-Ar^{SO3} and H^4-Ar^{1}Bp), 7.04–6.98 (br m, 1H, H^6-Ph^{OMe}), 6.98–6.9 (t, 2H, H^4-Ar^{2}Bp and H^5-Ph^{OMe}), 6.9–6.76 (br m,1H, H^3-Ph^{OMe}), 6.29 (br d, 2H, H^3-Ar^{2}Bp and H^3-Ar^{1}Bp), 5.84 (d, 1H, H^5-Ar^{2}Bp), 3.58 (s, 3H, C*H*$_3$-Ph^{OMe}), 3.46 (s, 3H, OC*H*$_3$^{1}-Ar^{2}Bp), 3.28 (s, 3H, C*H*$_3$^{1}-Lut), 3.19 (s, 3H, OC*H*$_3$^{2}-Ar2Bp), 2.97 (s, 3H, C*H*$_3$^{5}-Lut), 1.98 (s, 3H, C*H*$_3$-Ar^{SO3}), -0.02 (s, 3H, Pd-C*H*$_3$). ^{13}C{^{1}H} NMR (CD_2Cl_2): δ 159.8 (C^2-Ph^{OMe}), 159.4 (C^1-lut), 159.0 (C^5-lut), 158.3 (C^2-Ar^{2}Bp), 157.5 (C^6-Ar^{2}Bp), 146.3 (C^2-Ar^{SO3}), 140.9 (C^2-Ar^{1}Bp), 140.5 (J_{PC} = 150 Hz, C^1-

$Ar^{1}Bp$), 138.6 (C^{3}-lut), 138.6 (J_{CH} = 162 Hz, ^{5}C-Ar^{SO3}), 136.5 (J_{PC} = 9 Hz, J_{CH} = 173 Hz, C^{6}-Ph^{OMe}), 134.7 (J_{CH} = 171 Hz, C^{3}-$Ar^{1}Bp$), 134.1(J_{PC} = 6 Hz, J_{CH} = 161 Hz, C^{4}-$Ar^{1}Bp$), 132.5 (J_{CH} = 158 Hz, C^{4}-Ph^{OMe}), 131.0 (J_{CH} = 165 Hz, C^{5}-$Ar^{1}Bp$), 130.6 (J_{CH} = 161 Hz, C^{4}-Ar^{SO3}), 129.6 (J_{CH} = 158 Hz, C^{4}-$Ar^{2}Bp$), 129.1 (J_{PC} = 22 Hz, J_{CH} = 178 Hz, C^{6}-Ar^{SO3}), 127.3 (J_{PC} = 17.5 Hz, J_{CH} = 171 Hz, C^{6}-$Ar^{1}Bp$), 126.9 (J_{CH} = 164 Hz, C^{3}-Ar^{SO3}), 122.8 (J_{PC} = 2 Hz, J_{CH} = 164 Hz , C^{2}-lut), 122.6 (J_{PC} = 2 Hz, J_{CH} = 165 Hz, C^{4}-lut), 121.0 (C^{1}-Ph^{OMe}), 119.7 (J_{PC} = 9 Hz, J_{CH} = 170 Hz, C^{5}-Ph^{OMe}), 118.4 (C^{1}-Ar^{SO3}), 117.8 (J_{PC} = 14 Hz, C^{1}-$Ar^{2}Bp$), 110.4 (J_{CH} = 158 Hz, C^{3}-Ph^{OMe}), 103.1 (J_{CH} = 167 Hz, C^{3}-$Ar^{2}Bp$), 102.0 (J_{CH} = 158 Hz, C^{5}-$Ar^{2}Bp$), 55.2 (J_{CH} = 143 Hz, CH_3-Ph^{OMe}), 55.1 (J_{CH} = 143 Hz, OCH_3^{2}-$Ar^{2}Bp$), 54.9 (J_{CH} = 143 Hz, OCH_3^{6}-$Ar^{2}Bp$), 26.8 (J_{CH} = 127 Hz, CH_3^{1}-lut), 26.1 (J_{CH} = 127 Hz, CH_3^{5}-lut), 21.4 (J_{CH} = 126 Hz, CH_3-Ar^{SO3}), –4.2 (Pd*Me*). $^{31}P\{^{1}H\}$ NMR (CD_2Cl_2): δ 25.8 (s).

Figure 6.8. ^{1}H NMR of **2-lut** (CD_2Cl_2, 25 °C, 500 MHz).

(a) Full ^{1}H NMR spectrum

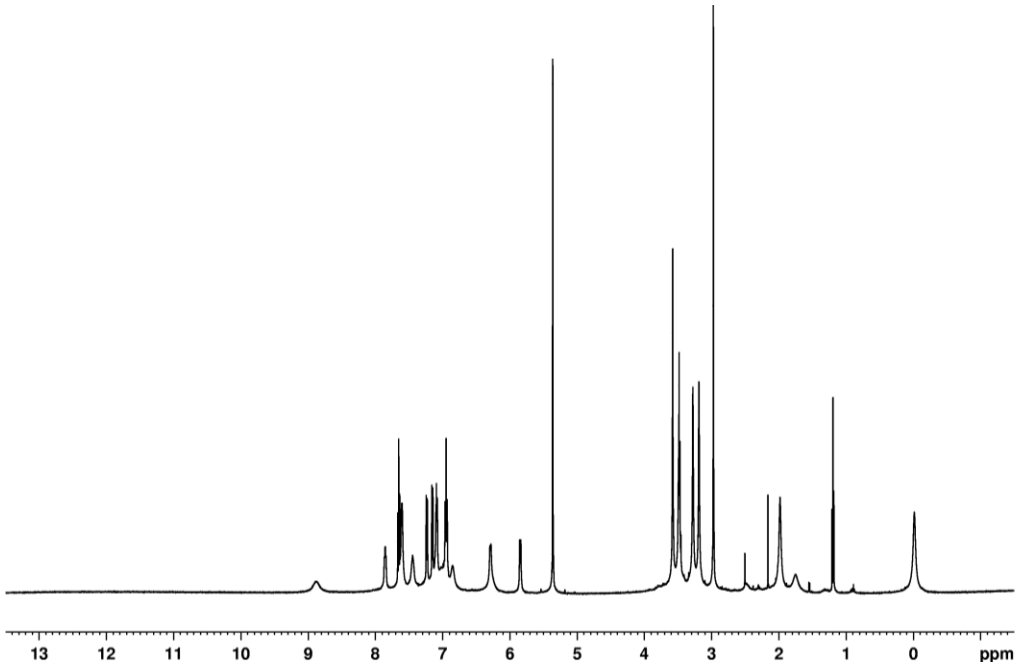

(b) Expansion of aromatic region

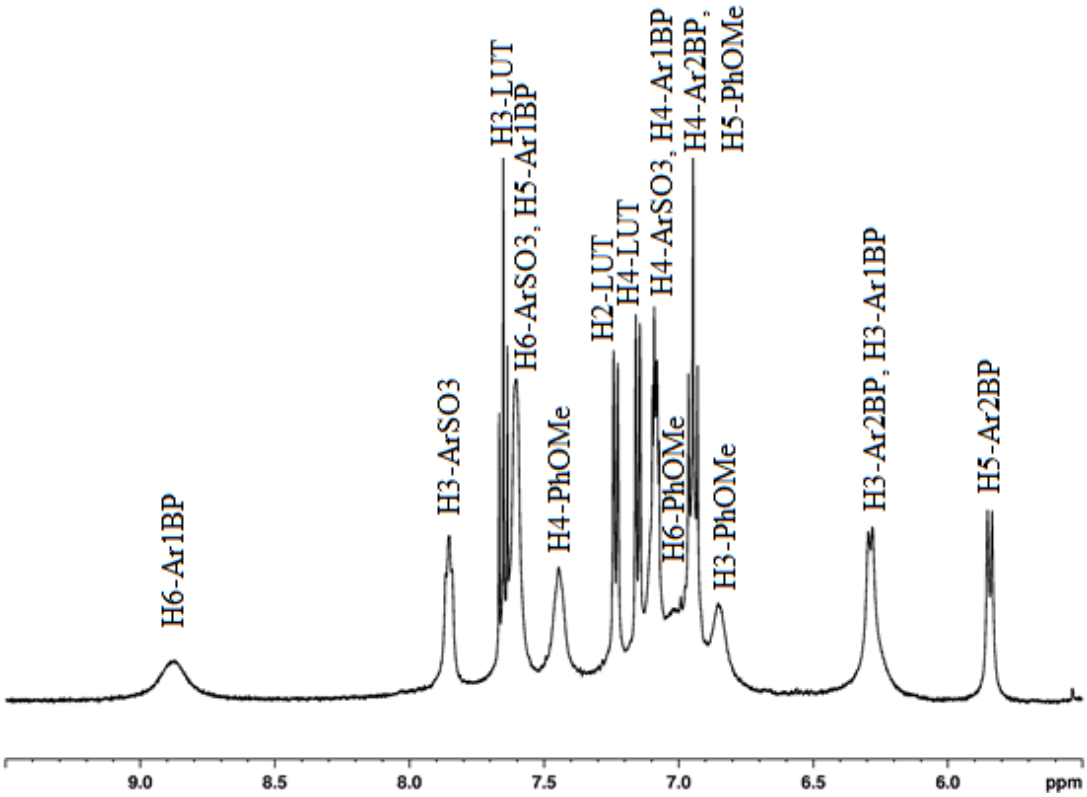

Figure 6.9. ^{1}H NMR of **2-lut** (CD_2Cl_2, 35 °C, 500 MHz).

(a) Full ^{1}H NMR spectrum

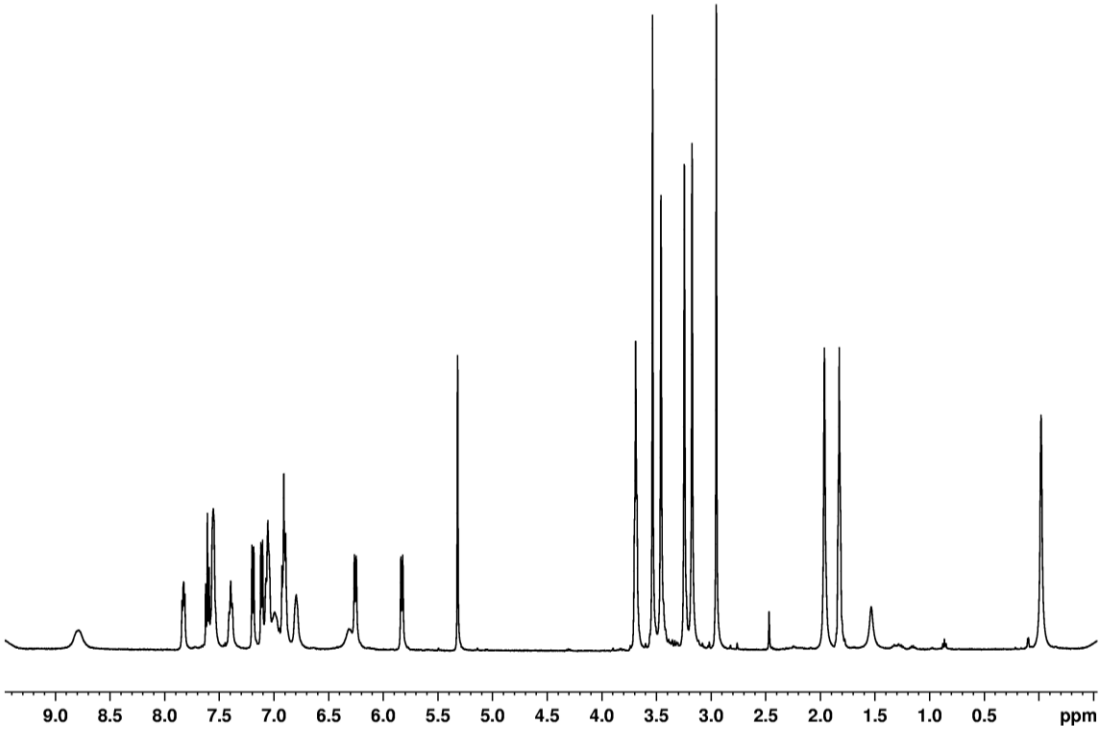

(b) Expansion of aromatic region

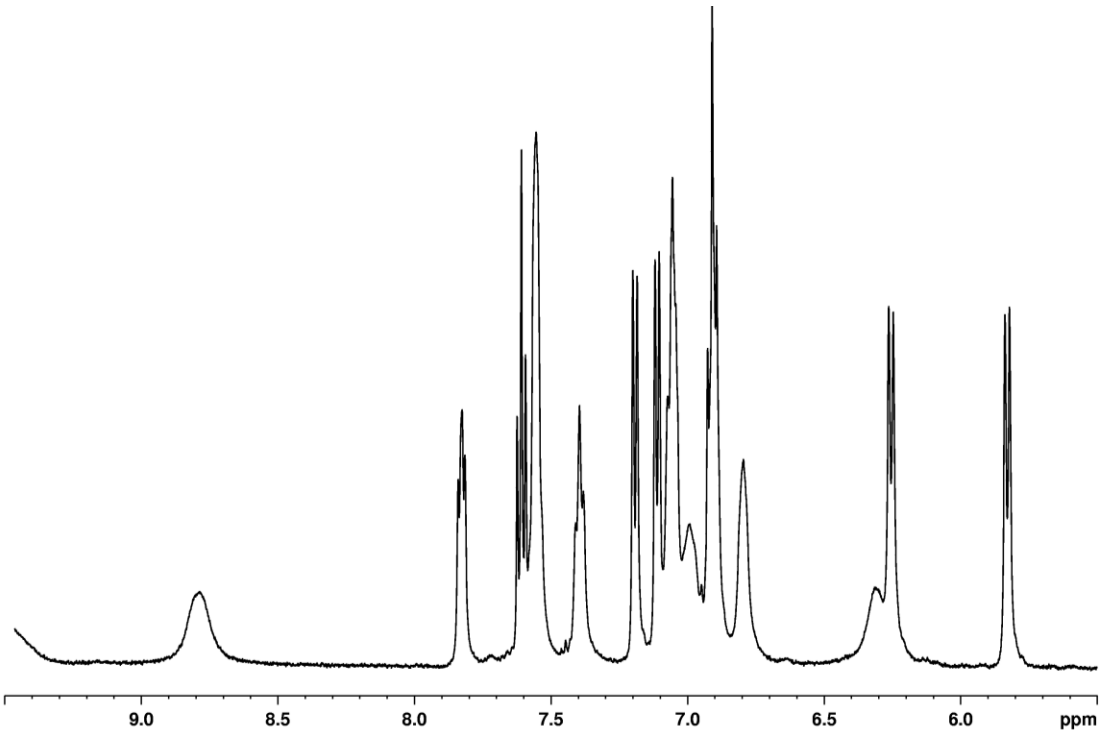

Figure 6.10. ^{1}H NMR of **2-lut** (CD_2Cl_2, –40 °C, 500 MHz).

(a) Full ^{1}H NMR spectrum.

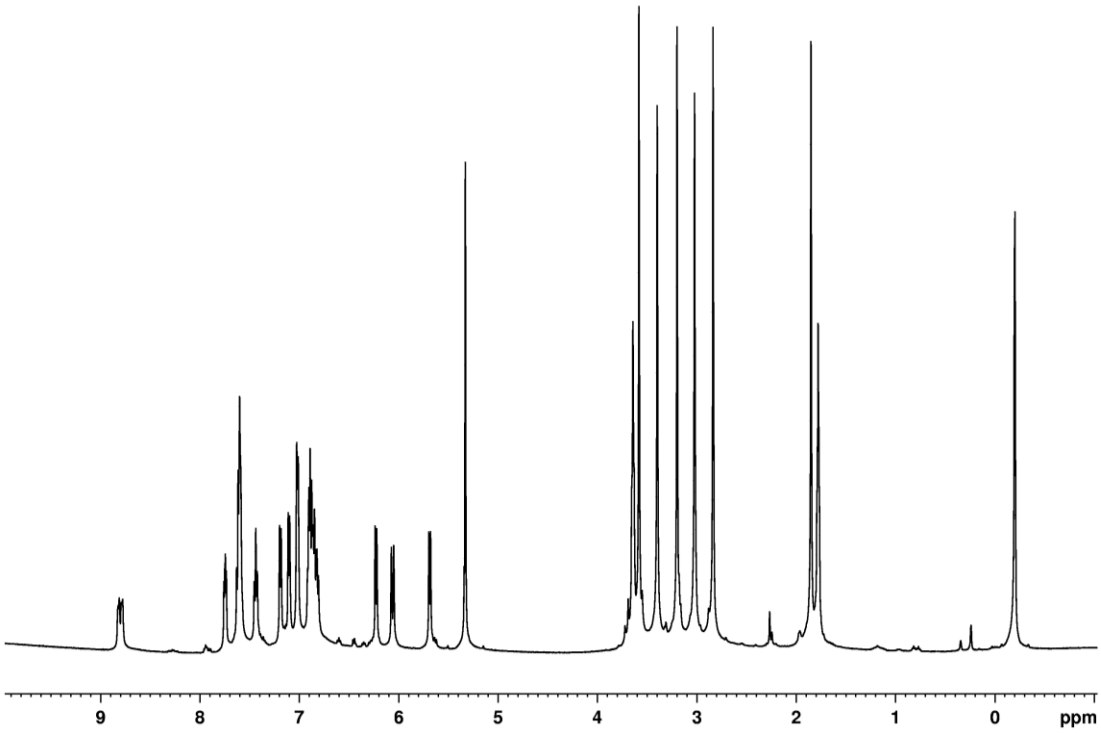

(b) Expansion of aromatic region

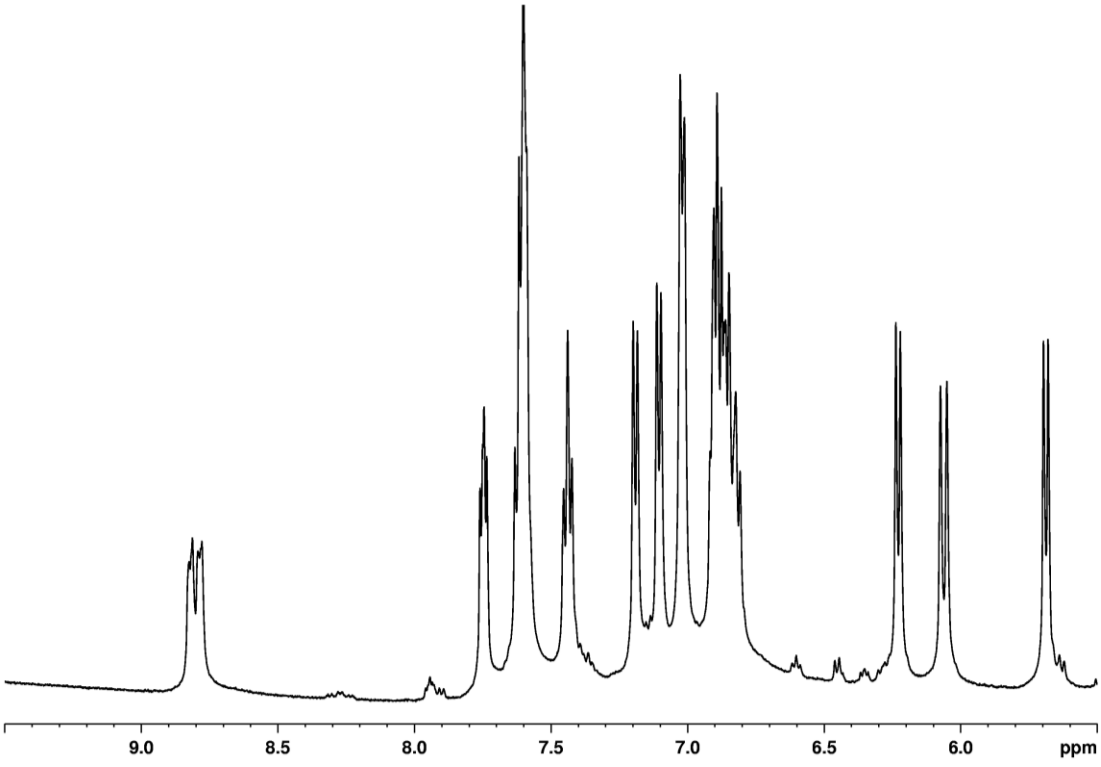

Figure 6.11. ^{1}H NMR of **2-lut** (CD_2Cl_2, 80 °C, 500 MHz).

(a) Full ^{1}H NMR spectrum

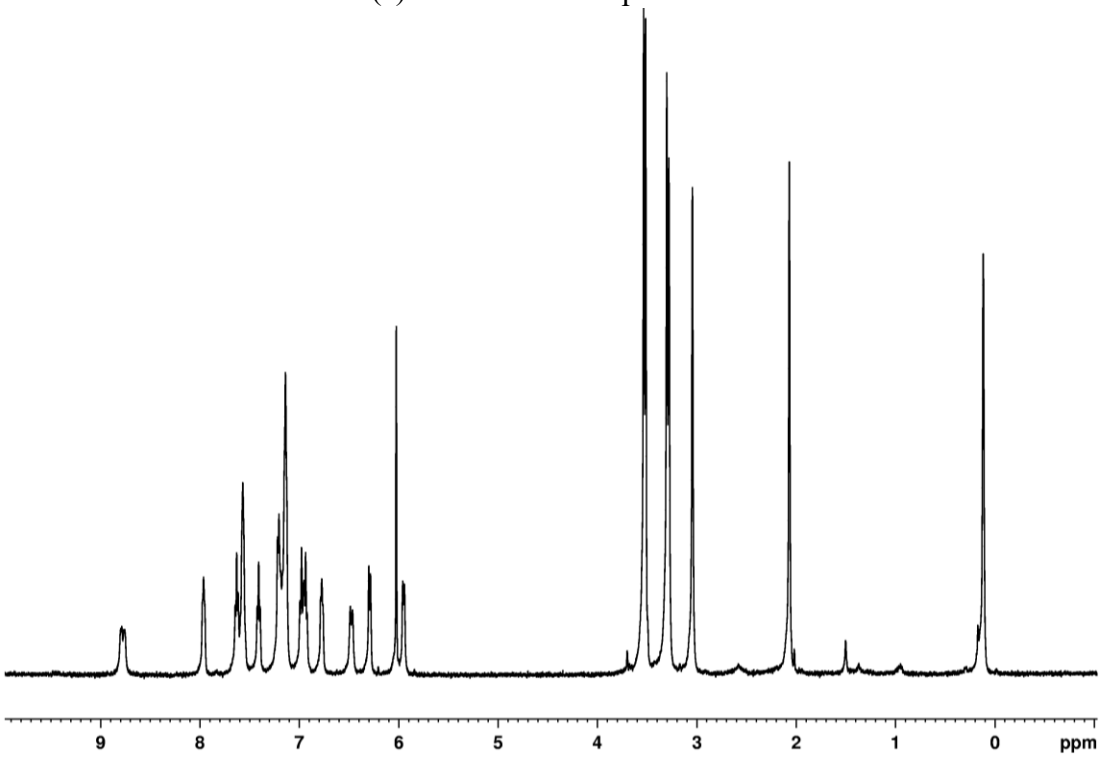

(b) Expansion of aromatic region

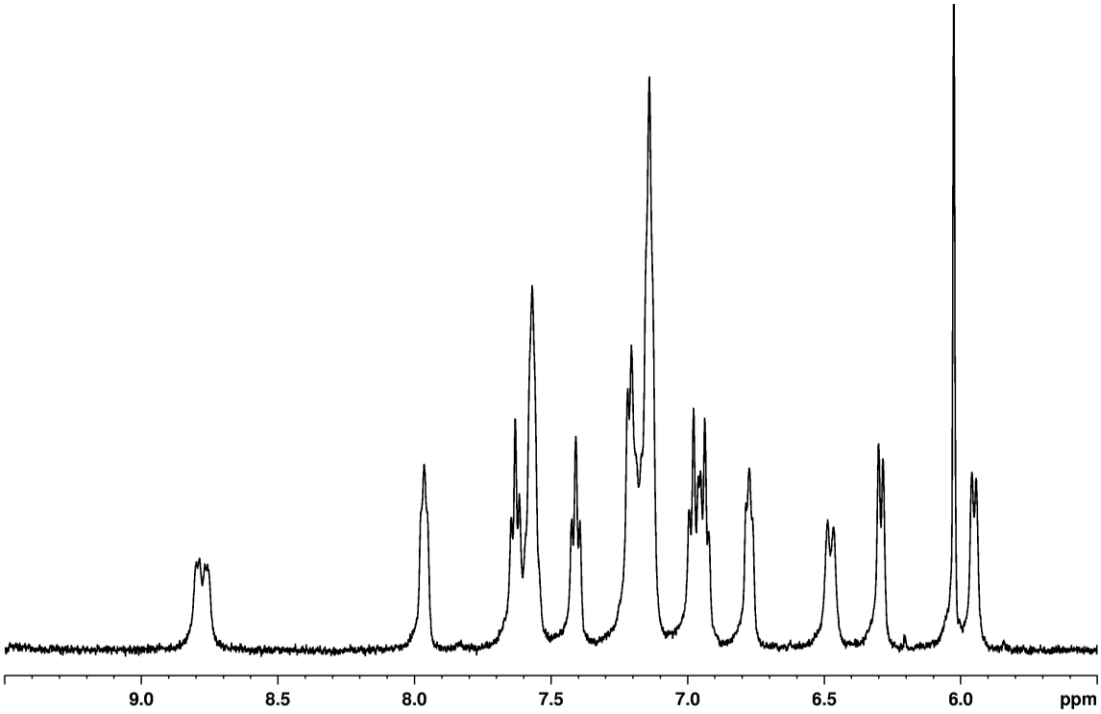

Figure 6.12. ^{13}C NMR of **2-lut** (CD_2Cl_2, 25 °C, 125 MHz).

(a) Full ^{13}C NMR spectrum

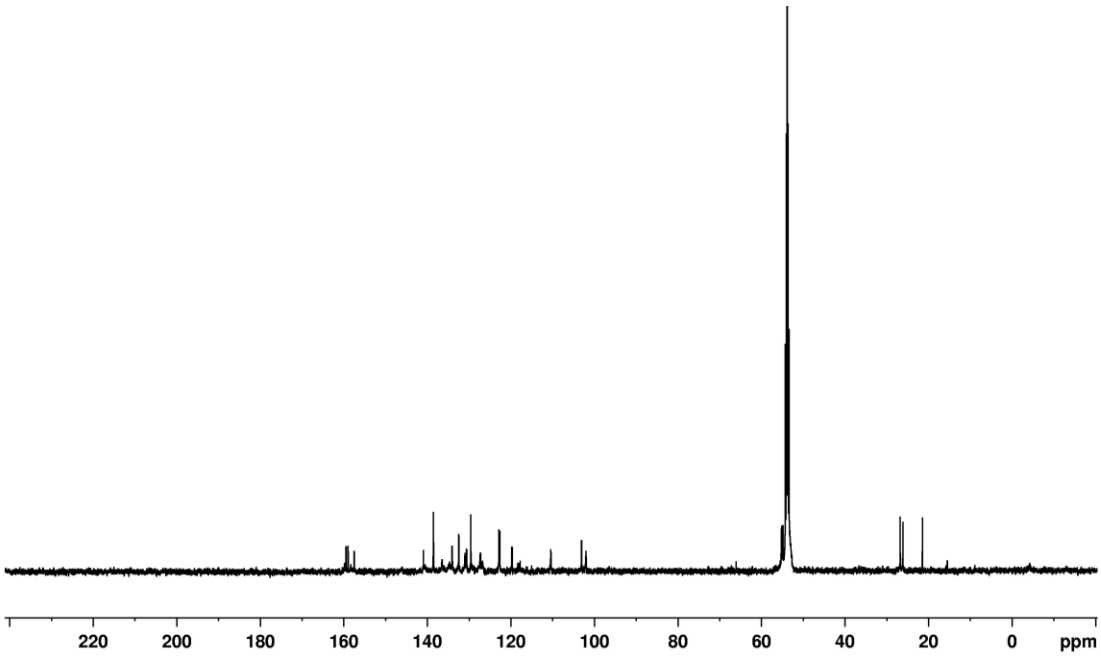

(b) Expansion of aromatic region

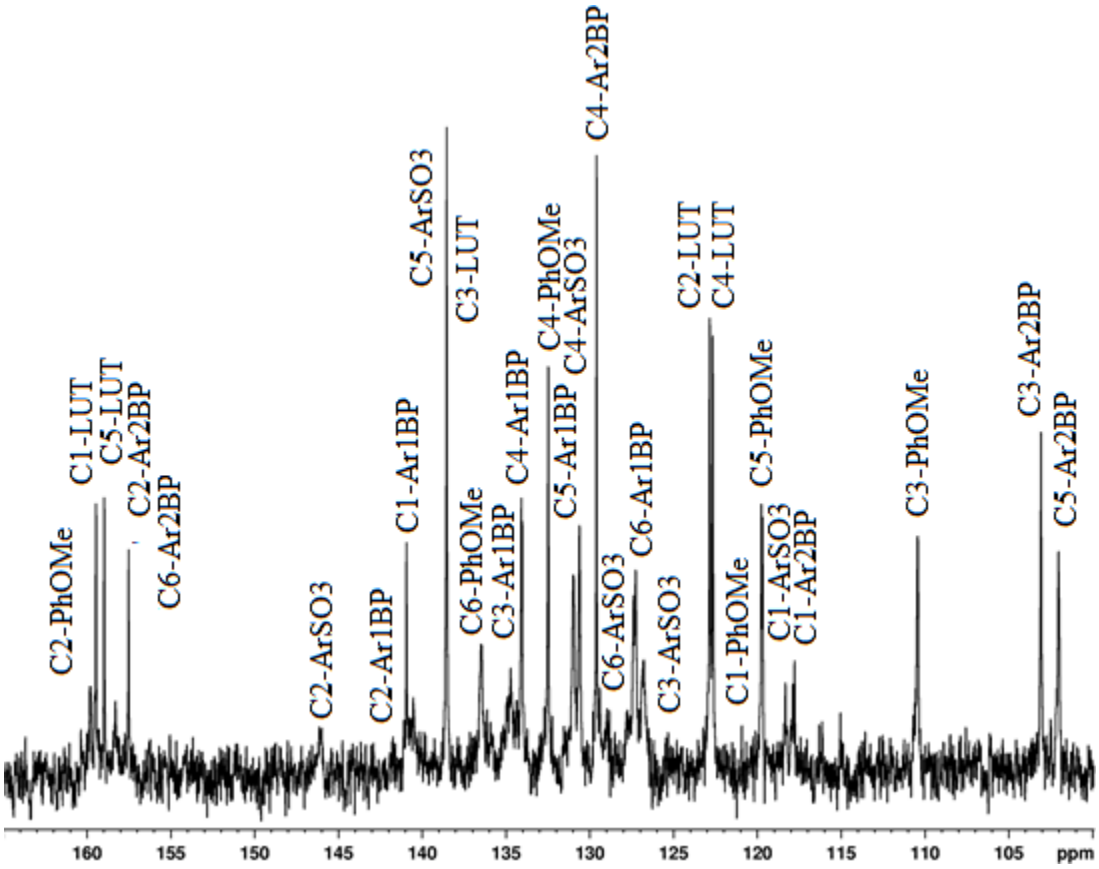

Figure 6.12, continued.

(c) Expansion of aliphatic region

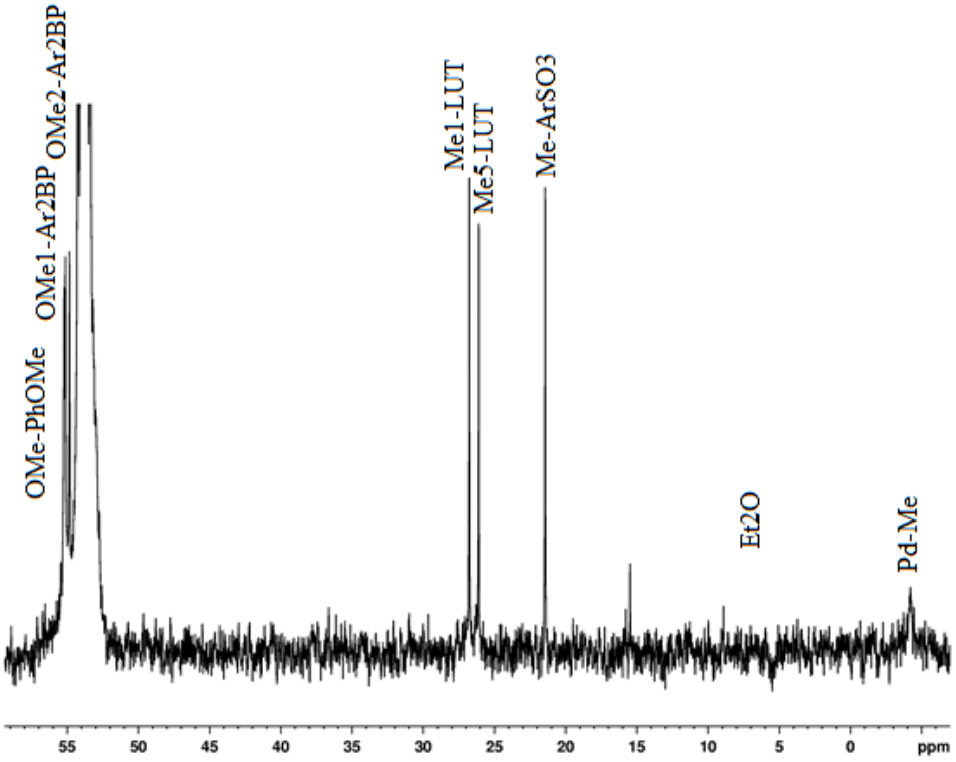

Figure 6.13. ^{13}C NMR of **2-lut** (CD_2Cl_2, –40 °C, 125 MHz).

(a) Full ^{13}C NMR spectrum

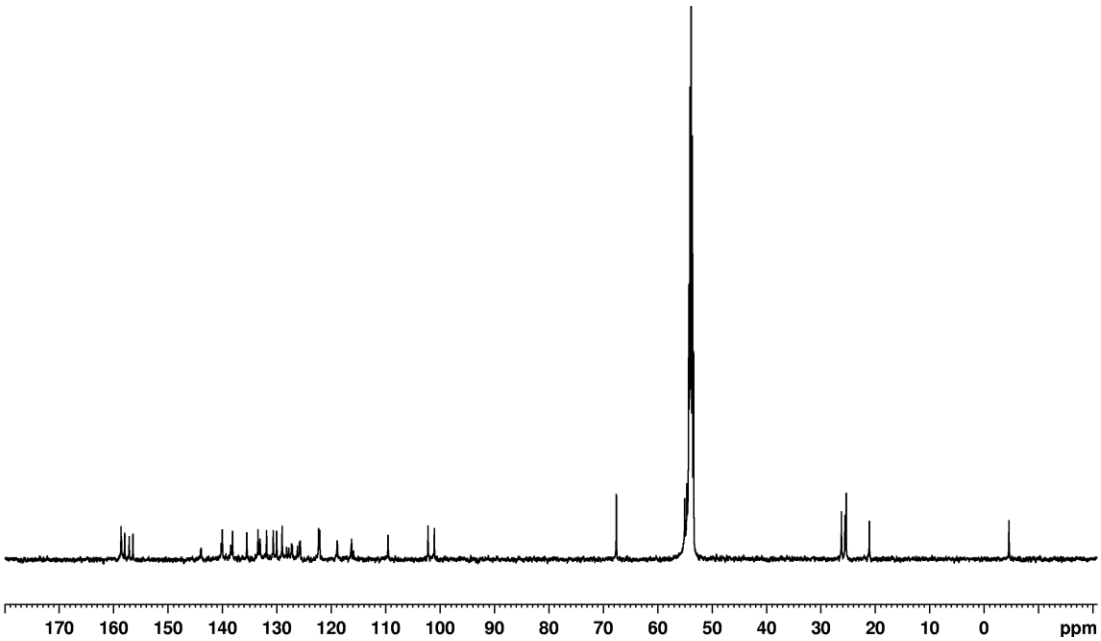

Figure 6.13, continued.

(b) Expansion of aromatic region

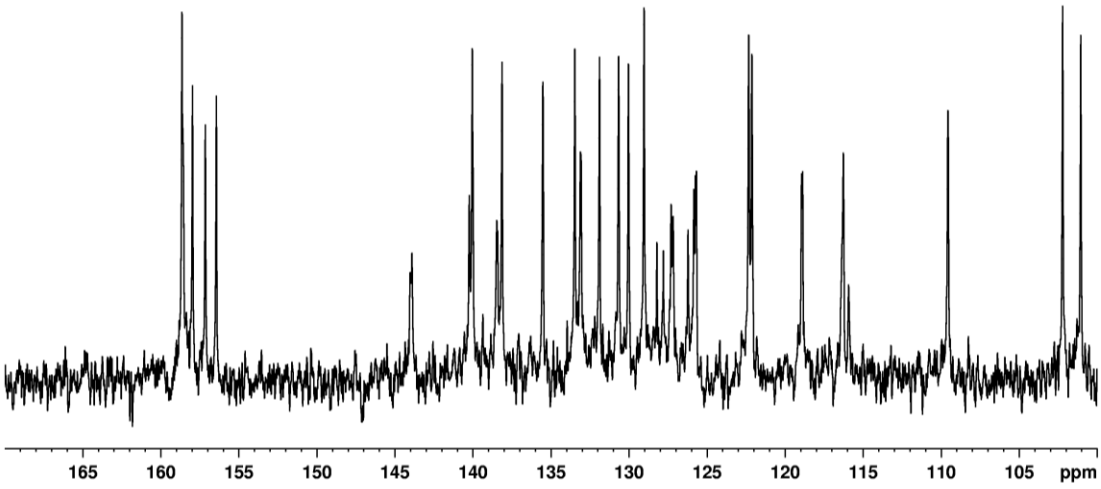

(c) Expansion of aromatic region

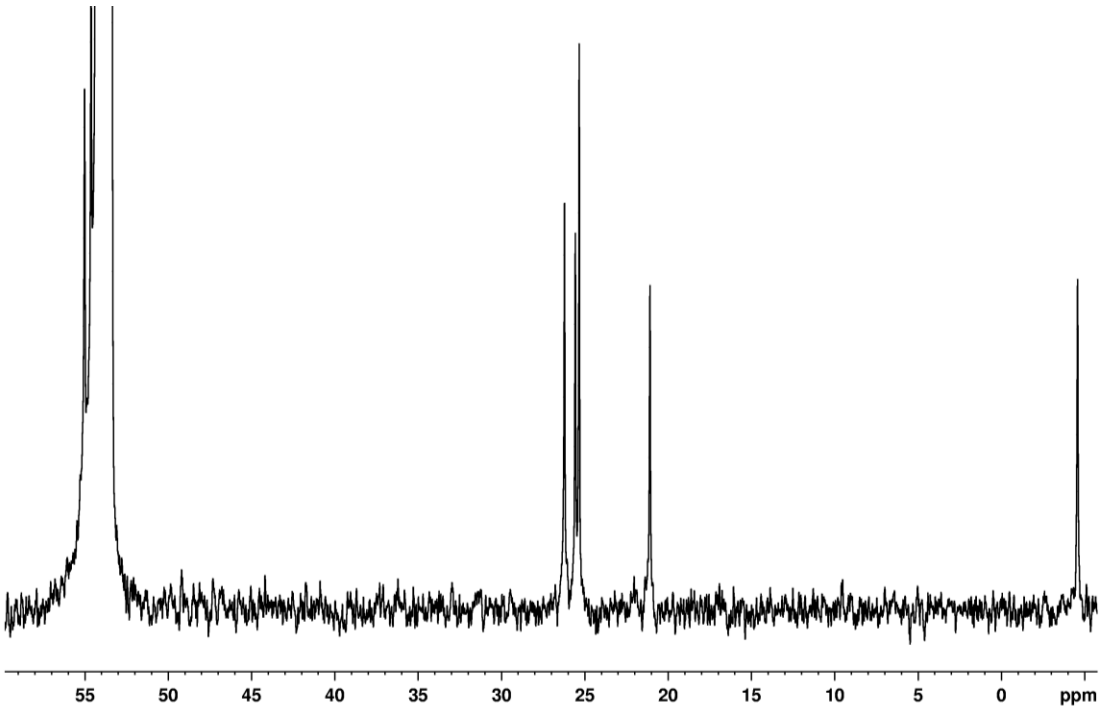

Figure 6.14. ^{1}H-^{1}H COSY NMR of **2-lut** (CD_2Cl_2, 25 °C, 500 MHz).

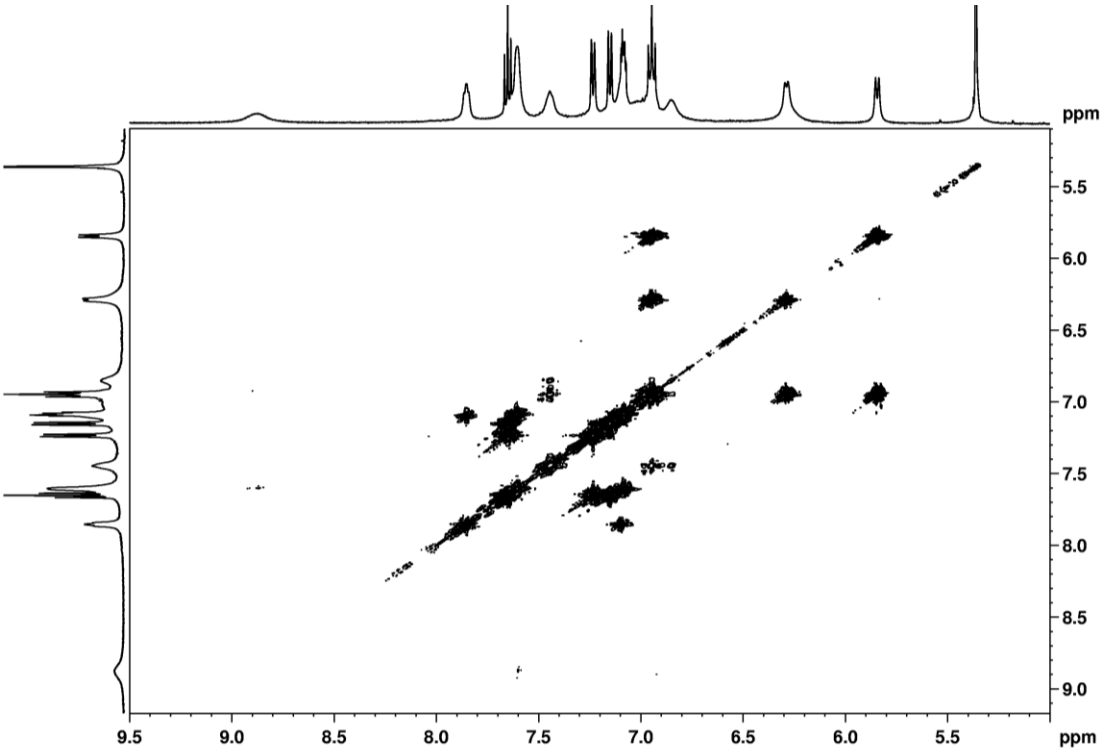

Figure 6.15. ^{1}H-^{1}H COSY NMR of **2-lut** (CD_2Cl_2, 35 °C, 500 MHz).

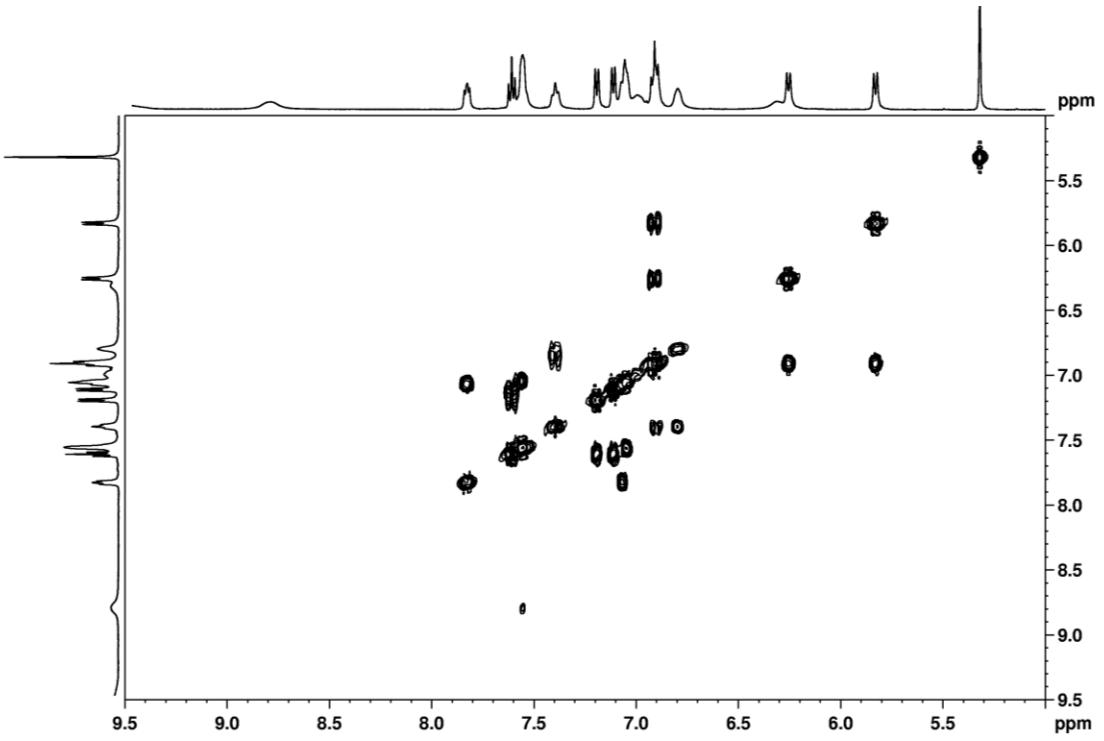

Figure 6.16. ^{1}H-^{1}H COSY NMR of **2-lut** (CD_2Cl_2, 80 °C, 500 MHz).

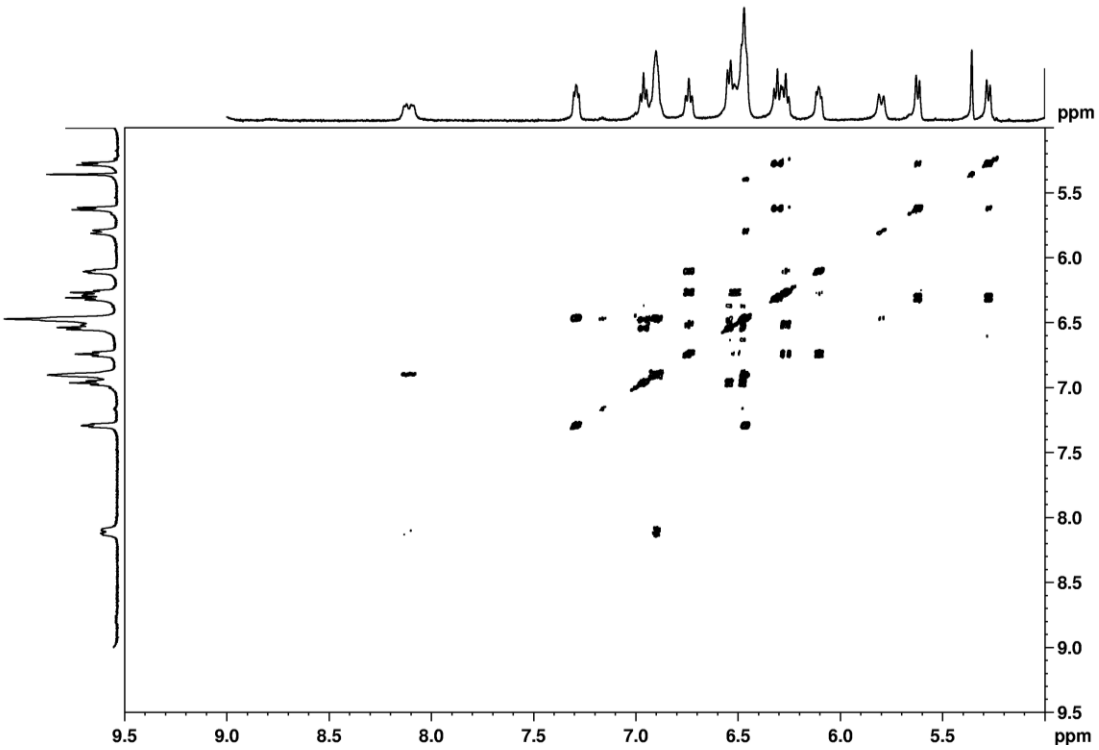

Figure 6.17. ^{1}H-^{1}H NOSY NMR of **2-lut** (CD_2Cl_2, 25 °C, 500 MHz).

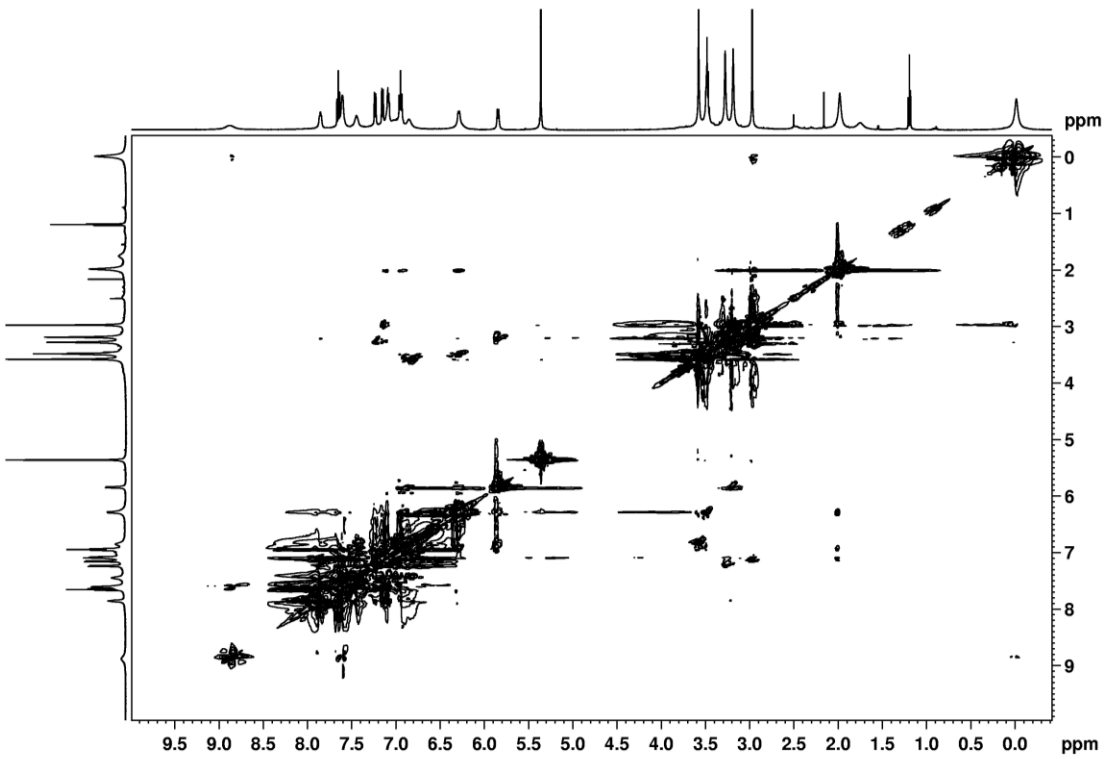

Figure 6.18. ^{1}H-^{1}H NOSY NMR of **2-lut** (CD_2Cl_2, –40 °C, 500 MHz).

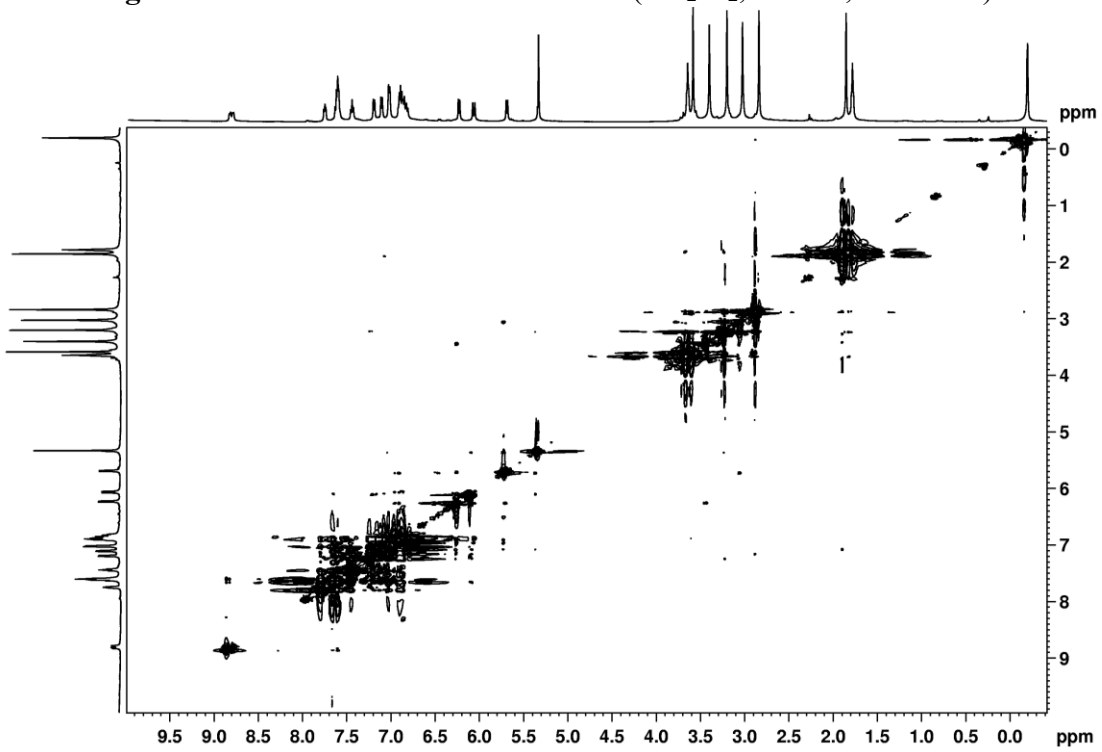

Figure 6.19. ^{1}H-^{13}C HMQC of **2-lut** (CD_2Cl_2, 25 °C, 500 MHz, 125 MHz).

(a) Full spectrum

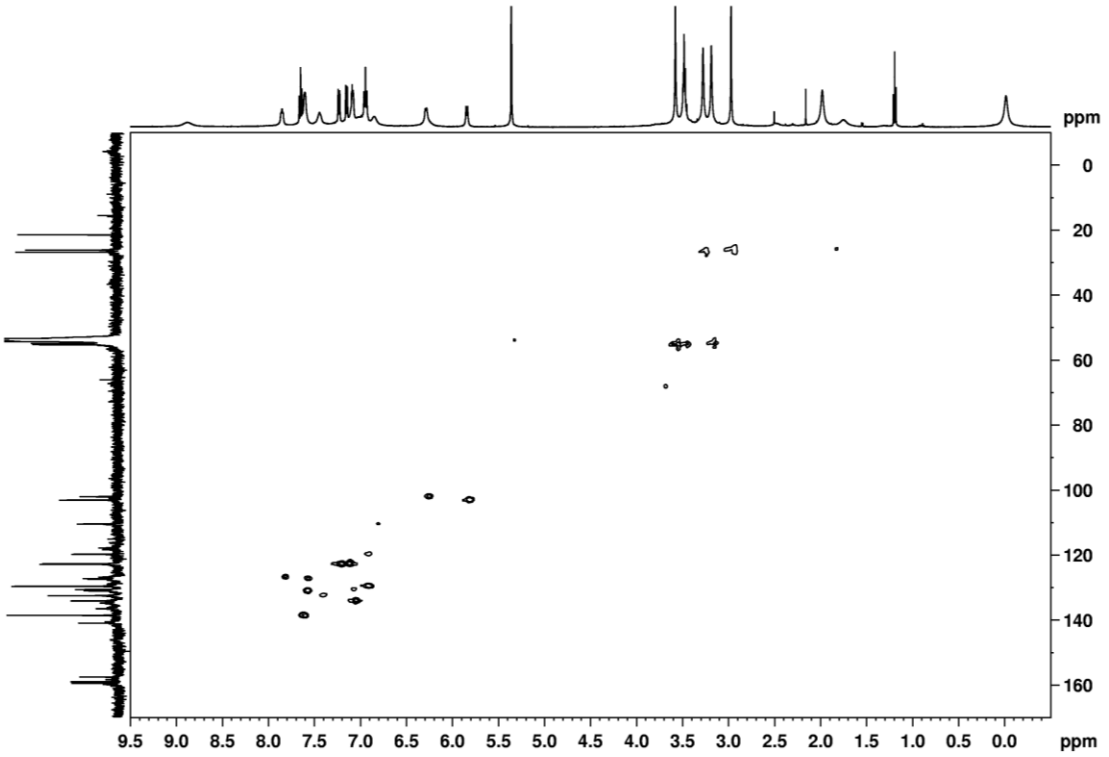

(b) Expansion of aromatic region

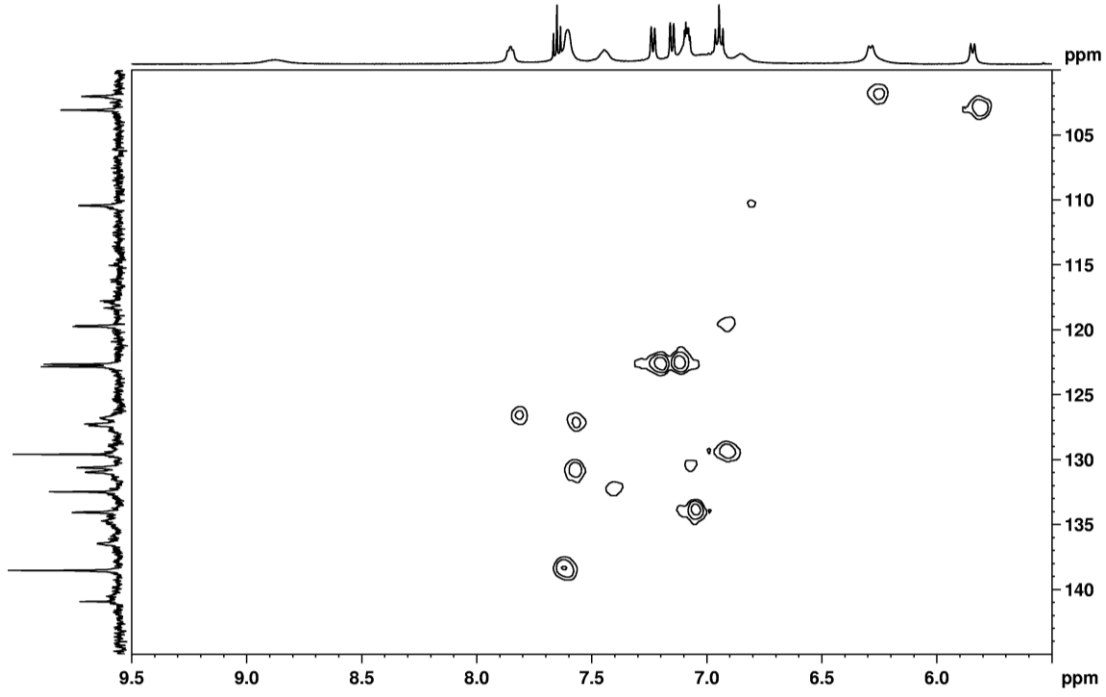

Figure 6.20. ^{1}H-^{13}C HMQC of **2-lut** (CD_2Cl_2, 35 °C, 500 MHz, 125 MHz).

(a) Full spectrum

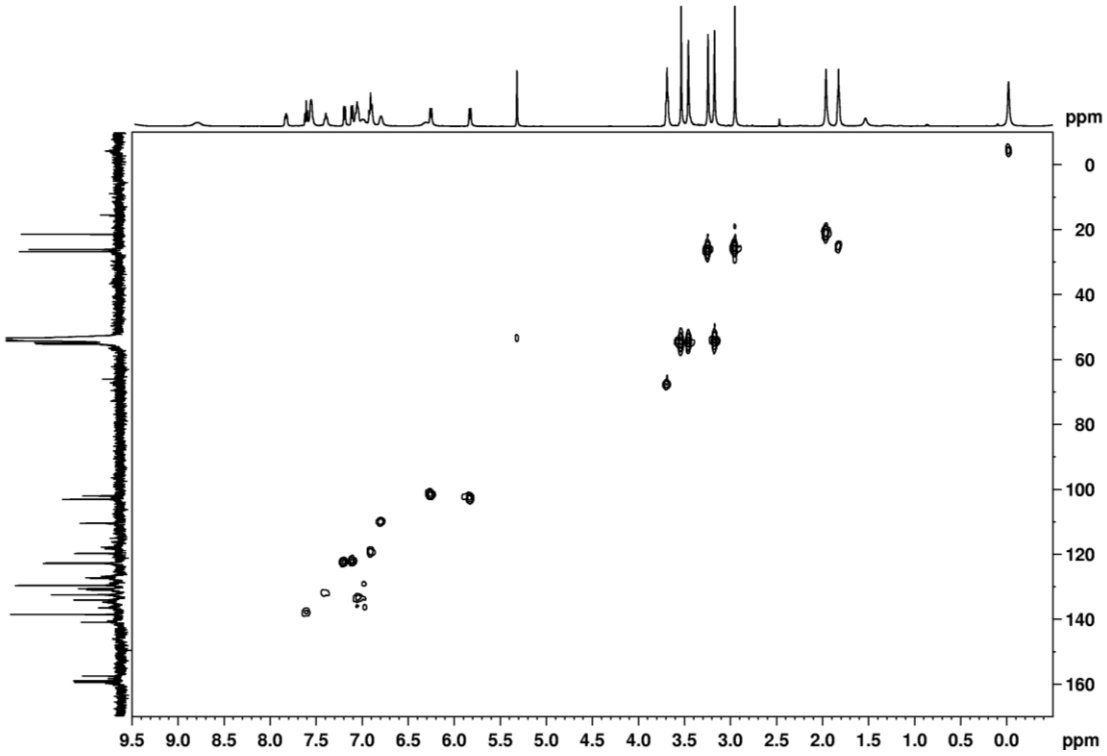

(b) Expansion of aromatic region

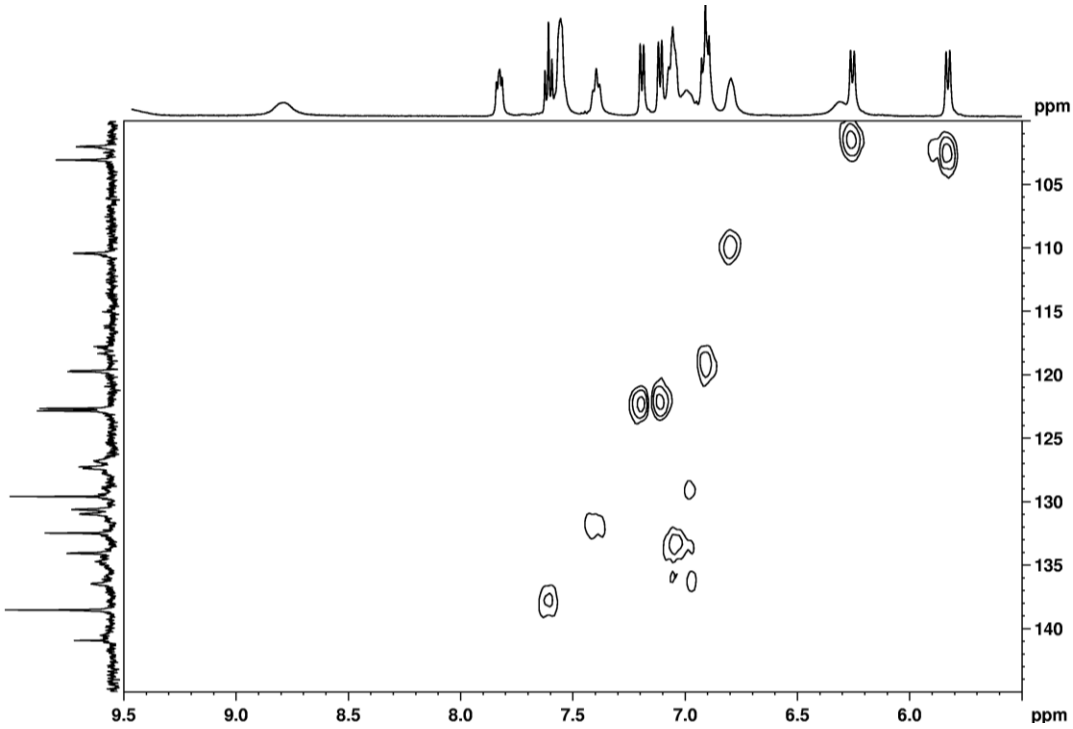

Figure 6.21. ^{1}H-^{13}C HMQC of **2-lut** (CD_2Cl_2, –40 °C, 500 MHz, 125 MHz).

(a) Full spectrum

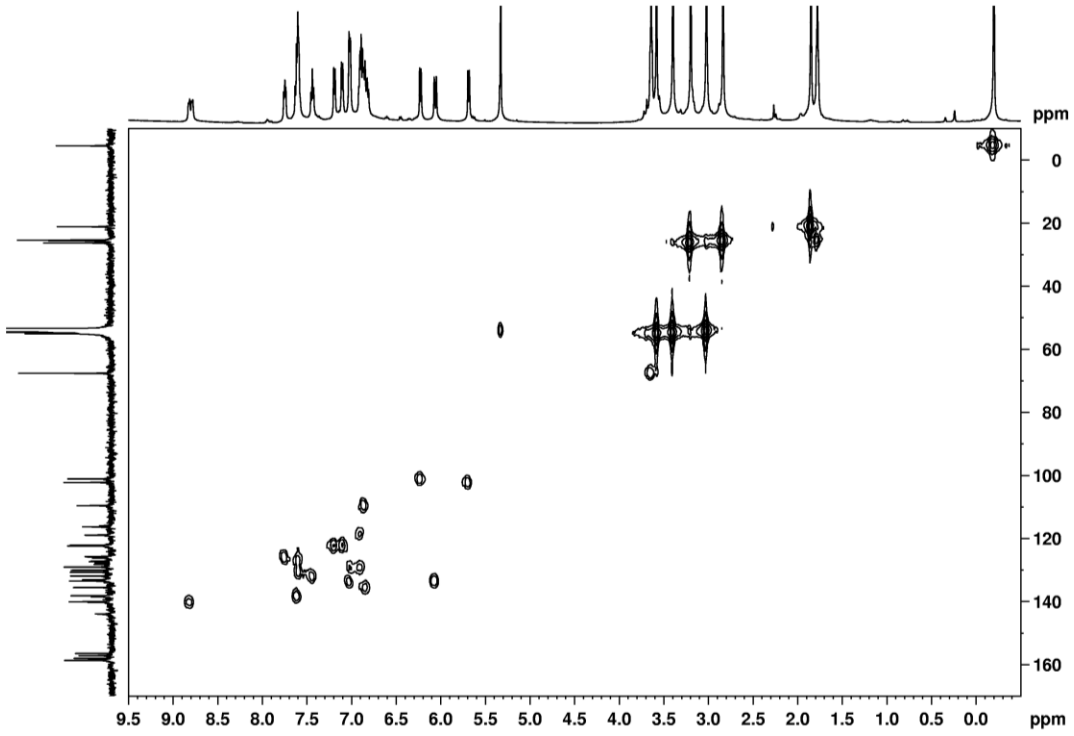

(b) Expansion of aromatic region

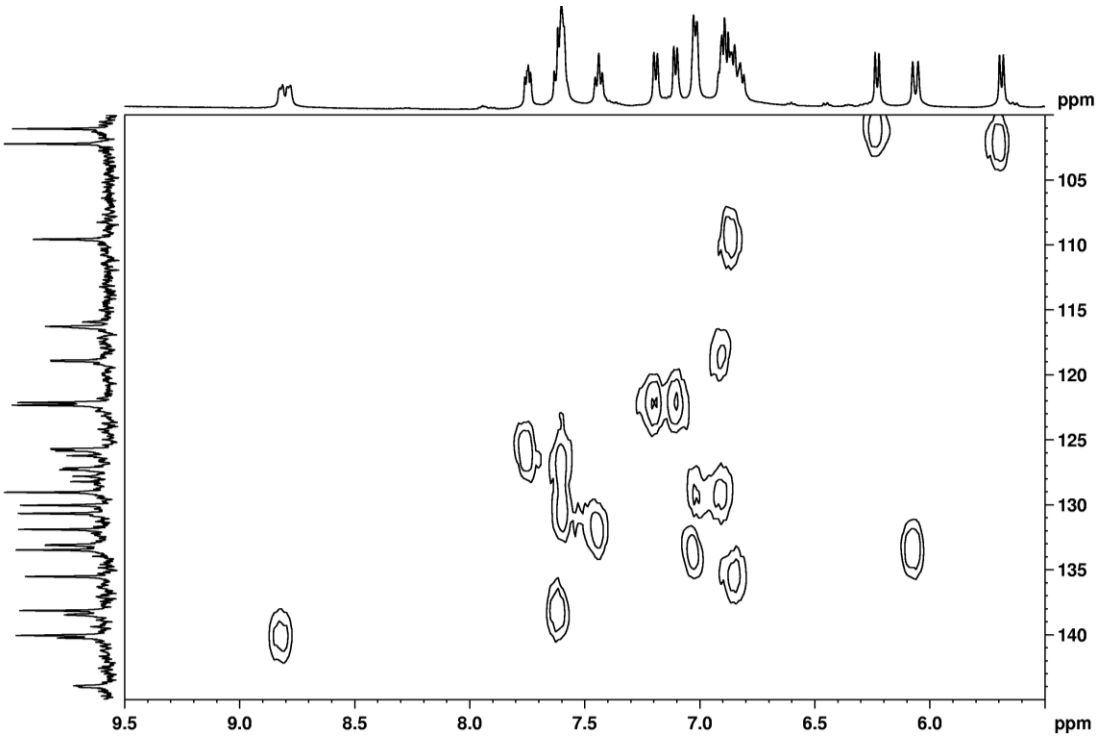

Figure 6.22. ^{1}H-^{13}C HMBC of **2-lut** (CD_2Cl_2, 25 °C, 500 MHz, 125 MHz).

(a) Full spectrum

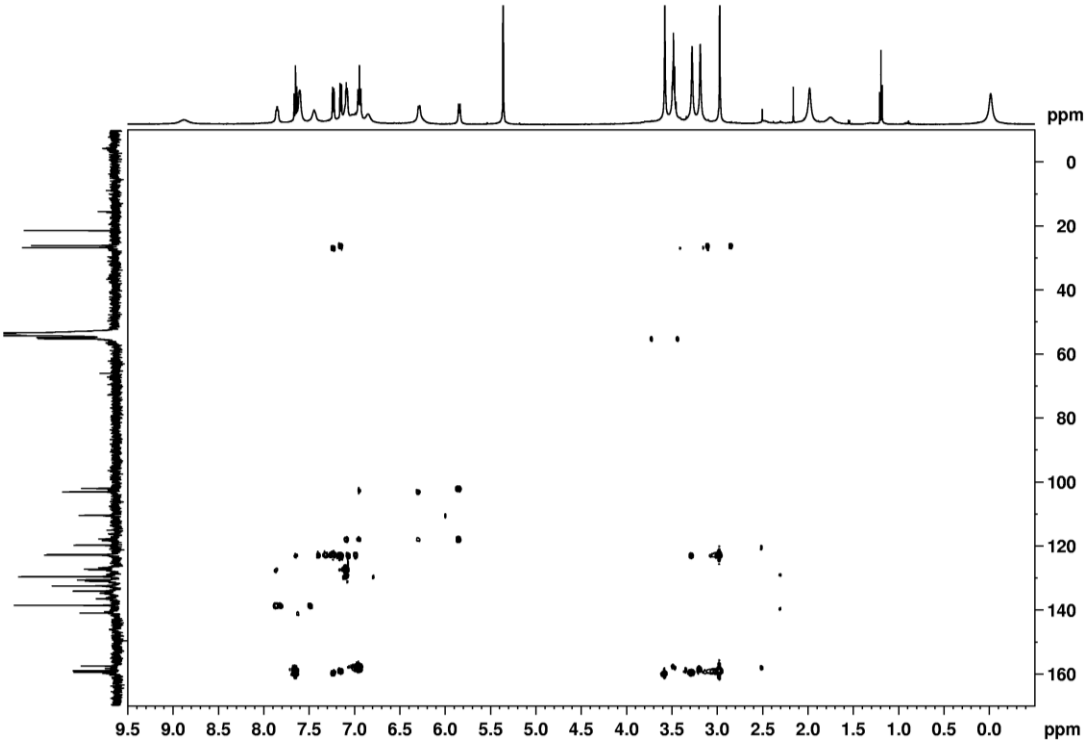

(b) Expansion of aromatic region

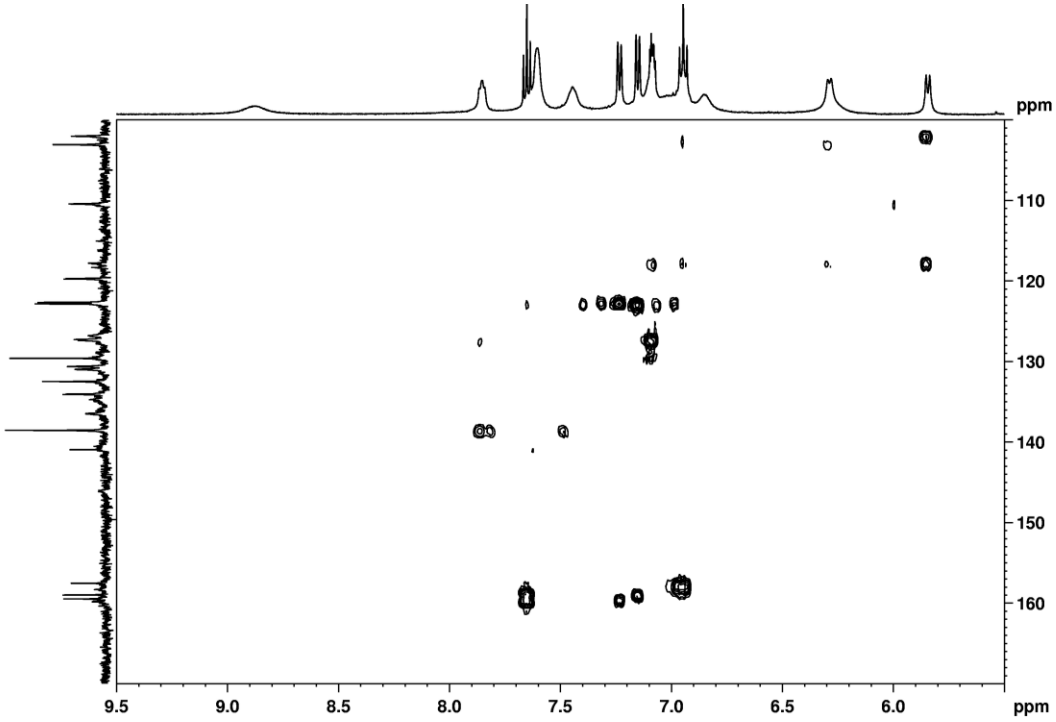

Figure 6.23. ^{1}H-^{13}C HMBC of **2-lut** (CD_2Cl_2, –40 °C, 500 MHz, 125 MHz).

(a) Full spectrum

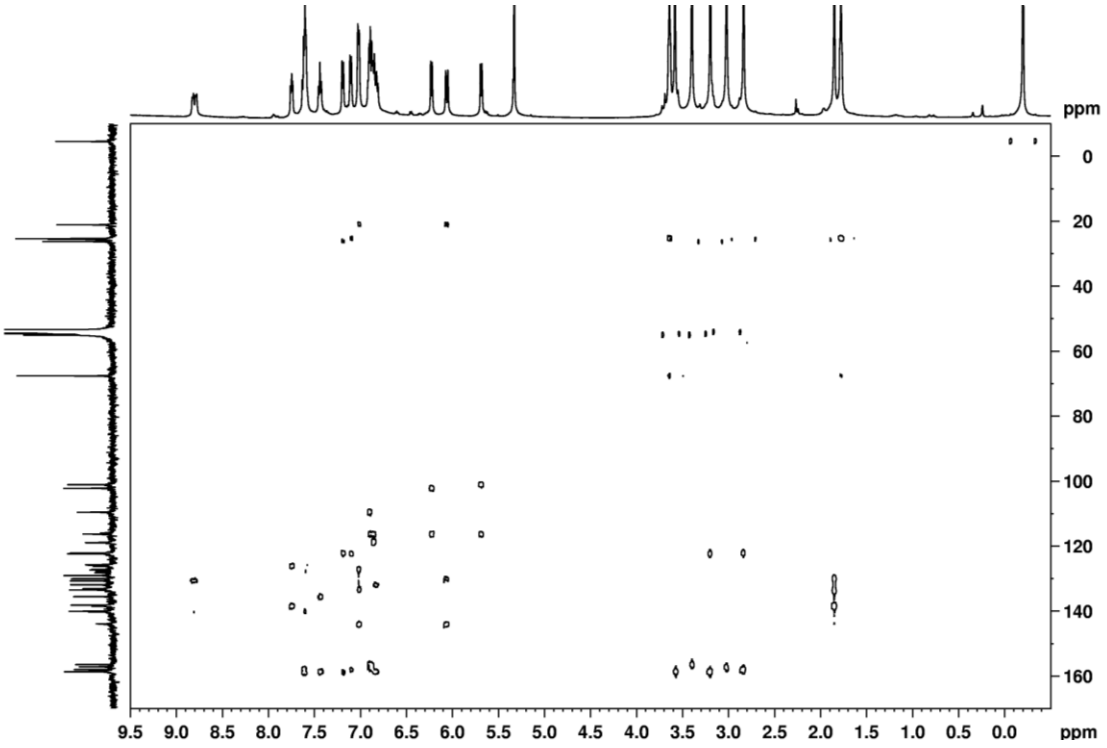

(b) Expansion of aromatic region

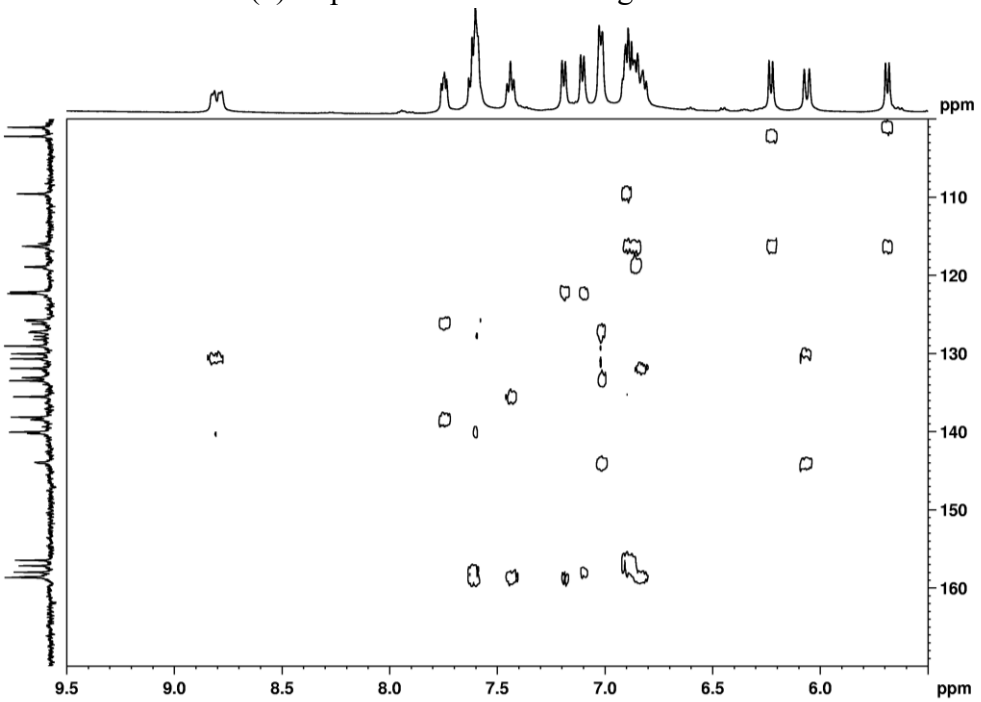

Table 6.4. Crystal data and structure refinement of **2-py** and, for comparison, **2-lut**.

	2-py	**2-lut**•2(THF)[14]
Identification code	1r	1-lut+2THF
Empirical formula	$C_{34}H_{34}NO_6PPdS$	C_{36} H_{38} N O_6 P Pd S,2(C_4 H_8 O)
Formula weight	722.05	894.31
Temperature (K)	100(2)	100(2)
Crystal system	monoclinic	triclinic
Space group	*C*2/*c*	P -1
a (Å)	25.9542(19)	10.2461(11)
b (Å)	15.3711(12)	10.4428(11)
c (Å)	18.1879(14)	20.089(2)
α (°)	90	76.3297(11)
β (°)	120.949(2)	78.2903(11)
γ (°)	90	87.3731(12)
Volume ($Å^3$)	6222.9(8)	2045.12
Z	8	2
Density (calculated) (Mg/m3)	1.541	1.458
Absorption coefficient (mm^{-1})	0.762	0.601
F(000)	2960.0	932
Crystal size (mm^3)	0.18 × 0.11 × 0.08	0.40 x 0.24 x 0.08
Radiation	MoKα (λ = 0.71073)	MoKα (λ = 0.71073)
Theta range for data collection (°)	4.584 to 50.722	2.01 to 28.28
Index ranges	-30 ≤ h ≤ 31, -18 ≤ k ≤ 18, -21 ≤ l ≤ 21	-13 ≤ h ≤ 13, -13 ≤ k ≤ 13, -26 ≤ l ≤ 26
Reflections collected	16637	24117
Independent reflections	5688 [R_{int} = 0.0826, R_{sigma} = 0.0897]	9689 (R_{int} = 0.0229)
Data / restraints / parameters	5688/204/507	9689/0/512
Goodness-of-fit on F^2	1.083	1.014
Final R indices [I>2sigma(I)]	R^1 = 0.0676, wR_2 = 0.1288	R^1 = 0.0316, wR_2 = 0.0805
R indices (all data)	R_1 = 0.1049, wR_2 = 0.1425	R_1 = 0.369, wR_2 = 0.0825
Largest diff. peak and hole (e.$Å^{-3}$)	0.57/-0.65	1.047/-0.490

6.5 References and Notes

(1) Berkefeld, A.; Mecking, S. *Angew. Chem. Int. Ed. Engl.* **2008**, *47*, 2538.

(2) Nakamura, A.; Ito, S.; Nozaki, K. *Chem. Rev.* **2009**, *109*, 5215.

(3) Ito, S.; Nozaki, K. *Chem. Rec.* **2010**, *10*, 315.

(4) Nakamura, A.; Anselment, T. M. J.; Claverie, J.; Goodall, B.; Jordan, R. F.; Mecking, S.; Rieger, B.; Sen, A.; van Leeuwen, P. W. N. M.; Nozaki, K. *Acc. Chem. Res.* **2013**, *46*, 1438.

(5) Franssen, N. M. G.; Reek, J. N. H.; de Bruin, B. *Chem. Soc. Rev.* **2013**, *42*, 5809.

(6) Britovsek, George J. P.; Gibson, V. C.; Wass, D. F. *Angew. Chem. Int. Ed.* **1999**, 428.

(7) Gibson, V. C.; Spitzmesser, S. K. *Chem. Rev.* **2003**, *103*, 283.

(8) Skupov, K. M.; Marella, P. R.; Simard, M.; Yap, G. P. A.; Allen, N.; Conner, D.; Goodall, B. L.; Claverie, J. P. *Macromol. Rapid Commun.* **2007**, *28*, 2033.

(9) Piche, L.; Daigle, J. C.; Rehse, G.; Claverie, J. P. *Chem. Eur. J.* **2012**, *18*, 3277.

(10) Neuwald, B.; Falivene, L.; Caporaso, L.; Cavallo, L.; Mecking, S. *Chem. Eur. J.* **2013**, *19*, 17773.

(11) Wucher, P.; Goldbach, V.; Mecking, S. *Organometallics* **2013**, *32*, 4516.

(12) Ota, Y.; Ito, S.; Kuroda, J.; Okumura, Y.; Nozaki, K. *J. Am. Chem. Soc.* **2014**, *136*, 11898.

(13) Piche, L.; Daigle, J.-C.; Poli, R.; Claverie, J. P. *Eur. J. Inorg. Chem.* **2010**, *2010*, 4595.

(14) Defoe, J., J. Doctoral dissertation, The University of Chicago, 2011.

(15) Johnson, A. M.; Contrella, N. D.; Sampson, J. R.; Zheng, M.; Jordan, R. F. *Organometallics* **2017**, *36*, 4990.

(16) Kochi, T.; Noda, S.; Yoshimura, K.; Nozaki, K. *J. Am. Chem. Soc.* **2007**, *129*, 8948.

(17) Falivene, L.; Credendino, R.; Poater, A.; Petta, A.; Serra, L.; Oliva, R.; Scarano, V.; Cavallo, L. *Organometallics* **2016**, *35*, 2286.

(18) Vela, J.; Lief, G. R.; Shen, Z.; Jordan, R. F. *Organometallics* **2007**, *26*, 6624.

(19) Neuwald, B.; Caporaso, L.; Cavallo, L.; Mecking, S. *J. Am. Chem. Soc.* **2013**, *135*, 1026.

(20) Keller, J.; Schlierf, C.; Nolte, C.; Mayer, P.; Straub, B. F. *Synthesis* **2006**, 354.

(21) Wife, R. L.; Van Oort, A. B.; Van Doorn, J. A.; Van Leeuwen, P. W. N. M. *Synthesis* **1983**, *1983*, 71.

(22) Aspinall, H. C.; Tillotson, M. R. *Inorg. Chem.* **1996**, *35*, 5.

(23) Aspinall, H. C.; Moore, S. R.; Smith, A. K. *Dalton Trans.* **1993**, 993.

(24) Bianchini, C.; Lenoble, G.; Oberhauser, W.; Parisel, S.; Zanobini, F. *Eur. J. Inorg. Chem.* **2005**, *2005*, 4794.

(25) De Graaf, W.; Boersma, J.; Smeets, W. J. J.; Spek, A. L.; Van Koten, G. *Organometallics* **1989**, *8*, 2907.